

**GEOMETRIC CONTROL THEORY AND ITS APPLICATION
TO UNDERWATER VEHICLES**

A DISSERTATION SUBMITTED TO THE GRADUATE DIVISION OF THE
UNIVERSITY OF HAWAI'I IN PARTIAL FULFILLMENT OF THE
REQUIREMENTS FOR THE DEGREE OF

DOCTOR OF PHILOSOPHY

IN

OCEAN & RESOURCES ENGINEERING

DECEMBER 2008

By
Ryan N. Smith

Dissertation Committee:

Monique Chyba, Chairperson
Song K. Choi
R. Cengiz Ertekin
Geno Pawlak
George R. Wilkens

We certify that we have read this dissertation and that, in our opinion, it is satisfactory in scope and quality as a dissertation for the degree of Doctor of Philosophy in Ocean & Resources Engineering.

DISSERTATION COMMITTEE

Chairperson

©2008, Ryan Neal Smith. All rights reserved.

To Neal

Acknowledgments

Of this entire dissertation, this single section has proven to be the most painful and difficult to write. Of course, after committing two-hundred and some odd pages to the discussion of my research over the last five years, I have few words left for the one section that will probably be read the most of any other in this dissertation. Additionally, recounting the memories of all the love and support which I have received from so many people brings tears to my eyes every time I have tried to work on this section. My cup runneth over.

I have written this acknowledgments section one hundred forty-three times; yes, I have been counting. I can not simply list every person who has participated in the success of this work, as the list would be longer than the dissertation itself. So, I must restrict myself to acknowledging only those whom have truly made this all possible, and at times, very worthwhile.

I will undoubtedly omit some individuals who do deserve recognition. For most of these, including you would require the inclusion of a multitude of others, as your contributions are of equivalent importance. I trust that these individuals know who they are, and willingly accept this blanket acknowledgment as sufficient recognition. Thank you!

I would first like to extend a huge thank you to the Mathematics Department for their continued support throughout my graduate career. Emotionally, academically and financially they have provided a stable foundation upon which I have based my studies. In particular, I would like to acknowledge my Hawaiian aunties, Susan and Shirley, for their guidance, wisdom and love.

I would like to thank the Ocean & Resources Engineering Department for taking me in and allowing me the freedom to follow my academic dreams. My experiences in this department have taught me things that I never knew I needed to know, and for this I am grateful. To Volker, Danny, Jordon, Kumar and Rob, I thank you for all your assistance that first year in teaching a mathematician how to be an engineer; I would not have made it through without you.

I owe a debt of gratitude to the past and present members of the Autonomous Systems Laboratory and employees of Mase, Inc. For your instruction and guidance in the operation and maintenance of ODIN, I am truly grateful. In particular, I would like to give a huge thank you to Chris McLeod for his patience, support and friendship over the years; all three of which were tested many times when troubleshooting a malfunctioning ODIN. I think that I also owe an homage to the robotic gods for for keeping ODIN operational during the last experimental stages of my research.

I want to extend a separate thank you to all of those students who assisted me in the collection and processing of the data gathered at the pool. Thank you Shashi, Jeff, Daniel, Will, Scott, Ben, Tim and Gina. Your dedicated efforts during those early morning experiments was greatly appreciated.

A key component to this research was the implementation of the control strategies onto ODIN at the Duke Kahanamoku Aquatic Complex. None of that would have been possible without the help of Bruce Kennard. I want to thank him for his flexibility and willingness to provide ample space and time at the pool to conduct the experiments presented in this dissertation.

I would like to thank Thomas Haberkorn for his guidance, assistance and tutelage over the past five years. And, of course, his persistence in treating every time we "took a coffee." Your padawan has finished his training.

I would also like to thank George Csordas for his mentorship over the entire course of my graduate career. He taught me that nothing is *obvious*, and anything that is implied as such, *clearly* needs to be checked. Dr. Csordas, for the many times you have asked "How is your thesis coming along?", I can finally and proudly reply, "It is finished."

I would also like to acknowledge Jonathan Gradie for his mentorship, support and friendship. Thank you for the opportunities, experiences, camaraderie and most of all, the stories. You are an inspiration.

It has been an amazing experience to work under and collaborate with Monique Chyba for the better part of the last six years. What started as a simple conversation after a colloquium has blossomed into the work presented in this dissertation. It has been exciting to be a part of her programs and visions from the very beginning. I can not thank Monique enough for her patience, guidance, support, enthusiasm, coaching and friendship.

Most of all, I would like to thank my family for providing a solid foundation of unconditional love and support. I thank my uncle Tom for the inspiration to follow my dreams. Thank you Mom and Dad for letting me lead during this journey; following, supporting and encouraging every decision along the way. Thank you Troy and York for never letting me forget who I am and where I came from.

To my wife Ellen, a woman who fell in love with, and married, a mathematician turned ocean engineer during the middle of his Ph.D. I will do my very best for the rest of my life

to return the love and support you have given me over the past four years. Without you, this would never have been possible.

Abstract

This dissertation is based on theoretical study and experiments which extend geometric control theory to practical applications within the field of ocean engineering. We present a method for path planning and control design for underwater vehicles by use of the architecture of differential geometry. In addition to the theoretical design of the trajectory and control strategy, we demonstrate the effectiveness of the method via the implementation onto a test-bed autonomous underwater vehicle.

Bridging the gap between theory and application is the ultimate goal of control theory. Major developments have occurred recently in the field of geometric control which narrow this gap and which promote research linking theory and application. In particular, Riemannian and affine differential geometry have proven to be a very effective approach to the modeling of mechanical systems such as underwater vehicles. In this framework, the application of a kinematic reduction allows us to calculate control strategies for fully and under-actuated vehicles via kinematic decoupled motion planning. However, this method has not yet been extended to account for external forces such as dissipative viscous drag and buoyancy induced potentials acting on a submerged vehicle. To fully bridge the gap between theory and application, this dissertation addresses the extension of this geometric control design method to include such forces.

We incorporate the hydrodynamic drag experienced by the vehicle by modifying the Levi-Civita affine connection and demonstrate a method for the compensation of potential forces experienced during a prescribed motion. We present the design method for multiple

different missions and include experimental results which validate both the extension of the theory and the ability to implement control strategies designed through the use of geometric techniques.

By use of the extension presented in this dissertation, the underwater vehicle application successfully demonstrates the applicability of geometric methods to design implementable motion planning solutions for complex mechanical systems having equal or fewer input forces than available degrees of freedom. Thus, we provide another tool with which to further increase the autonomy of underwater vehicles.

Contents

Acknowledgments	v
Abstract	ix
List of Tables	xvii
List of Figures	xix
List of Symbols	xxii
Chapter 1: Introduction	1
Chapter 2: Equations of Motion	13
2.1 Rigid Body Kinematics	14
2.2 Rigid Body Dynamics	21
2.3 Submerged Rigid Body Dynamics	29
2.3.1 Added Mass	29
2.3.2 Viscous Damping	31
2.3.3 Restoring Forces and Moments	33
2.4 Geometric Equations of Rigid-Body Dynamics	34
2.4.1 Ideal Fluid, Including Added Mass	36
2.4.2 Geometric Forces	48
2.4.3 Viscous Drag Geometrically	51
2.4.4 Restoring Forces Geometrically	54

2.4.5 Geometric Equations of Motion in a Viscous Fluid	56
2.5 Closing Remarks	63
Chapter 3: Control of Underwater Vehicles	64
3.1 Motion Planning for the Rigid Body	64
3.2 Motion Planning for the Submerged Rigid Body	67
3.3 Control of Autonomous Underwater Vehicles	68
3.3.1 PID Control	69
3.3.2 Adaptive Control	70
3.3.3 Sliding Mode Control	71
3.3.4 Neural Network Control	72
3.3.5 Fuzzy Logic	73
3.3.6 General Control	74
Chapter 4: Geometric Control of Underwater Vehicles	76
4.1 Literature Review	76
4.2 Research Motivation and Direction	78
4.3 Kinematic Reduction	80
4.3.1 Decoupling Vector Fields	85
4.3.2 Under-Actuation	86
4.4 Control Strategy Design Using Decoupling Vector Fields	87
Chapter 5: Application to the Omni Directional intelligent Navigator	97

5.1	Omni-Directional Intelligent Navigator (ODIN)	97
5.2	Calculated Decoupling Vector Fields	102
5.2.1	Covariant derivatives	104
5.2.2	One-input systems	111
5.2.3	Two-input systems	113
5.3	Covariant Derivatives for $\tilde{\nabla}$	117
5.4	Decoupling Vector Fields for ODIN	117
5.5	Calculated Control Strategies	123
5.5.1	Mission 1	125
5.5.2	Mission 2	127
5.5.3	Mission 3	129
5.5.4	Mission 4	137
5.5.5	Mission 5	140
5.5.6	Mission 6	146
5.5.7	Mission 7	150
Chapter 6: Experiments		156
6.1	Motivation	156
6.2	Testing Facility	156
6.3	From Theory to Implementation	158
6.4	Experimental Results	162
6.4.1	Mission 1	163

6.4.2 Mission 2	169
6.4.3 Mission 3	171
6.4.4 Mission 4	183
6.4.5 Mission 5	192
6.4.6 Mission 6	197
6.4.7 Mission 7	201
6.5 Experimental Summary	204
Chapter 7: Generalization to Other Vehicles	208
7.1 ODIN Generalization	209
7.2 Torpedo-Shaped Vehicle	211
Chapter 8: Further Research	218
8.1 Control Strategy Implementation onto other Vehicles	218
8.2 Alternate Inclusion of Restoring Forces	219
8.3 Design of Algorithm for On-Board Computations	225
Chapter 9: Conclusions and Recommendations	226
9.1 Theoretical Conclusions and Recommendations	226
9.2 Experimental Conclusions and Recommendations	228
Appendix A: Differential Geometry	231
A.1 Manifolds and Submanifolds	232
A.2 Tangent and Cotangent Bundles	237

A.3	Vector and Covector Fields	240
A.3.1	Lie Bracket	242
A.4	Affine Differential Geometry	246
A.4.1	Affine Connections	247
A.4.2	Symmetric Product	249
A.5	Lie Groups	249
A.5.1	Lie Algebras	251
Appendix B: Ancillary Data Collected		254
B.1	Drag Force Estimations	254
B.2	Thruster Calibrations	261
B.3	Water Sampling Data	265
B.4	Thruster Protection Circuit	266
Appendix C: Proof of Theorem 5.2		268
C.1	Three Input Systems	268
C.1.1	Three Translational Inputs	268
C.1.2	Three Rotational Inputs	270
C.1.3	Mixed Translational and Rotational Inputs	271
C.2	Four Input Systems	279
C.2.1	Three Translation, One Rotation	279
C.2.2	Three Rotation, One Translation	281
C.2.3	Two Translation, Two Rotation	283

C.3	Five Input Systems	289
C.3.1	Three Translation, Two Rotation	289
C.3.2	Two Translation, Three Rotation	292
C.4	Six Input Systems	294
References	295

List of Tables

1	SNAME notation for the study of underwater vehicles.	16
2	Notations for the study of underwater vehicles	17
3	Main dimensions and hydrodynamic parameters for ODIN.	99
4	Covariant derivatives in basis notation for the affine connection $\tilde{\nabla}$	118
5	Discretized control structure for 5m pure surge.	160
6	Discretized control structure for a 2.5 m pure heave without buoyancy compensation.	165
7	Discretized control structure for a 2.5 m pure heave including buoyancy compensation.	168
8	Discretized control structure for trajectory ending at $\eta_f = (1.25, 0, 3.665, 0, 0, 0)$ excluding potential forces.	172
9	Discretized control structure for trajectory ending at $\eta_f = (1.25, 0, 3.665, 0, 0, 0)$ including potential forces using only vertical thrusters.	176
10	Discretized control structure for trajectory ending at $\eta_f = (1.25, 0, 3.665, 0, 0, 0)$ including potential forces for a fully-actuated system.	176
11	Discretized control structure for trajectory ending at $\eta_f = (1.25, 0, 3.665, 0, 0, 0)$ including potential forces using alternate approach #1.	179
12	Discretized control structure for trajectory ending at $\eta_f = (1.25, 0, 3.665, 0, 0, 0)$ including potential forces using alternate approach #2 using only vertical thrusters.	180

13	Discretized control structure for trajectory ending at $(1.25, 0, 3.665, 0, 0, 0)$ including potential forces using alternate approach #2.	182
14	Discretized control structure for a pure roll of $\phi = \pi/8$ radians using the ramped control method.	188
15	Discretized control structure for a pure roll of $\phi = \pi/6$ radians using the ramped control method.	188
16	Discretized control structure for a pure roll of $\phi = \pi/4$ radians using the ramped control method.	189
17	Discretized control structure for a single transect of a seabed survey mission.	193
18	Discretized control structure for a concatenated sway motion of a transect of a seabed survey mission.	195
19	Discretized control structure for cylinder examination.	198
20	Modified cylinder examination control strategy #1.	199
21	Modified cylinder examination control strategy #2.	199
22	Discretized control structure for examination of a bulbous bow.	202
23	Quadratic Thrust/Voltage relationship for a control voltage range of $[-3, 3]$.	264
24	Piece-wise linear Thrust/Voltage relationship for a control voltage range of $[-3, 3]$	265

List of Figures

1	REMUS 600 AUV, Hydroid, LLC (2008).	4
2	SLOCUM Glider, Webb Research Corporation (2008).	4
3	Bluefin-12 AUV, Bluefin Robotics Corporation (2008).	5
4	DepthX AUV, StoneAerospace, Inc. (2008a).	6
5	ENDURANCE AUV, StoneAerospace, Inc. (2008b).	7
6	Earth-fixed and body-fixed coordinate reference frames.	16
7	Potential forces acting at C_G and C_B and the righting arm for a submerged spherical vehicle.	56
8	A block diagram of a PID controller, SilverStar (2008).	69
9	ODIN operating in the pool.	98
10	An inside look at ODIN.	98
11	Main external dimensions of ODIN.	99
12	Configurations for tether attachment to ODIN.	100
13	Trajectory around a cylinder for mission six.	148
14	USS George H.W. Bush (CVN 77), GlobalSecurity.org (2008).	151
15	Scaled trajectory for examining a bulbous bow.	152
16	Duke Kahanamoku Aquatic Complex.	157
17	Duke Kahanamoku Aquatic Complex diving well.	158
18	Control design to implementation flow chart.	161
19	Pure heave trajectory ending at $\eta_f = (0, 0, 4, 0, 0, 0)$ excluding buoyancy.	165

20	Pure heave trajectory ending at $\eta_f = (0, 0, 4, 0, 0, 0)$ including buoyancy. . .	168
21	Pure surge trajectory ending at $\eta_f = (5, 0, 1.5, 0, 0, 0)$ excluding buoyancy. .	170
22	Pure surge trajectory ending at $\eta_f = (5, 0, 1.5, 0, 0, 0)$ including buoyancy. .	171
23	Trajectory ending at $\eta_f = (1.25, 0, 3.665, 0, 0, 0)$ excluding potential forces.	173
24	Trajectory ending at $\eta_f = (1.25, 0, 3.665, 0, 0, 0)$ including potential forces using only vertical thrusters.	177
25	Trajectory ending at $\eta_f = (1.25, 0, 3.665, 0, 0, 0)$ including potential forces for a fully-actuated ODIN.	178
26	Trajectory ending at $\eta_f = (1.25, 0, 3.665, 0, 0, 0)$ including potential forces using alternate approach #1.	180
27	Trajectory ending at $\eta_f = (1.25, 0, 3.665, 0, 0, 0)$ including potential forces using alternate approach #2 using only vertical thrusters.	181
28	Trajectory ending at $\eta_f = (1.25, 0, 3.665, 0, 0, 0)$ including potential forces using alternate approach #2.	182
29	Pure roll for $\phi = \pi/8$ radians using the applied compensation control method.	185
30	Pure roll for $\phi = \pi/6$ radians using the applied compensation control method.	186
31	Pure roll for $\phi = \pi/4$ radians using the applied compensation control method.	187
32	Pure roll for $\phi = \pi/8$ radians designed from theory.	189
33	Pure roll for $\phi = \pi/6$ radians designed from theory.	190
34	Pure roll for $\phi = \pi/4$ radians designed from theory.	191
35	Single transect of the seabed survey mission.	194
36	Transect of the seabed survey mission with concatenated sway motion. . . .	196

37 Modified cylinder examination trajectory #1. 200

38 Modified cylinder examination trajectory #2. 201

39 Implementation of trajectory to examine a bulbous bow. 203

40 ODIN’s external dimensions. 210

41 Two transects connected by turn around loop. 217

42 Drag force versus velocity in the surge direction. 258

43 Drag force versus velocity in the sway direction. 259

44 Drag force versus velocity in the heave direction. 259

45 Drag moment versus velocity in the roll direction. 260

46 Drag moment versus velocity in the pitch direction. 260

47 Drag moment versus velocity in the yaw direction. 261

48 Lever and strain gauge set-up for thruster testing. 262

49 Example thruster testing experiment. 263

50 Circuit diagram for thruster protection. 267

List of Symbols

A_i	Projected surface area	32
$\text{ad}_{(\nu, \Omega)}$	Adjoint operator	106
b	Position in \mathbb{R}^3 of O_B with respect to O_I	16
B	Buoyancy force	33
C_B	Center of buoyancy	33
C_G	Center of gravity	23
C_D	Non-dimensional drag coefficient	32
C_f	Added mass moment cross terms	38
Cor_B	Coriolis force matrix	27
D_i	Dimensional drag coefficient	32
\mathcal{D}_i	Drag force or moment	53
$\Delta(X, Y)$	(1,2)-type tensor field	59
η	Position and orientation of O_B with respect to O_S	17
η_2	Orientation of O_B with respect to O_S	17
η_{init}	Initial configuration of the rigid body	88
η_{final}	Final configuration of the rigid body	88
F_{drag}	Drag force	53
$\mathcal{F}_t^{V_i}$	Flow along the vector field V_i for time t	91
g	Gravitational acceleration	33
$g(\eta)$	Restoring forces and moments matrix	33

\mathbb{G}	Kinetic energy metric	40
$\gamma(t)$	A differentiable curve in $SE(3)$	242
$\mathbb{G}_{\mathbb{R}^3}$	Standard inner product on \mathbb{R}^3	39
$\mathbb{G}^\#$	Inverse of the kinetic energy metric	50
$\Gamma^\infty(X)$	\mathcal{C}^∞ -sections of the distribution generated by X	241
H_{O_B}	Angular momentum about O_B	25
\mathbb{I}^{-1}	Set of input vector fields to the fully-actuated system ($m = 6$)	63
\mathbb{I}_i^{-1}	i^{th} column of $\mathbb{G}^\#$	63
\mathcal{I}_m^{-1}	Set of inputs to the underactuated system ($m < 6$)	63
\mathcal{I}^{-1}	Span \mathcal{I}_k^{-1}	63
J_b	Inertia tensor in the body-fixed frame	22
$J_f^{\Omega_i}$	Added mass moment of inertia matrix in the body-fixed frame	31
J_f	Added mass moment of inertia matrix	38
j_i	Inertia plus added mass moment of inertia	40
J	3×3 added mass moments of inertia matrix	40
$Lie^\infty(\mathcal{Y})$	Involutive closure of \mathcal{Y}	244
$\mathcal{L}_X f$	Lie derivative of f with respect to X	243
m	Mass	24
M_B	Rigid body inertia matrix	28
μ_{ij}	Added mass coefficient	30
$M_f^{\nu_i}$	Added mass matrix in the body-fixed reference frame	24

m_i	Mass plus added mass	40
M_f	Added mass matrix	38
M	3×3 added mass matrix	40
∇	Levi-Civita affine connection	40
$\tilde{\nabla}$	Levi-Civita affine connection including drag forces	60
$\nabla_{\gamma'(t)\gamma'(t)}$	Covariant derivative along the curve $\gamma'(t)$, acceleration in $SE(3)$	41
ν	Translational velocities in the body-fixed frame	17
∇_X	Covariant derivative with respect to the vector field X	247
$O(3)$	Orthogonal matrix group	18
Ω	Rotational velocities in the body-fixed frame	17
ω	Rotational velocities in the earth-fixed frame	22
ϕ	Rotation about the x-axis (roll)	16
ψ	Rotation about the z-axis (yaw)	16
p	Total translational momentum in the earth-fixed frame	37
π	Total rotational momentum in the earth-fixed frame	37
P	Total translational momentum in the body-fixed frame	37
Π	Total rotational momentum in the body-fixed frame	37
$P(\gamma(t))$	Restoring force from buoyancy and gravity	55
$\{\pi^1, \dots, \pi^6\}$	Dual basis for $SE(3)$	50
Q	Configuration manifold for a mechanical system	36
R	Orientation of the rigid body in $SO(3)$ with respect to Σ_I	19

ρ	Fluid mass density	32
ρ_B	Mass density of the rigid body	23
r_{C_G}	Vector from O_B to C_G	23
r_{C_B}	Vector from O_B to C_B	??
$R_{1,\phi}$	3×3 rigid body rotation matrix about the x-axis	19
$R_{2,\theta}$	3×3 rigid body rotation matrix about the y-axis	19
$R_{3,\psi}$	3×3 rigid body rotation matrix about the z-axis	19
(r, s) -tensor	\mathbb{R} -valued multilinear map taking r covectors and s vectors as inputs	241
Σ_B	Body-fixed reference system	15
Σ_I	Inertial (earth-fixed) reference frame	14
σ	Control forces	17
$SO(3)$	Special Orthogonal group	18
$SE(3)$	Special Euclidean group	19
$SE(3)$	Special Euclidean group	19
$\check{\sigma}(t)$	Dynamic controls including restoring forces	127
$\mathfrak{so}(3)$	Lie algebra of $SO(3)$	37
$\mathfrak{se}(3)$	Lie algebra of $SE(3)$	106
$S(b, R, \nu, \Omega)$	Geodesic Spray	45
θ	Rotation about the y-axis (pitch)	16
T_{body}	Kinetic energy of the rigid body	38
T_{fluid}	Kinetic energy of the fluid surrounding the rigid body	38

$\tau(t)$	Reparameterization of a curve	82
TQ	Tangent bundle of Q	238
T_qQ	Tangent space at $q \in Q$	238
T^*Q	Cotangent bundle of Q	239
\mathbb{T}_i	Input vector fields for a torpedo-shaped AUV	213
\mathcal{V}	Submerged volume of a rigid body	33
$V_G(\gamma(t))$	Gravitational potential function	55
$V_B(\gamma(t))$	Potential function from buoyancy	55
W	Weight of a submerged rigid body	33
$[X, Y]$	Lie bracket of X and Y	244
$\{X_1, \dots, X_6\}$	Standard basis for $SE(3)$	50
\mathcal{Y}	Distribution generated by the vector fields in the set \mathcal{Y}	83
Y_i, Z_i	General vector fields	241

Chapter 1

Introduction

At age 4, I was given a radio controlled submarine for my birthday. One can imagine my excitement as my father helped me put it together. I am not sure who was more excited about the vessel, my dad or I.

I grew up in northern Michigan in a small town surrounded by water, in a small house right on the lake. Water was as much a part of my everyday life as the air that I breathed. It fascinated me, and captivated my attention for hours on end. Whether fishing, diving, sailing, water skiing, or snowmobiling across the frozen expanse, I used the water everyday.

We finally finished the submarine and I immediately ran to the lake to try it out. With a preliminary surface test, we verified that all controls were functioning. My dad dropped the submarine in the water, I actuated the thrusters full throttle ahead, and aimed the craft a few degrees down bubble. The submarine tore ahead and headed down below the surface.

I never saw the submarine after that. It was supposed to surface upon losing radio contact, or if the batteries died, but it never did. I looked for days trying figure out where it went, and spent many hours holding my breath, scanning the lake bottom. Even after we moved from that house, I used to go back and snorkel or SCUBA dive around trying to find my lost ship. After a while, it just seemed pointless. I put it out of my mind and pursued other hobbies and interests. I got into model cars, and flying model airplanes and eventually rockets. I never lost a car, plane or rocket; they always came back. I will always wonder where that submarine went...and thus began my wonder of water and the ocean.

Many people query the location of ships, planes, or other vessels claimed by the waters of our earth. Some look to salvage the wreckage and determine the cause of the disaster while others are only interested in the supposed billions of dollars of treasure waiting to be found. Still others seek natural resources such as oil or precious minerals like methane hydrates. And the list goes on. Experts say that we have explored less than 5% of the underwater world on Earth (see Cousteau (2004)). Scientists know more about the entire surface of Mars and the dark side of the moon than they know about Earth's oceans. This may not strike one as odd, but think about how many people have been to Mars compared to the number of people who enter Earth's oceans each day. The ocean is not an exclusive playground for scientists, but a resource for everyone.

Both ocean and space exploration reveal great mysteries about how the universe, and Earth in particular, came to be as it is today, and how it may change over the years to come. With such a vast area of unknowns, it is illogical to think that human driven craft should attempt exploration missions. The first space missions, such as Sputnik, were simply robots controlled from Earth. Likewise, our ocean exploration should be conducted autonomously.

With advances in technology, and our ability to create smarter robots, more explorations are being conducted by autonomous vehicles. This allows for access to higher risk areas, longer time underwater, and more efficient exploration as compared to human occupied vehicles. The use of underwater vehicles is expanding in every area of ocean science. Such vehicles are used by oceanographers, archaeologists, geologists, ocean engineers, and many others. These vehicles are designed to be agile, versatile and robust. Autonomy of a vehicle only adds to the versatility and implementability of the vehicle. Much research

has gone into designing autonomous underwater vehicles that perform a multitude of tasks far surpassing the abilities of human divers and small human-driven submarines. Tasks range from long term gathering of ocean samples to 3-D mapping of underwater caverns and never before seen areas. Also, these vehicles can dive deeper and remain at depth longer without risking human lives.

Autonomous Underwater Vehicles (AUVs) come in a variety of shapes and sizes, and are built for a wide range of purposes. From continuous monitoring of coral reef ecosystems in a shallow marine environment to bringing back images of undiscovered marine species from depths of over 11 km in the Marianas Trench, AUVs are a major asset in ocean research today and for the future.

Multiple AUVs are currently in use today in a variety of fields. Scientists at California Polytechnic State University use a REMUS (Remote Environmental Monitoring Units) AUV, shown in Fig. 1, to monitor and map toxic blooms of *Karenia Brevis* on the west Florida coast. This project uses the AUV to continuously sample waters off the coast of Florida and alert scientists of an increase of *Karenia Brevis*, which is the cause of the *red tide*.

Researchers at the Massachusetts Institute of Technology (MIT) and Woods Hole Oceanographic Institute (WHOI) use Slocum gliders, shown in Fig. 2, to monitor ocean waters over long time scales. These gliders have large wings which create motion by moving a series of internal masses and controlling an internal bladder to adjust buoyancy. Slocum gliders are capable of 30+ day deployments and can monitor temperature, salinity, oxygen content, and even gather side scan sonar images during their missions.



Figure 1: REMUS 600 AUV, Hydroid, LLC (2008).



Figure 2: SLOCUM Glider, Webb Research Corporation (2008).

Professor Chryssostomidis, from the Hellenic Centre for Marine Research (HCMR) in Greece, along with students from MIT use AUVs such as the Odyssey type and Bluefin, shown in Fig. 3, to discover and inspect underwater archaeological sites. The AUV allows scientists to scan large sites very quickly and only send humans under water when a significant artifact has been potentially located.

Stone Aerospace is a leader in the utilization of AUVs to map previously unexplored areas. One long term goal is to create an underwater vehicle for unmanned exploration of



Figure 3: Bluefin-12 AUV, Bluefin Robotics Corporation (2008).

one of the moons of Jupiter. This craft will fly to the moon of Jupiter, bore through 1-1.5 km of ice, navigate and survey the aquatic environment, create a 3-D map, collect samples, and fly back to Earth. In preparation for this task, the DepthX AUV (shown in Fig. 4) was designed to explore and map the Zacaton cenote, an unexplored aquatic cave. Also, the Endurance vehicle (shown in Fig. 5) was designed to bore through ice and conduct a preprogrammed 3-D grid trajectory for mapping and sampling.

Not only are AUVs becoming more important to aquatic research here on earth, but they are helping push our knowledge further into the galaxy. And, we have not even begun to implement AUVs to their full potential.

Currently, in the search for a lost SCUBA diver, surfer, swimmer, or other water going individual, trained human divers meticulously comb the ocean floor in a predetermined pattern to find the lost person. But, as we know, humans can be quite imprecise. Thus, an AUV following a predetermined Search and Rescue (SAR) pattern would be more efficient,

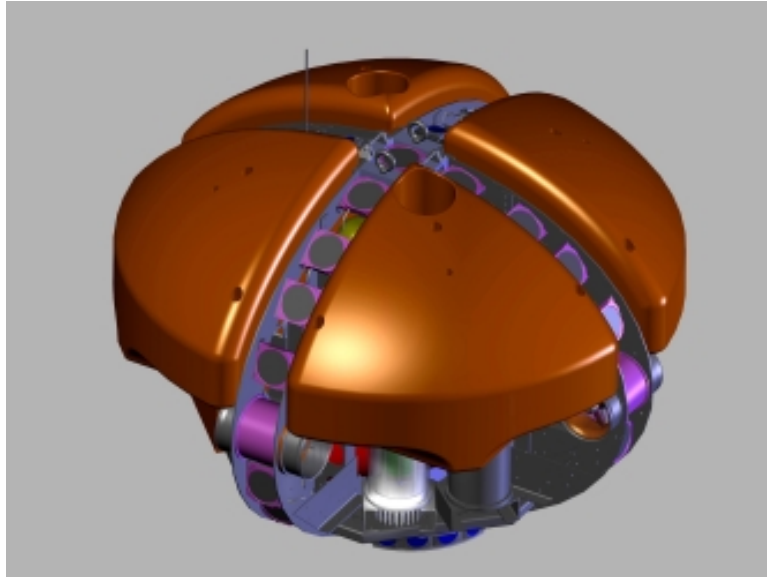


Figure 4: DepthX AUV, StoneAerospace, Inc. (2008a).

knowing that the vehicle was traveling the pattern in a time optimal method. And, in SAR, saving time saves lives. We can also look at SAR as search and recovery, in terms of recovering items that have fallen into a body of water. Similar to the work of Chryssostomidis, but using the AUV to also recover the artifacts as well. An AUV is an excellent choice since it has the ability to go places that may endanger humans, and they can handle caustic or harmful materials without endangering the lives of rescue/recovery personnel.

Other benefits include military applications such as mine counter measures, surveillance, defensive tactics, ship hull inspections and more. If AUVs are deployed around mobile ships, they could be an early detection system for torpedos or underwater attacks. In the case of a torpedo, the AUV could possibly sacrifice itself by getting in the way of the incoming threat. AUVs are also good candidates for mine countermeasures and mine field mapping because we can always build another AUV if one happens to set off a mine and destroy itself.

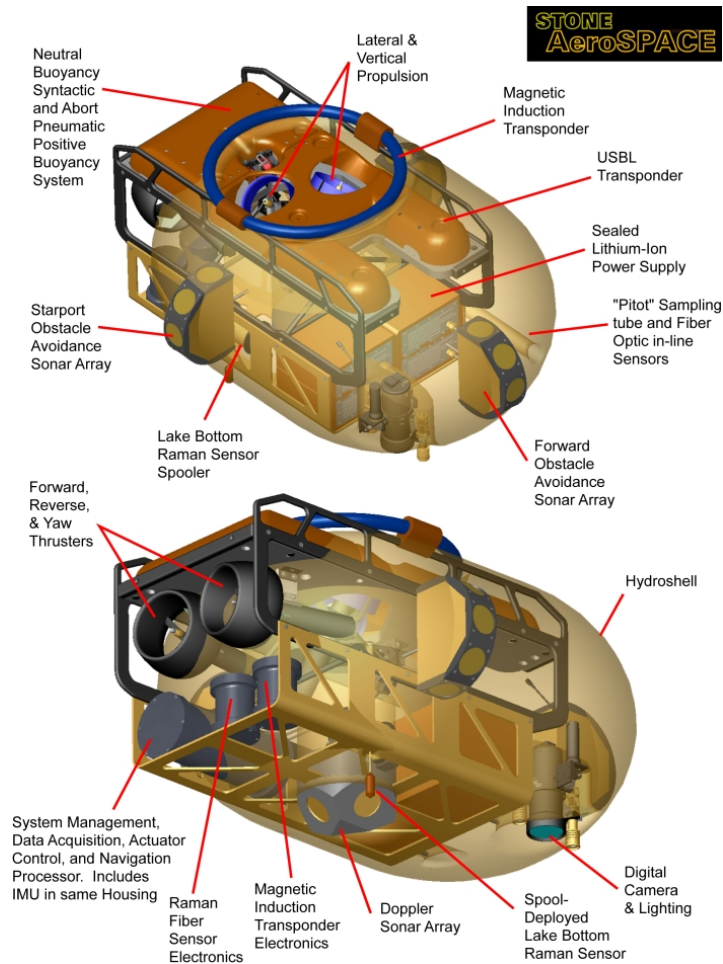


Figure 5: ENDURANCE AUV, StoneAerospace, Inc. (2008b).

With the applications for AUVs on the rise, the need for a better understanding of the dynamics of these vehicles rises as well. Like any other machine, we need the ability to control the AUV accurately to perform even the simplest of tasks. This control starts with the basic hydrodynamics of the vessel, and goes on to include the autonomy algorithm which the vessel uses to make its decisions.

As seen in Figs. 1, 2, and 3, most of today's research AUVs are designed with a torpedo-like shape. This design reduces the number of degrees of freedom (DOF) and thus makes the vehicle easier to understand from a control point of view. The shape also reduces drag

and enhances the efficiency of the vehicle. The downside of this shape is the lack of maneuverability of the vessel. For completing transects, and navigating over a long distance trip, an AUV does not have to be very agile. But, as AUVs enter more diverse areas of science and are asked to complete more complex tasks, other shapes such as ellipses or spheres, as seen in Fig. 4, need to be more closely examined. These shapes are more maneuverable, but require much more knowledge about control design as well as the hydrodynamics of the vehicle.

Independent of its shape, all underwater vehicles are confronted with the task of path planning and control design for each mission. This task is crucial for successful operation of the vehicle, and has yet to be fully investigated. This is because the general motion planning problem for a nonlinear mechanical system is very difficult. The purpose of this dissertation is to provide answers to the motion planning problem for underwater vehicles.

The general submerged rigid body belongs to a class of simple mechanical control systems whose Lagrangian is of the form kinetic energy minus potential energy. In literature, there are many formulations for modeling the mechanics of such systems. Here we consider a more recent development by use of a differential geometric formulation. One reason for choosing this approach is that the configurations defined by a simple mechanical system correspond naturally to a differentiable manifold in a one to one manner. A manifold is basically a set that locally looks like Euclidean space (\mathbb{R}^n). The differentiable manifold used is referred to as the configuration space for the system and is denoted by Q . On this space we are able to formulate a coordinate-independent model of the system. This allows us to deal with the actual structure of the problem without the unnecessary bulk, and some-

times false representations, associated with a certain choice of coordinates. An example demonstrating this invariance is presented in Chapter 2.

Associated to each point of a manifold is the set of all velocities possible from that point. This space is called the tangent space at $q \in Q$ and is denoted T_qQ . The union of all these vector spaces is called the tangent bundle TQ and is itself a differentiable manifold which is twice the dimension of Q . The dynamics of a mechanical system are uniquely determined by its initial conditions in the tangent bundle.

The formulation of external forces arises naturally as well in this geometric architecture as the set of \mathbb{R} -valued maps on the tangent space. This is the dual space to T_qQ and is referred to as the cotangent space. Remembering that work is the integral of the product of force with velocity, is represented by a scalar quantity and is linear with respect to velocity means that forces must find their home in the dual space of T_qQ .

Linking this all together, and really the heart of affine differential geometry as studied here, is the affine connection. This object adds extra structure to the manifold and arises from the formulation of the problem, as we will see later.

The formulation of mechanical systems using differential geometry and affine connections is a relatively new area of research. Bullo & Lewis (2005a) and Bloch (2003) provide a good foundation for the theoretical methods and formulations of geometric control of mechanical systems. Most contributions in this area can be found within the references of these texts.

In this dissertation, we start with the foundations presented in Bullo & Lewis (2005a) and work to extend these theoretical results to practical applications. In particular, we focus

on generating control strategies from the geometric control theory and implementing them onto a test-bed underwater vehicle. These control strategies are derived from a geometric reduction procedure and constructed using decoupled trajectory planning via primitives. Currently, this theory does not include external forces arising from hydrodynamic drag, gravity or buoyancy experienced by a vehicle submerged in a viscous fluid. To this end, we present an extension of this low level control theory and display implementation results as validation.

We begin this dissertation with a presentation of the equations of motion of a rigid body in the classical mechanics sense. We introduce hydrodynamic forces as they arise and conclude with a well known version of the second-order system of equations describing the motion of an underwater vehicle. Next, we derive the same equations under the framework of differential geometry paralleling the previous derivation so as to provide a heuristic proof of their equivalence.

With these equations defined, we examine their solution through the motion planning problem for general and submerged rigid bodies and reiterate the difficulty of the problem. A short survey of closed-loop control strategies is included to show current control system designs for autonomous underwater vehicles.

We begin Chapter 4 with a literature review on the geometric control of underwater vehicles and the motivation and direction of the body of this research. We continue on by defining the necessary tools and structure to design the open-loop control strategies, and present a step-by-step design process. Here we also present the theoretical extension which allows for practical implementation.

These control strategies are tailored for implementation onto a specific test-bed vehicle for validation. A description of this AUV along with the adaptation and control design are contained within Chapter 5. The actual implementation results are presented in Chapter 6. Continuing along the application thread, we present a short chapter on the generalization of this research to different vehicles from the test-bed AUV used in our experiments.

Chapter 9 is dedicated to the conclusions reached both theoretically and experimentally. We give a summary of the accomplishments and impacts of this research in each realm. This is followed by a chapter containing areas of further research and investigation including an alternate, albeit untested, formulation of the inclusion of the restoring forces arising from gravity and buoyancy.

There are three main contributions of this dissertation for which the author is solely responsible. The first is the introduction of the modified Levi-Civita affine connection presented in Section 2.4.5. Details on this connection and its application to the motion planning problem can be found in Chyba & Smith (2008) and Smith et al. (2008b). The second contribution is the calculation and characterization of the decoupling vector fields corresponding to both ∇ and $\tilde{\nabla}$ for the test-bed AUV considered in this study. Results of these calculations were initially included in Chyba et al. (2008c) and are extended in Chyba & Smith (2008) and Smith et al. (2008b). The third sole contribution made by the author of this dissertation is the calculation, adaptation and implementation of control strategies onto a test-bed vehicle designed by use of a kinematic reduction and decoupled trajectory planning as defined by Bullo & Lewis (2005a) and Bullo et al. (2002). Some preliminary implementation results can be found in Chyba & Smith (2008) and the forthcoming Smith

et al. (2008a). Further control design and implementation results are the focus of this dissertation and the details are included in Chapters 5 and 6.

Chapter 2

Equations of Motion

In this chapter, we develop a working model for the kinematics and dynamics of a submerged, three-dimensional rigid body that can move in six degrees-of-freedom. First, we consider the kinematics of a freely floating system and define the relevant frames of reference, including the transformation from one coordinate system to the other. The discussion on dynamics begins with the definition of the inertia tensor and ends with the six-degree-of-freedom equations of motion for the rigid body. From these equations, we move into the discussion of a rigid body submerged in a fluid and incorporate the additional forces and moments involved, including added mass, hydrodynamic damping, gravity and buoyancy.

The initial derivation of these equations of motion is presented similarly to that found in a classical mechanics text such as Lamb (1961), Ardema (2005) or Meriam & Kraige (1997). The addition of the hydrodynamic forces and moments into these general equations can be found in Lamb (1945) (see also Fossen 1994), with an in-depth treatment of these topics presented in Newman (1977). Since the goal of this dissertation is to extend and implement notions of geometric control theory, we provide a second derivation of these equations of motion. This alternate geometric representation will parallel the standard derivation as a means to heuristically demonstrate its equivalence as well as to alleviate the need to define a plethora of terms and notation. The equations of motion derived in the architecture of differential geometry will be the starting point from which we build the theory studied in this dissertation.

We intend that the application of the geometric theory developed within this paper be widely applicable rather than vehicle specific. Thus, we will first define the model and appropriate terms with generality, and then present a specific application to a test-bed AUV in a later section. This allows us to create a generalized model, as well as show the advantages of the model in the areas of control and analysis of vehicle dynamics.

2.1 Rigid Body Kinematics

For the analysis of AUVs, it is necessary to work with two right-handed, orthogonal coordinate systems. We first need a reference frame from which to measure distances and angles. This is done by choosing an earth-fixed reference frame. For low-speed marine vehicles such as those studied here, the Earth's movement has a negligible effect on the dynamics of the vehicle. Thus, the earth-fixed frame may be considered as an inertial frame. To precisely identify the configuration of a rigid body, we need to know the position and orientation of a point on the body with respect to the inertial reference frame. Thus, we will define a reference frame fixed to a chosen point on the body. These two reference frames are described in detail below.

The inertial frame is a right-handed, non-rotating, orthogonal reference frame and is taken to be earth fixed with accelerations neglected. This coordinate system $\Sigma_I : (O_I, \{s_1, s_2, s_3\})$ is defined with the s_1 and s_2 axes lying in the horizontal plane perpendicular to the direction of gravity, while the s_3 axis is orthogonal to the $s_1 - s_2$ plane and taken to be positive in the direction of gravity. We may also refer to this frame as the spatial reference

frame. This choice of inertial reference frame is consistent with current oceanography and AUV literature. With this choice of coordinates, we get a reference frame positioned at the free surface ($s_3 = 0$) and s_3 corresponds to depth. Since we are considering an unbounded fluid domain, we may select an arbitrary position for the inertial frame, preferably in a location such that the depth of the vehicle is non-negative. The inertial frame is shown in Fig. 6.

The body-fixed frame is a right-handed, orthogonal reference frame which is fixed to a point on the body. This coordinate system $\Sigma_B : (O_B, \{B_1, B_2, B_3\})$ is defined with O_B located at a chosen point and the body axes B_1, B_2 and B_3 coincide with the principle axes of inertia:

- B_1 - longitudinal axis (positive to fore)
- B_2 - transverse axis (positive to starboard)
- B_3 - normal axis (positive to the keel)

The body-fixed frame is shown in Fig. 6.

The above definitions of reference frames suggests that the position and orientation of the vehicle be expressed relative to the spatial frame while the linear and angular velocities are defined relative to the body-fixed frame. Standard notation for these quantities are defined in SNAME (1950) and are reproduced in Table 1. Through the development of the differential geometric theory, the SNAME (1950) standard notation will prove to be notationally cumbersome for summations and geometric representations. To this end, we choose an alternate notation to simplify the expressions. This notation is presented in

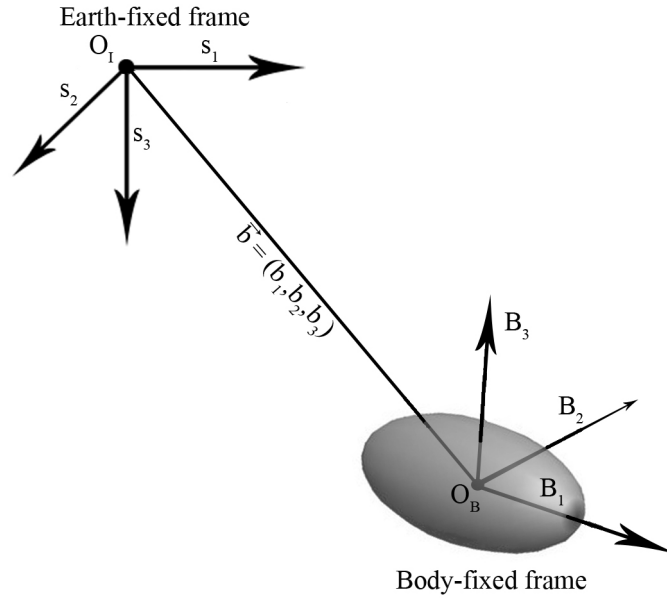


Figure 6: Earth-fixed and body-fixed coordinate reference frames.

Table 2. One reason why the standard notation will prove awkward is that SNAME (1950) notation presents the formulation in local coordinates, whereas the geometric formulation is constructed to be a coordinate free, and thus invariant, representation. We provide support of this later in this section.

As seen in Fig. 6, we let $\mathbf{b} = (b_1, b_2, b_3)$ be the vector from the origin of the inertial

DOF	Forces & moments	Linear & angular velocity (body-fixed frame)	Positions & Euler angles
Surge	X	u	x
Sway	Y	v	y
Heave	Z	w	z
Roll	K	p	ϕ
Pitch	M	q	θ
Yaw	N	r	ψ

Table 1: SNAME notation for the study of underwater vehicles.

DOF	External forces (φ_ν) & moments (τ_Ω) (body-fixed frame)	Linear (ν) & angular (Ω) velocity (body-fixed frame)	Positions & Euler angles
Surge	φ_1	ν_1	b_1
Sway	φ_2	ν_2	b_2
Heave	φ_3	ν_3	b_3
Roll	τ_1	Ω_1	ϕ
Pitch	τ_2	Ω_2	θ
Yaw	τ_3	Ω_3	ψ

Table 2: Notations for the study of underwater vehicles

frame to the origin of the body-fixed frame. The angular orientation of the body with respect to the earth-fixed frame can either be given using Euler angles or quaternions. In this dissertation, we choose to work with the Euler angles, accepting the fact that we may need two representations to fully avoid singularities. A kinematic approach using the quaternions is presented in Fossen (1994) for the interested reader.

Now, the motion of a rigid body in six degrees of freedom can be described using $\boldsymbol{\eta} = (b_1, b_2, b_3, \phi, \theta, \psi)^t = (\mathbf{b}, \phi, \theta, \psi)^t = (\mathbf{b}, \boldsymbol{\eta}_2)^t$, where $\boldsymbol{\eta}_2 = (\phi, \theta, \psi)$ for the orientation and position relative to the spatial frame. In the body frame, $\boldsymbol{\nu} = (\nu_1, \nu_2, \nu_3)^t$ is the linear velocity, $\boldsymbol{\Omega} = (\Omega_1, \Omega_2, \Omega_3)^t$ is the angular velocity and $\boldsymbol{\sigma} = (\varphi_1, \varphi_2, \varphi_3, \tau_1, \tau_2, \tau_3)^t = (\boldsymbol{\varphi}_\nu, \boldsymbol{\tau}_\Omega)^t$ accounts for the external forces and moments acting on the vehicle. Through the derivation we will break out each force individually with its own representation, this will eventually leave $\boldsymbol{\sigma}$ to represent only the input control forces from the actuators.

In this formulation, we will express the angular orientation of the body-fixed reference frame, with respect to the spatial reference frame, using a rotation matrix. This choice of notation motivates the need for the following definitions.

Definition 2.1 (Orthogonal matrix group). Given $n \in \mathbb{N}$ and a matrix $R \in \mathbb{R}^{n \times n}$, the *orthogonal matrix group*, denoted by $O(n)$, is defined by

$$O(n) = \{R \in \mathbb{R}^{n \times n} | RR^t = \mathbb{I}_n\}, \quad (2.1)$$

where \mathbb{I}_n is the $n \times n$ identity matrix. In particular, $R \in O(n)$ if $R^t = R^{-1}$.

Definition 2.2 (Special orthogonal matrix group). Given $n \in \mathbb{N}$ and a matrix $R \in \mathbb{R}^{n \times n}$, the *special orthogonal matrix group*, denoted by $SO(n)$, is defined by

$$SO(n) = \{R \in O(n) | \det R = 1\}. \quad (2.2)$$

For $n = 3$, the set $SO(3)$ is the group of rotations in \mathbb{R}^3 .

Definition 2.3 (Euclidean matrix group). Given $n \in \mathbb{N}$, the *Euclidean matrix group*, denoted by $E(n)$, is defined by

$$E(n) = \left\{ g \in \mathbb{R}^{(n+1) \times (n+1)} \mid g = \begin{bmatrix} R & r \\ 0_{1 \times n} & 1 \end{bmatrix}, R \in O(n), r \in \mathbb{R}^n \right\}. \quad (2.3)$$

Definition 2.4 (Special Euclidean matrix group). Given $n \in \mathbb{N}$, the *special Euclidean matrix group*, denoted by $SE(n)$, is defined by

$$SE(n) = \{g \in E(n) | \det g = 1\}. \quad (2.4)$$

The position and the orientation of a rigid body is expressed as an element of $\mathbb{R}^3 \times \text{SO}(3)$: (\mathbf{b}, R) . Here $\mathbf{b} = (b_1, b_2, b_3)^t \in \mathbb{R}^3$ denotes the position vector of the body, and $R \in \text{SO}(3)$ is a rotation matrix describing the orientation of the body. We will identify elements of $\mathbb{R}^3 \times \text{SO}(3)$ with elements of $\text{SE}(3)$ by means of the bijection

$$(\mathbf{b}, R) \mapsto \begin{bmatrix} R & \mathbf{b} \\ 0_{1 \times n} & 1 \end{bmatrix}. \quad (2.5)$$

By use of the Euler angle representation, we can use a rotation matrix $R_{i,\alpha}$ to express the rotation angle α of a vector about the i^{th} axis from one coordinate system to another. If we let $s \cdot = \sin(\cdot)$ and $c \cdot = \cos(\cdot)$, these matrices are given by:

$$R_{1,\phi} = \begin{bmatrix} 1 & 0 & 0 \\ 0 & c\phi & s\phi \\ 0 & -s\phi & c\phi \end{bmatrix}, R_{2,\theta} = \begin{bmatrix} c\theta & 0 & -s\theta \\ 0 & 1 & 0 \\ s\theta & 0 & c\theta \end{bmatrix}, R_{3,\psi} = \begin{bmatrix} c\psi & s\psi & 0 \\ -s\psi & c\psi & 0 \\ 0 & 0 & 1 \end{bmatrix}. \quad (2.6)$$

Note that each of these matrices is an element of $\text{O}(3)$, and since the two coordinate systems defined earlier share the same orientation (both right-handed), $R_{i,\alpha} \in \text{SO}(3)$. For a general rotation about all three axes, we can combine the above rotation matrices via matrix

multiplication by $R_{3,\psi}R_{2,\theta}R_{1,\phi}$ which yields the general rotation matrix, R :

$$R = \begin{bmatrix} c\psi c\theta & -s\psi c\phi + c\psi s\theta s\phi & s\psi s\phi + c\psi c\phi s\theta \\ s\psi c\theta & c\psi c\phi + s\phi s\theta s\psi & -c\psi s\phi + s\theta s\psi c\phi \\ -s\theta & c\theta s\phi & c\theta c\phi \end{bmatrix}. \quad (2.7)$$

It is easy to check that indeed $R \in \text{SO}(3)$, and as such, the inverse transformation is given by R^t . Note that the order of multiplication of these matrices is not arbitrary. As is common in guidance and control applications, the *xyz*-convention is adopted here.

To conclude our study of the kinematics of the rigid body we consider the transformation of the linear and angular velocities between the two reference frames. By construction, the matrix R given in Eq. (2.7) will transform the linear velocity in the body-fixed frame to the linear velocity in the earth-fixed frame. For the angular velocity, we note that the orientation of the body frame with respect to the inertial frame is given by

$$\Omega = \begin{bmatrix} \dot{\phi} \\ 0 \\ 0 \end{bmatrix} + R_{1,\phi} \begin{bmatrix} 0 \\ \dot{\theta} \\ 0 \end{bmatrix} + R_{1,\phi}R_{2,\theta} \begin{bmatrix} 0 \\ 0 \\ \dot{\psi} \end{bmatrix} = R_2^{-1}\dot{\eta}_2. \quad (2.8)$$

Inverting R_2^{-1} and combining the previously derived expressions, we arrive at a formulation

of the kinematic equations of motion for a rigid body moving in six degrees of freedom,

$$[\dot{\eta}] = \begin{bmatrix} R & 0_{3 \times 3} \\ 0_{3 \times 3} & R_2 \end{bmatrix} \begin{bmatrix} \nu \\ \Omega \end{bmatrix}. \quad (2.9)$$

2.2 Rigid Body Dynamics

There are two basic approaches to deriving the equations of motion for a rigid body moving in six degrees-of-freedom; the Newton-Euler and the Lagrangian formulations. The first is based on Newton's Second Law, the well known formulae:

$$\mathbf{F}_{net} = m\mathbf{a} \quad \text{and} \quad \mathbf{F}_{net} = J_b\boldsymbol{\alpha}, \quad (2.10)$$

where the net forces (\mathbf{F}_{net}) acting on the body are related to the mass (m) and translational acceleration (\mathbf{a}), and the moments (\mathbf{F}_{net}) are related to the inertia of the body (J_b) and the angular acceleration ($\boldsymbol{\alpha}$). The Eq. (2.10) was later expressed in terms of the conservation of linear and angular momentum by Euler. These Newton-Euler equations are the natural starting point for a vectorial approach to deriving the dynamic equations of motion. On the other hand, the Lagrangian approach describes the vehicle's dynamics in terms of energy. We first formulate expressions for the kinetic (T) and potential (V) energy and create a Lagrangian $L = T - V$ ¹. A set of six second-order differential equations describing the

¹There are alternate ways to define a Lagrangian, however this is the form used to describe the class of simple mechanical systems including underwater vehicles.

motion of the rigid body in six degrees-of-freedom are then calculated from the Lagrange equation:

$$\frac{d}{dt} \left(\frac{\partial L}{\partial \dot{\eta}} \right) - \frac{\partial L}{\partial \eta} = \sigma_S, \quad (2.11)$$

where σ_S is a vector of the control inputs expressed in the inertial frame. A detailed write-up using the Lagrangian approach including a non-zero potential (also referred to as a Quasi-Lagrangian approach) with applications to marine vehicles can be found in Sagatun (1992). The derivations included in this research follow the Newton-Euler approach.

We begin by defining the inertia tensor of the body J_b . Let $\boldsymbol{\omega} = (\omega_1, \omega_2, \omega_3)^t$ denote the angular velocity of the rigid body with respect to the inertial reference frame. Suppose that O_B is an arbitrary point in the body and that the body is rotating with angular velocity $\boldsymbol{\omega}$ about Σ_I . We then define the inertia tensor as:

$$J_b = \begin{bmatrix} I_{b_1} & -I_{b_1 b_2} & -I_{b_1 b_3} \\ -I_{b_2 b_1} & I_{b_2} & -I_{b_2 b_3} \\ -I_{b_3 b_1} & -I_{b_3 b_2} & I_{b_3} \end{bmatrix}, \quad (2.12)$$

where I_{b_1} , I_{b_2} and I_{b_3} are the moments of inertia about the B_1 , B_2 and B_3 axes, respectively, and the cross terms are products of inertia. We calculate these entries to the inertia matrix with the following integrals taken over the volume V of the rigid body:

$$\begin{aligned} I_{b_1} &= \int_V (b_2^2 + b_3^2) \rho_B dV; & I_{b_1 b_2} &= \int_V b_1 b_2 \rho_B dV = \int_V b_2 b_1 \rho_B dV = I_{b_2 b_1}, \\ I_{b_2} &= \int_V (b_1^2 + b_3^2) \rho_B dV; & I_{b_1 b_3} &= \int_V b_1 b_3 \rho_B dV = \int_V b_3 b_1 \rho_B dV = I_{b_3 b_1}, \end{aligned}$$

$$I_{b_3} = \int_V (b_1^2 + b_2^2) \rho_B dV; \quad I_{b_2 b_3} = \int_V b_2 b_3 \rho_B dV = \int_V b_3 b_2 \rho_B dV = I_{b_3 b_2},$$

where ρ_B is the mass density of the body. By use of ρ_B , we define the mass of the body as $\int_V \rho_B dV$; assumed constant with respect to time. Since the location of O_B is arbitrary, it will be useful to define $\mathbf{r}_{C_G} = \frac{1}{m} \int_V \mathbf{r} \rho_B dV$ as the vector from O_B to the center of gravity (C_G) of the rigid body, where \mathbf{r} denotes the vector from O_B to each infinitesimal volume element dV .

Since the study of dynamics involves examination of the time derivatives of vectors in two different reference frames, we use the relation

$$\dot{\mathbf{v}} = \dot{\mathbf{v}} + \boldsymbol{\omega} \times \mathbf{v}, \quad (2.13)$$

to relate the time derivative of a vector $\dot{\mathbf{v}}$ in the inertial frame to its time derivative in the body frame $\dot{\mathbf{v}} = d\mathbf{v}/dt$. Substituting $\boldsymbol{\omega}$ for \mathbf{v} in this relation shows that angular acceleration is invariant under change of frame.

Now, we begin with the conservation of linear momentum, or Euler's first axiom:

$$\dot{\mathbf{p}} \triangleq \mathbf{F}; \quad \mathbf{p} \triangleq m\boldsymbol{\nu}, \quad (2.14)$$

where \mathbf{p} is the linear momentum, m is the mass, \mathbf{F} represents the forces and $\boldsymbol{\nu}$ is the velocity. First, we define $\mathbf{b}_{C_G} = \mathbf{b} + \mathbf{r}_{C_G}$ to determine the position of C_G with respect to

the inertial frame. Thus, we can express the velocity of C_G as $\boldsymbol{\nu}_{C_G} = \dot{\mathbf{b}}_{C_G} = \dot{\mathbf{b}} + \dot{\mathbf{r}}_{C_G}$.

Since we assume that the mass of the rigid body is constant, we have that

$$\boldsymbol{\nu}_{C_G} = \boldsymbol{\nu}_{O_B} + \boldsymbol{\omega} \times \mathbf{r}_{C_G}, \quad (2.15)$$

where $\boldsymbol{\nu}_{O_B}$ represents the velocity of O_B . Taking the time derivative of this expression and substituting into Eq. (2.14), we get

$$m(\dot{\boldsymbol{\nu}}_{O_B} + \boldsymbol{\omega} \times \boldsymbol{\nu}_{O_B} + \dot{\boldsymbol{\omega}} \times \mathbf{r}_{C_G} + \boldsymbol{\omega} \times (\boldsymbol{\omega} \times \mathbf{r}_{C_G})) = \boldsymbol{\varphi}_{\nu}, \quad (2.16)$$

where m is the mass of the vehicle and the forces $\boldsymbol{\varphi}_{\nu}$ act at O_B . If we suppose that $O_B = C_G$, the above relation simplifies to

$$m(\dot{\boldsymbol{\nu}}_{C_G} + \boldsymbol{\omega} \times \boldsymbol{\nu}_{C_G}) = \boldsymbol{\varphi}_{\nu}, \quad (2.17)$$

and the forces $\boldsymbol{\varphi}_{\nu}$ now act at C_G .

Continuing on, we now consider the conservation of angular momentum, Euler's second axiom, to determine the dynamic equations for rotational motion. This axiom is given by:

$$\dot{\mathbf{H}} \triangleq \mathbf{F}; \quad \mathbf{H} \triangleq J_b \boldsymbol{\omega}, \quad (2.18)$$

where \mathbf{F} represents the moments about C_G and $\boldsymbol{\omega}$ is the angular velocity. We begin with

the absolute angular momentum about O_B :

$$\mathbf{H}_{O_B} \triangleq \int_V \mathbf{r} \times \boldsymbol{\nu} \rho_B dV. \quad (2.19)$$

We take the time derivative of this expression to get

$$\dot{\mathbf{H}}_{O_B} = \int_V \mathbf{r} \times \dot{\boldsymbol{\nu}} \rho_B dV + \int_V \dot{\mathbf{r}} \times \boldsymbol{\nu} \rho_B dV. \quad (2.20)$$

The first term on the right hand side of the above equation is the moment vector which we will call $\boldsymbol{\tau}_{\Omega_O}$. Since we can express the velocity of the rigid body as the sum of the velocity of O_I as seen in the body-fixed frame plus the velocity of a differential volume element with respect to O_B , we know that

$$\dot{\mathbf{r}} = \boldsymbol{\nu} - \boldsymbol{\nu}_{O_B}. \quad (2.21)$$

By use of this relation, we can rewrite Eq. (2.20) as

$$\dot{\mathbf{H}}_{O_B} = \boldsymbol{\tau}_{\Omega_O} - \boldsymbol{\nu}_{O_B} \times \int_V \boldsymbol{\nu} \rho_B dV = \boldsymbol{\tau}_{\Omega_O} - \boldsymbol{\nu}_{O_B} \times \int_V \dot{\mathbf{r}} \rho_B dV \quad (2.22)$$

along with the fact that $\boldsymbol{\nu} \times \boldsymbol{\nu} = 0$. Here we notice that the integral containing $\dot{\mathbf{r}}$ is equal to $m\dot{\mathbf{r}}_{C_G} = m(\boldsymbol{\omega} \times \mathbf{r}_{C_G})$ by taking the time derivative of the equation for \mathbf{r}_{C_G} given earlier.

Substituting this into Eq. (2.22) we have

$$\dot{\mathbf{H}}_{O_B} = \boldsymbol{\tau}_{\Omega_O} - m\boldsymbol{\nu}_{O_B} \times (\boldsymbol{\omega} \times \mathbf{r}_{C_G}). \quad (2.23)$$

Now, we go back to the beginning and rewrite Eq. (2.19) as

$$\mathbf{H}_{O_B} = \int_V \mathbf{r} \times \boldsymbol{\nu} \rho_B dV = \int_V \mathbf{r} \times \boldsymbol{\nu}_{O_B} \rho_B dV + \int_V \mathbf{r} \times (\boldsymbol{\omega} \times \mathbf{r}) \rho_B dV. \quad (2.24)$$

By utilizing the fact that $\int_V \mathbf{r} \times \boldsymbol{\nu}_{O_B} \rho_B dV = m\mathbf{r}_{C_G} \times \boldsymbol{\nu}_{O_B}$ from the equation for \mathbf{r}_{C_G} and that the integral on the far right is the inertia tensor represented in vectorial form, we obtain the following expression for \mathbf{H}_{O_B} :

$$\mathbf{H}_{O_B} = J_b \boldsymbol{\omega} + m\mathbf{r}_{C_G} \times \boldsymbol{\nu}_{O_B}. \quad (2.25)$$

Differentiating Eq. (2.25) with respect to time, assuming that J_b is constant, and eliminating $\dot{\mathbf{H}}_{O_B}$ from the expression, we arrive at the Euler equations:

$$J_b \dot{\boldsymbol{\omega}} + \boldsymbol{\omega} \times (J_b \boldsymbol{\omega}) + m\mathbf{r}_{C_G} \times (\dot{\boldsymbol{\nu}}_{O_B} + \boldsymbol{\omega} \times \boldsymbol{\nu}_{O_B}) = \boldsymbol{\tau}_{\Omega_O}. \quad (2.26)$$

As with the translational case, if we assume that $O_B = C_G$, then Eq. (2.26) reduces to

$$J_b \dot{\boldsymbol{\omega}} + \boldsymbol{\omega} \times (J_b \boldsymbol{\omega}) = \boldsymbol{\tau}_{\Omega}. \quad (2.27)$$

By use of the notation presented in Table 2 and defining $\mathbf{r}_{CG} = (x_G, y_G, z_G)$, we present the following Lemma containing the general equations of motion.

Lemma 2.1. *The general equations of motion, for a six degree-of-freedom rigid body, expressed in the chosen local coordinate system are given by:*

$$\begin{aligned}
m(\dot{v}_1 - \nu_2\Omega_3 + \nu_3\Omega_2 - x_G(\Omega_2^2 + \Omega_3^2) + y_G(\Omega_1\Omega_2 - \dot{\Omega}_3) + z_G(\Omega_1\Omega_3 - \dot{\Omega}_2)) &= \varphi_{\nu_1} \\
m(\dot{v}_2 - \nu_3\Omega_1 + \nu_1\Omega_3 - y_G(\Omega_3^2 + \Omega_1^2) + z_G(\Omega_2\Omega_3 - \dot{\Omega}_1) + x_G(\Omega_1\Omega_2 - \dot{\Omega}_3)) &= \varphi_{\nu_2} \\
m(\dot{v}_3 - \nu_1\Omega_2 + \nu_2\Omega_1 - z_G(\Omega_1^2 + \Omega_2^2) + x_G(\Omega_1\Omega_3 - \dot{\Omega}_2) + y_G(\Omega_3\Omega_2 - \dot{\Omega}_1)) &= \varphi_{\nu_3} \\
I_{b_1}\dot{\Omega}_1 + (I_{b_3} - I_{b_2})\Omega_2\Omega_3 - (\dot{\Omega}_3 + \Omega_1\Omega_2)I_{b_1b_3} + (\Omega_3^2 - \Omega_2^2)I_{b_2b_3} + (\Omega_1\Omega_3 - \dot{\Omega}_2)I_{b_1b_2} \\
+ m(y_G(\dot{v}_3 - \nu_1\Omega_2 + \nu_2\Omega_1) - z_G(\dot{v}_2 - \nu_3\Omega_1 + \nu_1\Omega_3)) &= \tau_{\Omega_1} \\
I_{b_2}\dot{\Omega}_2 + (I_{b_1} - I_{b_3})\Omega_1\Omega_3 - (\dot{\Omega}_1 + \Omega_3\Omega_2)I_{b_1b_2} + (\Omega_1^2 - \Omega_3^2)I_{b_3b_1} + (\Omega_1\Omega_2 - \dot{\Omega}_3)I_{b_2b_3} \\
+ m(z_G(\dot{v}_1 - \nu_2\Omega_3 + \nu_3\Omega_2) - x_G(\dot{v}_3 - \nu_1\Omega_2 + \nu_2\Omega_1)) &= \tau_{\Omega_2} \\
I_{b_3}\dot{\Omega}_3 + (I_{b_2} - I_{b_1})\Omega_2\Omega_1 - (\dot{\Omega}_2 + \Omega_1\Omega_3)I_{b_2b_3} + (\Omega_2^2 - \Omega_1^2)I_{b_1b_2} + (\Omega_3\Omega_2 - \dot{\Omega}_1)I_{b_3b_1} \\
+ m(x_G(\dot{v}_2 - \nu_3\Omega_1 + \nu_1\Omega_3) - y_G(\dot{v}_1 - \nu_2\Omega_3 + \nu_3\Omega_2)) &= \tau_{\Omega_3}
\end{aligned}$$

If we let $\mathbf{v} = (\boldsymbol{\nu}, \boldsymbol{\Omega})^t$, then these equations can be expressed vectorially as

$$M_B\dot{\mathbf{v}} - Cor_B(\mathbf{v})\mathbf{v} = \boldsymbol{\sigma}(t), \quad (2.28)$$

where M_B and Cor_B represent the rigid body inertia and Coriolis force matrices, respectively and $\boldsymbol{\sigma}(t)$ accounts for the external forces. The Coriolis matrix accounts for Coriolis and centripetal forces experienced by the body. These are pseudo forces which arise in the equations of motion when a body is viewed from a rotating frame of reference. Since there is more than one representation for Cor_B , and the geometric equations presented later account for these forces intrinsically, we will not examine them here. A detailed analysis can be found in any of the references mentioned at the beginning of this section. The inertia

matrix M_B is represented by the following matrix:

$$\begin{bmatrix} m & 0 & 0 & 0 & mz_G & -my_G \\ 0 & m & 0 & -mz_G & 0 & mx_G \\ 0 & 0 & m & my_G & -mx_G & 0 \\ 0 & mz_G & -my_G & I_{b_1} & -I_{b_1b_2} & -I_{b_1b_3} \\ -mz_G & 0 & mx_G & -I_{b_2b_1} & I_{b_2} & -I_{b_2b_3} \\ my_G & -mx_G & 0 & -I_{b_3b_1} & -I_{b_3b_2} & I_{b_3} \end{bmatrix}. \quad (2.29)$$

This concludes the derivation of the equations of motion for a rigid body in six degrees of freedom with a body-fixed reference frame in an arbitrary location. By making two non-limiting assumptions, we can simplify these equations quite a bit. The first assumption is that $O_B = C_G$ which implies that $\mathbf{r}_{C_G} = (0, 0, 0)^t$. The second assumption is that the axes of the body-fixed reference frame correspond with the principle axes of inertia of the rigid body. This later assumption yields a diagonal inertia tensor (i.e., $J_b = \text{diag}(I_{b_1}, I_{b_2}, I_{b_3})$), and coupled with the first assumption implies then that M_B is a diagonal matrix. In the local coordinate system chosen, under these two assumptions, the equations presented in Lemma 2.1 simplify to the following:

$$\begin{aligned} m(\dot{\nu}_1 - \nu_2\Omega_3 + \nu_3\Omega_2) &= \varphi_{\nu_1} \\ m(\dot{\nu}_2 - \nu_3\Omega_1 + \nu_1\Omega_3) &= \varphi_{\nu_2} \\ m(\dot{\nu}_3 - \nu_1\Omega_2 + \nu_2\Omega_1) &= \varphi_{\nu_3} \\ I_{b_1}\dot{\Omega}_1 + (I_{b_3} - I_{b_2})\Omega_2\Omega_3 &= \tau_{\Omega_1} \\ I_{b_2}\dot{\Omega}_2 + (I_{b_1} - I_{b_3})\Omega_1\Omega_3 &= \tau_{\Omega_2} \\ I_{b_3}\dot{\Omega}_3 + (I_{b_2} - I_{b_1})\Omega_2\Omega_1 &= \tau_{\Omega_3}. \end{aligned}$$

We are now ready to examine and include additional forces experienced when the rigid body is submerged in a fluid.

2.3 Submerged Rigid Body Dynamics

In this section, we examine the additional forces and moments acting on a rigid body which arise due to submersion in a fluid. We first consider the added mass and inertia resulting from the kinetic energy of the fluid caused by accelerations of the body. Next, we examine the damping and dissipation experienced by a body submerged in a viscous fluid. Finally, we consider the terms required to account for the restoring (conservative) forces and moments, which arise from gravity and buoyancy.

2.3.1 Added Mass

The added mass is a pressure-induced force due to the inertia of the surrounding fluid and is proportional to the acceleration of the rigid body. In particular, the added mass tensor μ_{ij} is the effective mass of the fluid that must be accelerated with the body. In the notation, the first subscript i refers to the *direction of the force/moment*, and the second subscript j refers to the *direction of motion*. The added mass coefficients are usually different depending on the direction of translation. This is contrary to Newton's second law where the mass, m , is independent of the direction of acceleration. Hence, this acts as the coefficient of proportion so that Newton's Laws hold in an ideal fluid. Without any

symmetry, the cross-coefficients ($\mu_{12}, \mu_{13}, \mu_{23}$) are non-zero, which further asserts the fact that the hydrodynamic force differs in direction from the acceleration. However, the added mass coefficients do display symmetry ($\mu_{ij} = \mu_{ji}$) due to the absence of a free surface in the study of underwater vehicles.

In total, there are 21 independent added mass coefficients; symmetry of the body further reduces the number of independent coefficients. In general, the added mass tensor is given by:

$$\mu_{ij} = \rho \int_{S_B} \phi_j^{(R)} \frac{\partial \phi_i^{(R)}}{\partial n} dS, \quad (2.30)$$

where $\phi_i^{(R)}$ is the real part of the potential function describing the fluid surrounding the body, S_B is the surface of the body and $\partial/\partial n$ is the derivative in the normal direction to the surface of the body.

In general, all 21 independent coefficients need to be computed for an accurate expression of the added mass for an arbitrary underwater vehicle. An in-depth analysis and presentation of these terms is presented in Imlay (1961). For typical AUV applications, the vehicle speed is low and symmetries of the body can be exploited to reduce the computations. Assuming three planes of symmetry, as is common for most AUVs, and specifically the test-bed vehicle used to conduct this research, we only need to compute μ_{ii} for $i = 1, \dots, 6$. Thus, in matrix form, the added mass matrix is diagonal and we express it as

$$\begin{pmatrix} M_f^\nu & 0_{3 \times 3} \\ 0_{3 \times 3} & J_f^\Omega \end{pmatrix}, \quad (2.31)$$

where $M_f^\nu = \text{diag}(M_f^{\nu_1}, M_f^{\nu_2}, M_f^{\nu_3})$ and $J_f^\Omega = \text{diag}(J_f^{\Omega_1}, J_f^{\Omega_2}, J_f^{\Omega_3})$ correspond to the translational forces and rotational moments, respectively.

Including this development within the previously derived equations gives us the following Lemma.

Lemma 2.2. *The equations of motion of a rigid body moving in six degrees of freedom submerged in an ideal fluid are given by*

$$\begin{pmatrix} m\mathbb{I}_3 + M_f & 0_{3 \times 3} \\ 0_{3 \times 3} & J_b + J_f \end{pmatrix} \begin{pmatrix} \dot{\mathbf{v}} \\ \dot{\mathbf{\Omega}} \end{pmatrix} - \text{Cor}_B(\mathbf{v})\mathbf{v} = \boldsymbol{\sigma}(t), \quad (2.32)$$

where \mathbb{I}_3 is the 3×3 identity matrix and $\mathbf{v} = (\boldsymbol{\nu}, \mathbf{\Omega})^t$ as before. Note that the matrix Cor_B is different from the previous presentation since the fluid does indeed contribute to the Coriolis and centripetal forces. However, as mentioned earlier, we will not need to detail the exact expression of this term as it will be accounted for when we present the equations of motion in a coordinate invariant setting.

2.3.2 Viscous Damping

Viscous damping and dissipation encountered by marine vehicles are caused by many factors. The major factors include radiation-induced potential damping from forced body oscillations in the presence of a free surface, linear and quadratic skin friction, wave drift damping and vortex shedding. A detailed breakdown of each of these factors related to

underwater vehicles can be found in Allmendinger (1990). Since the focus of this study is on the movement of a small, slow-moving, fully submerged AUV which is far from the free surface, we are not concerned with damping from the generation or interaction with waves. Of the remaining damping factors, pressure drag (form drag) is dominant based on the speed and shape of the test-bed vehicle considered. Since we also assume that the AUV has three planes of symmetry, the hydrodynamic drag matrix is diagonal and is given by $D(v) = \text{diag}(D_1\nu_1, D_2\nu_2, D_3\nu_3, D_4\Omega_1, D_5\Omega_2, D_6\Omega_3)$ where we define $D_i = 1/2C_{D_i}\rho A_i$ for $i = 1, 2, 3$ and $D_i = 1/2C_{D_i}\rho A_i r$ for $i = 4, 5, 6$. We let C_{D_i} denote the drag coefficient for the i^{th} direction of the velocity, ρ is the fluid density, A_i is the projected surface area in the i^{th} direction and r is the length of the moment arm. We remark here that for rotational motions, C_{D_i} , for $i = 4, 5, 6$, is not dimensionless as in the cases for $i = 1, 2, 3$. See Appendix B.1 for details on the calculation of $D(v)$. We note that we assume the viscous drag terms to be quadratic with respect to velocity. Adding this expression to the previous sections, we get the following Lemma.

Lemma 2.3. *The equations of motion of a rigid body moving in six degrees of freedom submerged in a viscous fluid are given by*

$$\begin{pmatrix} m\mathbb{I}_3 + M_f & 0_{3 \times 3} \\ 0_{3 \times 3} & J_b + J_f \end{pmatrix} \begin{pmatrix} \dot{\mathbf{v}} \\ \dot{\boldsymbol{\Omega}} \end{pmatrix} - D(\mathbf{v})\mathbf{v} - Cor_B(\mathbf{v})\mathbf{v} = \boldsymbol{\sigma}(t). \quad (2.33)$$

2.3.3 Restoring Forces and Moments

For the restoring forces and moments, we adopt the SNAME (1950) notation for the submerged weight $W = mg$ and buoyancy force $B = \rho g \mathcal{V}$ where ρ is the fluid density, g is the gravitational acceleration, m is the mass of the vehicle and \mathcal{V} is the submerged volume of the fluid² displaced by the vehicle. Since the gravitational force (\mathbf{f}_G) will act through $\mathbf{C}_G = (x_G, y_G, z_G)$ and the buoyancy force (\mathbf{f}_B) will act through the center of buoyancy ($\mathbf{C}_B = (x_B, y_B, z_B)$), we express the restoring forces as

$$g(\boldsymbol{\eta}) = - \begin{bmatrix} \mathbf{f}_G(\boldsymbol{\eta}) + \mathbf{f}_B(\boldsymbol{\eta}) \\ \mathbf{C}_G \times \mathbf{f}_G(\boldsymbol{\eta}) + \mathbf{C}_B \times \mathbf{f}_B(\boldsymbol{\eta}) \end{bmatrix}. \quad (2.34)$$

Expanding the expression in Eq. (2.34), we arrive at

$$g(\boldsymbol{\eta}) = \begin{bmatrix} (W - B)s\theta \\ -(W - B)c\theta s\phi \\ -(W - B)c\theta c\phi \\ -(y_G W - y_B B)c\theta c\phi + (z_G W - z_B B)c\theta s\phi \\ (z_G W - z_B B)s\theta + (x_G W - x_B B)c\theta c\phi \\ -(x_G W - x_B B)c\theta s\phi - (y_G W - y_B B)s\theta \end{bmatrix}. \quad (2.35)$$

²Here we choose to denote the submerged volume as \mathcal{V} rather than the conventional ∇ since ∇ will be used to represent an affine connection on a manifold.

Combining Eq. (2.35) with the equations presented in Lemma 2.3, we present the following Lemma giving the equations of motion for a rigid body subjected to restoring forces and moments.

Lemma 2.4. *The equations of motion of a rigid body moving in six degrees of freedom submerged in a viscous fluid and subject to the restoring forces and moments of gravity and buoyancy are given by:*

$$\begin{pmatrix} m\mathbb{I}_3 + M_f & 0_{3 \times 3} \\ 0_{3 \times 3} & J_b + J_f \end{pmatrix} \begin{pmatrix} \dot{\boldsymbol{\nu}} \\ \dot{\boldsymbol{\Omega}} \end{pmatrix} - D(\mathbf{v})\mathbf{v} - Cor_B(\mathbf{v})\mathbf{v} + g(\boldsymbol{\eta}) = \boldsymbol{\sigma}(t), \quad (2.36)$$

where $\mathbf{v} = (\boldsymbol{\nu}, \boldsymbol{\Omega})^t$ as before.

Rewriting these equations in the standard Newton-Euler notation ($F=ma$) and separating translational and rotational motion results in the following equivalent expressions:

$$M\dot{\boldsymbol{\nu}} = -\boldsymbol{\Omega} \times M\boldsymbol{\nu} + D_{\boldsymbol{\nu}}(\boldsymbol{\nu})\boldsymbol{\nu} - g(\mathbf{b}) + \boldsymbol{\varphi}_{\boldsymbol{\nu}} \quad (2.37)$$

$$J\dot{\boldsymbol{\Omega}} = -\boldsymbol{\Omega} \times J\boldsymbol{\Omega} - \boldsymbol{\nu} \times M\boldsymbol{\nu} + D_{\boldsymbol{\Omega}}(\boldsymbol{\Omega})\boldsymbol{\Omega} - g(\boldsymbol{\eta}_2) + \boldsymbol{\tau}_{\boldsymbol{\Omega}}, \quad (2.38)$$

where $M\boldsymbol{\nu} \times \boldsymbol{\Omega}$ and $J\boldsymbol{\Omega} \times \boldsymbol{\Omega}$ account for the Coriolis and centripetal forces. Note that $\boldsymbol{\varphi}_{\boldsymbol{\nu}}$ and $\boldsymbol{\tau}_{\boldsymbol{\Omega}}$ now only include the external control forces acting on the submerged rigid body.

This concludes a typical derivation of the general equations of motion for a submerged rigid body. We continue in the following section by paralleling this derivation to express the same equations of motion in the language of differential geometry.

2.4 Geometric Equations of Rigid-Body Dynamics

The Eqs. (2.36) or Eqs. (2.37) and (2.38) are usually taken as the general equations of motion for an underwater vehicle moving in six degrees-of-freedom, however they are actually a coordinate representation of a more general set of equations living on a differentiable manifold³. A specific choice of parameterization (i.e., coordinates) for these general equations is convenient in some applications and allows us to work locally and temporarily believe that we are working with familiar calculus in Euclidean space, but this also can be quite restrictive based on the configuration manifold of the system in question. In addition, a coordinate expression may omit inherent global properties of the mechanical system and manifold structure since the coordinates are only valid for a portion of the configuration space. For example, there is no global parameterization (i.e., single set of coordinates) which completely defines $\mathbb{S}^1 = \{(x, y) \in M | x^2 + y^2 = 1\}$, the circle in \mathbb{R}^2 . By use of a manifold, we force the problem formulation to be coordinate independent, and thus we can tackle the real geometric structure of the problem.

To this end, we continue the derivation of the equations of motion by examining them through the framework of differential geometry. Here, we will produce a coordinate-invariant system of equations to describe the motion of a rigid body moving in six degrees-of-freedom. The motivation for this derivation is to exploit inherent geometric properties and symmetries of the mechanical system to provide solutions to the motion planning problem. We note here that a general understanding of manifolds, differential geometry,

³A manifold is, essentially a set that can locally be parameterized by Euclidean space

Lie groups, affine geometry and tensor analysis is assumed for uninterrupted reading. The readers unfamiliar with some of the terminology and concepts are referred to Appendix A for clarification. We also refer the interested reader to the works of do Carmo (1992), Bullo & Lewis (2005a), Boothby (1986), Abraham et al. (1986) and Warner (1971) for a more in-depth treatment of these topics.

For the geometrical derivation, we will also choose to follow the Newton-Euler formulation. Since we have laid quite a bit of groundwork in the previous sections, we begin here with the kinematic equations of motion and build up to the expression of kinetic energy of the rigid body and the surrounding fluid. From these expressions, we create the geometric architecture used to examine the submerged rigid body as a mechanical system on a differentiable manifold.

2.4.1 Ideal Fluid, Including Added Mass

As previously mentioned, we can express the position and the orientation of a rigid body as an element of $SE(3)$: (\mathbf{b}, R) . In the following sections, we will refer to $Q = SE(3)$ as the configuration manifold for our system. It is on this differentiable manifold that we will build the equations to describe the motion of the submerged rigid body and present them as an affine connection control system. As done in the previous derivation, we begin with the system kinematics.

By use of the previously defined notation, we can write the kinematic equations for a rigid body as:

$$\dot{\mathbf{b}} = R \boldsymbol{\nu}, \quad (2.39)$$

$$\dot{R} = R \hat{\boldsymbol{\Omega}}, \quad (2.40)$$

where the operator $\hat{\cdot} : \mathbb{R}^3 \rightarrow \mathfrak{so}(3)$ is defined by $\hat{\mathbf{y}} \mathbf{z} = \mathbf{y} \times \mathbf{z}$. The space $\mathfrak{so}(3)$ is the Lie algebra associated to the Lie group $SO(3)$, and is the space of skew-symmetric 3×3 matrices (i.e., $\mathfrak{so}(3) = \{R \in \mathbb{R}^{3 \times 3} | R^t = -R\}$).

To derive the dynamic equations of motion for a rigid body, we let \mathbf{p} be the total translational momentum and $\boldsymbol{\pi}$ be the total angular momentum, in the inertial frame. Let \mathbf{P} and $\boldsymbol{\Pi}$ be the respective quantities in the body-fixed frame. It follows that $\dot{\mathbf{p}} = \sum_{i=1}^k \mathbf{f}_i$, $\dot{\boldsymbol{\pi}} = \sum_{i=1}^k (\hat{\mathbf{x}}_i \mathbf{f}_i) + \sum_{i=1}^l \boldsymbol{\tau}_i$ where \mathbf{f}_i ($\boldsymbol{\tau}_i$) are the external forces (torques), given in the inertial frame, and \mathbf{x}_i is the vector from the origin of the inertial frame to the line of action of the force \mathbf{f}_i .

To represent the equations of motion in the body-fixed frame, we differentiate the relations $\mathbf{p} = R \mathbf{P}$, $\boldsymbol{\pi} = R \boldsymbol{\Pi} + \hat{\mathbf{b}} \mathbf{p}$ to obtain

$$\dot{\mathbf{P}} = \hat{\mathbf{P}} \boldsymbol{\Omega} + \boldsymbol{\varphi}_\nu, \quad (2.41)$$

$$\dot{\boldsymbol{\Pi}} = \hat{\boldsymbol{\Pi}} \boldsymbol{\Omega} + \hat{\mathbf{P}} \boldsymbol{\nu} + \sum_{i=1}^k (R^t (\mathbf{x}_i - \mathbf{b})) \times R^t \mathbf{f}_i + \boldsymbol{\tau}_\Omega, \quad (2.42)$$

where $\boldsymbol{\varphi}_\nu$ ($\boldsymbol{\tau}_\Omega$) represents the external forces (torques) in the body-fixed frame.

To obtain the equations of motion of a rigid body in terms of the linear and angular velocities, we need to calculate the total kinetic energy of the system. The kinetic energy of the rigid body, T_{body} , is given by:

$$T_{body} = \frac{1}{2} \begin{pmatrix} \mathbf{v} \\ \boldsymbol{\Omega} \end{pmatrix}^t \begin{pmatrix} m\mathbb{I}_3 & -m\hat{\mathbf{r}}_{C_G} \\ m\hat{\mathbf{r}}_{C_G} & J_b \end{pmatrix} \begin{pmatrix} \mathbf{v} \\ \boldsymbol{\Omega} \end{pmatrix}, \quad (2.43)$$

where m is the mass of the rigid body and J_b is the body inertia matrix as defined before.

Based on Kirchhoff's equations, as seen in Lamb (1945), the kinetic energy of the fluid, T_{fluid} , is given by

$$T_{fluid} = \frac{1}{2} \begin{pmatrix} \mathbf{v} \\ \boldsymbol{\Omega} \end{pmatrix}^t \begin{pmatrix} M_f & C_f^t \\ C_f & J_f \end{pmatrix} \begin{pmatrix} \mathbf{v} \\ \boldsymbol{\Omega} \end{pmatrix}, \quad (2.44)$$

where M_f , J_f and C_f are, respectively, referred to as the added mass, the added mass moments of inertia and the added mass cross-terms.

Combining Eqs. (2.43) and (2.44), the total kinetic energy for a rigid body submerged in a fluid is given by

$$T = \frac{1}{2} \begin{pmatrix} \mathbf{v} \\ \boldsymbol{\Omega} \end{pmatrix}^t \begin{pmatrix} M & C_f^t - m\hat{\mathbf{r}}_{C_G} \\ C_f + m\hat{\mathbf{r}}_{C_G} & J \end{pmatrix} \begin{pmatrix} \mathbf{v} \\ \boldsymbol{\Omega} \end{pmatrix}, \quad (2.45)$$

where $M = m\mathbb{I}_3 + M_f$ and $J = J_b + J_f$. As before, we assume that $O_B = C_G$ and the body has three planes of symmetry, thus $\hat{\mathbf{r}}_{C_G} = [0_{3 \times 3}] = C_f$.

Now, we can use Eq. (2.45) to define a Riemannian metric on the manifold Q . First, let us just examine the rigid body without the fluid. If we let \mathbf{r} represent the vector from O_B to an arbitrary point in the rigid body as before, then at time t , the location of this point can be parameterized by $\mathbf{x}(t) = \mathbf{b}(t) + R(t)\mathbf{r}$. Then, we can write the kinetic energy of the rigid body as a function of time as

$$T_{body}(t) = \frac{1}{2} \int_V \|\dot{\mathbf{b}}(t) + \dot{R}(t)\mathbf{r}\|_{\mathbb{R}^3}^2 \rho_B dV. \quad (2.46)$$

This equation can be broken down into the translational and rotational parts separately by use of the body angular velocity:

$$T_{trans}(t) = \frac{1}{2} m \|\dot{\mathbf{b}}(t)\|_{\mathbb{R}^3}^2, \quad T_{rot}(t) = \frac{1}{2} \mathbb{G}_{\mathbb{R}^3}(J_b(\boldsymbol{\Omega}(t), \boldsymbol{\Omega}(t))), \quad (2.47)$$

where $\mathbb{G}_{\mathbb{R}^3}$ is the standard inner product on \mathbb{R}^3 . Now, let $\gamma : I \rightarrow Q$ be a differentiable curve at $q_0 \in Q$. By use of the forward kinematic map $\Pi : Q \rightarrow \text{SO}(3) \times \mathbb{R}^3$ we induce a differentiable curve $\gamma_1 = \Pi \circ \gamma : I \rightarrow \text{SO}(3) \times \mathbb{R}^3$ at $(R_0, \mathbf{b}_0) \triangleq \Pi(q_0)$. If we assign a nonnegative number $KE(\mathbf{v}_0)$ to the tangent vector $\mathbf{v}_0 = [\gamma]_{q_0} \in T_{q_0}Q$, we define the kinetic energy of the rigid body at time zero along the curve γ_1 . Repeating this process for every tangent vector in TQ , we generate a function $KE : TQ \rightarrow \mathbb{R}$ which defines the kinetic energy. It is shown in Bullo & Lewis (2005a) that there exists a C^∞ , positive-semidefinite $(0, 2)$ -tensor field G such that $KE(\mathbf{v}_q) = \frac{1}{2} G(\mathbf{v}_q, \mathbf{v}_q)$. This is the inner product which we will use in our equations.

Thus, the kinetic energy of a rigid body in an interconnected-mechanical system is represented by a positive-semidefinite $(0, 2)$ -tensor field on the configuration manifold Q . We refer to this object as the *kinetic energy metric* for the system. In a similar fashion, we can construct the kinetic energy for the fluid as another $(0, 2)$ -type tensor field. The sum of this tensor field and G defines the kinetic energy for the submerged rigid body.

Putting this together, we have that the kinetic energy metric for the submerged rigid body is the unique Riemannian metric on $Q = \mathbb{R}^3 \times \text{SO}(3)$ given by:

$$\mathbb{G} = \begin{pmatrix} M & 0 \\ 0 & J \end{pmatrix}, \quad (2.48)$$

where $M = m\mathbb{I}_3 + M_f$ and $J = J_b + J_f$. In the sequel, we will use $m_i = m + M_f^{\nu_i}$ and $j_i = J_b^{\Omega_i} + J_f^{\Omega_i}$, for $i = 1, 2, 3$. Thus, $M = \text{diag}(m_1, m_2, m_3)$ and $J = \text{diag}(j_1, j_2, j_3)$.

The following Lemma demonstrates how to compute \mathbb{G} in a coordinate chart.

Lemma 2.5. *Let \mathbb{G} be a C^∞ , $(0, 2)$ -tensor field defined above. Let (q^1, \dots, q^n) be the coordinates for Q in the chosen chart, and let $((q^1, \dots, q^n), (v^1, \dots, v^n))$ be the corresponding natural coordinates for TQ . Then, the components of \mathbb{G} in the chosen chart are given by*

$$\mathbb{G}_{ij} = \frac{\partial^2 KE}{\partial v^i \partial v^j}, \quad i, j \in \{1, \dots, n\}. \quad (2.49)$$

As with any Riemannian metric, associated to \mathbb{G} is its *Levi-Civita connection*: the unique affine connection that is both symmetric and metric compatible. The Levi-Civita connection provides the appropriate notion of acceleration for a curve in the configuration

space by guaranteeing that the acceleration is in fact a tangent vector field along a curve γ ; the Levi-Civita connection can be studied in more depth in do Carmo (1992). The connection also accounts for the Coriolis and centripetal forces acting on the system. Explicitly, if $\gamma(t) = (\mathbf{b}(t), R(t))$ is a curve in $SE(3)$, and $\gamma'(t) = (\boldsymbol{\nu}(t), \boldsymbol{\Omega}(t))$ is its pseudo-velocity as given in Eqs. (2.39) and (2.40), the accelerations are given by

$$\nabla_{\gamma'}\gamma' = \begin{pmatrix} \dot{\boldsymbol{\nu}} + M^{-1}(\boldsymbol{\Omega} \times M\boldsymbol{\nu}) \\ \dot{\boldsymbol{\Omega}} + J^{-1}(\boldsymbol{\Omega} \times J\boldsymbol{\Omega} + \boldsymbol{\nu} \times M\boldsymbol{\nu}) \end{pmatrix}, \quad (2.50)$$

where ∇ denotes the Levi-Civita connection⁴ and $\nabla_{\gamma'}\gamma'$ is the covariant derivative of γ' with respect to itself. We refer to $\nabla_{\gamma'}\gamma'$ as the *geometric acceleration* with respect to ∇ and note that Eq. (2.50) is Newton's Second Law expressed geometrically as $a = \sum_i F_i/m$. With no external forces, Eq. (2.50) becomes $\nabla_{\gamma'}\gamma' = 0$ which are the geodesics for the affine connection ∇ . It is important here to note that this geometric acceleration is the proper way to consider acceleration, in a general sense, since it is invariant under change of coordinates. This is easily seen through a simple example.

Example 2.1. Suppose that $Q = \mathbb{R}^2$ and consider the curve $\gamma : \mathbb{R} \mapsto Q$ defined in Cartesian coordinates by $\gamma(t) = (\cos t, \sin t)$. Thus, we have $\text{image}(\gamma) = \mathbb{S}^1$ and in coordinates $(x(t), y(t)) = (\cos t, \sin t)$. Under the Cartesian coordinate system chosen, the definition

⁴Here we remind the reader that ∇ is not the submerged volume of fluid displaced by a rigid body, but denotes an affine connection on Q .

that acceleration is the second derivative with respect to time yields

$$(\dot{x}(t), \dot{y}(t)) = (-\sin t, \cos t), \quad (\ddot{x}(t), \ddot{y}(t)) = (-\cos t, -\sin t). \quad (2.51)$$

In polar coordinates, we represent the curve by $(r(t), \theta(t)) = (1, t)$, taking note that $r(t)$ and $\theta(t)$ are only defined for $t \in (-\pi, \pi)$. Thus,

$$(\dot{r}(t), \dot{\theta}(t)) = (0, 1), \quad (\ddot{r}(t), \ddot{\theta}(t)) = (0, 0). \quad (2.52)$$

Since the acceleration is zero in polar coordinates and non-zero in Cartesian coordinates, this notion of acceleration can not be a tangent vector since a tangent vector cannot be both zero and non-zero.

Now, consider the geometric acceleration with respect to the Levi-Civita connection corresponding to the Riemannian metric $\mathbb{G} = dx \otimes dx + dy \otimes dy$. The corresponding Christoffel symbols are zero in Cartesian coordinates and thus we get

$$\nabla_{\gamma'} \gamma' = \ddot{x} \frac{\partial}{\partial x} + \ddot{y} \frac{\partial}{\partial y} = -\cos t \frac{\partial}{\partial x} - \sin t \frac{\partial}{\partial y}. \quad (2.53)$$

In polar coordinates, the nonzero Christoffel symbols are $\Gamma_{\theta\theta}^r = -r$ and $\Gamma_{r\theta}^\theta = \Gamma_{\theta r}^\theta = \frac{1}{r}$ and we have

$$\nabla_{\gamma'} \gamma' = (\ddot{r} - r\dot{\theta}^2) \frac{\partial}{\partial r} + \left(\ddot{\theta} + \frac{2}{r} \dot{r}\dot{\theta} \right) \frac{\partial}{\partial \theta} = -\frac{\partial}{\partial r}. \quad (2.54)$$

Here, we see that $\nabla_{\gamma'} \gamma'$ is indeed a tangent vector with base point $\gamma(t)$, of unit length with

respect to the standard Riemannian metric on \mathbb{R}^2 , and pointing toward the origin. In both cases, $\nabla_{\gamma'}\gamma'$ represents what one would normally refer to as acceleration, and hence, it is invariant under change of coordinates.

To continue deriving the equations of motion, we need the following definition.

Definition 2.5 (Affine connection control system). A C^∞ -affine connection control system is a 5-tuple $(Q, \nabla, \mathcal{D}, \mathcal{Y} = \{Y_1, \dots, Y_m\}, U)$ where

- (i) Q is a manifold,
 - (ii) ∇ is an affine connection on Q ,
 - (iii) \mathcal{D} is a regular linear velocity constraint such that ∇ restricts to \mathcal{D} ,
 - (iv) \mathcal{Y} is a set of input vector fields, usually taken to be the external control of the system,
 - (v) $U \in \mathbb{R}^m$ is the control set in which the input controls take their values,
- with all items assumed to be C^∞ .

We now have the tools to present the equations of motion for a neutrally buoyant rigid body submerged in an ideal fluid. We remind the reader that we assume that $O_B = C_G$ and that the body has three planes of symmetry. Note that as in Section 2.3.1 we neglect the external forces resulting from hydrodynamic damping and those forces resulting from a gravitational potential. The combination of all these assumptions physically implies that the vehicle is submerged in an ideal fluid and is neutrally buoyant with C_G coincident with C_B . We remark here that this situation implies that the metacentric height of the vehicle is zero, which is a state of neutral equilibrium and unstable for practical applications. However, we must understand the dynamics of the vehicle in this simplified case before

we include the interaction with external forces and moments. To this end, we present the following Lemma as the geometric parallel to Lemma 2.2 presented in Section 2.3.1. In the sections to follow, we will examine external forces and moments which act upon a submerged rigid body and incorporate these into our equations of motion.

Lemma 2.6. *Let $Q = \text{SE}(3)$, ∇ be the Levi-Civita connection on Q associated with the Riemannian metric \mathbb{G} and let the set of input control vector fields be given by $\mathcal{I} = \{\mathbb{I}_1^{-1}, \dots, \mathbb{I}_6^{-1}\}$. Then the equations of motion of a rigid body submerged in an ideal fluid and subjected only to input control forces are given by the affine connection control system:*

$$\nabla_{\gamma'} \gamma' = \sum_{i=1}^6 \mathbb{I}_i^{-1}(\gamma(t)) \sigma_i(t), \quad (2.55)$$

where the input control vector fields are $\mathbb{I}_i^{-1} = \mathbb{G}^\# \pi_i = \mathbb{G}^{ij} X_i$, which may be represented as the i^{th} column of the matrix $\mathbb{I}^{-1} = \begin{pmatrix} M^{-1} & 0 \\ 0 & J^{-1} \end{pmatrix}$, and $\sigma_i(t)$ are the controls.

Note that this affine connection control system is a second-order system on the manifold Q . We can also express an affine connection control system as an affine control system on TQ with a drift. This equivalence is realized via the *geodesic spray* of an affine connection and the *vertical lift* of tangent vectors to Q .

Definition 2.6 (Drift vector field). In the context of differential geometry, a *drift vector field* or *drift* is a vector field which specifies the dynamics of the system in the absence of controls. A drift vector field arises from the inertia of the system as well as the interaction with external (non-control) forces.

Definition 2.7 (Vertical lift). Let $v \in T_q Q \subset TQ$, then the *vertical lift* at v is a map

$\text{vlft}_v : T_q Q \rightarrow T_v TQ$. For $w \in T_q Q$, we define $\text{vlft}_v(w) = \frac{d}{dt}(v + tw)|_{t=0}$. In components,

$$\text{vlft}_v(w) = \begin{pmatrix} 0 \\ w \end{pmatrix} \in T_v TQ.$$

Definition 2.8 (Geodesic spray). The *geodesic spray* of ∇ is the vector field S , on TQ ,

that generates geodesic flow. Specifically, for $v \in T_q Q$, $S(v) = \frac{d}{dt}\gamma'_v(t)|_{t=0}$ where γ_v is the

unique ∇ -geodesic such that $\gamma_v(0) = q$ and $\gamma_v'(0) = v$.

By use of the above definitions, we can define the equations of motion, Eq. (2.55), as an affine control system on TQ by

$$\Upsilon'(t) = S(\Upsilon(t)) + \sum_{i=1}^m \text{vlft} \mathbb{I}_i^{-1}(\Upsilon(t)) \sigma_i(t), \quad (2.56)$$

for a locally absolutely continuous trajectory $\Upsilon : I \mapsto TQ$ and where $S(\Upsilon(t))$ is the geodesic spray, which in the special case of our Levi-Civita connection, is given by:

$$S(\mathbf{b}, R, \boldsymbol{\nu}, \boldsymbol{\Omega}) = \begin{pmatrix} \boldsymbol{\nu} \\ \boldsymbol{\Omega} \\ -M^{-1}(\boldsymbol{\Omega} \times M\boldsymbol{\nu}) \\ -J^{-1}(\boldsymbol{\Omega} \times J\boldsymbol{\Omega} + \boldsymbol{\nu} \times M\boldsymbol{\nu}) \end{pmatrix}. \quad (2.57)$$

For this presentation of $S(\mathbf{b}, R, \boldsymbol{\nu}, \boldsymbol{\Omega})$, the components are expressed relative to the standard left-invariant basis of vector fields on $TSE(3)$ rather than coordinate vector fields. The Eqs. (2.39) and (2.40) can be used to recover expressions for $\dot{\mathbf{b}}$ and \dot{R} .

In Bullo & Lewis (2005a), p. 224, the authors show that trajectories for the affine connection control system on Q map bijectively to trajectories for the affine control system on TQ whose initial points lie on the zero-section. The bijection maps the trajectory $\gamma : [0, T] \rightarrow Q$ to the trajectory $\Upsilon = \gamma' : [0, T] \rightarrow TQ$.

Another representation of Eq. (2.55) is to choose a set of coordinates and express the equations of motion locally. We include this expression for completeness, but will not heavily rely on this formulation in the sequel. The Eqs. (2.39) and (2.40) can be written in the local coordinates given in Section 2.1 as

$$\dot{\boldsymbol{\eta}} = \begin{pmatrix} R & 0 \\ 0 & \Theta \end{pmatrix} \begin{pmatrix} \boldsymbol{\nu} \\ \boldsymbol{\Omega} \end{pmatrix}, \quad (2.58)$$

where

$$R(\boldsymbol{\eta}) = \begin{pmatrix} \cos \psi \cos \theta & R^{12} & R^{13} \\ \sin \psi \cos \theta & R^{22} & R^{23} \\ -\sin \theta & \cos \theta \sin \phi & \cos \theta \cos \phi \end{pmatrix} \quad (2.59)$$

and

$$\Theta(\boldsymbol{\eta}) = \begin{pmatrix} 1 & \sin \phi \tan \theta & \cos \phi \tan \theta \\ 0 & \cos \phi & -\sin \phi \\ 0 & \frac{\sin \phi}{\cos \theta} & \frac{\cos \phi}{\cos \theta} \end{pmatrix} \quad (2.60)$$

where $R^{12} = -\sin \psi \cos \phi + \cos \psi \sin \theta \sin \phi$, $R^{13} = \sin \psi \sin \phi + \cos \psi \cos \phi \sin \theta$, $R^{22} = \cos \psi \cos \phi + \sin \phi \sin \theta \sin \psi$ and $R^{23} = -\cos \psi \sin \phi + \sin \psi \cos \phi \sin \theta$. Note that this transformation depends on the convention used for the Euler angles. Our choice reflects

a singularity for an inclination of $\pm\pi/2$. By use of the above expressions, we can now present the equations given in Lemma 2.6 in a local coordinate system with the following Lemma.

Lemma 2.7. *The equations of motion for a neutrally buoyant, submerged rigid body in an ideal fluid expressed in the coordinates presented in Section 2.1 are given by the following affine control system:*

$$\dot{b}_1 = \nu_1 \cos \psi \cos \theta + \nu_2 R^{12} + \nu_3 R^{13} \quad (2.61)$$

$$\dot{b}_2 = \nu_1 \sin \psi \cos \theta + \nu_2 R^{22} + \nu_3 R^{23} \quad (2.62)$$

$$\dot{b}_3 = -\nu_1 \sin \theta + \nu_2 \cos \theta \sin \phi + \nu_3 \cos \theta \cos \phi \quad (2.63)$$

$$\dot{\phi} = \Omega_1 + \Omega_2 \sin \phi \tan \theta + \Omega_3 \cos \phi \tan \theta \quad (2.64)$$

$$\dot{\theta} = \Omega_2 \cos \phi - \Omega_3 \sin \phi \quad (2.65)$$

$$\dot{\psi} = \frac{\sin \phi}{\cos \theta} \Omega_2 + \frac{\cos \phi}{\cos \theta} \Omega_3 \quad (2.66)$$

$$\dot{\nu}_1 = \frac{1}{m + M_f^{\nu_1}} [-(m + M_f^{\nu_3})\nu_3\Omega_2 + (m + M_f^{\nu_2})\nu_2\Omega_3 + \varphi_{\nu_1}] \quad (2.67)$$

$$\dot{\nu}_2 = \frac{1}{m + M_f^{\nu_2}} [(m + M_f^{\nu_3})\nu_3\Omega_1 - (m + M_f^{\nu_1})\nu_1\Omega_3 + \varphi_{\nu_2}] \quad (2.68)$$

$$\dot{\nu}_3 = \frac{1}{m + M_f^{\nu_3}} [(m + M_f^{\nu_2})\nu_2\Omega_1 - (m + M_f^{\nu_1})\nu_1\Omega_2 + \varphi_{\nu_3}] \quad (2.69)$$

$$\dot{\Omega}_1 = \frac{1}{I_{b_1} + J_f^{\Omega_1}} [(I_{b_2} - I_{b_3} + J_f^{\Omega_2} - J_f^{\Omega_3})\Omega_2\Omega_3 + (M_f^{\nu_2} - M_f^{\nu_3})\nu_2\nu_3 + \tau_{\Omega_1}] \quad (2.70)$$

$$\dot{\Omega}_2 = \frac{1}{I_{b_2} + J_f^{\Omega_2}} [(I_{b_3} - I_{b_1} + J_f^{\Omega_3} - J_f^{\Omega_1})\Omega_1\Omega_3 + (M_f^{\nu_3} - M_f^{\nu_1})\nu_1\nu_3 + \tau_{\Omega_2}] \quad (2.71)$$

$$\dot{\Omega}_3 = \frac{1}{I_{b_3} + J_f^{\Omega_3}} [(I_{b_1} - I_{b_2} + J_f^{\Omega_1} - J_f^{\Omega_2})\Omega_1\Omega_2 + (M_f^{\nu_1} - M_f^{\nu_2})\nu_1\nu_2 + \tau_{\Omega_3}]. \quad (2.72)$$

Remark 2.1. We note here that from the point of view of geometric control literature, the equations of motion presented in Eq. (2.55) are the general equations of motion for a submerged rigid body. This phrase *submerged rigid body* may have different connotations and assumptions depending on the area of study.

We now carry on by examining external forces in the framework of differential geometry to develop equivalent equations to those presented in Eqs. (2.37) and (2.38).

2.4.2 Geometric Forces

Now that we have the notion of geometric acceleration and the base for Newton's Second Law, we continue building the equations which define our mechanical system. To consider a complete model for rigid body motion in a viscous fluid, we must incorporate external interaction into the equations of motion. These interactions come in the form of control inputs, buoyancy and friction, among others. These are characterized as forces.

The main external forces experienced by a submerged rigid body are added mass, viscous drag, restoring forces and moments from buoyancy and gravity and environmental disturbances such as ocean currents. The inertial force of added mass is included in the affine connection, and hence, does not need to be further examined here. Environmental disturbances can be very complex and nearly impossible to model without some *a priori* knowledge of their effects. Since this is a first extension of geometric control theory to practical application and our tests are conducted in a very controlled environment, we

omit the inclusion of such factors. Thus, viscous drag and restoring forces and moments are the main external forces acting on a submerged rigid body which are studied in this dissertation.

Since this theory is expressed in the differential geometric framework, the notion of a force is not as obvious as when viewed from the Newtonian point of view. The following describes how we will incorporate the external forces considered above into the geometric equations of motion.

Suppose that a rigid body is subjected to a Newtonian force (\mathbf{f}) or torque ($\boldsymbol{\tau}$). Due to the forces considered, we allow a general external-geometric force F to depend on position $((\mathbf{b}, R) \in \mathbb{R}^3 \times \text{SO}(3))$, on velocities $((\dot{\mathbf{b}}, \dot{R}) \in T_{(\mathbf{b}, R)}(\mathbb{R}^3 \times \text{SO}(3)))$ and on time. We also assume that the effects of forces on a system are linear; the effect of two forces is the sum of their individual effects and, scaling a force similarly scales the effect upon the system. Given these assumptions, a force arises geometrically as a cotangent bundle-valued function, since the cotangent bundle is the set of linear functionals on the tangent bundle. Thus, for each $v_{(\mathbf{b}, R)} \in TQ$, we define an element $F_{\mathbf{f}, \boldsymbol{\tau}}(t, v_{(\mathbf{b}, R)}) \in T_{(\mathbf{b}, R)}^*Q$ which models the effects of \mathbf{f} and $\boldsymbol{\tau}$ in the differential geometry framework. The details are contained within the following Definition.

Definition 2.9 (Force). For $r \in \mathbb{N} \cup \{\infty\}$, a C^r -force on a manifold Q is a map $F : \mathbb{R} \times TQ \rightarrow T^*Q$ with the property that F is a locally integrally class C^r bundle map over id_Q . A C^r -force is

- (i) *time-independent* if there exists a C^r -fiber bundle map $F_0 : TQ \rightarrow T^*Q$ over id_Q with

the property that $F(t, v_{(b,R)}) = F_0(v_{(b,R)})$, and is

(ii) *basic* if there exists a C^r -covector field F_0 on Q such that $F(t, v_{(b,R)}) = F_0(b, R)$.

Here id_Q represents the identity map on Q (i.e., $\text{id}_Q(x) = x$ for all $x \in Q$)

If $\gamma : I \rightarrow Q$ is a C^r -curve, then a C^r -force along γ is a C^r -covector field $F : I \rightarrow T^*Q$ along γ .

Now, let $\{X_1, \dots, X_6\}$ be the standard left-invariant basis for $\text{SE}(3)$ and let $\{\pi^1, \dots, \pi^6\}$ be its dual basis. Then, we can express an external force acting on the system as a one form:

$$F_{f,\tau}(t, v_{(b,R)}) = \sum_{i=1}^6 F_i(t, \mathbf{b}, R, \boldsymbol{\nu}, \boldsymbol{\Omega}) \pi^i, \quad (2.73)$$

where F_i is the i^{th} component of the force, $i = 1, \dots, 6$. By definition, this force is an element of T^*M and thus not a geometric acceleration. This is remedied by applying $\mathbb{G}^\#$, the inverse of the kinetic energy metric \mathbb{G} . Multiplication by the matrix $\mathbb{G}^\#$ represents a vector bundle isomorphism which essentially means divide by mass, hence $\mathbb{G}^\#(F(\gamma'(t))) \in TM$ and is an acceleration as desired:

$$\mathbb{G}^\# = \text{diag} \left(\frac{1}{m_1}, \frac{1}{m_2}, \frac{1}{m_3}, \frac{1}{j_1}, \frac{1}{j_2}, \frac{1}{j_3} \right). \quad (2.74)$$

Thus, in matrix form, the external accelerations become

$$\mathbb{G}^\#(F(\gamma'(t))) = \left(\frac{F_1}{m_1}, \frac{F_2}{m_2}, \frac{F_3}{m_3}, \frac{F_4}{j_1}, \frac{F_5}{j_2}, \frac{F_6}{j_3} \right). \quad (2.75)$$

Now we have an object which represents the external Newtonian forces as an acceleration in the language of differential geometry. As mentioned before, these external forces will be used to model the drag, buoyancy, restorative and control forces that act upon the rigid body.

Another external forces which we consider are the control forces. These are the forces with which we move the rigid body through the surrounding fluid. Throughout this dissertation, we assume that we have three forces acting at the center of gravity along the body-fixed axes and that we have three pure torques about these three axes. We will refer to these controls as the six degree-of-freedom (6-DOF) controls. We denote the controls by: $\sigma = (\varphi_\nu, \tau_\Omega) = (\varphi_{\nu_1}, \varphi_{\nu_2}, \varphi_{\nu_3}, \tau_{\Omega_1}, \tau_{\Omega_2}, \tau_{\Omega_3})$.

Remark 2.2. The above notion of control forces is not realistic from a practical point of view since underwater vehicle controls may represent the action of the vehicle's thrusters or actuators. The forces from these actuators generally do not act at the center of gravity and the torques are obtained from the momenta created by the forces. We will address this issue when we discuss the test-bed vehicle used in this study. We also present an alternate formulation of the input control forces in Section 7.1.

2.4.3 Viscous Drag Geometrically

In this section, we use the tools developed in Section 2.4.2 to model the forces and moments resulting from viscous drag. As previously mentioned, due to the shape and veloc-

ity of the test-bed vehicle under consideration, the dominant contribution of viscous drag comes from separation of the fluid from the body. This is commonly referred to as pressure (or form) drag. This force arises due to the pressure difference between the front and rear of the vehicle. More details on the viscous drag can be found in Appendix B.1. These forces and moments are called dissipative, since they dissipate energy from the system. In particular, we have the following definition.

Definition 2.10. (Dissipative force/moment) A time-independent force $F : TQ \rightarrow T^*Q$ is *dissipative* if $\langle F(v_q); v_q \rangle \leq 0$ for each $v_q \in TQ$.

It is commonly known in hydrodynamics that for flows at high Reynolds number, or those characterized by flow separation, the drag force and moment is proportional to $\nu|\nu|$ and $\Omega|\Omega|$, respectively. For this research, we make the assumption that we have a drag force $D_\nu(\nu)$ and a drag momentum $D_\Omega(\Omega)$ implying that there are no off-diagonal terms, repeating the assumption made in Section 2.3.2. The contribution of these forces with respect to the velocities is given by

$$D_\nu(\nu_i) = \frac{1}{2}C_D\rho A_i\nu_i|\nu_i|, \quad D_\Omega(\Omega_i) = \frac{1}{2}C_D\rho A_i\Omega_i|\Omega_i| \quad (2.76)$$

where C_D is the appropriate drag coefficient for the prescribed direction of motion⁵, ρ is the density of the fluid, A_i is the projected surface area of the body in the direction of the velocity, ν_i are the translational velocities and Ω_i are the rotational velocities.

⁵As previously mentioned, C_D may not be dimensionless

Remark 2.3. Note that in Eq. (2.76), we express the drag force (moment) as proportional to $\nu|\nu|$ ($\Omega|\Omega|$). Since the velocities ν and Ω correspond to the velocities of the test-bed vehicle whose motions are in a single direction with respect to the surrounding fluid, we may assume that $\nu|\nu| = \nu^2$ and $\Omega|\Omega| = \Omega^2$.

Since a vehicle may have different drag coefficients and different projected areas depending on the direction of the velocity, we define $F_i(\gamma'(t)) = D_i$ such that the total drag relation is given by $D_{total} = D_i|v_i|v_i$ for $i \in \{1, \dots, 6\}$ and $v = (\nu_1, \nu_2, \nu_3, \Omega_1, \Omega_2, \Omega_3)$. Then we let $\mathcal{D}_i = -\frac{D_i}{m_i}\nu_i^2$ for $i = 1, 2, 3$ and $\mathcal{D}_i = -\frac{D_i}{j_{i-3}}\Omega_{i-3}^2$ for $i = 4, 5, 6$. Again, we assume that pressure drag is dominant for our application and estimate the drag coefficient accordingly (see Appendix B.1).

In our case, the dissipative forces and moments (viscous drag forces and moments) depend on the square of the velocity of the body along a given trajectory γ . Hence, we can write $F_{drag}(\gamma'(t)) = \sum_{i=1}^6 F_i(\gamma'(t))\pi^i(\gamma'(t))$ which expands to

$$F_{drag}(\gamma'(t)) = \sum_1^3 F_i(\gamma'(t))\nu_i^2\pi^i + \sum_{i=1}^3 F_{i+3}(\gamma'(t))\Omega_i^2\pi^i. \quad (2.77)$$

Thus, we have the following expression

$$\begin{aligned} & \mathbb{G}^\#(F_{drag}(\gamma'(t))) \\ &= \sum_{i=1}^3 \frac{F_i(\gamma'(t))}{\mathbb{G}_{ii}} \nu_i^2 X_i + \sum_{i=4}^6 \frac{F_i(\gamma'(t))}{\mathbb{G}_{ii}} \Omega_{i-3}^2 X_i \\ &= \sum_{i=1}^6 \mathcal{D}_i X_i, \end{aligned} \quad (2.78)$$

where \mathbb{G}_{ij} is the i, j -entry of the kinetic energy matrix \mathbb{G} as given before. The result is that the drag force is expressed as a geometric acceleration given by $\mathbb{G}^\#(F_{drag}(\gamma'(t)))$ which we can incorporate into the differential geometric equations of motion.

Remark 2.4. The drag forces $F_i(\gamma'(t)) = D_i$ for $i = 1, \dots, 6$ are estimated for the test-bed vehicle used to conduct this research. Since the data are lengthy, we omit the details here, but refer the reader to Appendix B.1 for further information and a detailed explanation on the estimation of the drag forces.

2.4.4 Restoring Forces Geometrically

Now, we consider the conservative or restoring forces and moments from buoyancy and gravity. These are forces and moments which arise from a potential function, and thus, in the context of differential geometry are referred to as *potential forces*. Throughout this dissertation, we will use the terms restoring force/moment and potential force/moment interchangeably to refer to the conservative forces/moments arising from buoyancy and gravity.

Restoring forces (moments) can be viewed as a force (torque) which acts to pull the rigid body back to a stable equilibrium position or orientation. Restoring functions are commonly known to store energy to be turned into kinetic energy later. In particular, given a potential function $V \in \mathcal{C}^\infty(Q)$ on Q its *potential (restoring) force* is the basic force (see Def. 2.9) given by $F(t, v_q) = -\text{grad } V(q) = -dV(q)$ for $q \in Q$. In this dissertation,

we concern ourselves with potential forces which are independent of time, velocity and acceleration. The differential geometric theory supports potential functions which depend on position, velocity and time, however, our application does not require considering these cases. In the case of the submerged rigid body, we encounter a potential force from gravity and a potential force from buoyancy.

We denote by $\mathbf{r}_{C_G} = (x_G, y_G, z_G)$ ($\mathbf{r}_{C_B} = (x_B, y_B, z_B)$) the location of C_G (C_B) with respect to O_B . Now, the potential force from the acceleration due to gravity acts directly at C_G , and is given by the potential function $V_G(\gamma(t)) = W(R\mathbf{r}_B + \mathbf{b}) \cdot \mathbf{s}_3$ where \cdot denotes the inner product. Similarly, the force arising from the buoyancy is the force exerted by the fluid on the submerged volume of the vessel and acts at C_B and is given by the potential function $V_B(\gamma(t)) = B(R\mathbf{r}_B + \mathbf{b}) \cdot \mathbf{s}_3$. These two potential forces can be combined into one term denoted by $F(t, v_q) = P(\gamma(t)) = -(dV_G + dV_B)$. Writing this in matrix form, we can express the potential forces from gravity and buoyancy as accelerations (via multiplication by $\mathbb{G}^\#$) with the following:

$$\mathbb{G}^\# P(\gamma(t)) = \begin{bmatrix} -\frac{1}{m_1}(W - B)s\theta \\ \frac{1}{m_2}(W - B)c\theta s\phi \\ \frac{1}{m_3}(W - B)c\theta c\phi \\ \frac{1}{j_1}((y_G W - y_B B)c\theta c\phi - (z_G W - z_B B)c\theta s\phi) \\ -\frac{1}{j_2}((z_G W - z_B B)s\theta - (x_G W - x_B B)c\theta c\phi) \\ \frac{1}{j_3}((x_G W - x_B B)c\theta s\phi + (y_G W - y_B B)s\theta) \end{bmatrix}, \quad (2.79)$$

where $c \cdot = \cos(\cdot)$ and $s \cdot = \sin(\cdot)$. Here we see that the restoring acceleration represented in the right-hand side of Eq. (2.79) is actually $-g(\boldsymbol{\eta})$ from an earlier section multiplied by the inverse of the kinetic energy metric \mathbb{G} . Again, the musical exponent $\#$ implies a tangent bundle isomorphism which literally means *divide by mass*. This term is the opposite sign from $g(\boldsymbol{\eta})$ given in Eq. (2.35) since here we take $dV = g(\boldsymbol{\eta})$ and define $P(\gamma(t)) = -dV$. Note that if $C_G \neq C_B$, the two opposing potential forces will induce a torque, referred to as the righting moment, if the vehicle rotates. The righting arm GZ depends on the distance between C_G and C_B and the list angle ϕ as seen in Fig. 7. On the other hand, if $C_G = C_B$, then the vehicle will experience no torque that opposes orientational displacements.

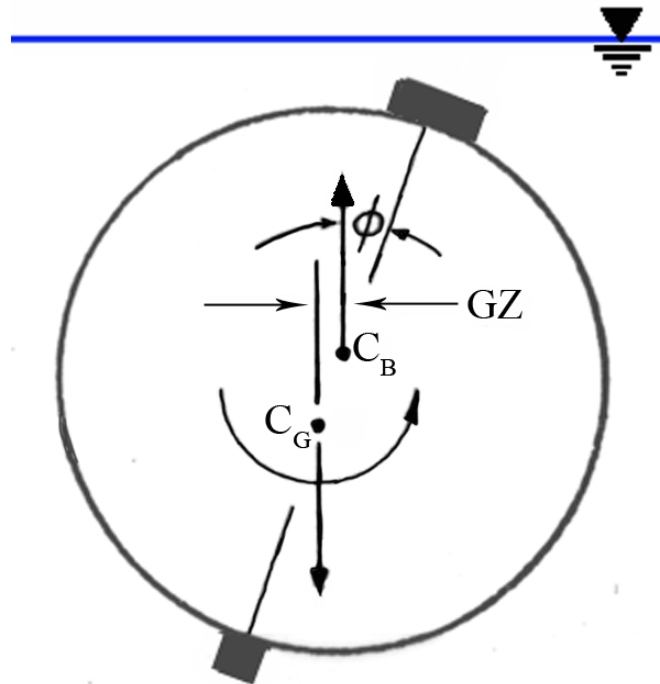


Figure 7: Potential forces acting at C_G and C_B and the righting arm for a submerged spherical vehicle.

2.4.5 Geometric Equations of Motion in a Viscous Fluid

In this section, we present the equations of motion for a rigid body submerged in a viscous fluid and subject to restoring forces and moments. To include viscous drag and the restoring forces and moments, we need the following Definition.

Definition 2.11 (Forced affine connection control system). A C^∞ -forced affine connection control system is a 6-tuple $(Q, \nabla, \mathcal{D}, Y, \mathcal{Y} = \{Y_1, \dots, Y_m\}, U)$ where

- (i) Q is a manifold,
 - (ii) ∇ is an affine connection on Q ,
 - (iii) \mathcal{D} is a regular linear velocity constraint such that ∇ restricts to \mathcal{D} ,
 - (iv) Y is a vector force,
 - (v) \mathcal{Y} is a set of input vector fields, usually taken to be the external control of the system,
 - (vi) $U \in \mathbb{R}^m$ is the control set in which the input controls take their values,
- with all items assumed to be C^∞ .

Note the difference between the *forced* affine connection control system above and the affine connection control system presented in Definition 2.5 is the vector field Y acting as an external force. Here, Y is a *drift vector field* as defined in Definition 2.6. It is via such drift vector fields that we will incorporate the external forces and moments arising from viscous drag, gravity and buoyancy.

Following the Newton-Euler formulation of the equations of motion, we can now set the geometric acceleration equal to the sum of the forces and moments (divided by mass)

acting upon the rigid body. The following Lemma combines the previously addressed forces and moments from Sections 2.4.3 and 2.4.4 along with the control forces to define the general equations of motion for an underwater vehicle submerged in a viscous fluid using the Levi-Civita affine connection.

Lemma 2.8. *Let $Q = \text{SE}(3)$, ∇ be the Levi-Civita connection on Q associated with the Riemannian metric \mathbb{G} and let the set of input control vector fields be given by $\mathcal{I} = \{\mathbb{I}_1^{-1}, \dots, \mathbb{I}_6^{-1}\}$. Let $\mathbb{G}^\#(F_{drag}(\gamma'(t)))$ represent the dissipative forces resulting from hydrodynamic drag. Let $\mathbb{G}^\#P(\gamma(t))$ represent the potential forces arising from gravity and buoyancy. Then the equations of motion of a rigid body submerged in a viscous fluid and subjected to dissipative and potential forces are given by the forced affine connection control system:*

$$\nabla_{\gamma'}\gamma' = \mathbb{G}^\#P(\gamma(t)) + \mathbb{G}^\#(F_{drag}(\gamma'(t))) + \sum_{i=1}^6 \mathbb{I}_i^{-1}(\gamma(t))\sigma_i(t), \quad (2.80)$$

where $\sigma_i(t)$ represents the controls.

Here, we point out the major difference between the two affine connection control systems given in Eqs. (2.55) and (2.80). The Eq. (2.55) is known as a *driftless* system, as there are no vector fields which specify the dynamics of the system in the absence of the control forces. The terms $\mathbb{G}^\#(F_{drag}(\gamma'(t)))$ and $\mathbb{G}^\#P(\gamma(t))$ in Eq. (2.80) represent drift vector fields, and thus this *forced* affine connection control system represents an entirely different geometric object from the driftless system presented in Section 2.4.1. As we will see later in Section 4.3, it will be advantageous to work with a driftless system whenever possible.

To this end, we present the development of a new affine connection which will allow us to eliminate one of the drift vector fields in Eq. (2.80).

As previously mentioned, the magnitude of the drag force acting on a rigid body is proportional to the square of the velocity of the body and we assume that the drag coefficient matrix is diagonal. This relationship allows us to describe the geometric acceleration associated to the viscous drag forces as a symmetric type (1, 2)-tensor field on $\mathbb{R}^3 \times \text{SO}(3)$. The difference between any two affine connections is a type (1, 2)-tensor field Δ . If we let $\tilde{\nabla}$ represent an affine connection and ∇ the Levi-Civita affine connection, we can write

$$\tilde{\nabla}_X Y = \nabla_X Y + \Delta(X, Y), \quad (2.81)$$

for any vector fields $X, Y \in Q$. Thus, by modifying the Levi-Civita affine connection, we are able to include the hydrodynamic drag forces inside the new affine connection $\tilde{\nabla}$. We continue with some background and further details to validate this claim.

In general, a symmetric type (1,2)-tensor is given by

$$\Delta = \sum_{i,j,k} \Delta_{jk}^i X_i \otimes \pi^j \otimes \pi^k, \quad (2.82)$$

where $\Delta_{kj}^i = \Delta_{jk}^i$, and thus when we evaluate Δ along the trajectory we get

$$\begin{aligned} \Delta|_{(b,R)}(\gamma', \gamma') &= \sum_{i=1}^6 \left(\sum_{j,k=1}^3 \Delta_{jk}^i(b, R) \nu^j \nu^k \right. \\ &\quad \left. + 2 \sum_{j=1}^3 \sum_{k=4}^6 \Delta_{jk}^i(b, R) \nu^j \Omega^k + \sum_{j,k=4}^6 \Delta_{jk}^i(b, R) \Omega^j \Omega^k \right) X_i. \end{aligned} \quad (2.83)$$

Computing the above using the standard basis $\{X_1, \dots, X_6\}$ from before, we get that

$$\Delta(X_i, X_j) = \Delta_{ij}^1 X_1 + \dots + \Delta_{ij}^6 X_6. \quad (2.84)$$

By use of Eq. (2.78), we see that the only non-zero terms occur when $i = j = k$, and we have that $\Delta(X_i, X_i) = \Delta_{ii}^i X_i = -\frac{D_i}{\mathbb{G}_{ii}} X_i$. Thus, we are able to define the modified Levi-Civita connection in the following manner

$$\tilde{\nabla}_{X_i} X_j = \begin{cases} -\frac{D_i}{\mathbb{G}_{ii}} X_i & i = j \\ \nabla_{X_i} X_j & i \neq j \end{cases}, \quad (2.85)$$

since we know $\nabla_{X_i} X_i = 0$.

We can now use the affine connection $\tilde{\nabla}$ to express Eq. (2.80) in a more compact form. Under the assumptions that $C_G \neq C_B$ and $W \neq B$, we can not express Eq. (2.80) as a driftless system due to the fact that the restoring forces and moments do not directly depend on the velocity of the body. We will present an approach to handle the restoring forces when we discuss the design of the control strategy. For now, we present the simplification of Eq. 2.80 in the following Lemma.

Lemma 2.9. *Let $Q = \text{SE}(3)$, $\tilde{\nabla}$ be the modified Levi-Civita connection on Q associated with the Riemannian metric \mathbb{G} and let the set of input control vector fields be given by $\mathcal{I} = \{\mathbb{I}_1^{-1}, \dots, \mathbb{I}_6^{-1}\}$. Let $G^\# P(\gamma(t))$ represent the restoring forces arising from gravity and buoyancy. Then the equations of motion of a rigid body submerged in a viscous fluid are*

given by the forced affine connection control system:

$$\tilde{\nabla}_{\gamma'}\gamma' = \mathbb{G}^\#P(\gamma(t)) + \sum_{i=1}^6 \mathbb{I}_i^{-1}(\gamma(t))\sigma_i(t), \quad (2.86)$$

where $\sigma_i(t)$ represents the controls.

The Eq. (2.86) can be simplified further using more restrictive assumptions. As mentioned in Section 2.4.4, if $W = B$ and $C_G = C_B$, then the vehicle will experience no restoring forces or moments. Again, this situation implies that the metacentric height of the vehicle is zero, which is a state of neutral equilibrium and unstable for practical applications. However, we include the following for completeness as it will be put to use in Chapter 4.

Under the assumptions that $W = B$ and $C_G = C_B$, $\mathbb{G}^\#P(\gamma(t)) = 0$ and Eq. (2.80) simplifies to the following forced affine connection control system:

$$\nabla_{\gamma'}\gamma' = \mathbb{G}^\#(F_{drag}(\gamma'(t))) + \sum_{i=1}^6 \mathbb{I}_i^{-1}(\gamma(t))\sigma_i(t). \quad (2.87)$$

With the new connection, $\tilde{\nabla}$, the equations of motion presented by Eq. (2.87) become an affine connection control system given by

$$\tilde{\nabla}_{\gamma'}\gamma' = \sum_{i=1}^6 \sigma^i(t)\mathbb{I}_i^{-1}(\gamma(t)). \quad (2.88)$$

The above system is a second-order affine connection control system on Q , just as we saw

in Section 2.4.1. As in Eq. (2.86), it initially looks as though we neglect the viscous drag forces and moments, but they are now hidden in the affine connection $\tilde{\nabla}$. Essentially, we have modified the acceleration of the system to account for the dissipation. These terms resurface when we write Eq. (2.88) as a first-order system on TQ as

$$\Upsilon'(t) = \tilde{S}(\Upsilon(t)) + \sum_{i=1}^m \text{vlf} \mathbb{I}_i^{-1}(\Upsilon(t)) \sigma_i(t), \quad (2.89)$$

where the geodesic spray, \tilde{S} , associated with $\tilde{\nabla}$ is given by

$$\tilde{S}(\mathbf{b}, R, \boldsymbol{\nu}, \boldsymbol{\Omega}) = \begin{pmatrix} \boldsymbol{\nu} \\ \boldsymbol{\Omega} \\ -M^{-1}(\boldsymbol{\Omega} \times M\boldsymbol{\nu} + D_{\boldsymbol{\nu}}(\boldsymbol{\nu})) \\ -J^{-1}(\boldsymbol{\Omega} \times J\boldsymbol{\Omega} + \boldsymbol{\nu} \times M\boldsymbol{\nu} + D_{\boldsymbol{\Omega}}(\boldsymbol{\Omega})) \end{pmatrix}. \quad (2.90)$$

Clearly, it is seen that along with the Coriolis and centripetal terms, the drag force $D_{\boldsymbol{\nu}}(\boldsymbol{\nu})$ and drag momentum $D_{\boldsymbol{\Omega}}(\boldsymbol{\Omega})$ are accounted for within the affine connection $\tilde{\nabla}$.

Although Eq. 2.88 represents an unstable system in practice, it is interesting from a theoretical geometric control viewpoint that Eq. 2.87 can be represented by the *driftless* system in Eq. 2.88. The affine connection $\tilde{\nabla}$ enables the current control strategy design method, studied in this dissertation, to account for dissipation from viscous drag experienced by a submerged rigid body. This modification to the Levi-Civita affine connection is a development of the author of this dissertation and can be studied in more detail in Chyba & Smith (2008) and Smith et al. (2008b).

2.5 Closing Remarks

In the sequel, we denote by \mathbb{I}^{-1} the matrix whose columns are the six input vector fields to the fully actuated system: $\mathbb{I}^{-1} = (\mathbb{I}_1^{-1}, \mathbb{I}_2^{-1}, \mathbb{I}_3^{-1}, \mathbb{I}_4^{-1}, \mathbb{I}_5^{-1}, \mathbb{I}_6^{-1})$. We also define $\mathcal{I}_m^{-1} = \{\tilde{\mathbb{I}}_1^{-1}, \dots, \tilde{\mathbb{I}}_m^{-1}\}$ to represent a set of input vector fields to an under-actuated system ($m < 6$). We denote the span of the under-actuated system by \mathcal{I}^{-1} . We note here that under our assumptions, \mathbb{I}^{-1} is diagonal, and thus each \mathbb{I}_i^{-1} and $\tilde{\mathbb{I}}_i^{-1}$, $i \in \{1, \dots, 6\}$, represents a single degree of freedom input vector field to the system.

Chapter 3

Control of Underwater Vehicles

The term *Motion Planning* has had many different definitions and connotations over the years. Arguably, the first emergence of a motion planning problem was through graph theory in 1736 when Leonard Euler proved it was impossible to design a continuous route traversing all seven of Königsberg's bridges exactly once. Over the years, this simply posed problem has evolved into an entire field of research, where problems are referred to as a *travelling salesman problem*, *highway inspector's dilemma*, or the *general movers' problem*.

When considering motion planning problems such as those mentioned above, two distinct questions arise. First, is it possible to find a path from a given initial configuration to any desired final configuration? If the answer to the first question is affirmative, then the second question is how do we realize this motion? With respect to control theory, the first question refers to the controllability of the system, while the second question is what is referred to as the *motion planning problem* in literature.

In this chapter, we examine the motion planning problem for a rigid body and a submerged rigid body. This motivates the need for the design of path planning techniques and algorithms. We then proceed on to discuss some currently implemented feedback control algorithms which provide assistance to autonomous vehicles in realizing a chosen trajectory.

3.1 Motion Planning for the Rigid Body

Asking the questions presented above with respect to the research presented in this study amounts to asking if and how one could maneuver a six degree of freedom rigid body from a given initial configuration to any final configuration. In general, Reif (1987) showed that the controllability question for such a system with movable obstacles is PSPACE-hard⁶. An introduction and analysis of controllability for robot motion is presented in Canny (1988) and has been built upon by many over the years. One approach to consider controllability, which is most linked to the mathematical theory presented here, is through the treatment of an accessibility set, fundamentally developed by Sussmann & Jurdjevic (1972). And, probably the earliest approach, specifically on mechanical systems on Lie groups, is presented in Bonnard (1984). Many other approaches have been presented over the years, yet providing general conditions for the determination of controllability is still an open question. When we are able to determine that the rigid body is controllable, we are then posed with the task of designing a control strategy which steers the vehicle to the prescribed final configuration.

In this section, we consider the motion planning problem for the rigid body. As mentioned in Remark 2.1, we include added mass in the formulation of the equations of motion, but neglect dissipation and gravitational forces acting upon the body. This results in the consideration of the driftless affine connection control system presented by Eq. (2.55). For

⁶PSPACE is the set of all problems which can be solved by programs which only need a polynomial (in the length of the problem instance specification) amount of memory to run.

such a system, determining the controllability is simple and results in determining whether or not the involutive distribution of Lie brackets generated by the input control vector fields $\mathcal{Y} = \{Y_1, \dots, Y_6\}$ span the tangent space of the configuration manifold, see Chapter 7 of Bullo & Lewis (2005a) for more details on this and other controllability results. Given that the system is indeed controllable, we are then posed with the following problem.

Problem 3.1. Given the driftless system presented in Eq. (2.55), let \mathcal{U} be a collection of U -valued locally integrable inputs. Then the \mathcal{U} -motion planning problem is:

Given $\eta_0, \eta_f \in Q$, find $u \in \mathcal{U}$, defined on $[0, T]$, such that the controlled trajectory (γ, u) with $\gamma(0) = \eta_0$ has the property that $\gamma(T) = \eta_f$.

From here, it is a matter of determining the types of controls we are able to, or wish to apply in a given situation. One approach is via the use of primitives and utilizes a piece-wise constant control structure. An alternative analytic approach is using locally absolutely continuous controls which often results in periodic (sinusoidal) control structures. If an analytic solution is unavailable, numerical methods may be implemented to generate solutions. Under these circumstances, optimization of some form along the trajectory is also being addressed.

For this dissertation, we focus on a kinematic approach using primitives. We demonstrate how to compute piece-wise constant velocity controls by following the flows of specific vector fields. These controls are then used to generate an absolutely continuous control strategy for the dynamic system. In the next chapter, we will define a kinematic reduction and describe how to generate these controls by following decoupling vector fields. We also

examine the current limitations of this method with respect to its direct application to actual AUVs, and present new extensions which reduce these limitations.

3.2 Motion Planning for the Submerged Rigid Body

In the previous section, we saw that the controllability for a rigid body was somewhat simple to determine and the motion planning problem could be solved with the appropriate choice of control inputs. For the case of the submerged rigid body, where we include external forces arising from hydrodynamic damping, gravity and buoyancy, the situation is much different. The equations of motion for a mechanical system of this type, given by Eq. (2.86), represent a forced affine connection control system which has a nonzero drift vector field.

For a system of equations which include a drift vector field, the notion of a kinematic reduction, as studied in this dissertation, is not defined, and hence motion planning using this geometric method does not exist. Moreover, current kinematic, holonomic path and motion planning do not account for the additional dynamics and constraints experienced by a submerged rigid body. Numerical techniques can still provide solutions, but these can be computationally expensive and may possibly diverge depending upon the choice of the final configuration. To this end, the efforts of the research in this dissertation strive to extend current results of geometric control theory in the area of kinematic decoupled path planning so that we may generate open-loop controls which can be implemented onto actual AUVs.

We focus our efforts on the design of open-loop controls, as their successful implementation can lead to enhanced accuracy with reduced control effort by the vehicle. Acting as a control in the feedforward path of the control system, the open-loop controls steer the vehicle using an understanding of the vehicle's dynamic response to each type of control input.

Since open-loop controls are based on the *a priori* knowledge of the inputs to the system, they are not robust against unknown disturbances. To remedy this, AUVs are typically controlled using a feedback or adaptive control law. Such a control feeds back an estimated correction factor into the actuation signal. In this manner, the vehicle can compensate or adapt to changes in the environment or correct for inaccuracies present in the hydrodynamic model. In the sections to follow, we examine some of the popular feedback control algorithms currently used in the AUV community.

The use of a feedback control is useful as long as there is a way to determine or estimate the error along the chosen trajectory. For underwater applications, vehicle navigation and positioning still present large problems to be addressed in this area. To this end, a hybrid system between open and closed-loop controls would provide a robust controller which utilizes the benefits of each.

3.3 Control of Autonomous Underwater Vehicles

In the following sections, we present a basic definition and application of some of the more popular feedback controls used in AUV control. This is by no means an exhaustive

list, and since the scope of this dissertation is not on closed-loop control laws, we do not discuss the precise details of the design or implementation of the presented controllers.

3.3.1 PID Control

A proportional–integral–derivative controller (PID controller) is a widely used generic feedback control mechanism. Given a desired set point, this controller attempts to correct the error by calculating a corrective action that can adjust the process accordingly. This correction factor is calculated by use of a subset of three separate parameters; the Proportional, the Integral and Derivative values. A general PID controller is displayed in Fig. 8.

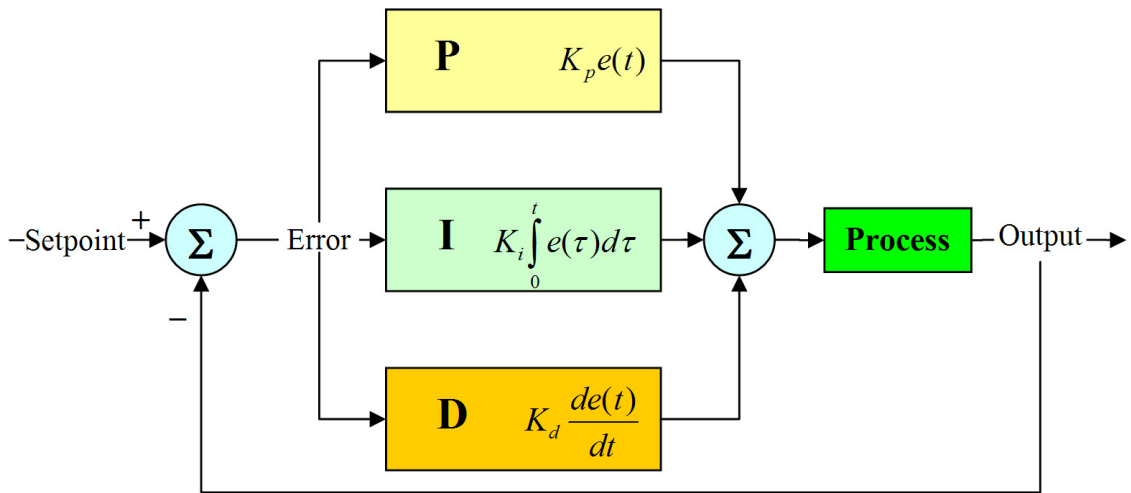


Figure 8: A block diagram of a PID controller, SilverStar (2008).

The proportional value determines the direct reaction to the current error, the integral value determines the reaction based on the sum of recent errors and the derivative deter-

mines the reaction to the rate at which the error has been changing. The weighted sum of these three actions is used as the corrective feedback to the system. By changing the weights or gains on each of the P, I and D parameters, the controller can be fine tuned for specific requirements. Note that the use of the PID algorithm for control does not guarantee optimal control of the system or system stability.

The name PID controller is a general name for the class of subsets of this type of controller. Certain applications may require using only one or two parameters to appropriately control the system. This is achieved by setting the gain of undesired control outputs to zero. A PID controller is referred to as a PI, PD, P or I controller in the absence of the unnamed control parameters. PI controllers are particularly common, since derivative action is very sensitive to measurement noise. The absence of an integral parameter in the controller may prevent the system from reaching its target value.

The application of PID controllers to underwater vehicles has been phased out over the last few years as more advanced alternatives become available. Although they are not completely obsolete, PID controllers are rarely found as the sole controller for an AUV. They are usually combined with or integrated into one of the more recently developed controllers listed in the following sections.

3.3.2 Adaptive Control

Adaptive control modifies the control law used by a controller to cope with the fact that the parameters of the system are time-varying or uncertain. Adaptive control does not need

a priori information about the bounds on these uncertain or time-varying parameters, it is only concerned with control law changes. Adaptive control can be either feedforward adaptive control or feedback adaptive control. One successful implementation of adaptive control of which the author is particularly familiar, is the Multiple Input Multiple Output (MIMO) adaptive controller which uses bound estimation developed for ODIN. The details of this design and implementation can be found in Yuh (1996) and Choi & Yuh (1996). Due to the broad implications of its name, there are many different flavors of adaptive control with applications to underwater vehicles.

3.3.3 Sliding Mode Control

Sliding mode control is a state feedback control scheme. This variable structure control alters the dynamics of the nonlinear system by applying a high-frequency switching control. Here, the feedback is not a continuous function of time. The basic implementation involves selecting a hypersurface or a manifold such that the system trajectory exhibits desirable behavior when confined to this space, and then finding appropriate feedback gains so that the system trajectory intersects and stays on the selected manifold.

The principle of a sliding mode control is to forcibly constrain the system to remain on the manifold (sliding surface) on which the system will exhibit desirable features. On this space, the system dynamics are then governed by a reduced-order system.

The use of sliding mode control with applications to AUVs can be found in e.g., Yoerger & Slotine (1985) and Healey & Lienard (1993).

3.3.4 Neural Network Control

The term neural network stems from the biological reference of a network or circuit of neurons. This biological mimicry now functions to control mechanical systems through a sort of artificial intelligence. A control theoretical neural network involves a network of simple processing elements which are able to control complex global behavior determined by the connections between the processing elements and element parameters.

In a neural network model, simple nodes, or processing elements, are connected together to form a network hence the term "neural network". While a neural network does not have to be adaptive, its practical use is realized with algorithms designed to alter the weights applied to each of the connections in the network to produce a desired signal flow. Some neural networks, or parts of neural networks are used as components in larger systems that combine both adaptive and non-adaptive elements.

Artificial neural network models can be used to infer a function from observations and also apply it. This is very useful in applications where a desired function may not be available in closed form. Applications of neural networks include system identification and control (underwater vehicle application), game-playing and decision making, pattern recognition, medical diagnosis, financial applications and e-mail spam filtering. A neural network control system was also tested on ODIN (see e.g., Yuh (1990)). Without an explicit model of the vehicle, the controller was able to update model parameters in real time using a recursive adaptation algorithm in the neural network.

3.3.5 Fuzzy Logic

A fuzzy control system is one based on fuzzy logic; a mathematical system that analyzes analog input values in terms of logical variables that take on continuous values between zero and one. Fuzzy logic is widely used in robotic control and has the advantage that the solution to the problem can be formulated in terms that human operators can understand, thus their experience can be exploited in the design phase of the controller. This characteristic makes it relatively easy to mechanize tasks which are already performed by humans.

Fuzzy control system design is based on empirical methods which is a methodical approach to trial-and-error. The general design process is to document the system's dynamics, inputs and outputs and then determine the fuzzy sets for the inputs. After this, one can lay out the set of rules and determine the defuzzification method. Fuzzy controllers are conceptually very simple, generally consisting of only an input stage, a processing stage, and an output stage. For more information on fuzzy control we refer the interested reader to Lewis (1997).

In the application to underwater vehicles, a fuzzy logic controller can be used as a stand alone solution, or in combination with a neural network or alternate type of adaptive controller. One specific application using only a fuzzy logic controller can be found in Kato (1995).

3.3.6 General Control

In this chapter, we have gone from describing the motion planning problem for the rigid body to detailing some particular control algorithms used in the operation of underwater vehicles. As should be clear from the discussion, choosing the method of control for an underwater vehicle is highly dependent on the specific applications and tasks that the vehicle is designed to perform. Most autonomous underwater vehicles in operation today use a combination or hybridization of control methods to provide the appropriate robustness and performance characteristics. For example, Tsukamoto et al. (1999) experimented with the combination of an on-line neural-net controller, off-line neural-net controller, a fuzzy controller and a non-regressor based adaptive controller for position and velocity control of their system. Hybrid controllers such as this, and each of the five individual controllers presented in the previous sections, can provide good experimental results, however they all share the characteristic that they all are model-free. This means that vehicle parameters are either estimated or learned by the system and the controllers need to be adjusted and/or tuned for the specific vehicle and application. For some vehicles, this tuning is implemented at the beginning of each mission

With so many different vehicles in operation, model-free controllers have become widespread in AUV applications. There is no need for a precise hydrodynamic model, and these controllers provide robustness with respect to environmental disturbances. However, there is still need for improvement.

Improvement may come by reverting back to the original motion planning question; how does one calculate the controls which steer a vehicle from one configuration to another? To answer this question, we need to examine the mechanical system at hand. However, many current models do not entirely describe a submerged rigid body. For this we turn to a differential geometric architecture and utilize the equations of motion presented in Section 2.4. With this formulation, we are able to exploit the symmetries, geometry and the inherent non-linearities of an underwater vehicle to produce control strategies based on the model. Also, the coordinate invariant formulation on a differentiable manifold allows us to consider the intrinsic structure of the problem rather than a pseudo-structure attached through the choice of a specific coordinate system. For those readers still wondering why a new formulation is necessary or if it is really worth substantial consideration, I refer you to Lewis (2007) where the author presents a straightforward and colloquially written article on why differential geometric modeling is important. For those remaining readers, we will now proceed with a geometric formulation of solutions to the motion planning problem for a submerged rigid body.

Combining these solutions with the advanced control techniques and algorithms described in Sections 3.3.1-3.3.5 can only increase the autonomy experienced by AUVs today. With increased autonomy we are creating the opportunity for new applications and tasks which can be carried out by the autonomous vessels.

Chapter 4

Geometric Control of Underwater Vehicles

As many may not be familiar with the geometric equations of motion presented in Section 2.4 or the use of these equations to model mechanical systems, we begin this chapter with a brief literature survey on the topic commonly referred to as geometric mechanics. Although this area has recently become an area of active interest, the foundations and beginnings were set in motion almost 30 years ago.

4.1 Literature Review

In the early stages, the geometric approach was a Hamiltonian viewpoint driven by its success with problems in dynamics. Introductory texts establishing the geometric groundwork in this area are Arnol'd (1978) and Abraham & Marsden (1978). From this base, an extensive amount of work has been done following the Hamiltonian point of view. Advancements along these lines can be found in Marsden (1992), Abraham & Ratiu (1999), van der Schaft (2000) and Dalsmo & van der Schaft (1998).

As research continued, the Lagrangian formulation surfaced as a preferred option. As the role of external forces and constraints in mechanical systems became more obvious, more research emphasis was directed toward this view. Under the Lagrangian setting, these external constraints arise more naturally. One reference, which derives geometric mechanics from first principles by use of the Lagrangian point of view, and is the foundation for

the research in this dissertation, is Bullo & Lewis (2005a). Other major contributors to the recent development of geometric modeling of mechanical systems include Anthony Bloch of the University of Michigan, Peter Crouch of the University of Hawaii, Naomi Leonard of Princeton University, P.S. Krishnaprasad of the University of Maryland, Monique Chyba of the University of Hawaii, Richard Murray of the California Institute of Technology, Jorge Cortés of the University of California, San Diego and Kevin Lynch of Northwestern University.

As the focus of this study is on the motion planning of an underwater vehicle, we turn now to examine recent literature on this specific issue with reference to a presentation in the formulation of geometric mechanics. As mentioned earlier, the foundations for this research begin with Bullo & Lewis (2005a). Early applications of geometric mechanics to autonomous underwater vehicles can be found in Leonard (1994), Leonard (1996) and Leonard (1997). These treatments utilize averaging techniques on the associated Lie group and produce periodic control structures. The applications of these techniques are also applicable to under-actuated systems.

An alternative approach is calculating kinematic controls for an under-actuated mechanical system as presented in Bullo & Lynch (2001). By use of a geometric reduction, the second-order system is reduced to a first-order, and solutions are found in the integral curves of certain vector fields. It is this approach which is the focus of the research contained in this dissertation.

4.2 Research Motivation and Direction

From the previous sections, it is obvious that the state of the art of AUV control is currently at a high level, however improvements can always be made. Each addition further enhances the autonomy of the vehicles and extends their capabilities. To this end, this dissertation examines an extension of low-level control results to create kinematically controlled trajectories which are implementable onto a test-bed AUV.

The motivation for this study began with the introduction of decoupling vector fields presented in Bullo & Lynch (2001) and with the expansion of this work in Bullo & Lewis (2005*b*). The first article presents the definitions and lays the foundation for the more detailed controllability results and motion planning techniques contained within the later reference as well as within the text of Bullo & Lewis (2005*a*). The geometric formulation and approach to the submerged rigid body problem not only allows for a kinematic reduction to a first-order system, but makes analysis of under-actuated systems quite simple from the motion planning perspective.

Controllability of these under-actuated systems, from a kinematic standpoint, is checked via the Lie bracket distribution, for which computations can be lengthy but are not difficult. For an under-actuated, controllable system, we decouple the trajectory planning between zero velocity states following the integral curves of decoupling vector fields. These vector fields are defined on the configuration space Q and define time scalable trajectories which do not violate the under-actuated constraints on the system. This method for trajectory

planning and design was first seen in Lynch et al. (1998) and Lynch et al. (2000) with application to a three degrees-of-freedom robot with a passive third joint.

When considering the motion planning problem in the case of an autonomous underwater vehicle, under-actuation is of major concern for many reasons. First of all, the vehicle needs to be prepared to deal with actuator failure(s) resulting from any number of mechanical issues. Secondly, since AUVs are limited by the power carried on-board, it may be beneficial to operate in an under-actuated, but fully controllable condition in an effort to conserve energy. Additionally, early consideration of these path planning results may assist in vehicle design to implement effective redundancy. Such consideration at the design stage could also aid in the construction of a fully controllable but under-actuated vehicle for more cost-effective applications.

Since this geometric formulation is model based, any symmetry and inherent geometric structure is exploited in the trajectory construction. For these reasons, along with the pure mathematical beauty of the geometric mechanics involved, we consider extending this theory to design and implement control strategies onto a test-bed AUV with six DOF.

The geometric theory as presented in the prior references presented in this section, with direct regard to the concepts of a kinematic reduction and decoupling vector fields, is not directly applicable for implementation onto a test-bed AUV. Current results have only been applied to drift-free affine connection control systems. As seen in Eqs. (2.80) - (2.86), we are presented with a forced affine connection control system describing the dynamics of a submerged rigid body. Hence, an extension of the current theory is necessary in real world applications.

In the following sections of this chapter, we define a kinematic reduction and decoupling vector field and present an extension of these definitions which incorporate dissipative forces. We then go on to describe the control strategy design in the presence of potential forces. In Chapter 5, we apply the trajectory design method to the Omni-Directional Intelligent Navigator (ODIN). We compute the decoupling vector fields for each of the under-actuated situations and calculate multiple control strategies which are implemented onto the vehicle. Experimental results from this implementation are presented in Chapter 6.

4.3 Kinematic Reduction

In this section, we present a formal definition and a characterization of a kinematic reduction. This geometric reduction reposes the second-order problem on Q (dynamic system) as a driftless, first-order system on Q (kinematic system), with the property that the controlled trajectories (i.e., solutions) of the reduced system are also controlled trajectories of the original second-order system. The dynamic system has a 12-dimensional state space (i.e., six positions and six velocities), and the control inputs are accelerations. The kinematic system uses velocity control inputs, and hence, the state space has half the dimension of the dynamic system. One advantage to the reduction in complexity of the system representation is the subsequent simplification of related control problems including stabilization, motion planning and optimal control.

Motivation for a reduction in complexity of the system representation is derived from previous efforts on general dynamic control systems including work on hybrid models for

motion control systems by Brockett (1993), oscillatory motion primitives by Bullo et al. (2000), consistent control abstractions by Pappas et al. (2000), hierarchical steering algorithms by McIsaac & Ostrowski (2001) and maneuver automata by Frazzoli et al. (2002).

First, we need a few preliminaries to distinguish between the different types of controls which will be considered for the two separate systems. As previously mentioned, the second-order system takes dynamic control inputs (accelerations), whereas the first-order system uses kinematic (velocity) control inputs. We demonstrate the need for this distinction by use of an example from Bullo & Lewis (2005a).

Example 4.1. Consider the simple mechanical system of a particle moving on a line under the influence of a control force. If we denote the configuration as x and the velocity as v , then the governing equations are:

$$\dot{x} = v, \quad \dot{v} = \frac{u}{m}, \quad (4.1)$$

where u is the input control force and $m > 0$ is the mass of the particle. If we suppose that u is locally integrable, and that we start at $t = 0$, then Eq. (4.1) is equivalent to the control system $\dot{x} = \tilde{u}$, where

$$\tilde{u}(t) = \frac{1}{m} \int_0^t u(s) ds. \quad (4.2)$$

Here we see that this simple system is reducible as long as the velocity input, \tilde{u} , is locally absolutely continuous. Note that the trajectories of the system $\dot{x} = \tilde{u}$ where \tilde{u} is only locally integrable are not realizable trajectories of Eq. (4.1) when the inputs are

bounded. Physically speaking, locally integrable velocity inputs imply that the velocity can change instantaneously, a phenomenon which is impossible with bounded controls due to the inertia of the system.

Now we are posed with two classes of systems; dynamic and kinematic. Both of these systems require the examination of different classes of inputs. The dynamic class of inputs includes functions $\sigma : [0, T] \rightarrow \mathbb{R}^m$ which are locally integrable and is denoted by \mathcal{U}_{dyn}^m . The kinematic class of inputs includes functions $\tilde{\sigma} : [0, T] \rightarrow \mathbb{R}^{\tilde{m}}$ which are locally absolutely continuous and is denoted by $\mathcal{U}_{kin}^{\tilde{m}}$. Note that $\mathcal{U}_{kin}^{\tilde{m}} \in \mathcal{U}_{dyn}^m$.

Definition 4.1 (Reparameterization). Given an interval $I \in \mathbb{R}$, a *reparameterization of I* is a map $\tau : J \rightarrow I$ with the properties

- i) τ is surjective
- ii) τ is either strictly increasing (i.e., $\tau(t_1) > \tau(t_2)$ if $t_1 > t_2$) or strictly decreasing (i.e., $\tau(t_1) < \tau(t_2)$ if $t_1 > t_2$), and
- iii) τ is locally absolutely continuous

If $\gamma : I \rightarrow Q$ is a locally absolutely continuous curve, a *reparameterization of γ* is a curve $\gamma \circ \tau : J \rightarrow Q$, where τ is a reparameterization of I .

Note that a reparameterization only alters the speed at which one travels along the curve, whereas the image of the reparameterized curve is the same as the original.

We denote an affine connection control system (dynamic) by $\Sigma_{dyn} = (Q, \nabla, \mathcal{Y}, \mathbb{R}^m)$. The associated driftless system (kinematic) is the triple $\Sigma_{kin} = (Q, \mathcal{X} = \{X_1, \dots, X_{\tilde{m}}\}, U)$, where $\mathcal{X} \in \Gamma^\infty(TQ)$, $U \subset \mathbb{R}^{\tilde{m}}$ and $\tilde{m} \leq 6$. This driftless system is associated to the affine

control system defined by

$$\gamma'(t) = \sum_{\alpha=1}^{\tilde{m}} \tilde{u}^\alpha(t) X_\alpha(\gamma(t)), \quad (4.3)$$

where a controlled trajectory is a pair (γ, \tilde{u}) such that

- i) $\gamma : I \rightarrow Q$ and $\tilde{u} : I \rightarrow U$ are both defined on the same interval $I \subset \mathbb{R}$,
- ii) \tilde{u} belongs to the class of kinematic inputs $\mathcal{U}_{kin}^{\tilde{m}}$
- iii) (γ, \tilde{u}) together satisfy Eq. 4.3.

We now have the tools to state the definition and characterization of a *kinematic reduction* for a controlled mechanical system. We will denote the distribution generated by \mathcal{Y} (resp. \mathcal{X}) by Y (resp. X).

Definition 4.2 (Kinematic reduction). Let $\Sigma_{dyn} = (Q, \nabla, \mathcal{Y}, \mathbb{R}^6)$ be a \mathcal{C}^∞ affine connection control system with Y having locally constant rank. A driftless system $\Sigma_{kin} = (Q, \mathcal{X}, \mathbb{R}^{\tilde{m}})$ ($\tilde{m} \leq 6$) is a *kinematic reduction* of Σ_{dyn} if

- i) X is a locally constant rank subbundle of TQ and if,
- ii) for every controlled trajectory (γ, u_{kin}) for Σ_{kin} , there exists u_{dyn} such that (γ, u_{dyn}) is a controlled trajectory of Σ_{dyn} .

The rank of the kinematic reduction Σ_{kin} at q is the rank of X at q .

Hence, we transform the motion planning problem into a first-order system on the configuration space by use of a kinematic reduction. The controlled trajectories for this new kinematic system are also controlled trajectories for Σ_{dyn} , with the exception of a possible reparameterization.

Now, given the assumption of locally constant rank, for an affine connection ∇ and a family of vector fields $\mathcal{Y} = \{Y_1, \dots, Y_m\}$ on Q we may define

$$B_{\mathcal{Y}}(S_q) : Y_q \times Y_q \rightarrow T_q Q / S_q \quad (4.4)$$

as the $T_q Q / S_q$ -valued symmetric-bilinear map on Y_q given by

$$B_{\mathcal{Y}_q}(S_q)(u, v) = \pi_{S_q}(\langle U : V \rangle(q)), \quad (4.5)$$

where $S_q \subset T_q Q$ is a subspace, U and V are vector fields extending $u, v \in Y_q$ and where $\pi_{S_q} : T_q Q \rightarrow T_q Q / S_q$ is the canonical projection. Using this map, we define a map $Q_{B_{\mathcal{Y}}} : \Gamma^\infty(TQ) \rightarrow \Gamma^\infty(TQ/\mathcal{Y})$ by

$$Q_{B_{\mathcal{Y}}}(X)(q) = B_{\mathcal{Y}}(q)(X(q), X(q)). \quad (4.6)$$

This allows us to characterize kinematic reductions with the following theorem. A proof of this result can be found in Bullo & Lewis (2005a).

Theorem 4.1 (Characterization of kinematic reductions). *Let $\Sigma_{dyn} = (Q, \nabla, \mathcal{Y}, \mathbb{R}^m)$ be a C^∞ -affine connection control system with \mathcal{Y} of locally constant rank and let $\Sigma_{kin} = (Q, \mathcal{X}, \mathbb{R}^{\tilde{m}})$ be a driftless system with \mathcal{X} of locally constant rank. The following statements are equivalent:*

- i) Σ_{kin} is a kinematic reduction of Σ_{dyn} ;

- ii) $Sym^{(1)}(\mathcal{X}) \subset Y$;
- iii) $X \subset Y$ and $Q_{B_Y}|_X = 0$.

Remark 4.1. As presented above, the definition and characterization of a kinematic reduction are only defined for an affine connection control system. Thus, the forced affine-connection control systems such as those given in Eqs. (2.87) and (2.86) do not have a kinematic reduction in the sense of Theorem 4.1.

4.3.1 Decoupling Vector Fields

Of particular interest and a main focus of this research are kinematic reductions of rank one. The rank of a kinematic reduction is the rank of the distribution generated by the input control vector fields for the kinematic system. Rank-one kinematic reductions are called decoupling vector fields and are of interest because they describe motions which are easy to implement onto underwater vehicles. Through the use of decoupling vector fields, we are also able to calculate implementable control strategies for under-actuated vehicles.

Given a rank one kinematic reduction $\Sigma_{kin} = (Q, X_1, \mathbb{R})$, we say that any vector field of the form $X = \phi X_1$, where $\phi \in C^\infty(Q)$ is nowhere vanishing, is a *decoupling vector field*. These are the vector fields with which we will plan the motion for our underwater vehicle. Theorem 4.1 gives us the following Corollary.

Corollary 4.1 (Characterization of decoupling vector fields). *A vector field $X \in \Gamma^\infty(TQ)$ is a decoupling vector field for Σ_{dyn} if and only if $X, \nabla_X X \in \Gamma^\infty(Y)$.*

Practically speaking, $X \in \Gamma^\infty(Y)$ ensures that the vehicle will be able to speed up and slow down while traveling along the integral curves of X , and $\nabla_X X \in \Gamma^\infty(Y)$ guarantees that motion along X at a constant velocity is feasible. Corollary 4.1 gives rise to the following definition of decoupling vector fields.

Definition 4.3 (Decoupling vector field). A *decoupling vector field* for an affine connection control system is a vector field V on Q having the property that every reparametrized integral curve for V is a trajectory for the affine connection control system. More precisely, let $\gamma : [0, S] \rightarrow Q$ be a solution for $\gamma'(s) = V(\gamma(s))$ and let $s : [0, T] \rightarrow [0, S]$ satisfy $s(0) = s'(0) = s'(T) = 0$, $s(T) = S$, $s'(t) > 0$ for $t \in (0, T)$, and $(\gamma \circ s)' : [0, T] \rightarrow TQ$ is absolutely continuous. Then $\gamma \circ s : [0, T] \rightarrow Q$ is a trajectory for the affine connection control system. Additionally, an integral curve of V is called a *kinematic motion* for the affine connection control system.

Note that in every case the zero vector field is a decoupling vector field since $\mathbf{0}$ and $\nabla_0 \mathbf{0}$ are both in \mathcal{I}_m^{-1} for all m . We omit the inclusion of this vector field in the computations in the sequel since the zero vector field has no application to the motion planning problem.

4.3.2 Under-Actuation

When we consider the scenario of an under-actuated underwater vehicle, we consider a control system which has less than six degrees-of-freedom. For an affine connection con-

trol system, the under-actuated vehicle is represented by

$$\nabla_{\gamma'} \gamma' = \sum_{a=1}^m \sigma^a(t) \tilde{\mathbb{I}}_a^{-1}(\gamma(t)), \quad (4.7)$$

where $\tilde{\mathbb{I}}_a^{-1} \in \mathcal{I}_m^{-1}$ for $m < 6$. Notice that if $\mathcal{I}_m^{-1} = \mathbb{I}^{-1} = TQ$ (i.e., Eq. (4.7) is fully-actuated) then every vector field is a decoupling vector field, and if \mathcal{I}^{-1} has rank $m = 1$ (i.e., (4.7) is single-input) then V is a decoupling vector field if and only if both V and $\nabla_V V$ are multiples of $\tilde{\mathbb{I}}_1^{-1}$. However, the situation is not as straightforward in other under-actuated scenarios. Here we assume that the body is unable to apply a force or torque in one or more of the six degrees-of-freedom, which in turn restricts the vehicle's controllability. This is very interesting since it is rather likely that an underwater vehicle loses actuator power for one reason or another but still needs to move. In particular, we would at least like the vehicle to be able to return home in a distressed situation. In the under-actuated setting, decoupling vector fields are found by solving a system of homogeneous quadratic polynomials in several variables. The details of this will be discussed in the next chapter with the application of this theory to the AUV ODIN.

4.4 Control Strategy Design Using Decoupling Vector Fields

We are now ready to discuss the procedure of motion planning via decoupled kinematic motions. We remark here that the method presented provides motion planning solutions for affine connection control systems only. These are control systems without an associ-

ated drift vector field. At the end of this section, we propose a method to handle systems with drift vector fields (e.g., restoring forces), such as the system given in Eq. (2.86). Additionally, we will assume that the given control system is under-actuated since, in the motion planning problem for a fully-actuated system, every vector field is decoupling.

First, we define the initial (η_{init}) and final (η_{final}) configurations of the system. We make the assumption that the initial configuration is the current vehicle configuration, or is realizable by the vehicle, otherwise the problem is not well stated. We do not put restrictions on the final configuration.

The trajectory design is based on what is commonly known in control literature as *motion planning by use of primitives*. This basically involves concatenating the integral curves of the calculated decoupling vector fields to create a realizable path connecting η_{init} and η_{final} . Determining whether or not the final configuration is reachable by use of only kinematic motions defined by the decoupling vector fields is not trivial. This condition is dependent upon the set of input control vector fields available as well as the final configuration. As a general result, we supply the following definition and proposition regarding the controllability of kinematic systems.

Definition 4.4. (Kinematic controllability) A C^∞ affine connection control system Σ_{dyn} is *kinematically controllable* if the system can reach any configuration $\eta_{final} \in SE(3)$ from any starting configuration $\eta_{init} \in SE(3)$ in finite time by using only kinematic motions.

This definition invokes the following proposition for computationally determining the kinematic controllability of a given system.

Proposition 4.1. *A C^∞ affine connection control system $\tilde{\Sigma}_{dyn}$ is kinematically controllable from a configuration $\eta_{init} \in \text{SE}(3)$ if there exists a finite collection*

$$\Sigma_{kin,1} = (Q, \mathcal{Z}_1, \mathbb{R}^{m_1}), \dots, \Sigma_{kin,k} = (Q, \mathcal{Z}_k, \mathbb{R}^{m_k})$$

of kinematic reductions for Σ_{dyn} such that

$\text{Lie}^{(\infty)}(\mathcal{Z}_1, \dots, \mathcal{Z}_k)_{\eta_{init}} = T_{\eta_{init}}Q$. Here, \mathcal{Z}_i represents the collection of input control vector fields to the kinematic system for each kinematic reduction and $\text{Lie}^{(\infty)}(W)$ is the involutive distribution generated by the family of vector fields W .

We refer the interested reader to Bullo & Lewis (2005a) for an overview of controllability results for mechanical systems which leads to this result.

Depending upon the actuation available to the vehicle, the system may not satisfy Proposition 4.1 but may still be able to realize a path from η_{init} to η_{final} by use of kinematic motions.

Example 4.2. Given an affine connection control system representing a neutrally buoyant, six degrees-of-freedom rigid body submerged in an ideal fluid with $C_G = C_B$ as presented in Eq. (2.55). Suppose that $Q = \text{SE}(3)$, $\eta_{init} = (0, 0, 0, 0, 0, 0)^t$, $\eta_{final} = (5, 0, 0, 0, 0, 0)^t$ and $\mathcal{I}_2^{-1} = \{\tilde{\mathbb{I}}_1^{-1}, \tilde{\mathbb{I}}_2^{-1}\} = \{\mathbb{I}_1^{-1}, \mathbb{I}_2^{-1}\}$. Then, the under-actuated scenario is expressed as

$$\nabla_{\gamma'} \gamma' = \sum_{i=1}^2 \tilde{\mathbb{I}}_i^{-1}(\gamma(t)) \sigma_i(t), \quad (4.8)$$

and the decoupling vector fields are given by $V_1 = \alpha \tilde{\mathbb{I}}_1^{-1}$ and $V_2 = \beta \tilde{\mathbb{I}}_2^{-1}$ for $\alpha, \beta \in \mathbb{R}$. The motion planning problem breaks down to being able to realize a pure surge of five units

when the vehicle only has direct control over surge and sway. It is clear that $\text{Lie}^{(\infty)}(\mathcal{I}_2^{-1}) \neq T_{\eta_{init}}Q$, and hence by Proposition 4.1, this system is not kinematically controllable. However, it is obvious that the motion can be realized by following the integral curves of V_1 .

Through this example, we see that although the system may not be kinematically controllable, we might still be able to design a path connecting η_{init} and η_{final} by use of only kinematic motions. We note that in general, the choice of kinematic motions may not be as obvious as in the example presented.

Once we have determined that the final configuration is reachable, we are ready to design the trajectory and control structure. Here we assume that we have a driftless affine-connection control system with associated decoupling vector fields $\{V_1, \dots, V_{\tilde{m}}\}$ for $\tilde{m} < 6$. Next we solve the motion planning problem by determining the sequence of integral curves of the decoupling vector fields (primitives) to follow to get from η_{init} to η_{final} . We then parameterize each segment to start and end at zero velocity so that each segment begins with the same initial conditions and we can concatenate these motions to build the entire trajectory. From this reparameterized, concatenated, kinematic motion trajectory, we can construct the dynamic controls which steer the vehicle between the initial and final configurations. With this heuristic blueprint in place, we now present the details of the construction.

Suppose that we have a C^∞ affine connection control system $\Sigma_{dyn} = (Q, \nabla, \mathcal{I}^{-1}, \mathbb{R}^m)$ that is either kinematically controllable, or the available actuation and final configuration allow for kinematic motion planning. Calculate the decoupling vector fields for the driftless

kinematic system $\Sigma_{kin} = (Q, \mathcal{V} = \{V_1, \dots, V_{\tilde{m}}\}, \mathbb{R}^{\tilde{m}})$. Let $\mathcal{F}_t^{V_i}$ represent the flow along the integral curve of the vector field V_i for a duration $[0, t]$. Set the initial configuration as η_{init} and the final configuration as η_{final} . Then, solve the kinematic motion planning problem by concatenating the flows of the decoupling vector fields from η_{init} to η_{final} by finding $k \in \mathbb{N}$, $a_1, \dots, a_k \in \{1, \dots, \tilde{m}\}$, $t_1, \dots, t_k \in \mathbb{R}^+$ and $\epsilon_1, \dots, \epsilon_k \in \{1, -1\}$ such that:

$$\mathcal{F}_{t_k}^{\epsilon_k V_{a_k}} \circ \dots \circ \mathcal{F}_{t_1}^{\epsilon_1 V_{a_1}}(\eta_{init}) = \eta_{final}. \quad (4.9)$$

Define $\bar{\eta}_{init} = \eta_{init}$ and $\bar{\eta}_j = \mathcal{F}_{t_j}^{\epsilon_j V_{a_j}} \circ \dots \circ \mathcal{F}_{t_1}^{\epsilon_1 V_{a_1}}(\eta_{init})$ for $j \in \{1, \dots, k\}$. For each $j \in \{1, \dots, k\}$, choose a C^2 -reparameterization $\tau_j : [0, \bar{t}_j] \rightarrow [0, t_j]$ such that $\tau'(0) = \tau'(\bar{t}_j) = 0$ so that the kinematic motion begins and ends at rest. Define $\gamma : [0, t_j] \rightarrow Q$ as the integral curve $t \mapsto \mathcal{F}_t^{\epsilon_j V_{a_j}}$. Then the dynamic control $\sigma_j : [0, \bar{t}_j] \rightarrow \mathbb{R}^m$ is defined by

$$\sigma^\alpha(t) \mathbb{I}_\alpha^{-1}(\gamma \circ \tau(t)) = (\tau'(t))^2 \nabla_{V_{a_j}} V_{a_j}(\gamma \circ \tau(t)) + \tau''(t) V_{a_j}(\gamma \circ \tau(t)), \quad (4.10)$$

where Einstein's summation convention is used on the variable α . By letting $u : [0, T] \rightarrow \mathbb{R}^m$ be the control formed by the concatenation of $\sigma_1, \dots, \sigma_k$, (γ, u) is then a controlled trajectory for Σ_{dyn} . This general method of calculating the controls for a dynamic system following decoupling vector fields was taken from Bullo & Lewis (2005a) and is adapted for our specific application.

As presented, this technique allows us to calculate a control strategy for a drift-free affine connection control system similar to the one in Eq. (2.55). Under the assumptions

for the system in Eq. (2.55), we consider a neutrally buoyant rigid body submerged in an ideal fluid with $C_G = C_B$. Hence, there are no external forces acting on the system, and thus we have a driftless system. To calculate the controls for a system such as that given in Eq. (2.80), we need to find a way to deal with the drift vector fields.

In light of the construction of $\tilde{\nabla}$ presented in Section 2.4.5, we can extend this control design technique to compensate for dissipative forces experienced in a viscous fluid. If we replace the Levi-Civita affine connection ∇ with the affine connection $\tilde{\nabla}$ in the Eq. (4.10), we are able to compute the dynamic controls for the affine connection control system given in Eq. (2.88). Since the forces and moments resulting from viscous drag are incorporated into the affine connection, Eq. (2.88) is a drift-free affine connection control system, and the previously presented control design technique is applicable.

Here we see that with the design of the affine connection $\tilde{\nabla}$, we were able to extend the current kinematic control theory to include dissipative forces experienced in a viscous fluid. The control strategy design is exactly the same, except that in calculating the dynamic controls, we use $\tilde{\nabla}$ instead of the Levi-Civita affine connection. Thus, the characterization of a kinematic reduction remains as presented earlier and hence the definition of a decoupling vector field does not change either. There is a slight modification with regard to the calculation of decoupling vector fields for the system, however, that is handled within the calculation of the covariant derivative and does not affect the method in which we calculate the dynamic controls for the trajectory.

The extension of this control-design method to include forces arising from a potential function such as gravity and buoyancy must be handled in a different way. Since these

forces do not depend on time, velocity or acceleration of the body, they can not be handled within the affine connection. Many methods have been tried to modify the kinematic reduction in an attempt to include potential forces without any success. The essence of the natural kinematic reduction presented relies on the reduced system being driftless. Since the potential forces are based on physical characteristics of the rigid body (placement of C_B with respect to C_G and angular displacement) under certain conditions, a drift will always exist in the reduced system. Hence, a general theory along these lines is a very difficult problem and remains an open question.

Since the inclusion of the potential forces within the kinematic reduction has eluded us, we sought out different methods to account for these forces. As the main goal of this research is to successfully implement trajectories developed from geometric control theory by use of a kinematic reduction technique, we turned to the experiments for assistance.

Neglecting potential forces, we designed control strategies by use of the method described earlier. Since the test-bed vehicle is slightly positively buoyant, each of these strategies was subjected to the potential force of buoyancy. Some trajectories were designed to perform, and maintain, pitch and roll displacements which subjected the body to righting moments, since $C_B \neq C_G$ on the test-bed vehicle. Experimental results showed that the designed control strategies correctly maneuvered the vehicle to the desired location with two exceptions. The first exception is that the small ($\approx 1.3\text{N}$) net buoyancy force had noticeable effect when the vehicle did not realize any heave displacement. When a heave displacement was prescribed during a given trajectory, the buoyancy force had little to no effect. We make note that when prescribed, the control force in heave was a full order

of magnitude larger than the 1.3N buoyancy force which is the main reason we observe a negligible effect of the buoyancy for these types of evolutions. Detailed results are presented and discussed in Chapter 6. The second exception is related to the induced righting moments when the prescribed trajectory required the vehicle to maintain a pitch and/or roll angle. Experiments showed that the control strategy correctly oriented the vehicle to the appropriate angle, but the righting moments quickly brought the vehicle back to its equilibrium position. Again, we present and discuss these implemented experiments in detail in Chapter 6.

During the general operation of an underwater vehicle, environmental and mechanical disturbances will cause the vehicle to deal with induced forces and moments arising from changes in pitch and roll. By design, the vehicle should be robust enough to limit these small perturbations with the stability provided by the righting arm of the vessel. Preparing or correcting for these minor disturbances over the duration of a trajectory is not the focus of the path planning and control design contained within this dissertation. Here we present a method for the compensation of restoring forces which are known or estimated *a priori*. These include the constant buoyant force on the vehicle, forces and moments induced via the request to maintain a given pitch and/or roll angle and constant currents.

We further assert that since the control strategies are constructed for full open-loop implementation, it is impossible to adjust for unforeseen disturbances without using a feedback loop. As this research is dedicated to providing solutions to the motion planning problem and not to trajectory tracking, we consider only those restoring forces mentioned above. With this understanding of the type of restoring forces and moments considered, we

continue presenting a method to include them into the geometric framework of kinematic motion planning.

Many control strategies which neglected all restoring forces and moments were designed and implemented onto the test-bed vehicle. The vehicle's behavior and performance during these experiments lead us to consider an *ad hoc* method for compensating for the restoring forces and moments. We consider the addition of the potential forces and moments into the dynamic controls after they have been calculated by use of the kinematic reduction technique described earlier. Since the issue comes in maintaining a prescribed inclination angle or compensating for a constant buoyancy factor; $g(\eta)$ does not depend on time while the angle is maintained. By computing $g(\eta)$ for $\mathcal{F}_t^{\epsilon_j V_{a_j}}$ for each $j \in \{1, \dots, k\}$, we then have the restoring forces and moments for each concatenated section, call them $g_j(\eta)$. By adding $g_j(\eta)$ to $u_j(t)$ we get the dynamic controls including restoring forces and moments. The only adjustment to the control design procedure described above is that $\tau(t)$ must still be at least C^2 and we must guarantee that $\tau''(\bar{t}_j) = 0$ when kinematic motion involving a pitch or roll is followed. Experimental implementations of such trajectories matched well with theoretical predictions and details are presented in Chapter 6.

Since an angular displacement invokes forces in other degrees-of-freedom (see Eq. (2.79)), an under-actuated vehicle may not be able to apply the actual computed controls. This issue is discussed in Section 5.5 when we compute the controls for implementation.

Remark 4.2. As a closure to this section, we would like to make a few remarks regarding the reparameterization along the kinematic motions. Since the speed along a given inte-

gral curve can arbitrarily be chosen, the parameterization thus depends upon the physical bounds of the thrusters or actuators of the vehicle. Additionally, with different choices of $\tau(t)$, we can somewhat control the time and energy efficiency of the vehicle over the duration of a given path. Note, however, that if the realization of the path requires the concatenation of two or more integral curves, we can never achieve time optimality along that path. This fact is because the concatenation is made through states of zero velocity, and it is obvious that such a strategy can never be time optimal.

Chapter 5

Application to the Omni-Directional intelligent Navigator

5.1 Omni-Directional Intelligent Navigator (ODIN)

The test-bed vehicle used to conduct the research for this dissertation is the Omni-Directional Intelligent Navigator (ODIN), shown in Figs. 9, 10 and 11. ODIN is an AUV which is owned by the Autonomous Systems Laboratory (ASL), College of Engineering, University of Hawaii. The vehicle's main body is a 0.64m diameter sphere made of anodized aluminum (AL 6061-T6). Eight Tecnydyne brushless thrusters are attached to the sphere via four fabricated mounts, each holding two thrusters. These thrusters are evenly distributed around the sphere with four oriented vertically and four oriented horizontally. The placement of these thrusters is shown in Fig. 11.

Fully assembled, ODIN's mass is 123.8 kg and she is positively buoyant by 1.3N. ODIN is capable of unbiased movement in six degrees-of-freedom from either a tethered or autonomous mode. The numerical values of additional various parameters used for modeling ODIN are given in Table 3. These values were derived from estimations and experiments performed on ODIN. The added mass and drag terms were estimated from formulas found in Allmendinger (1990) and Imlay (1961). The details of the estimation of the drag coefficients are contained in Appendix B.1. We do not list the drag coefficients used since the

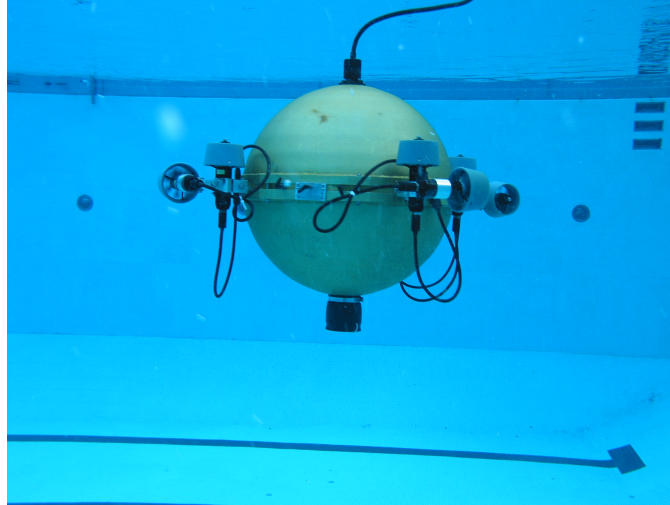


Figure 9: ODIN operating in the pool.

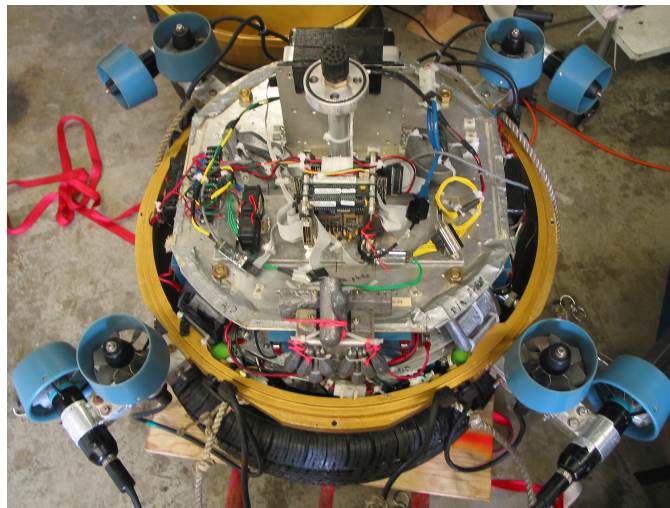


Figure 10: An inside look at ODIN.

value depends upon the reparameterization $\tau(t)$ in the computation of the controls and is different for each experiment. Moments of inertia were calculated using experiments outlined in Bhattacharyya (1978). We used inclining experiments to locate C_G , which we take as the center of our body-fixed reference frame (i.e., $C_G = O_B$). Due to the symmetry of the vehicle, the center of buoyancy C_B , is assumed to be the center of the spherical body of ODIN. The location of C_B is measured from $C_G = O_B$, and is given in Table 3. Along with

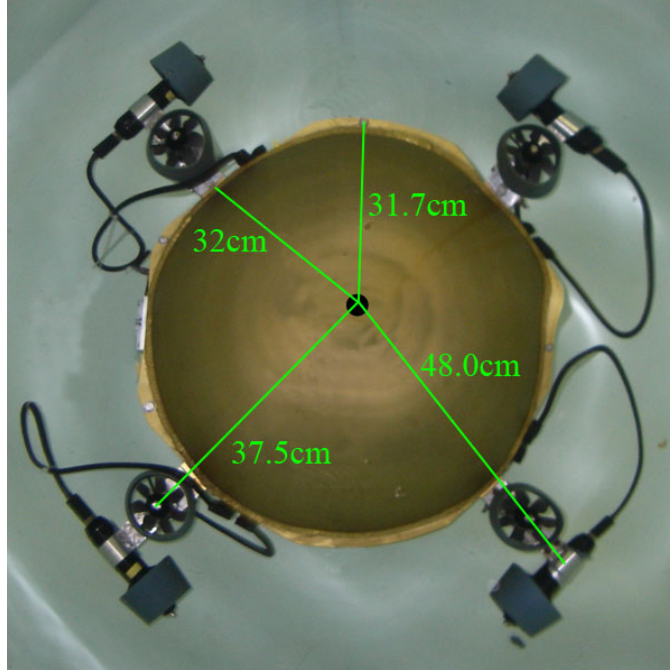


Figure 11: Main external dimensions of ODIN.

Mass	123.8 kg	$B = \rho g \mathcal{V}$	1215.8 N	C_B	(0, 0, -7) mm
Diameter	0.64 m	$W = mg$	1214.5 N	C_G	(0, 0, 0) mm
$M_f^{\nu_1}$	70 kg	$M_f^{\nu_2}$	70 kg	$M_f^{\nu_3}$	70 kg
I_{xx}	5.46kg m ²	I_{yy}	5.29kg m ²	I_{zz}	5.72kg m ²
$J_f^{\Omega_1}$	0kg m ²	$J_f^{\Omega_2}$	0kg m ²	$J_f^{\Omega_3}$	0kg m ²

Table 3: Main dimensions and hydrodynamic parameters for ODIN.

the tests to determine the values in Table 3, we also tested the thrusters. Each thruster has a unique voltage input to power output relationship. This relationship is highly nonlinear and is approximated using a piecewise linear function which we refer to as our thruster model. More information regarding the thruster modeling can be found in Appendix B.2

For the experiments in this dissertation, ODIN was operated from a tethered configuration, but the tether was only used to send commands to be run in autonomous mode. This setup allows for multiple tests to be conducted without removing ODIN from the water to

upload mission sorties, and allows for ODIN to be immediately shut down in the event of an emergency.

To reduce the dynamic effects of the tether upon ODIN's movement, it was fixed to the rear and bottom of the vehicle with excess slack allowed to gather at the bottom of the pool. Many different configurations were examined and a detailed discussion on this topic can be found in Chyba et al. (2008b). The three main configurations analyzed are shown in Fig. 12, with the implemented configuration displayed in the image on the far left of the figure.

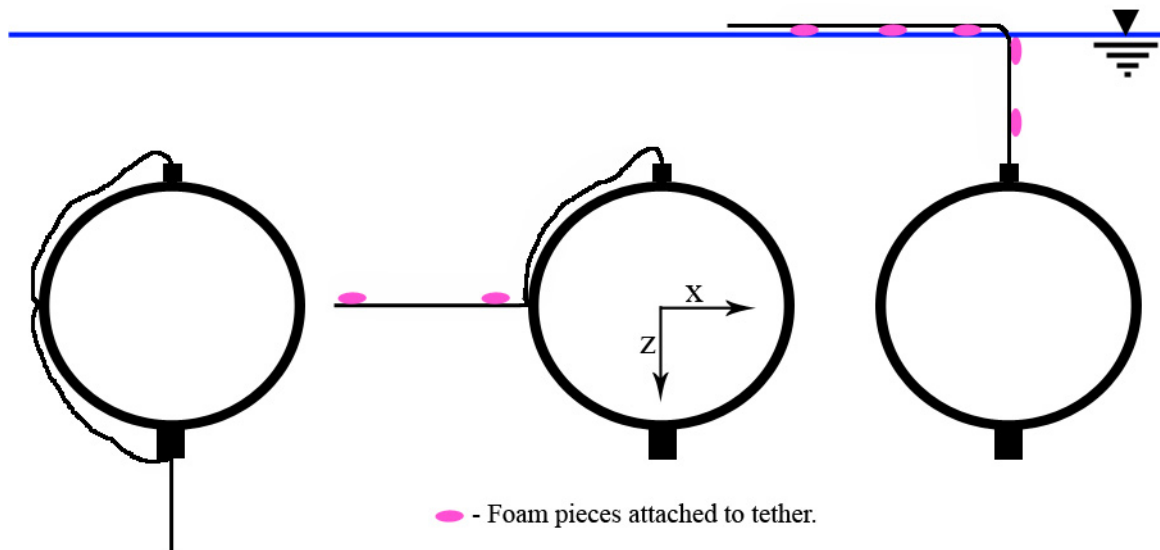


Figure 12: Configurations for tether attachment to ODIN.

ODIN's internal CPU is a 800 MHz Intel based processor running on a PC104+ form factor with two external I/O boards providing A/D and D/A operations. The software is divided into two components. The first component is based on a real time extension to the Windows 2000 operating system, which provides ODIN real time autonomous control. The second component runs on the remote laptop and allows the operator to upload autonomous mission profiles to ODIN on the fly during testing, as well as monitor ODIN in real time

during such missions. The communication from ODIN to the remote laptop is via a RS232c serial protocol.

Major internal components include a pressure sensor, inertial measurement unit, leakage sensor, heat sensor and 24 batteries (20 for the thrusters and four for the CPU). ODIN is able to compute and communicate real time, yaw, pitch, roll, and depth and can run autonomously for up to five hours.

ODIN does not have real time sensors to detect horizontal ($x - y$) position. Instead, experiments are videotaped from a platform 10m above the water's surface, giving us a near nadir view of ODIN's movements. Videos are saved and horizontal position data are post-processed for later analysis. A real-time system utilizing sonar was available on ODIN, but was abandoned for two main reasons. First, the sonar created too much noise in the diving well and led to inaccuracies. More significantly, in the implementation of our control strategies, ODIN is often required to achieve large ($> 15^\circ$) list angles which render the sonars useless for horizontal position. Many alternative solutions were attempted and video provided a cost-effective solution which produced accurate results. We are able to determine ODIN's relative position in the testing pool to ± 10 cm.

Unique to ODIN's construction is the control from an eight dimensional thrust to move in six degrees-of-freedom. To calculate the six-dimensional thrust σ resulting from the eight-dimensional thrust ζ (from the thrusters), or vice-versa, we need to apply a linear transformation to ζ . Since the separation between C_G and C_B is small with respect to the diameter of ODIN, we can decouple the action of the four vertical and four horizontal thrusters. We assume that the vertical thrusters only contribute to the heave, pitch and

roll, while the horizontal thrusters are responsible for surge, sway and yaw. Thus, we can decouple the transformation into two linear transformations from \mathbb{R}^4 to \mathbb{R}^3 which are given by the following Thrust Conversion Matrices (TCM's).

$$\text{TCMhorizontal} = \begin{bmatrix} -0.707 & 0.707 & 0.707 & -0.707 \\ 0.707 & 0.707 & -0.707 & -0.707 \\ 0.48160 & -0.48160 & 0.48160 & -0.48160 \end{bmatrix} \quad (5.1)$$

$$\text{TCMvertical} = \begin{bmatrix} -1.0 & -1.0 & -1.0 & -1.0 \\ -0.26989 & -0.26989 & 0.26989 & 0.26989 \\ 0.26989 & -0.26989 & -0.26989 & 0.26989 \end{bmatrix} \quad (5.2)$$

The input control strategies to ODIN take the form of the six degree of freedom controls which are converted onboard ODIN to the eight actual thrusters using the pseudo-inverse of the TCMs.

ODIN's thruster configuration puts redundancy into the system in case of actuator failure or need to conserve energy. ODIN is able to operate in an *under-actuated* condition if necessary, and this is one of the main topics addressed through the design of control strategies using the procedures outlined in this dissertation. The fact that ODIN is controlled by eight thrusters and the controls are designed using six input control vector fields does lead to a some ambiguity in the definition of under-actuated. However, this is not the case for the missions presented in this dissertation. A control strategy design using eight input vector fields is discussed in Section 7.1.

5.2 Calculated Decoupling Vector Fields

In Chapter 4, we discussed the motivation and construction of control strategies developed by use of a kinematic reduction procedure for an under-actuated, submerged rigid body. Since the goal of this research is to merge theory and application with regard to the motion planning problem for underwater vehicles, we use the data presented in the previous sections to design control strategies for ODIN.

The first step is to calculate the decoupling vector fields which will define the admissible kinematic motions. Here we will present the method of calculation of decoupling vector fields for every under-actuated scenario. We note that under-actuation here refers to the loss of one or more degrees of freedom which is different from the loss of a physical actuator or thruster.

Since we consider the under-actuated scenario, we are dealing with the case where the input control vector fields are a proper subset of $\mathbb{I}^{-1} = \{\mathbb{I}_1^{-1}, \dots, \mathbb{I}_6^{-1}\}$. We refer to the set of input control vector fields to the under-actuated system as $\mathcal{I}_m^{-1} = \{\tilde{\mathbb{I}}_1^{-1}, \dots, \tilde{\mathbb{I}}_m^{-1}\}$ for $m < 6$, where the $\tilde{\cdot}$ signifies a reindexing of $\mathbb{I}_i^{-1} \in \mathbb{I}^{-1}$. With these vector fields as inputs, the equations of motion for an under-actuated ODIN are given by the following affine connection control system:

$$\tilde{\nabla}_{\gamma'} \gamma' = \sum_{i=1}^m \tilde{\mathbb{I}}_i^{-1}(\gamma(t)) \sigma_i(t). \quad (5.3)$$

Remember here that we are neglecting the potential forces while applying the kinematic

reduction and computing the decoupling vector fields. We will include these forces when we consider the final control design. Now we concern ourselves only with the computation of the decoupling vector fields for each under-actuated scenario.

5.2.1 Covariant derivatives

From Corollary 4.1, we see that to calculate decoupling vector fields, we must be able to calculate the covariant derivative of one vector field with respect to another. This section is devoted to such calculations. For the remainder of the dissertation, we assume that $\{X_1, \dots, X_6\}$ is the standard basis for $SE(3) = \mathbb{R}^3 \times SO(3)$. Thus, we will use the indices 1, 2 and 3 to correspond to the translational inputs, while 4, 5 and 6 correspond to the rotational inputs.

As mentioned in Section 4.7, decoupling vector fields are found by solving a system of homogeneous polynomials in several variables. We now explain and expand upon that statement. We first present a general method for the calculation of decoupling vector fields for an arbitrary affine connection ∇ . After it is clear how the procedure works, we calculate the decoupling vector fields for ODIN by use of the affine connection $\tilde{\nabla}$ developed in Section 2.87.

Given a set of input vector fields $\mathcal{Z} = \{Z_1, \dots, Z_m\}$ and using Corollary 4.1, we know that, for a vector field V to be decoupling, we must have $V = \sum_{a=1}^m h^a Z_a$ for $h^a \in \mathbb{R}$ since we must have $V \in \text{Span} \{Z_1, \dots, Z_m\}$. Now, since we must also guarantee $\nabla_V V \in$

Span $\{Z_1, \dots, Z_m\}$, we want

$$\nabla_V V = \nabla_{\sum h^a Z_a} \sum h^b Z_b \equiv 0 \pmod{\mathcal{Z}}. \quad (5.4)$$

Starting with the middle of the above equation, we get that

$$\begin{aligned} \nabla_{\sum h^a Z_a} \sum h^b Z_b &= \sum h^a \nabla_{Z_a} \sum h^b Z_b = \sum \sum h^a \nabla_{Z_a} (h^b Z_b) \\ &= \sum \sum h^a [Z_a(h^b) Z_b + h^b \nabla_{Z_a} Z_b] \\ &\equiv \sum \sum h^a h^b \nabla_{Z_a} Z_b \pmod{\mathcal{Z}} \\ &\equiv \frac{1}{2} \sum \sum h^a h^b (\nabla_{Z_a} Z_b + \nabla_{Z_b} Z_a) \pmod{\mathcal{Z}}. \end{aligned} \quad (5.5)$$

Thus, we are concerned with calculating $\nabla_{Z_a} Z_b$ for $a, b \in \{1, \dots, m\}$ to find the coefficients h^1, \dots, h^m such that V is decoupling.

To calculate $\nabla_{Z_a} Z_b$, we use the following equation

$$\begin{aligned} \mathbb{G}(\nabla_{Z_a} Z_b, X_m) &= \\ \frac{1}{2} [\mathcal{L}_{Z_a}(\mathbb{G}(Z_b, X_m)) + \mathcal{L}_{Z_b}(\mathbb{G}(X_m, Z_a)) - \mathcal{L}_{X_m}(\mathbb{G}(Z_a, Z_b))] & \quad (5.6) \\ + \mathbb{G}([Z_a, Z_b], X_m) - \mathbb{G}([Z_a, X_m], Z_b) - \mathbb{G}([Z_b, X_m], Z_a), & \end{aligned}$$

where $\mathbb{G}(Z_i, Z_j) = Z_i^t \mathbb{G} Z_j$ is the inner product which represents the kinetic energy metric on $SE(3)$. For any left-invariant frame field Z_1, \dots, Z_m on $SE(3)$, the Lie derivative $\mathcal{L}_*(\mathbb{G}(*, *)) = 0$, so we need to calculate only the last three terms in Eq. (5.6). To calculate these terms, we need to know how to calculate the Lie bracket of vector fields. We pro-

vide a brief overview of this computation and refer the interested reader to a more detailed treatment contained in Appendix A and the references contained therein.

Since our configuration space is the Lie group $SE(3)$, the linear space of body-fixed velocities is represented by the Lie algebra $\mathfrak{se}(3)$:

$$\mathfrak{se}(3) = \left\{ \begin{bmatrix} 0 & 0 \\ \nu & \hat{\Omega} \end{bmatrix} \mid \nu \in \mathbb{R}^3, \Omega \in \mathbb{R}^3 \right\}, \quad (5.7)$$

where ν represents the translational velocities and Ω represents the rotational velocities. In this Lie algebra, we know that

$$\left[\begin{bmatrix} 0 & 0 \\ \nu_1 & \hat{\Omega}_1 \end{bmatrix}, \begin{bmatrix} 0 & 0 \\ \nu_2 & \hat{\Omega}_2 \end{bmatrix} \right] = \begin{bmatrix} 0 & 0 \\ \hat{\Omega}_1 \nu_2 - \hat{\Omega}_2 \nu_1 & \hat{\Omega}_1 \hat{\Omega}_2 - \hat{\Omega}_2 \hat{\Omega}_1 \end{bmatrix}, \quad (5.8)$$

and since $\mathfrak{se}(3) \cong \mathbb{R}^3 \times \mathbb{R}^3 \ni (\nu, \Omega)$, we can write

$$[(\nu_1, \Omega_1), (\nu_2, \Omega_2)] = (\Omega_1 \times \nu_2 - \Omega_2 \times \nu_1, \Omega_1 \times \Omega_2). \quad (5.9)$$

Thus, we can define the adjoint operator $\text{ad}_{(\nu, \Omega)} : \mathfrak{se}(3) \rightarrow \mathfrak{se}(3)$ as

$$\text{ad}_{(\nu_1, \Omega_1)}(\nu_2, \Omega_2) = [(\nu_1, \Omega_1), (\nu_2, \Omega_2)], \quad (5.10)$$

which can be written as the matrix operator: $\text{ad}_{(\nu, \Omega)} = \begin{bmatrix} \hat{\Omega} & \hat{\nu} \\ 0 & \hat{\Omega} \end{bmatrix}$.

Next, we define the adjoint operator for each vector field in $\{X_1, \dots, X_6\}$. Here, remember that indices 1, 2 and 3 correspond to the translational inputs (ν), while 4, 5 and 6 correspond to the rotational inputs (Ω).

$$\text{ad}_{X_1} = \begin{bmatrix} 0 & 0 & 0 & 0 & 0 & 0 \\ 0 & 0 & 0 & 0 & 0 & -1 \\ 0 & 0 & 0 & 0 & 1 & 0 \\ 0 & 0 & 0 & 0 & 0 & 0 \\ 0 & 0 & 0 & 0 & 0 & 0 \\ 0 & 0 & 0 & 0 & 0 & 0 \end{bmatrix} \quad (5.11)$$

$$\text{ad}_{X_2} = \begin{bmatrix} 0 & 0 & 0 & 0 & 0 & 1 \\ 0 & 0 & 0 & 0 & 0 & 0 \\ 0 & 0 & 0 & -1 & 0 & 0 \\ 0 & 0 & 0 & 0 & 0 & 0 \\ 0 & 0 & 0 & 0 & 0 & 0 \\ 0 & 0 & 0 & 0 & 0 & 0 \end{bmatrix} \quad (5.12)$$

$$\text{ad}_{X_3} = \begin{bmatrix} 0 & 0 & 0 & 0 & -1 & 0 \\ 0 & 0 & 0 & 1 & 0 & 0 \\ 0 & 0 & 0 & 0 & 0 & 0 \\ 0 & 0 & 0 & 0 & 0 & 0 \\ 0 & 0 & 0 & 0 & 0 & 0 \\ 0 & 0 & 0 & 0 & 0 & 0 \end{bmatrix} \quad (5.13)$$

$$\text{ad}_{X_4} = \begin{bmatrix} 0 & 0 & 0 & 0 & 0 & 0 \\ 0 & 0 & -1 & 0 & 0 & 0 \\ 0 & 1 & 0 & 0 & 0 & 0 \\ 0 & 0 & 0 & 0 & 0 & 0 \\ 0 & 0 & 0 & 0 & 0 & -1 \\ 0 & 0 & 0 & 0 & 1 & 0 \end{bmatrix} \quad (5.14)$$

$$\text{ad}_{X_5} = \begin{bmatrix} 0 & 0 & 1 & 0 & 0 & 0 \\ 0 & 0 & 0 & 0 & 0 & 0 \\ -1 & 0 & 0 & 0 & 0 & 0 \\ 0 & 0 & 0 & 0 & 0 & 1 \\ 0 & 0 & 0 & 0 & 0 & 0 \\ 0 & 0 & 0 & -1 & 0 & 0 \end{bmatrix} \quad (5.15)$$

$$\text{ad}_{X_6} = \begin{bmatrix} 0 & -1 & 0 & 0 & 0 & 0 \\ 1 & 0 & 0 & 0 & 0 & 0 \\ 0 & 0 & 0 & 0 & 0 & 0 \\ 0 & 0 & 0 & 0 & -1 & 0 \\ 0 & 0 & 0 & 1 & 0 & 0 \\ 0 & 0 & 0 & 0 & 0 & 0 \end{bmatrix} \quad (5.16)$$

These matrices allow us to calculate Lie brackets via matrix multiplication of elements in the Lie algebra. We list the results here for each of the six basis vectors:

$$[X_1, X_k] = \text{ad}_{X_1} X_k = \begin{cases} 0 & k = 1, 2, 3, 4 \\ X_3 & k = 5 \\ -X_2 & k = 6 \end{cases} \quad (5.17)$$

$$[X_2, X_k] = \text{ad}_{X_2} X_k = \begin{cases} 0 & k = 1, 2, 3, 5 \\ -X_3 & k = 4 \\ X_1 & k = 6 \end{cases} \quad (5.18)$$

$$[X_3, X_k] = \text{ad}_{X_3} X_k = \begin{cases} 0 & k = 1, 2, 3, 6 \\ X_2 & k = 4 \\ -X_1 & k = 5 \end{cases} \quad (5.19)$$

$$[X_4, X_k] = \text{ad}_{X_4} X_k = \begin{cases} 0 & k = 1, 4 \\ X_3 & k = 2 \\ -X_2 & k = 3 \\ X_6 & k = 5 \\ -X_5 & k = 6 \end{cases} \quad (5.20)$$

$$[X_5, X_k] = \text{ad}_{X_5} X_k = \begin{cases} 0 & k = 2, 5 \\ -X_3 & k = 1 \\ X_1 & k = 3 \\ -X_6 & k = 4 \\ X_4 & k = 6 \end{cases} \quad (5.21)$$

$$[X_6, X_k] = \text{ad}_{X_6} X_k = \begin{cases} 0 & k = 3, 6 \\ X_2 & k = 1 \\ -X_1 & k = 2 \\ X_5 & k = 4 \\ -X_4 & k = 5 \end{cases} \quad (5.22)$$

Remembering from Eq. (2.48) that the kinetic energy metric for this system is given by

$$\mathbb{G} = \text{diag}(m_1, m_2, m_3, j_1, j_2, j_3), \quad (5.23)$$

where $m_i = m + M_f^{\nu_i}$ and $j_i = J_{b_i} + J_f^{\Omega_i}$, we are equipped to calculate Eq. (5.6) and the covariant derivative between the two input vector fields.

5.2.2 One-input systems

For each under-actuated setting, we will calculate the decoupling vector fields based on the available number of degrees of freedom; a one-input system can be controlled in only one degree-of-freedom. Since our results depend on the symmetries of the rigid body, we introduce the following terminology.

Definition 5.1 (Kinetically unique). We will call our system *kinetically unique* if all the eigenvalues in the kinetic energy metric \mathbb{G} are distinct. In particular, the added mass $m_i = m + M_f^{\nu_i}$, and added moment of inertia $j_i = J_{b_i} + J_f^{\Omega_i}$ coefficients are all distinct. Unless otherwise stated, we will assume that all systems are kinetically unique.

We also introduce $\mathcal{U} = \{1, 2, 3\}$ and $\mathcal{V} = \{4, 5, 6\}$ ⁷. We refer to $\mathbb{I}_i^{-1}, i \in \mathcal{U}$ as a translational control vector field and $\mathbb{I}_j^{-1}, j \in \mathcal{V}$ a rotational control vector field.

Now, let us first discuss the degenerate situation of ODIN in an ideal fluid controlled by only a single input vector field: ($m = 1$). This can also be viewed as a loss of 5 degrees

⁷Here we abuse notation and reuse the variable \mathcal{V} which was previously defined as the submerged volume of a vessel. Due to the distinct nature of each object, there will be no confusion between their usage, as the definition will be clear from context.

of freedom. The single input geometric acceleration is given by

$$\nabla_{\gamma'} \gamma' = \tilde{\mathbb{I}}_1^{-1}(\gamma(t))\sigma(t), \quad (5.24)$$

for $\tilde{\mathbb{I}}_1^{-1} \in \mathcal{I}_1^{-1}$, and $\sigma(t)$ is the control force. Since there is only one input vector, we are only interested in calculating $\nabla_{\tilde{\mathbb{I}}_1^{-1}} \tilde{\mathbb{I}}_1^{-1}$. Hence, Eq. (5.6) becomes

$$\begin{aligned} \mathbb{G}(\nabla_{\tilde{\mathbb{I}}_1^{-1}} \tilde{\mathbb{I}}_1^{-1}, X_k) = \\ \frac{1}{2} [\mathbb{G}([\tilde{\mathbb{I}}_1^{-1}, \tilde{\mathbb{I}}_1^{-1}], X_k) - \mathbb{G}([\tilde{\mathbb{I}}_1^{-1}, X_k], \tilde{\mathbb{I}}_1^{-1}) - \mathbb{G}([\tilde{\mathbb{I}}_1^{-1}, X_k], \tilde{\mathbb{I}}_1^{-1})]. \end{aligned} \quad (5.25)$$

The first term on the right-hand-side, $\mathbb{G}([\tilde{\mathbb{I}}_1^{-1}, \tilde{\mathbb{I}}_1^{-1}], X_k)$ is zero because $[\tilde{\mathbb{I}}_1^{-1}, \tilde{\mathbb{I}}_1^{-1}] = 0$ since the input control vector fields are constant. The next two terms are identical since we are only considering one input vector field. These two terms are zero since $\tilde{\mathbb{I}}_1^{-1} = \mathbb{I}_i^{-1} = \alpha X_i$ for $\alpha \in \mathbb{R}$ and $i \in \{1, \dots, 6\}$ which implies that $[\tilde{\mathbb{I}}_1^{-1}, X_k] = 0$ for $k = i$. Thus, $\mathbb{G}([\tilde{\mathbb{I}}_1^{-1}, X_k], \tilde{\mathbb{I}}_1^{-1}) = \mathbb{G}([X_i, X_k], X_i) = [0, 0, 0, 0, 0, 0]$. This gives us

$$\mathbb{G}(\nabla_{\tilde{\mathbb{I}}_1^{-1}} \tilde{\mathbb{I}}_1^{-1}, X_k) = \begin{bmatrix} 0 \\ 0 \\ 0 \\ 0 \\ 0 \\ 0 \end{bmatrix}, \quad (5.26)$$

which in turn implies that $\nabla_{\tilde{\mathbb{I}}_1^{-1}} \tilde{\mathbb{I}}_1^{-1} = 0$. Hence, it is obvious that the decoupling vector fields $V \in \mathcal{I}_1^{-1}$ are simply multiples of the input vector field $\tilde{\mathbb{I}}_1^{-1}$ since $\nabla_V V = 0 \in \mathcal{I}_1^{-1}$. These motions are then either purely translational or purely rotational corresponding to exactly one principal axis of inertia. This gives us the following definition.

Definition 5.2 (Pure vector field). A *pure vector field* is a single input vector field \mathbb{I}_i^{-1} , $i \in \{1, \dots, 6\}$. Its action corresponds to a single principal axis of inertia of the body-fixed reference frame; the integral curves of the vector field are either purely translational *or* purely rotational. We call the integral curves of such a vector field the *pure motions*.

Note that generic single-input affine connection control systems may have no decoupling vector fields since a generic vector field may not satisfy the condition that $\nabla_Z Z \in \text{Span}\{Z\}$. However, if a vector field Z does satisfy $\nabla_Z Z \in \text{Span}\{Z\}$, then, via a reparameterization, we get $\nabla_Z Z = 0$. Geometrically, we refer to Z as *auto-parallel*; the integral curves of Z are geodesics for the corresponding affine connection ∇ .

5.2.3 Two-input systems

Suppose now that we consider two input vector fields for ODIN in an ideal fluid. Hence, $m = 2$ and $\mathcal{I}^{-1} = \mathcal{I}_2^{-1} = \{\tilde{\mathbb{I}}_1^{-1}, \tilde{\mathbb{I}}_2^{-1}\}$. The geometric acceleration is given by the affine connection control system

$$\nabla_{\gamma'} \gamma' = \sum_{a=1}^2 \tilde{\mathbb{I}}_a^{-1}(\gamma(t)) \sigma^a(t). \quad (5.27)$$

First assume that, $\mathcal{I}^{-1} = \{\mathbb{I}_1^{-1}, \mathbb{I}_2^{-1}\}$. From Section 5.2.2, we know that

$$\mathbb{G}(\nabla_{\mathbb{I}_1^{-1}} \mathbb{I}_1^{-1}, X_i) = 0, \quad (5.28)$$

and

$$\mathbb{G}(\nabla_{\mathbb{I}_2^{-1}} \mathbb{I}_2^{-1}, X_i) = 0, \quad (5.29)$$

for $i = 1, \dots, 6$, which implies $\nabla_{\mathbb{I}_1^{-1}} \mathbb{I}_1^{-1} = 0 = \nabla_{\mathbb{I}_2^{-1}} \mathbb{I}_2^{-1}$.

To calculate $\nabla_{\mathbb{I}_1^{-1}} \mathbb{I}_2^{-1}$, we rewrite Eq. (5.6) as

$$\begin{aligned} \mathbb{G}(\nabla_{\mathbb{I}_1^{-1}} \mathbb{I}_2^{-1}, X_k) = & \\ & \frac{1}{2} [\mathcal{L}_{\mathbb{I}_1^{-1}}(\mathbb{G}(\mathbb{I}_2^{-1}, X_k)) + \mathcal{L}_{\mathbb{I}_2^{-1}}(\mathbb{G}(X_k, \mathbb{I}_1^{-1}))] \\ & - \mathcal{L}_{X_k}(\mathbb{G}(\mathbb{I}_1^{-1}, \mathbb{I}_2^{-1})) + \mathbb{G}([\mathbb{I}_1^{-1}, \mathbb{I}_2^{-1}], X_k) \\ & - \mathbb{G}([\mathbb{I}_1^{-1}, X_k], \mathbb{I}_2^{-1}) - \mathbb{G}([\mathbb{I}_2^{-1}, X_k], \mathbb{I}_1^{-1}), \end{aligned} \quad (5.30)$$

where $k = 1, \dots, 6$. Then,

$$\mathbb{G}(\nabla_{\mathbb{I}_1^{-1}} \mathbb{I}_2^{-1}, X_i) = 0 \quad i = 1, \dots, 5 \quad (5.31)$$

$$\mathbb{G}(\nabla_{\mathbb{I}_1^{-1}} \mathbb{I}_2^{-1}, X_6) = -\frac{1}{2j_3}(m_1 - m_2), \quad (5.32)$$

which implies $\nabla_{\mathbb{I}_1^{-1}\mathbb{I}_2^{-1}} = -\frac{1}{2j_3}(m_1 - m_2)X_6$. Now consider $\nabla_{\mathbb{I}_2^{-1}\mathbb{I}_1^{-1}}$

$$\mathbb{G}(\nabla_{\mathbb{I}_2^{-1}\mathbb{I}_1^{-1}}, X_i) = 0 \quad i = 1, \dots, 5 \quad (5.33)$$

$$\mathbb{G}(\nabla_{\mathbb{I}_2^{-1}\mathbb{I}_1^{-1}}, X_6) = -\frac{1}{2j_3}(m_1 - m_2), \quad (5.34)$$

which implies $\nabla_{\mathbb{I}_2^{-1}\mathbb{I}_1^{-1}} = -\frac{1}{2j_3}(m_1 - m_2)X_6$.

Thus for a vector field to be decoupling, we must find coefficients h_1 and h_2 such that

$$h_1 h_2 \left(-\frac{1}{j_3}(m_1 - m_2) \right) X_6 \equiv 0 \pmod{\mathcal{I}_2^{-1}}. \quad (5.35)$$

Under the kinetically unique assumption ($m_1 \neq m_2$), it is clear that either h_1 or h_2 must be zero. Thus, the decoupling vector fields for this system are $V = h_1 \mathbb{I}_1^{-1}$ or $V = h_2 \mathbb{I}_2^{-1}$. Continuing in the same manner, we can compute the decoupling vector fields for all other two-input systems. The results for the rest of these cases of the two-input systems are presented in Eq. (5.36) and these results lead to Theorem 5.1 and Corollaries 5.1 and 5.2.

Let $a, b \in \{1, \dots, 6\}$, where $a < b$, and let $\mathcal{U} = \{1, 2, 3\}$, $\mathcal{V} = \{4, 5, 6\}$. Let $V \in \mathcal{I}_2^{-1}$, ϵ_{ijk} be the standard permutation symbol and $\{X_1, \dots, X_6\}$ the standard basis vectors for \mathbb{R}^6 .

Then,

$$\nabla_V V \equiv \begin{cases} h_a h_b \left((-1)^c \frac{1}{j_c} (m_a - m_b) X_{c+3} \right) \\ \quad \text{if } a, b \in \mathcal{U} \text{ and } c \in \mathcal{U} \setminus \{a, b\} \\ h_a h_b \left((-1)^{c+1} \frac{1}{j_c} (j_b - j_a) X_c \right) \\ \quad \text{if } a, b \in \mathcal{V} \text{ and } c \in \mathcal{V} \setminus \{a, b\} \\ h_a h_b \left(\epsilon_{abc} \left(\frac{m_a}{m_c} \right) X_c \right) \\ \quad \text{if } a \in \mathcal{U} \text{ and } b \in \mathcal{V} \\ \quad \text{and } c \in \mathcal{U} \setminus \{a, b-3\} \\ 0 \quad \text{if } a = b \text{ or } a = b-3 \end{cases}, \quad (5.36)$$

where the equivalence is $(\text{mod } \mathcal{I}_2^{-1})$. The above calculations give rise to the following theorem.

Theorem 5.1. *Suppose we have a kinetically unique two input system $(\mathcal{I}_2^{-1} = \{\tilde{\mathbb{I}}_1^{-1}, \tilde{\mathbb{I}}_2^{-1}\})$ in which both inputs do not act upon the same principal axis of inertia. Then, a vector field $V \in \mathcal{I}^{-1}$ is decoupling if and only if V has all but one of its components equal to zero. In particular, it has the form $V = h_1 \tilde{\mathbb{I}}_1^{-1}$ or $V = h_2 \tilde{\mathbb{I}}_2^{-1}$; these are the pure vector fields.*

Corollary 5.1. *If both inputs act on the same principal axis of inertia ($a \equiv b+3 \pmod{6}$), then every vector field $V \in \mathcal{I}^{-1}$ is decoupling since $\nabla_V V = 0$.*

Corollary 5.2. *If we loosen the kinetically unique assumption and let $m_a = m_b$ for $a, b \in \mathcal{U}$ or $j_c = j_d$ for $c, d \in \mathcal{V}$, then every vector field $V \in \mathcal{I}^{-1}$ is decoupling.*

5.3 Covariant Derivatives for $\tilde{\nabla}$

With the developments presented in Sections 5.2.2 and 5.2.3, by use of the equations from Section 5.2.1 and combining that with the properties of $\tilde{\nabla}$ given in Section 2.87, we can calculate the covariant derivatives in standard basis notation for $\tilde{\nabla}$. The results of these computations are shown in Table 4, where we use the notation $(i, j) = \tilde{\nabla}_{\mathbb{I}_i^{-1}} \mathbb{I}_j^{-1}$. By Eq. (2.85), we note that the results are the same as those presented in Chyba et al. (2008c) for the Levi-Civita connection, except for the case of $\tilde{\nabla}_{\mathbb{I}_i^{-1}} \mathbb{I}_i^{-1}$.

Proposition 5.1. *By use of the Levi-Civita connection, we can define an affine connection $\tilde{\nabla}$ which includes external dissipative drag terms for the submerged rigid body and has the property that*

$$\tilde{\nabla}_{\mathbb{I}_i^{-1}} \mathbb{I}_j^{-1} = \begin{cases} \nabla_{\mathbb{I}_i^{-1}} \mathbb{I}_j^{-1} & i \neq j \\ -\frac{D_i}{G_{ii}} X_i & i = j. \end{cases}$$

Proof: Apply the results of Eq. (2.85) to the control input vector fields \mathbb{I}_k^{-1} for $k = 1, \dots, 6$.

5.4 Decoupling Vector Fields for ODIN

Covariant derivatives and decoupling vector fields for ODIN in an ideal fluid are presented in Chyba et al. (2008c). The work presented in this dissertation extends these results to account for hydrodynamic damping in the form of viscous drag. Thus, we present the decoupling vector fields used for kinematic motion planning for the AUV ODIN calculated

(1, 1)	$\frac{D_1}{m_1} X_1$	(2, 1)	$\frac{-(m_1-m_2)X_6}{2j_3}$
(1, 2)	$\frac{-(m_1-m_2)X_6}{2j_3}$	(2, 2)	$\frac{D_2}{m_2} X_2$
(1, 3)	$\frac{-(m_3-m_1)X_5}{2j_2}$	(2, 3)	$\frac{(m_3-m_2)X_4}{2j_1}$
(1, 4)	0	(2, 4)	$\frac{-(m_3-m_2)X_3}{2m_3}$
(1, 5)	$\frac{(m_3-m_1)X_3}{2m_3}$	(2, 5)	0
(1, 6)	$\frac{(m_1-m_2)X_2}{2m_2}$	(2, 6)	$\frac{(m_1-m_2)X_1}{2m_1}$
(3, 1)	$\frac{-(m_3-m_1)X_5}{2j_2}$	(4, 1)	0
(3, 2)	$\frac{(m_3-m_2)X_4}{2j_1}$	(4, 2)	$\frac{(m_3+m_2)X_3}{2m_3}$
(3, 3)	$\frac{D_3}{m_3} X_3$	(4, 3)	$\frac{-(m_3+m_2)X_2}{2m_2}$
(3, 4)	$\frac{-(m_3-m_2)X_2}{2m_2}$	(4, 4)	$\frac{D_4}{j_1} X_4$
(3, 5)	$\frac{(m_3-m_1)X_1}{2m_1}$	(4, 5)	$\frac{(j_3+j_2-j_1)X_6}{2j_3}$
(3, 6)	0	(4, 6)	$\frac{-(j_3+j_2-j_1)X_5}{2j_2}$
(5, 1)	$\frac{-(m_3+m_1)X_3}{2m_3}$	(6, 1)	$\frac{(m_2+m_1)X_2}{2m_2}$
(5, 2)	0	(6, 2)	$\frac{-(m_2+m_1)X_1}{2m_1}$
(5, 3)	$\frac{(m_3+m_1)X_1}{2m_1}$	(6, 3)	0
(5, 4)	$\frac{-(j_3-j_2+j_1)X_6}{2j_3}$	(6, 4)	$\frac{-(j_3-j_2-j_1)X_5}{2j_2}$
(5, 5)	$\frac{D_5}{j_2} X_5$	(6, 5)	$\frac{(j_3-j_2-j_1)X_4}{2j_1}$
(5, 6)	$\frac{(j_3-j_2+j_1)X_4}{2j_1}$	(6, 6)	$\frac{D_6}{j_3} X_6$

Table 4: Covariant derivatives in basis notation for the affine connection $\tilde{\nabla}$.

by use of the affine connection $\tilde{\nabla}$. Before we present the results, we first introduce the definitions of an axial and coordinate vector field which will help to ease later discussions.

Definition 5.3 (Axial field). A vector field V is called an *axial field* if it is of the form

$$V = h_i \mathbb{I}_i^{-1} + h_{i+3} \mathbb{I}_{i+3}^{-1} \text{ where } i \in \mathcal{U}.$$

The term axial field was coined by the author of this dissertation in Chyba et al. (2008c), and refers to a vector field whose integral curves represent a translation and a rotation acting on the same principal axis of inertia. The motion is *axial* in the sense that it deals with only one axis. We call the integral curves of such a vector field *axial motions*.

Definition 5.4 (Coordinate field). A vector field V is called a *coordinate field* if it is of the form $V = h_i \mathbb{I}_i^{-1} + h_j \mathbb{I}_j^{-1} + h_k \mathbb{I}_k^{-1}$ where $i = 1$ or 4 , $j = 2$ or 5 and $k = 3$ or 6 .

The term coordinate field was also coined by the author of this dissertation in Chyba et al. (2008c), and refers to a vector field whose integral curves represent one motion (translation or rotation) on or about each of the three principal axes of inertia. An integral curve for such a vector field is referred to as a *coordinate motion*.

A characterization of the decoupling vector fields for ODIN are stated in the following theorem.

Theorem 5.2. *Suppose that we consider a neutrally-buoyant ODIN subjected to viscous dissipation and $C_G = C_B$. Then we have the following characterization for the decoupling vector fields in terms of the number of degrees-of-freedom we can input to the system.*

Case 1: Single-input system, $\mathcal{I}_1^{-1} = \{\tilde{\mathbb{I}}_1^{-1}\}$. *The decoupling vector fields are multiples of $\tilde{\mathbb{I}}_1^{-1}$; these are pure motions.*

Case 2: Two-input system, $\mathcal{I}_2^{-1} = \{\tilde{\mathbb{I}}_1^{-1}, \tilde{\mathbb{I}}_2^{-1}\}$ *in which both inputs do not act upon the same principle axis of inertia. Then, for a kinetically unique system, a vector field $V \in \mathcal{I}^{-1}$ is decoupling if and only if V has all but one of its components equal to zero. In particular, it has the form $V = h_1 \tilde{\mathbb{I}}_1^{-1}$ or $V = h_2 \tilde{\mathbb{I}}_2^{-1}$; these are pure motions. If the input vector fields act on the same principal axis of inertia, then every vector field in \mathcal{I} is decoupling.*

Case 3: Three-input system.

1. *Three Translational Inputs:* $\mathcal{I}_3^{-1} = \{\mathbb{I}_1^{-1}, \mathbb{I}_2^{-1}, \mathbb{I}_3^{-1}\}$. For a kinetically unique system, a vector field $V \in \mathcal{I}^{-1}$ is decoupling if and only if V has all but one of its components equal to zero. In particular, it has the form $V = h_i \mathbb{I}_i^{-1}$ for $i \in \mathcal{U}$; these are the pure translational motions. Assuming exactly two of the m_i 's are equal, we get the axial motions as additional decoupling vector fields: $V = h_i \mathbb{I}_i^{-1} + h_j \mathbb{I}_j^{-1}$, where $m_i = m_j$ and $m_i \neq m_k$. If $m_i = m_j = m_k$, then every vector field $V \in \mathcal{I}^{-1}$ is decoupling since $\nabla_V V \in \mathcal{I}^{-1}$.
2. *Three Rotational Inputs:* $\mathcal{I}_3^{-1} = \{\mathbb{I}_4^{-1}, \mathbb{I}_5^{-1}, \mathbb{I}_6^{-1}\}$. In this case, $\nabla_V V \in \mathcal{I}^{-1}$ for all $V \in \mathcal{I}^{-1}$, thus each vector field $V \in \mathcal{I}^{-1}$ is decoupling.
3. *Mixed Translational and Rotational Inputs.* Suppose we have a kinetically unique three input system such that the inputs are not all translational or all rotational but represent motions along three distinct axes. Then, every vector field $V \in \mathcal{I}^{-1}$ is decoupling. If the three input system is such that it represents an axial motion plus another input vector field, the decoupling vector fields are the axial motions, $V = h_i \mathbb{I}_i^{-1} + h_{i+3} \mathbb{I}_{i+3}^{-1}$ for $i \in \mathcal{U}$, and the pure motions, $V = h_j \mathbb{I}_j^{-1}$, where $j \neq i$ and $j \neq i + 3$. The remarks about the symmetries in the case of three translational input are valid in this case also.

Case 4: Four input system.

1. Three Translation, One Rotation:

$\mathcal{I}_4^{-1} = \{\mathbb{I}_1^{-1}, \mathbb{I}_2^{-1}, \mathbb{I}_3^{-1}, \mathbb{I}_k^{-1}\}$ where $k \in \mathcal{V}$. For a kinetically unique system the decoupling vector fields are the axial motions $V = h_{k-3} \mathbb{I}_{k-3}^{-1} + h_k \mathbb{I}_k^{-1}$ or the coordinate motions $V = h_i \mathbb{I}_i^{-1} + h_j \mathbb{I}_j^{-1} + h_k \mathbb{I}_k^{-1}$ with $i, j \in \mathcal{U}$, $i, j \neq k - 3$. If $m_{k-3} = m_i$ for $i \in \mathcal{U}$ and $i \neq k - 3$, then $V = h_i \mathbb{I}_i^{-1} + h_{k-3} \mathbb{I}_{k-3}^{-1} + h_k \mathbb{I}_k^{-1}$ is also a decoupling vector field. If $m_1 = m_2 = m_3$, then every vector field $V \in \mathcal{I}^{-1}$ is a decoupling vector field.

2. Three Rotations, One Translation:

$\mathcal{I}_4^{-1} = \{\mathbb{I}_i^{-1}, \mathbb{I}_4^{-1}, \mathbb{I}_5^{-1}, \mathbb{I}_6^{-1}\}$ where $i \in \mathcal{U}$. Then the decoupling vector fields are the axial motions $V = h_i \mathbb{I}_i^{-1} + h_{i+3} \mathbb{I}_{i+3}^{-1}$ or the coordinate motions $V = h_4 \mathbb{I}_4^{-1} + h_5 \mathbb{I}_5^{-1} + h_6 \mathbb{I}_6^{-1}$.

3. Two Translations, Two Rotations. For a kinetically unique system, if two principle axes are repeated, $\mathcal{I}_4^{-1} = \{\mathbb{I}_i^{-1}, \mathbb{I}_j^{-1}, \mathbb{I}_{i+3}^{-1}, \mathbb{I}_{j+3}^{-1}\}$, where $i, j \in \mathcal{U}$, then the decoupling vector fields are either the pure motions $V = h_a \mathbb{I}_a^{-1}$ for $a \in \{i, j, i + 3, j + 3\}$ or the axial motions $V = h_a \mathbb{I}_a^{-1} + h_{a+3} \mathbb{I}_{a+3}^{-1}$ where $a = 1$ or $a = j$. If $m_i = m_j$, then additional decoupling vector fields for the system are the axial motions plus a multiple of the other translational input vector field: $V = h_i \mathbb{I}_i^{-1} + h_j \mathbb{I}_j^{-1} + h_k \mathbb{I}_k^{-1}$, where $k = i + 3$ or $k = j + 3$. And, if $J_b^{\Omega_i} + J_f^{\Omega_i} = J_b^{\Omega_j} + J_f^{\Omega_j}$, then additional decoupling vector fields for the system are of the form $V = h_{i+3} \mathbb{I}_{i+3}^{-1} + h_{j+3} \mathbb{I}_{j+3}^{-1}$. For a kinetically unique system, if

one principle axis is repeated: $\mathcal{I}_4^{-1} = \{\mathbb{I}_i^{-1}, \mathbb{I}_j^{-1}, \mathbb{I}_{i+3}^{-1}, \mathbb{I}_{k+3}^{-1}\}$, where $i, j, k \in \mathcal{U}$, then the decoupling vector fields are the axial motions $V = h_i \mathbb{I}_i^{-1} + h_{i+3} \mathbb{I}_{i+3}^{-1}$ or the coordinate motions $V = h_i \mathbb{I}_i^{-1} + h_j \mathbb{I}_j^{-1} + h_{k+3} \mathbb{I}_{k+3}^{-1}$. If $J_b^{\Omega_i} + J_f^{\Omega_i} = J_b^{\Omega_k} + J_f^{\Omega_k}$ then h_j or h_{i+3} must be zero, and additional decoupling vector fields are the axial motions plus a multiple of the other rotational input vector field:

$$V = h_i \mathbb{I}_i^{-1} + h_{i+3} \mathbb{I}_{i+3}^{-1} + h_{k+3} \mathbb{I}_{k+3}^{-1}.$$

Case 5: Five input system.

1. Three Translations, Two Rotations: $\mathcal{I}_5^{-1} = \{\mathbb{I}_1^{-1}, \mathbb{I}_2^{-1}, \mathbb{I}_3^{-1}, \mathbb{I}_i^{-1}, \mathbb{I}_j^{-1}\}$, where $i, j \in \mathcal{V}$, and let $k \in \mathcal{V}$ such that $k \neq i$ or j . For a kinetically unique system, the decoupling vector fields are:

(a) The axial motions plus a multiple of a translational input $V = h_a \mathbb{I}_a^{-1} + h_{a+3} \mathbb{I}_{a+3}^{-1} + h_{k-3} \mathbb{I}_{k-3}^{-1}$ where $a \in \mathcal{U} - (k - 3)$.

(b) The coordinate motions $V = h_a \mathbb{I}_a^{-1} + h_b \mathbb{I}_b^{-1} + h_{k-3} \mathbb{I}_{k-3}^{-1}$, where $a, b \in \mathcal{U} - (k - 3)$.

(c) The motions defined by $V = h_{k-3} \mathbb{I}_{k-3}^{-1} + h_b \mathbb{I}_b^{-1}$, where $b \in \mathcal{U} - (k - 3)$.

(d) The pure motion: $V = h_{k-3} \mathbb{I}_{k-3}^{-1}$

Assuming that $m_{i-3} = m_{j-3}$, additional decoupling vector fields are given by $V = h_a \mathbb{I}_a^{-1} + h_k \mathbb{I}_k^{-1} + h_i \mathbb{I}_i^{-1} + h_j \mathbb{I}_j^{-1}$, where $a = i - 3$ or $a = j - 3$ and $k \in \mathcal{U} - \{i - 3, j - 3\}$. Assuming that $J_b^{\Omega_{i-3}} + J_f^{\Omega_{i-3}} = J_b^{\Omega_{j-3}} + J_f^{\Omega_{j-3}}$, additional decoupling vector fields are given by $V = h_1 \mathbb{I}_1^{-1} + h_2 \mathbb{I}_2^{-1} + h_3 \mathbb{I}_3^{-1} + h_a \mathbb{I}_a^{-1}$, where $a = i$ or $a = j$.

2. Two Translations, Three Rotations: $\mathcal{I}_5^{-1} = \{\mathbb{I}_i^{-1}, \mathbb{I}_j^{-1}, \mathbb{I}_4^{-1}, \mathbb{I}_5^{-1}, \mathbb{I}_6^{-1}\}$, where $i, j \in \mathcal{U}$, and let $k \in \mathcal{U}$ such that $k \neq i$ or j . For a kinetically unique system, the decoupling vector fields are:

(a) The axial motions plus a multiple of a rotational input $V = h_a \mathbb{I}_a^{-1} + h_{a+3} \mathbb{I}_{a+3}^{-1} + h_{k+3} \mathbb{I}_{k+3}^{-1}$ where $a \in \mathcal{V} - (k+3)$.

(b) The coordinate motions: $V = h_a \mathbb{I}_a^{-1} + h_b \mathbb{I}_b^{-1} + h_{k+3} \mathbb{I}_{k+3}^{-1}$, where $a, b \in \mathcal{V} - (k+3)$.

(c) The motions defined by $V = h_{k+3} \mathbb{I}_{k+3}^{-1} + h_b \mathbb{I}_b^{-1}$ where $b \in \mathcal{V} - (k+3)$.

(d) The pure motion: $V = h_{k+3} \mathbb{I}_{k+3}^{-1}$

Loosening the kinetic uniqueness assumption does not provide any additional decoupling vector fields in this case.

Case 6: Six input system. Every vector field is decoupling.

Proof: Case 1 and Case 2 are detailed in Sections 5.2.2 and 5.2.3, respectively. For the other four cases, the results are directly calculated following the examples of the first two cases and by use of the calculated covariant derivatives located in Table 4. These calculations are presented in Appendix C.

Theorem 5.3. *The decoupling vector fields for ODIN calculated by use of the connection $\tilde{\nabla}$ are the same as for ODIN submerged in an ideal fluid.*

Proof: Using Proposition 5.1 and the fact that $\nabla_{\mathbb{I}_i^{-1}} \mathbb{I}_i^{-1} = -\frac{D_i}{G_{ii}} X_i \in \text{Span } \mathcal{I}_k^{-1}$ leads to the proof.

5.5 Calculated Control Strategies

Now that we have calculated all the decoupling vector fields for each of the under-actuated scenarios for ODIN, it is time to present the design of some control strategies utilizing the kinematic motion planning techniques we have developed. In each of the following sections, we will present one mission scenario for which we will calculate the desired controls. Some missions will serve to validate the techniques developed in this research while others will have real-life applications. Each mission scenario developed here was implemented onto ODIN. The results of the implementations are presented in Chapter 6.

We begin by calculating control strategies for some simple motions as a way to validate the construction process. We then proceed to consider more complex motions which are application oriented and consider some under-actuated scenarios as well.

For all of the controls and experiments presented in this study, we assume that $\eta_{init} = (0, 0, 0, 0, 0, 0)$, or in particular, every trajectory begins at the origin. Thus, we will only specify $\eta_{final} = \eta_f$ for a given mission.

By definition the integral curves of the input control vector fields $\mathbb{I}^{-1} = \{\mathbb{I}_1^{-1}, \dots, \mathbb{I}_6^{-1}\}$ define motions along or about the principle axes of the body-fixed reference frame. These six motions are called the pure motions as presented in Definition 5.2. To avoid confusion when we discuss the motions defined by the integral curves of the input vector fields and the calculated decoupling vector fields, we introduce the following terminology.

Definition 5.5. (Body-pure motion) A *body-pure motion* is motion of the vehicle along or about an axis of the body-fixed reference frame. For example, a *body-pure heave* is a pure translation along the B_3 axis.

5.5.1 Mission 1

The first mission which we choose to consider is a pure heave motion of 2.5 m. This simple motion serves many purposes. First, we are able to validate the design of a trajectory using the decoupling vector field method as outlined previously in this chapter. Secondly, we are able to verify the drag coefficient estimate in the heave direction. Additionally, since this trajectory does not prescribe any rotations, we do not invoke any righting moments and the inclusion of the potential force (i.e., only buoyancy in this case) is straightforward.

We consider the design of a control strategy to realize this motion from an under-actuated scenario. Here we assume that only the vertically oriented thrusters are available for use. Under this assumption, the input control vector fields are $\mathcal{I}_3^{-1} = \{\tilde{\mathbb{I}}_1^{-1} = \mathbb{I}_3^{-1}, \tilde{\mathbb{I}}_2^{-1} = \mathbb{I}_4^{-1}, \tilde{\mathbb{I}}_3^{-1} = \mathbb{I}_5^{-1}\}$. Although we will not fully exploit it here, we make note that since $\{\mathbb{I}_3^{-1}, \mathbb{I}_4^{-1}, \mathbb{I}_5^{-1}, [\mathbb{I}_3^{-1}, \mathbb{I}_4^{-1}], [\mathbb{I}_3^{-1}, \mathbb{I}_5^{-1}], [\mathbb{I}_4^{-1}, \mathbb{I}_5^{-1}]\}$ are a set of six linearly independent vector fields, by Proposition 4.1 this under-actuated system is kinematically controllable. By Case 3 of Theorem 5.2, every vector field $V \in \mathcal{I}_3^{-1}$ is decoupling. In particular, $m_3 \mathbb{I}_3^{-1} = X_3 = (0, 0, 1, 0, 0, 0)$ is a decoupling vector field, and the one of specific interest for this trajectory design.

We need only consider the integral curves of the decoupling vector field X_3 to realize the desired motion. There is only one integral curve to follow, and $\mathcal{F}_{2.5}^{X_3}(\eta_{init}) = \eta_{final}$. Thus, the trajectory $\gamma(t) : [0, 2.5] \rightarrow Q$ is simply the straight line from $(0, 0, 0, 0, 0, 0)$ to $(0, 0, 2.5, 0, 0, 0)$. We choose to reparameterize $\gamma(t)$ using $\tau(t) : [0, 8] \rightarrow [0, 2.5]$ so that the motion lasts for eight seconds. This reparameterization gives an average velocity for the trajectory of 0.3125 m/s. Referring to the data presented in Appendix B.1, the drag coefficient for this velocity is $D_3 = 115 \text{ kg/m}$. Hence, we can compute the dynamic control structure by use of Eq. (4.10) as

$$\sigma^3(t)\mathbb{I}_3^{-1}(\gamma \circ \tau(t)) = (\tau'(t))^2 \tilde{\nabla}_{X_3} X_3(\gamma \circ \tau(t)) + \tau''(t) X_3(\gamma \circ \tau(t)), \quad (5.37)$$

where $\tau(t) = \frac{5t^2(12-t)}{512}$ which ensures that the vehicle will begin and end the motion with zero velocity. By use of Table 4 for the calculation of the covariant derivative, Eq. (5.37) becomes

$$\begin{aligned} \sigma^3(t) &= D_3(\tau'(t))^2 + m_3 \tau''(t) \\ &= 115 \left(\frac{15t(8-t)}{512} \right)^2 + 196 \left(\frac{15(4-t)}{256} \right). \end{aligned} \quad (5.38)$$

This gives the control strategy for ODIN to realize a pure heave of 2.5 m with the inclusion of dissipative drag forces. However, here, the effect of buoyancy is not accounted for.

From Table 3, ODIN's weight is $W = mg = 123.8 \times 9.81 = 1214.5 \text{ N}$ and her buoyancy is $B = \rho g \mathcal{V} = 997 \times 9.81 \times 0.1243 = 1215.8 \text{ N}$. Thus, ODIN is positively buoyant by 1.3N. Since we choose to orient the inertial frame z -axis such that positive is in

the direction of gravity, there is a force of -1.3 N exerted on the body due to the positive buoyancy. This force happens to be along the same axis as our desired motion, but in the opposite direction. To account for the buoyancy, we must subtract it from the computed control $\sigma^3(t)$. We denote the new control as $\check{\sigma}^3(t) = \sigma^3(t) - (-1.3) = \sigma^3(t) + 1.3$.

From this point forward, a control strategy including compensation for the potential forces and moments arising from gravity and buoyancy will be denoted using $\check{\sigma}^i(t)$ for $i = 1, \dots, 6$.

5.5.2 Mission 2

The next motion which we investigate is a five meter pure surge evolution, thus we have $\eta_{final} = (5, 0, 0, 0, 0, 0)$. Similar to the pure heave motion, we use this trajectory to verify the drag coefficient used for the surge (and symmetrically sway) direction as well as validate the technique of including the viscous drag in the kinematic motion planning procedure.

We will consider and present two scenarios for this motion. The first scenario will represent an under-actuated scenario where ODIN only has the use of her horizontal thrusters. This three input system has input control vector fields $\mathcal{I}_3^{-1} = \{\tilde{\mathbb{I}}_1^{-1} = \mathbb{I}_1^{-1}, \tilde{\mathbb{I}}_2^{-1} = \mathbb{I}_2^{-1}, \tilde{\mathbb{I}}_3^{-1} = \mathbb{I}_6^{-1}\}$. By Case 3 of Theorem 5.2, every vector field $V \in \mathcal{I}_3^{-1}$ is decoupling. Hence, the decoupling vector fields for this system are the constant multiples and linear combinations of the set $\mathcal{D} = \{X_1 = (1, 0, 0, 0, 0, 0), X_2 = (0, 1, 0, 0, 0, 0), X_6 = (0, 0, 0, 0, 0, 1)\}$.

We note here, assuming neutral buoyancy, that the vehicle motions, in this under-actuated scenario, are restricted to a plane, see Chyba et al. (2008c). As presented, this system is not kinematically controllable (see Definition 4.4), however it should be obvious that the motion can be realized by use of the available controls.

For this motion, we need only consider the integral curves of the decoupling vector field X_1 . There is only one integral curve to follow, and $\mathcal{F}_5^{X_1}(\eta_{init}) = \eta_{final}$. Thus, the trajectory $\gamma(t) : [0, 5] \rightarrow Q$ is simply the straight line from $(0, 0, 0, 0, 0, 0)$ to $(5, 0, 0, 0, 0, 0)$. We choose to reparameterize $\gamma(t)$ using $\tau(t) : [0, 30] \rightarrow [0, 5]$ so that the motion lasts for 30 seconds. This reparameterization gives an average velocity for the trajectory of 0.167 m/s. From the data presented in Appendix B.1, the drag coefficient for this velocity is $D_1 = 231$ kg/m. Hence, we can calculate the dynamic control structure by use of Eq. (4.10) as

$$\sigma^1(t)\mathbb{I}_1^{-1}(\gamma \circ \tau(t)) = (\tau'(t))^2 \tilde{\nabla}_{X_1} X_1(\gamma \circ \tau(t)) + \tau''(t) X_1(\gamma \circ \tau(t)), \quad (5.39)$$

where $\tau(t) = \frac{t^2(45-t)}{2700}$, which ensures that the vehicle will begin and end the motion with zero velocity. By use of Table 4 for the computation of the covariant derivative, Eq. (5.39) becomes

$$\begin{aligned} \sigma^1(t) &= D_1(\tau'(t))^2 + m_1\tau''(t) \\ &= 231 \left(\frac{t(30-t)}{900} \right)^2 + 196 \left(\frac{15-t}{450} \right) \\ &= \frac{7(11t^4 - 660t^3 + 9900t^2 - 16800t + 252000)}{270000}. \end{aligned} \quad (5.40)$$

For the second scenario, we will assume that ODIN is fully actuated and compensate for the fact that ODIN is positively buoyant by additionally applying a pure heave control $\sigma^3(t)$ over the duration of the trajectory. Since this control will be compensating for the potential force arising from buoyancy, we use the control as computed in Eq. (5.40) as the base for our design. As computed previously, ODIN is positively buoyant by 1.3 N. Applying a constant control of $\sigma^3(t) = 1.3$ N while implementing the previously calculated pure surge control should compensate for the buoyancy. This gives the control structure

$$\check{\sigma}(t) = \begin{cases} \sigma^1(t) = \frac{7(11t^4 - 660t^3 + 9900t^2 - 16800t + 252000)}{270000} \\ \sigma^3(t) = 1.3, \end{cases} \quad (5.41)$$

for the prescribed motion ending at $\eta_{final} = (5, 0, 0, 0, 0, 0)$.

5.5.3 Mission 3

For this scenario, we expand upon Mission 2 given in Section 5.5.2. In particular, suppose that we would like ODIN to realize a pure surge displacement, except we do not have the use of the input control vector field \mathbb{I}_1^{-1} . Further, we assume that ODIN is in an under-actuated situation and does not have the use of the horizontally-mounted thrusters. Thus, ODIN only has the use of the vertically-mounted thrusters, and has direct control only upon roll, pitch and heave (i.e., $\{\mathbb{I}_3^{-1}, \mathbb{I}_4^{-1}, \mathbb{I}_5^{-1}\}$). Is it possible to reach $\eta_{final} = (a, 0, 0, 0, 0, 0)$, for $a \in \mathbb{R}$, in the proposed under-actuated condition? From Proposition 4.1, we can com-

pute that ODIN is kinematically controllable, and hence, the answer to the question is yes; any configuration is reachable from any other via kinematic motions. This fact is proved in Chyba et al. (2008c), however, a simple calculation shows that $\text{Lie}^\infty(\mathbb{I}_3^{-1}, \mathbb{I}_4^{-1}, \mathbb{I}_5^{-1}) = TQ$. Next, we discuss one way to accomplish this displacement.

The motivation for this trajectory is to demonstrate the ability of ODIN to realize a motion in an under-actuated scenario, to demonstrate the necessity of the inclusion of the restoring forces arising from $C_G \neq C_B$ and demonstrate the concatenation of integral curves to construct a control strategy.

Let us choose $a = 1.25$ m. Since the pure heave motion is directly controllable, and ODIN is positively buoyant, it is clear that reaching the configuration $\eta_{final} = (1.25, 0, b, 0, 0, 0)$, for $b \in \mathbb{R}$, will prove that ODIN can realize the prescribed surge displacement. One way to reach the desired configuration is to pitch the vehicle an angle α and hold this pitch angle while applying a body-pure heave (i.e., apply a control along the B_3 axis) until the vehicle realizes the 1.25 m surge displacement. The value of b depends upon the pitch angle α . For this experiment, we choose $\alpha = 30^\circ$, which corresponds to $b = 2.165$ m, and thus, we choose $\eta_{final} = (1.25, 0, 2.165, 0, 0, 0)$.

During implementation, we are limited by the size of the testing facility (see Section 6.2 for details on the testing site) and the output bounds of the thrusters. Thus, some motions need to be scaled down. In particular, for this trajectory, we could not prescribe a 5 m pure surge with $\alpha = 30^\circ$ since we are depth limited.

With $\eta_{final} = (1.25, 0, 2.165, 0, 0, 0)$, we present two separate control strategy designs for this mission. Given that the set of input control vector fields is $\mathcal{I}_3^{-1} = \{\mathbb{I}_3^{-1}, \mathbb{I}_4^{-1}, \mathbb{I}_5^{-1}\}$,

the decoupling vector fields for this system are the constant multiples and linear combinations of the set $\mathcal{D} = \{X_3 = (0, 0, 1, 0, 0, 0), X_4 = (0, 0, 0, 1, 0, 0), X_5 = (0, 0, 0, 0, 1, 0)\}$.

The basic idea of this motion is to point the bottom of ODIN at η_{final} by following the integral curves of X_4 (pitch motion), then follow the integral curves of X_3 (body-pure heave motion) to realize the displacement. At the end of the body-pure heave motion, the vehicle will be in the configuration $(1.25, 0, 2.165, 0, 30^\circ, 0)$. We can undo the pitch motion by following the integral curves of $-X_4$, however, through experimentation we have found that the righting moments take care of this angular displacement without having to apply any control. This mission is an example where an AUV needs to maintain a specific list angle over the duration of a trajectory to realize a given motion.

If we want ODIN to realize a surge displacement greater than 1.25 m, we may concatenate the following designed trajectory with one using the negative of the prescribed roll angle and body-pure heave control to create a V -shaped motion. This would have ODIN realize a 2.5 m displacement. Concatenating more V -shaped motions will allow ODIN to realize a greater surge displacement. On the other hand, we could successively implement the trajectory given here followed by a pure heave motion of 2.165 m. This would create a sawtooth-type trajectory. The distance of 1.25 m is arbitrarily chosen and depends upon the pitch angle prescribed and the length of the pure heave motion. Altering each of these, we can also create different surge displacements.

For the first scenario, we will calculate the control strategy as if there were no potential forces. This example will demonstrate the need to include such forces. In the second scenario, we add the potential forces using the procedure described earlier in this chapter.

We would like to realize a pitch angle of $30^\circ = \pi/6$ radians to point ODIN at η_{final} . After the pitch displacement, we require a 2.5 m pure heave. We can define this motion along the flows of the integral curves by $\mathcal{F}_{2.5}^{X_3} \circ \mathcal{F}_{\frac{\pi}{6}}^{X_5}(\eta_{init}) = \eta_{final}$. Remember that we are allowing the righting moments to undo the rotation so we do not need to include $\mathcal{F}_{\frac{\pi}{6}}^{-X_5}$ in the concatenation. For the initial rotation, we let $\tau_\theta(t) : [0, 5] \rightarrow [0, \frac{\pi}{6}]$ by $\tau_\theta(t) = \frac{\pi t^2(15-2t)}{750}$ so that the motion begins and ends with zero velocity. For a rotational velocity of 0.105 rad/s we have $D_5 = 37.2 \text{ kg m}^2$. We reparameterize the body-pure heave motion to last for 8 seconds by use of $\tau_z(t) : [0, 8] \rightarrow [0, 2.5]$ defined by $\tau_z(t) = \frac{5t^2(12-t)}{512}$. For a heave velocity of 0.3125 m/s we have $D_3 = 115 \text{ kg/m}$. Hence, we can compute the dynamic control structure for each motion by use of Eq. (4.10). For the pitch motion, we have

$$\sigma^5(t)\mathbb{I}_5^{-1}(\gamma \circ \tau_\theta(t)) = (\tau_\theta'(t))^2 \tilde{\nabla}_{X_5} X_5(\gamma \circ \tau_\theta(t)) + \tau_\theta''(t) X_5(\gamma \circ \tau_\theta(t)). \quad (5.42)$$

By use of Table 4 for the calculation of the covariant derivative, Eq. (5.42) becomes

$$\begin{aligned} \sigma^5(t) &= D_5(\tau_\theta'(t))^2 + j_2 \tau_\theta''(t) \\ &= 37.2 \left(\frac{\pi t(5-t)}{125} \right)^2 + 5.29 \left(\frac{\pi(5-2t)}{125} \right). \end{aligned} \quad (5.43)$$

And, for the body-pure heave motion, we have

$$\sigma^3(t)\mathbb{I}_3^{-1}(\gamma \circ \tau_z(t)) = (\tau_z'(t))^2 \tilde{\nabla}_{X_3} X_3(\gamma \circ \tau_z(t)) + \tau_z''(t) X_3(\gamma \circ \tau_z(t)). \quad (5.44)$$

By use of Table 4 for the calculation of the covariant derivative, Eq. (5.44) becomes

$$\begin{aligned}\sigma^3(t) &= D_3(\tau_z'(t))^2 + m_3\tau_z''(t) \\ &= 115 \left(\frac{15t(8-t)}{512} \right)^2 + 196 \left(\frac{15(4-t)}{256} \right).\end{aligned}\tag{5.45}$$

The control strategy to complete the desired motion is then the concatenated controls calculated above. We apply $\sigma^5(t)$ for 5 seconds and then apply $\sigma^3(t)$ for 8 seconds. Since this control strategy does not consider the restoring forces, the model assumes that the pitch angle achieved in the first five seconds can be maintained throughout the trajectory. Since $C_G \neq C_B$ for ODIN, this is definitely not the case as the experimental data will show in Section 6.4.2. Thus, we now consider the addition of controls to compensate for the potential forces arising from the righting moment in pitch.

From Eq. (2.79) and Table 3, the righting moment to be compensated for, to maintain a $\theta = 30^\circ$ pitch angle is given by

$$\begin{bmatrix} -(W - B) \sin \theta \\ (W - B) \cos \theta \sin \phi \\ (W - B) \cos \theta \cos \phi \\ z_B B \cos \theta \sin \phi \\ z_B B \sin \theta \\ 0 \end{bmatrix} = \begin{bmatrix} -(-1.3) \times 0.5 \\ 0 \\ (-1.3) \times 0.866 \\ 0 \\ (-0.007) \times 1215.8 \times 0.5 \\ 0 \end{bmatrix} = \begin{bmatrix} 0.65 \\ 0 \\ -1.126 \\ 0 \\ -4.2553 \\ 0 \end{bmatrix}.\tag{5.46}$$

Here we see the coupling effect that $C_G \neq C_B$ causes. If we retain the assumption that

the horizontal thrusters are not operational, we can not apply the prescribed 0.65N force in surge to properly compensate for the induced forces and moments for maintaining the prescribed pitch angle. To demonstrate for this trajectory that the surge control is negligible we will implement the control strategy with and without this force.

Now we are ready to design the control strategy which includes compensation for the righting moment.⁸ For this mission, we need to maintain a precise pitch angle while we apply a control in body-pure heave. From the calculation above, we know the force that we need to apply during the heave motion to maintain the desired pitch angle. While maintaining this pitch angle, we want the velocity and acceleration in pitch to be zero. In particular, we want the velocity and acceleration along the integral curves of X_5 to be zero. To do this, we choose $\tau(t)$ as defined in Section 4.4 with the additional assumption that $\tau''(\bar{t}_j) = 0$. Thus, when the control $\sigma^5(t)$ is calculated, it has zero value at time \bar{t}_j . We then simply use the control $\check{\sigma}^5 = \sigma^5(t) - (z_B B \sin \theta)$ as the control for the first section of this concatenated strategy. At time $t = \bar{t}_j$ we then subtract the control $\sigma_{pot} = (0.65, 0, -1.126, 0, -4.2553, 0)^t$ to the calculated control for the body-pure heave motion to realize the desired trajectory. Note that this method simply adds the negative of the potential forces induced from maintaining a prescribed pitch angle. We demonstrate this technique by computing the control strategy for this mission including potential forces.

The idea is the same as before, except we now let $\tau_\theta(t) : [0, 5] \rightarrow [0, \frac{\pi}{6}]$ by $\tau_\theta(t) = \frac{\pi t^3(6t^2 - 75t + 250)}{18750}$ so that the motion begins and ends with zero velocity as well as ends with

⁸As mentioned previously, since ODIN is nearly neutrally buoyant, for trajectories which include a heave displacement the small effect of the 1.3N buoyancy force can be neglected.

zero acceleration. For a rotational velocity of 0.105 rad/s we have $D_5 = 37.2 \text{ kg m}^2$. We reparameterize the body-pure heave motion exactly the same as above. Hence, we can calculate the dynamic control structure for each motion by use of Eq. (4.10). For the pitch motion, we have

$$\sigma^5(t)\mathbb{I}_5^{-1}(\gamma \circ \tau_\theta(t)) = (\tau'(t))^2 \tilde{\nabla}_{X_5} X_5(\gamma \circ \tau_\theta(t)) + \tau_\theta''(t) X_5(\gamma \circ \tau_\theta(t)). \quad (5.47)$$

By use of Table 4 for the calculation of the covariant derivative, Eq. (5.47) becomes

$$\begin{aligned} \sigma^5(t) &= D_5(\tau_\theta'(t))^2 + j_2 \tau_\theta''(t) \\ &= 37.2 \left(\frac{\pi t^2(t^2 - 10t + 25)}{625} \right)^2 + 5.29 \left(\frac{2\pi t(t^2 - 10t + 25)}{625} \right). \end{aligned} \quad (5.48)$$

Adding in the potential forces, we obtain the applied control for $t \in [0, 5]$: $\check{\sigma}^5(t) = \sigma^5(t) + 4.2553$. And, for the heave motion we repeat what was done earlier to obtain

$$\begin{aligned} \sigma^3(t) &= D_3(\tau_z'(t))^2 + m_3 \tau_z''(t) \\ &= 115 \left(\frac{15t(8-t)}{512} \right)^2 + 196 \left(\frac{15(4-t)}{256} \right). \end{aligned} \quad (5.49)$$

Including the potential forces to maintain the 30° pitch, the applied control for $t \in [5, 13]$ becomes $\check{\sigma}(t) = \sigma^3(t) - (0.65, 0, -1.126, 0, -4.2553, 0)^t$. In Section 6.4.2, we present this trajectory with and without the applied control in the surge direction to display the fully-actuated and under-actuated cases as defined at the beginning of this mission. The under

and fully-actuated controls are given by the following equations, respectively:

$$\ddot{\sigma}(t) = \begin{cases} \sigma^3(t) = \begin{cases} 1.006 & t \in [0, 5] \\ 115 \left(\frac{15t(8-t)}{512} \right)^2 + 196 \left(\frac{15(4-t)}{256} \right) + 1.126 & t \in [5, 13] \end{cases} \\ \sigma^5(t) = \begin{cases} 37.2 \left(\frac{\pi t^2(t^2-10t+25)}{625} \right)^2 + 5.29 \left(\frac{2\pi t(t^2-10t+25)}{625} \right) + 4.2553 & t \in [0, 5] \\ 4.2553 & t \in [5, 13] \end{cases} \end{cases} \quad (5.50)$$

$$\ddot{\sigma}(t) = \begin{cases} \sigma^1(t) = \begin{cases} -0.824 & t \in [0, 5] \\ -0.65 & t \in [5, 13] \end{cases} \\ \sigma^3(t) = \begin{cases} 1.006 & t \in [0, 5] \\ 115 \left(\frac{15t(8-t)}{512} \right)^2 + 196 \left(\frac{15(4-t)}{256} \right) + 1.126 & t \in [5, 13] \end{cases} \\ \sigma^5(t) = \begin{cases} 37.2 \left(\frac{\pi t^2(t^2-10t+25)}{625} \right)^2 + 5.29 \left(\frac{2\pi t(t^2-10t+25)}{625} \right) + 4.2553 & t \in [0, 5] \\ 4.2553 & t \in [5, 13] \end{cases} \end{cases} \quad (5.51)$$

Here, we would like to make a few remarks concerning the initial leg of this concatenated trajectory.

Remark 5.1. Successive implementations of only the pitching motion have shown that even for values of $\bar{t}_j \leq 5$, the effect of the coupled surge and heave forces is not negligible.

Even though the vehicle is unable to reach a state of equilibrium in such a short time

interval, the omission of these forces is noticeable. Upon reaching a steady state (i.e., maintaining a desired pitch angle) the effect of these forces is obvious as the vehicle will tend to drift slightly if the surge and heave forces are not counteracted. In the following section, we examine the pure rotation scenario to address such issues and present multiple control schemes to address the compensation for these forces.

Remark 5.2. Since we have a continuous, analytic expression for the control $\check{\sigma}^5(t)$, we could compute a continuous, analytic expression for $\check{\sigma}^1(t)$ and $\check{\sigma}^3(t)$ for $t \in [0, 5]$. We do not proceed down this route due to the method of implementation of the control strategies onto the test-bed vehicle. We will discuss this method further in Section 6.3, but in short, ODIN is not designed to handle continuously evolving control inputs. In the fully actuated case presented in Eq. (5.51) we present a constant control for $t \in [0, 5]$ for $\sigma^1(t)$ and $\sigma^3(t)$. This is related to the design of ODIN's input controls and will be explained in the implementations in Chapter 6.

5.5.4 Mission 4

From the design of Mission 3 presented in Section 5.5.3, it is clear that the pure rotation evolution needs to be examined independently. In this section, we consider a pure roll motion by use of three different methods to compensate for the righting moments. The basic idea of these motions is to consider the integral curves of the vector field X_4 , and choose $\tau(t)$ such that we apply a control for the first 5 seconds to reach the prescribed

orientation $\eta = (0, 0, 0, \phi, 0, 0)$, and then maintain that configuration for 5 seconds. In particular, $\bar{t}_j = 5$. In this section, we will assume that ODIN is fully actuated and include compensative forces in all necessary degrees of freedom. In the implementation section for these control strategies, we consider $\phi = \frac{\pi}{8}, \frac{\pi}{6}$ and $\frac{\pi}{4}$ radians.

For the first method, we abandon the differential geometric framework for a moment and simply require that the control be set constant to oppose the righting moments for the prescribed angle. Thus, the control for $t \in [0, 10]$ is given by

$$\ddot{\sigma}(t) = - \begin{pmatrix} 0 \\ (-1.3) \sin \phi \\ (-1.3) \cos \phi \\ (-0.007 \times 1215.8) \sin \phi \\ 0 \\ 0 \end{pmatrix}, \quad (5.52)$$

for the desired roll angle ϕ . Note that this is the negative of $P(\gamma(t))$, the righting moments acting on the vehicle for an angle ϕ , since the input controls are compensating for these moments. We will refer to this as the applied compensation control.

The next method goes back to the geometric construction method, with the exception that we do not choose $\tau''(\bar{t}_j) = 0$. This is to demonstrate that it is important to ensure that the acceleration is zero at the end of the angular evolution. Here we present two separate control designs for consideration.

For the first design, we use the same idea as before, except we now we let $\tau_\theta(t) : [0, 5] \rightarrow [0, \phi]$ by $\tau_\phi(t) = \frac{\phi t^2(15-2t)}{125}$ so that the motion begins and ends with zero velocity but does not end with zero acceleration. The dynamic control structure for the motion is calculated by use of Eq. (4.10):

$$\sigma^4(t)\mathbb{I}_5^{-1}(\gamma \circ \tau_\phi(t)) = (\tau'(t))^2 \tilde{\nabla}_{X_4} X_4(\gamma \circ \tau_\phi(t)) + \tau_\phi''(t) X_4(\gamma \circ \tau_\phi(t)). \quad (5.53)$$

By use of Table 4 for the calculation of the covariant derivative, Eq. (5.53) becomes

$$\sigma^4(t) = D_4 \left(\frac{6\phi t(5-t)}{125} \right)^2 + j_1 \left(\frac{6\phi(5-2t)}{125} \right). \quad (5.54)$$

Now, this control alone will not achieve much of a rotation at all. Thus, we subtract the force required to compensate for the righting moment in roll. This gives the applied control for $t \in [0, 5]$ as $\check{\sigma}^4(t) = \sigma^4(t) - (-0.007 \times 1215.8) \sin \phi$. Now, we wish to include the respective controls for sway and heave to compensate for the induced forces in these directions upon rotation. As mentioned in Remark 5.2, we can calculate a continuous control structure for $\sigma^1(t)$ and $\sigma^3(t)$ for $t \in [0, 5]$. Given the control force $\sigma^4(t)$ as calculated above, we know that the angle ϕ evolves as

$$\phi(t) = \arcsin \left(\frac{D_4(\tau_\phi'(t))^2 + j_1 \tau_\phi''(t)}{-(z_B B)} \right). \quad (5.55)$$

We can now compute a continuous control for $\sigma^2(t)$ and $\sigma^3(t)$ for $t \in [0, 5]$ by use of Eq. (5.52). The control $\check{\sigma}(t)$ for $t \in [5, 10]$ is then given by Eq. (5.52) with ϕ constant.

This design is similar to that done for the first concatenated leg of Mission 3, however, we do not guarantee that the acceleration is zero at $t = 5$, and in fact by the choice of $\tau(t)$, it is indeed not zero.

The second design is to choose $\tau''(5) = 0$ and include continuous controls for sway and heave for $t \in [0, 5]$. Here, $\tau_\phi(t) = \frac{\phi t^3(6t^2 - 75t + 250)}{3125}$. By use of this definition of $\tau(t)$, Eq. (5.54) becomes

$$\sigma^4(t) = D_4 \left(\frac{6\phi t^2(t^2 - 10t + 25)}{625} \right)^2 + j_1 \left(\frac{12\phi t(2t^2 - 15t + 25)}{625} \right). \quad (5.56)$$

Since the rest of the calculations for this method follow similarly to those done previously, we do not include them here.

The final method considered for constructing a control strategy for the pure roll follows exactly the same as the last two methods presented in the design of $\sigma^4(t)$. However, instead of including the full force for compensation of the righting moment in roll for the prescribed value of ϕ , we calculate the appropriate force needed for each $t \in [0, 5]$ from the theoretical evolution desired for the angular displacement. We do this by defining

$$\check{\sigma}^4(t) = \sigma^4(t) - (-0.007 \times 1215.8) \sin \phi(t), \quad (5.57)$$

where $\phi(t)$ is given by Eq. (5.55) and $\sigma^4(t)$ is calculated by use of either of Eq. (5.54) or Eq. (5.56).

5.5.5 Mission 5

Now that we have presented the control strategies for some basic motions, we continue with a practical mission for which an AUV may need to solve the motion planning problem. Suppose that the vehicle is affixed with a forward looking video camera. Additionally, suppose that we are interested in obtaining a video of the seabed in a given area. This scenario is quite common for applications involving coral reef monitoring, seabed mapping and search and recovery. Depending upon the specific application, the design of the search pattern may be different, however the vehicle must be able to rotate so that the camera can see the sea bed and maneuver while holding this prescribed angle.

To demonstrate this mission, we choose a pitch angle of $\theta = -20^\circ$ and apply a five meter surge while maintaining this pitch angle and constant depth. We will assume that ODIN is fully-actuated and thus every vector field in \mathbb{I}^{-1} is decoupling. We design the control strategy as follows. First, we apply a control to realize the pitch angle, then we follow the integral curves of $V_1 = \cos \theta X_1 + \sin \theta X_3$ to realize the surge motion.

For this mission, we will realize the pitch motion by simply applying the control to counter the righting moments for maintaining a pitch angle of $\theta = -0.35$ radians. We apply this control for $t = 5$ seconds so that the orientation is stabilized. This applied

control is given by

$$\sigma(t) = \begin{pmatrix} 0.445 \\ 0 \\ -1.221 \\ 0 \\ -2.911 \\ 0 \end{pmatrix}, \quad t \in [0, 5]. \quad (5.58)$$

Now to design the surge motion control strategy. We choose $\tau(t) : [0, 30] \rightarrow [5.323]$. Since we wish to realize a five meter surge while maintaining $\theta = -20^\circ$, we must consider the reparameterization over the length of the hypotenuse of the triangle which has base 5 m and adjacent angle θ . For this choice of reparameterization,

$$\tau(t) = \frac{5323(t^2(45 - t))}{13500000}. \quad (5.59)$$

The dynamic control structure given in Eq. (4.10) becomes

$$\sigma^a(t)\mathbb{I}_a^{-1}(\gamma \circ \tau(t)) = (\tau'(t))^2 \tilde{\nabla}_{V_1} V_1(\gamma \circ \tau(t)) + \tau''(t) V_1(\gamma \circ \tau(t)), \quad (5.60)$$

where we recall that Einstein's summation convention is used on the variable a . Since we prescribe $\theta = -20^\circ$, V_1 is a constant vector field. Since $\tilde{\nabla}$ is bilinear over \mathbb{R} , we can

calculate the covariant derivative $\tilde{\nabla}_{V_1} V_1$ as

$$\begin{aligned}
\tilde{\nabla}_{V_1} V_1 &= \tilde{\nabla}_{(\cos \theta X_1 + \sin \theta X_3)} (\cos \theta X_1 + \sin \theta X_3) \\
&= \tilde{\nabla}_{(\cos \theta X_1)} (\cos \theta X_1) + \tilde{\nabla}_{(\cos \theta X_1)} (\sin \theta X_3) \\
&\quad + \tilde{\nabla}_{(\sin \theta X_3)} (\cos \theta X_1) + \tilde{\nabla}_{(\sin \theta X_3)} (\sin \theta X_3) \\
&= \cos^2 \theta \tilde{\nabla}_{X_1} X_1 + 2 \sin \theta \cos \theta \tilde{\nabla}_{X_1} X_3 + \sin^2 \theta \tilde{\nabla}_{X_3} X_3 \\
&= \cos^2 \theta \tilde{\nabla}_{X_1} X_1 + \sin^2 \theta \tilde{\nabla}_{X_3} X_3.
\end{aligned} \tag{5.61}$$

Hence, we write the controls as

$$\sigma^a(t) \mathbb{I}_a^{-1}(\gamma \circ \tau(t)) = \begin{pmatrix} \frac{D_1}{m_1} \cos^2 \theta (\tau'(t))^2 + \cos \theta \tau''(t) \\ 0 \\ \frac{D_3}{m_3} \sin^2 \theta (\tau'(t))^2 + \sin \theta \tau''(t) \\ 0 \\ 0 \\ 0 \end{pmatrix}. \tag{5.62}$$

The surge and heave controls are then given by

$$\begin{aligned}
\sigma^1(t) &= D_1 \cos^2 \theta (\tau'(t))^2 + m_1 \cos \theta \tau''(t) \\
&= 231 \cos^2 \theta \left(\frac{5323t(30-t)}{4500000} \right)^2 + 196 \cos \theta \left(\frac{5323(15-t)}{2250000} \right),
\end{aligned} \tag{5.63}$$

and

$$\begin{aligned}\sigma^3(t) &= D_3 \sin^2 \theta (\tau'(t))^2 + m_3 \sin \theta \tau''(t) \\ &= 120 \sin^2 \theta \left(\frac{5323t(30-t)}{4500000} \right)^2 + 196 \sin \theta \left(\frac{5323(15-t)}{2250000} \right),\end{aligned}\quad (5.64)$$

where D_1 and D_3 were calculated as outlined previously. Since we wish to maintain the angle θ for $t \in [5, 35]$, the computed control for the main transect portion of the trajectory is given by adding the compensations control given in Eq. (5.58).

$$\ddot{\sigma}(t) = \begin{pmatrix} 231 \cos^2 \theta \left(\frac{5323t(30-t)}{4500000} \right)^2 + 196 \cos \theta \left(\frac{5323(15-t)}{2250000} \right) + 0.445 \\ 0 \\ 120 \sin^2 \theta \left(\frac{5323t(30-t)}{4500000} \right)^2 + 196 \sin \theta \left(\frac{5323(15-t)}{2250000} \right) - 1.221 + 1.3 \\ 0 \\ -2.911 \\ 0 \end{pmatrix}. \quad (5.65)$$

Note in the above control strategy that we also account for the buoyancy force of -1.3N along the transect to maintain a constant depth.

If we assume that this is a classic mowing-the-lawn search pattern, we need only add one more piece to give the complete control strategy. At the end of the surge motion, we can add a pure sway motion to move the vehicle so that it can begin another transect. For this pure sway, we wish to maintain the pitch angle and follow the integral curves of X_2 to realize the motion. Assuming that we wish to move over two meters, we choose

$\tau(t) : [0, 12] \rightarrow [0, 2]$ to be $\tau(t) = \frac{t^2(18-t)}{432}$ and calculate the control to be

$$\begin{aligned}\sigma^2(t) &= D_2(\tau'(t))^2 + m_3\tau''(t) \\ &= 231 \left(\frac{t(12-t)}{144} \right)^2 + 196 \left(\frac{6-t}{72} \right).\end{aligned}\tag{5.66}$$

Putting this all together, we can define a U-shaped trajectory (with right-angle corners) lasting 77 seconds and which represents two transects of a back and forth search plan. The controls are given below:

$$\sigma(t) = \begin{pmatrix} 0.445 \\ 0 \\ -1.221 \\ 0 \\ -2.911 \\ 0 \end{pmatrix} \quad t \in [0, 5]$$

$$\check{\sigma}(t) = \begin{pmatrix} 231 \cos^2 \theta \left(\frac{5323t(30-t)}{4500000} \right)^2 + 196 \cos \theta \left(\frac{5323(15-t)}{2250000} \right) + 0.445 \\ 0 \\ 120 \sin^2 \theta \left(\frac{5323t(30-t)}{4500000} \right)^2 + 196 \sin \theta \left(\frac{5323(15-t)}{2250000} \right) - 1.221 + 1.3 \\ 0 \\ -2.911 \\ 0 \end{pmatrix} \quad t \in [5, 35]$$

$$\sigma(t) = \begin{pmatrix} 0.445 \\ 231 \left(\frac{t(12-t)}{144} \right)^2 + 196 \left(\frac{6-t}{72} \right) \\ -1.221 + 1.3 \\ 0 \\ -2.911 \\ 0 \end{pmatrix} \quad t \in [35, 47]$$

$$\check{\sigma}(t) = \begin{pmatrix} - \left[231 \cos^2 \theta \left(\frac{5323t(30-t)}{4500000} \right)^2 + 196 \cos \theta \left(\frac{5323(15-t)}{2250000} \right) \right] + 0.445 \\ 0 \\ - \left[120 \sin^2 \theta \left(\frac{5323t(30-t)}{4500000} \right)^2 + 196 \sin \theta \left(\frac{5323(15-t)}{2250000} \right) \right] - 1.221 + 1.3 \\ 0 \\ -2.911 \\ 0 \end{pmatrix} \quad t \in [47, 77].$$

We remark that we do not turn the vehicle around, but go backwards along the transect instead. This eliminates the need to change the pitch and yaw angles.

5.5.6 Mission 6

Another practical application for an AUV is to survey the cables or legs of an offshore platform. The vehicle would be equipped again with a forward facing camera to collect video of the supports and rigging. In this case, we will imagine a submerged vertical cylin-

der with a one-meter radius to be examined. We would like to design a trajectory which keeps the camera facing along a line normal to the surface of the cylinder to give the best view of the entire beam. One way to achieve this goal is to design a spiral trajectory around the cylinder. Depending on the vehicle, this may be a difficult motion to construct. To this end, we present an alternate solution.

Maintaining a view normal to a curved surface can be accomplished by following a straight line while simultaneously yawing. The distance from the object may vary, however this motion is much easier to design than the spiral.

For our example, we suppose that the center of the vehicle is positioned 1.25 meters from the surface of the pre-described cylinder. The initial position and orientation is depicted in Fig. 13 along with the proposed path and ending configuration. The basic idea is to first rotate 45° , by use of the vector field X_6 , to face the cylinder, then follow the integral curves of $V_6 = 3X_2 - \frac{\pi}{2}X_6$ to effectively move in a straight line while rotating to maintain a head-on view of the cylinder.

For the first segment of the motion, we choose $\tau_\psi(t) : [0, 3] \rightarrow [0, \frac{\pi}{4}]$ to be $\tau_\psi(t) = \frac{\pi t^2(9-2t)}{108}$, and estimate $D_6 = 28.57 \text{ kg m}^2$. The dynamic control structure is again calculated by use of Eq. (4.10):

$$\sigma^6(t)\mathbb{I}_6^{-1}(\gamma \circ \tau_\psi(t)) = (\tau_\psi'(t))^2 \tilde{\nabla}_{X_6} X_6(\gamma \circ \tau_\psi(t)) + \tau_\psi''(t) X_6(\gamma \circ \tau_\psi(t)). \quad (5.67)$$

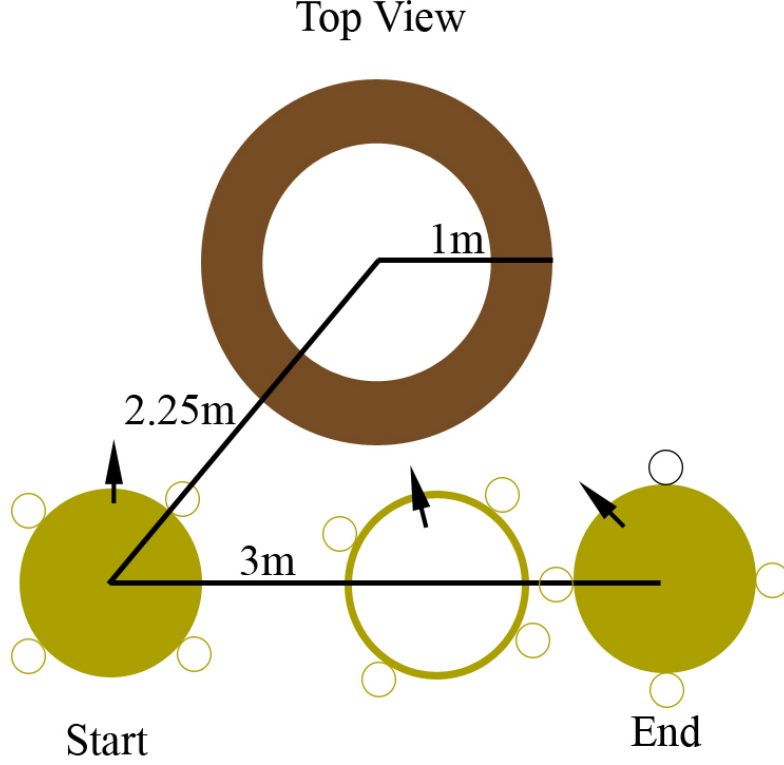


Figure 13: Trajectory around a cylinder for mission six.

By use of Table 4 for the calculation of the covariant derivative, Eq. (5.67) becomes

$$\begin{aligned}
 \sigma^6(t) &= D_6(\tau_\psi'(t))^2 + j_2\tau_\psi''(t) \\
 &= 28.57 \left(\frac{\pi t(3-t)}{18} \right)^2 + 5.72 \left(\frac{\pi(3-2t)}{18} \right).
 \end{aligned} \tag{5.68}$$

Now that the vehicle is rotated and facing normal to the cylinder, we can begin the sway and yaw trajectory. Here, we choose $\tau_y(t) : [0, 10] \rightarrow [0, 1]$ to be $\tau_y(t) = \frac{t^2(15-t)}{500}$, and calculate $D_6 = 28.56 \text{ kg m}^2$ and $D_2 = 120 \text{ kg/m}$ for the respective velocities in yaw and sway. The dynamic control structure given in Eq. (4.10) becomes

$$\sigma^a(t)\mathbb{I}_a^{-1}(\gamma \circ \tau_y(t)) = (\tau_y'(t))^2 \tilde{\nabla}_{V_6} V_6(\gamma \circ \tau_y(t)) + \tau_y''(t) V_6(\gamma \circ \tau(t)), \tag{5.69}$$

where the covariant derivative is given by

$$\begin{aligned}
\tilde{\nabla}_{V_6} V_6 &= \tilde{\nabla}_{(3X_2 - \frac{\pi}{2}X_6)} (3X_2 - \frac{\pi}{2}X_6) \\
&= \tilde{\nabla}_{(3X_2)} (3X_2) + \tilde{\nabla}_{(3X_2)} (-\frac{\pi}{2}X_6) + \tilde{\nabla}_{(-\frac{\pi}{2}X_6)} (3X_2) + \tilde{\nabla}_{(-\frac{\pi}{2}X_6)} (-\frac{\pi}{2}X_6) \quad (5.70) \\
&= \frac{9D_2}{196} X_2 + 0 + \frac{3\pi}{2} X_1 + \frac{\pi^2 D_6}{4 \times 5.72} X_6.
\end{aligned}$$

Note that in computing the covariant derivative the term $(3\pi/2)X_1$ appears. This is intuitive since a pure sway motion would move us away from the cylinder and not along the proposed trajectory. We need a surge component in the control structure. Here we see a glimpse of the important role that the affine connection plays in the control design for mechanical systems.

Inserting the calculation for the covariant derivative, the control strategy is given by

$$\check{\sigma}(t) = \begin{pmatrix} \frac{196 \times 3\pi}{2} \left(\frac{3t(10-t)}{500} \right)^2 \\ 9 \times 120 \left(\frac{3t(10-t)}{500} \right)^2 + 3 \times 196 \left(\frac{3(5-t)}{250} \right) \\ 1.3 \\ 0 \\ 0 \\ \frac{28.57\pi^2}{4} \left(\frac{3t(10-t)}{500} \right)^2 - \frac{5.72\pi}{2} \left(\frac{3(5-t)}{250} \right) \end{pmatrix}, \quad (5.71)$$

and we add in the appropriate buoyancy compensation to maintain a constant depth.

The entire control strategy is arrived at by applying the yaw control calculated in Eq. (5.68) with the appropriate buoyancy compensation for $t \in [0, 3]$ and then applying the

control given by Eq. (5.71) for $t \in [3, 13]$. We remark here that at the end of this trajectory, the vehicle is in the appropriate position to directly apply the control given by Eq. (5.71) for another ten seconds. After four applications of this control, the vehicle will have traversed around the cylinder via a square trajectory while keeping the camera view normal to the cylinder's surface.

5.5.7 Mission 7

Recently, it has been an interest of homeland security to examine the hulls of ships before they enter port. This mission has attracted recent research interest in the AUV community and is currently still under much investigation. We do not propose to solve the matter here, but instead, offer a possible solution to a motion planning problem which is motivated by ship hull inspections.

Many of the large vessels which would require examination before entering a harbor have a bulbous bow. An example of a bulbous bow can be seen on the USS George H.W. Bush (CVN 77) shown in Fig. 14. This bulb is positioned to sit just below the design water line and has the purpose of reducing the height of the bow wake of the vessel which in turn reduces the hull drag which implies better efficiency. These bulbs come in all different sizes and are optimized for a given ship design.

For this mission, we will design a trajectory for an underwater vehicle to examine the bulbous bow of a ship in the vertical direction. We assume here that the bulb is almond shaped with the point at the top. Since we are depth limited in the testing facility (see



Figure 14: USS George H.W. Bush (CVN 77), GlobalSecurity.org (2008).

Section 6.2 for details on the testing facility), we will scale down the path to fit within our constraints. The general shape we assume for the bulb and the associated trajectory are displayed in Fig. 15.

Again, we assume that the instrument used to gather data during the examination is front mounted and forward facing. The trajectory for this mission consists of a -22.5° pitch to point the instrument at the bulb, a one meter body-pure pure heave to move along the top portion, a pitch rotation to 30° and a 2.5 m body-pure heave to examine the lower part of the bulb. Since the second pitch and body-pure heave controls are determined in Section 5.5.3, we only focus on the design of the first segment. The complete strategy will be the concatenation of the two segments.

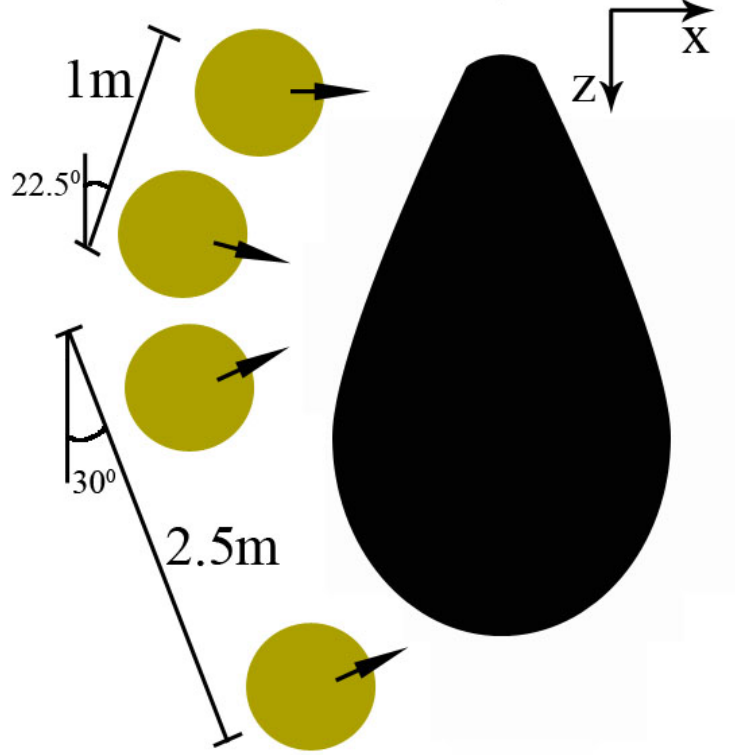


Figure 15: Scaled trajectory for examining a bulbous bow.

We continue as before and would like to realize a pitch angle of $-22.5^\circ = -\pi/8$ radians. After the pitch displacement, we require a 1 m pure heave. We can define this motion along the flows of the integral curves by $\mathcal{F}_1^{X_3} \circ \mathcal{F}_{-\pi/8}^{X_5}(\eta_{init}) = \eta_{final}$. For the initial rotation of this mission, we will realize the pitch motion by simply applying the control to counter the righting moments as done in Section 5.5.5. We apply this control for $t = 5$ seconds so that the orientation is stabilized. This control is given by

$$\sigma(t) = \begin{pmatrix} 0.497 & 0 & -1.201 & 0 & -3.257 & 0 \end{pmatrix}^t. \quad (5.72)$$

We reparameterize the body-pure heave motion to last for 10 seconds by use of $\tau_z(t) : [0, 10] \rightarrow [0, 1]$ defined by $\tau_z(t) = \frac{t^2(15-t)}{500}$. For a heave velocity of 0.1 m/s we have

$D_3 = 119 \text{ kg/m}$. Hence, we can calculate the dynamic control structure for each motion by use of Eq. (4.10),

$$\sigma^3(t)\mathbb{I}_3^{-1}(\gamma \circ \tau_z(t)) = (\tau_z'(t))^2 \tilde{\nabla}_{X_3} X_3(\gamma \circ \tau_z(t)) + \tau_z''(t) X_3(\gamma \circ \tau_z(t)). \quad (5.73)$$

By use of Table 4 for the calculation of the covariant derivative, Eq. (5.73) becomes

$$\begin{aligned} \sigma^3(t) &= D_3(\tau_z'(t))^2 + m_3 \tau_z''(t) \\ &= 119 \left(\frac{3t(10-t)}{500} \right)^2 + 196 \left(\frac{3(5-t)}{250} \right). \end{aligned} \quad (5.74)$$

At $t = 15$ seconds, we directly apply the control to counter the righting moment for $\theta = 30^\circ$ which is given by

$$\sigma(t) = \begin{pmatrix} -0.65 \\ 0 \\ 1.126 \\ 0 \\ 4.2553 \\ 0 \end{pmatrix}. \quad (5.75)$$

As mentioned previously, the body-pure heave portion is calculated in Section 5.5.3 and is not repeated here. The control strategy for the entire trajectory is given by the following

time discretized controls:

$$\ddot{\sigma}(t) = \begin{pmatrix} 0.497 \\ 0 \\ -1.201 + 1.3 \\ 0 \\ -3.257 \\ 0 \end{pmatrix} \quad t \in [0, 5], \quad (5.76)$$

$$\ddot{\sigma}(t) = \begin{pmatrix} 0.497 \\ 0 \\ 119 \left(\frac{3t(10-t)}{500} \right)^2 + 196 \left(\frac{3(5-t)}{250} \right) - 1.201 + 1.3 \\ 0 \\ -3.257 \\ 0 \end{pmatrix} \quad t \in [5, 15], \quad (5.77)$$

$$\ddot{\sigma}(t) = \begin{pmatrix} -0.65 \\ 0 \\ 1.126 \\ 0 \\ 4.2553 \\ 0 \end{pmatrix} \quad t \in [15, 20], \quad (5.78)$$

$$\ddot{\sigma}(t) = \begin{pmatrix} -0.65 \\ 0 \\ 115 \left(\frac{15t(8-t)}{512} \right)^2 + 196 \left(\frac{15(4-t)}{256} \right) + 1.126 + 1.3 \\ 0 \\ 4.2553 \\ 0 \end{pmatrix} \quad t \in [20, 28]. \quad (5.79)$$

Chapter 6

Experiments

6.1 Motivation

All of the previous chapters have focused upon the development of a geometric technique to provide solutions to the motion planning problem for the submerged rigid body. The particular extension presented in this dissertation allows for control strategies to be calculated by use of a kinematic reduction on systems which are subjected to dissipative drag and potential forces arising from gravity and buoyancy.

Demonstrating the inclusion of these forces into the construction of the control strategies achieves one part of the research objective to bridge the gap between geometric control theory and practical applications. The other portion is realized through the testing of the control strategies on an actual underwater vehicle.

In the following sections, we present the results obtained from the implementation of the control strategies discussed in Sections 5.5.1-5.5.7.

6.2 Testing Facility

The experiments for this research were all conducted in the diving well at the Duke Kahanamoku Aquatic Complex at the University of Hawaii. The well is 25m×25m by five

meters deep, and provides a constant and controlled environment for our experiments. A picture of the pool is shown in Fig. 16. The diving well is in the far pool seen in the photo. A close up of the diving well with appropriate dimensions and ODIN as seen from the 10



Figure 16: Duke Kahanamoku Aquatic Complex.

meter platform is presented in Fig. 17. Note that Fig. 17 is only a representative image of the diving well as it was not possible to obtain a picture from above which captured the entire pool. The black lines in the diving well are the lane lines for instances when the well is used for lap swimming.

The water temperature in the pool was a consistent 28° Centigrade and the density of the water is taken to be 997 kg m^{-3} (see Appendix B for details). The only other environmental factor to consider is a small current created by the pool's circulation pumps. Many drifter tests were performed at multiple depths in and around the testing area. The pool's current travels in a direction from West to East at an average rate of 0.016 m/s . The effect of

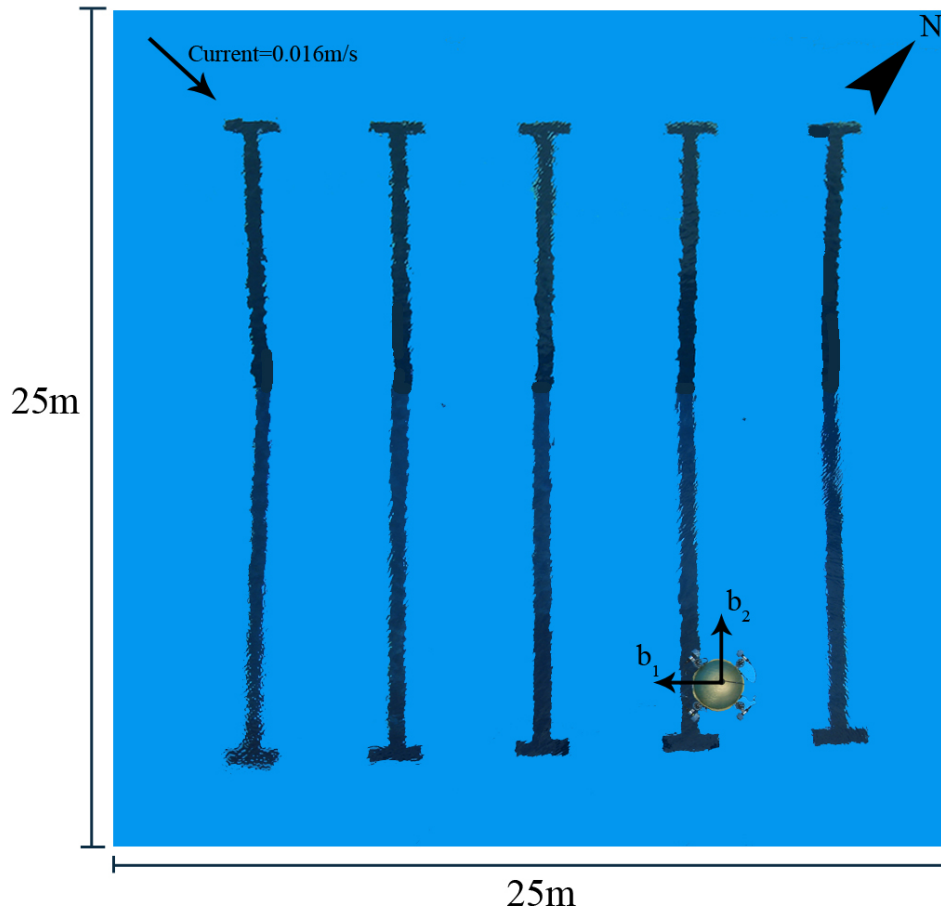


Figure 17: Duke Kahanamoku Aquatic Complex diving well.

this environmental disturbance is considered to be negligible. Although, accounting for the effect of the current can be handled in exactly the same way as the buoyancy force discussed in Section 5.5.1.

6.3 From Theory to Implementation

At this point, we have all the necessary tools from both theoretical and experimental points of view. We now must merge these two areas together through the implementation of the

calculated control strategies onto ODIN. Here, we present the method along with a flow chart (e.g., Fig. 18) to describe the transformation from theory to implementation.

Unfortunately, as designed, the control strategies can not directly be implemented onto ODIN. The geometric control theory generates continuous controls as a function of time, whereas ODIN's input requires a piece-wise constant control structure over discretized time intervals. The reason for this type of input is based on the combination of the refresh rate of the controller, the voltage to thrust relation used for the thrusters and an effort to keep the thrusters operating in a steady state to reduce their transient output response. In addition to the control structure, we must also link the piece-wise constant thrusts via a linear function since it is impossible for a physical actuator to change outputs instantaneously.

To test our strategies on ODIN, we must adapt the continuous control into piece-wise constant (PWC) controls. To do this, we must consider the work which is required to perform a desired motion and ensure that equivalent work is being done by both the continuous and PWC controls. We can calculate the work done over a given time interval by integrating the control. Thus, by appropriately choosing the actuator switching times, we can design a PWC control from a given continuous control where the work done on the system is equivalent.

For example, consider the pure surge strategy designed in Section 5.5.2. The calculated strategy for this motion is given by Eq. (5.40) as $\sigma^1(t) = \frac{7(11t^4 - 660t^3 + 9900t^2 - 16800t + 252000)}{270000}$. This control has a positive portion to accelerate the vehicle from rest and realize the motion and a negative section to slow the vehicle to a complete stop in the prescribed location. The

control is zero at 25.05 s. To convert $\sigma^1(t)$ into a PWC control, we consider

$$s_1 = \frac{1}{25.05} \int_0^{25.05} \sigma^1(t) dt, \quad s_2 = \frac{1}{4.95} \int_{25.05}^{30} \sigma^1(t) dt. \quad (6.1)$$

Calculating, we get $s_1 = 9.98$ N and $s_2 = -3.84$ N. Thus, we can write the PWC control as

$$s^1(t) = \begin{cases} 9.98 \text{ N} & t \in [0, 25.05] \\ -3.84 \text{ N} & t \in [25.05, 30] \end{cases}. \quad (6.2)$$

To implement this onto ODIN, we simply connect these two constant controls via a linear junction of 0.9 seconds to avoid instantaneous switching of the thrust command sent to the thrusters. The duration of this junction is based upon the refresh rate of ODIN's CPU and the avoidance of large voltage changes which may damage ODIN's thrusters (see also, Chyba et al. (2008a) for more information).

The resulting discretized control structure which is implemented onto ODIN is listed in Table 5, where the six-dimensional control structure is given by $\sigma = (\sigma^1, \sigma^2, \dots, \sigma^6)$.

Time (s)	Applied Thrust (6-dim.) (N)
0	(0,0,0,0,0,0)
0.9	(9.98,0,0,0,0,0)
25.95	(9.98,0,0,0,0,0)
26.85	(-3.84,0,0,0,0,0)
31.8	(-3.84,0,0,0,0,0)
32.7	(0,0,0,0,0,0)

Table 5: Discretized control structure for 5m pure surge.

Another aspect of the implementation which needs to be addressed is the initializa-

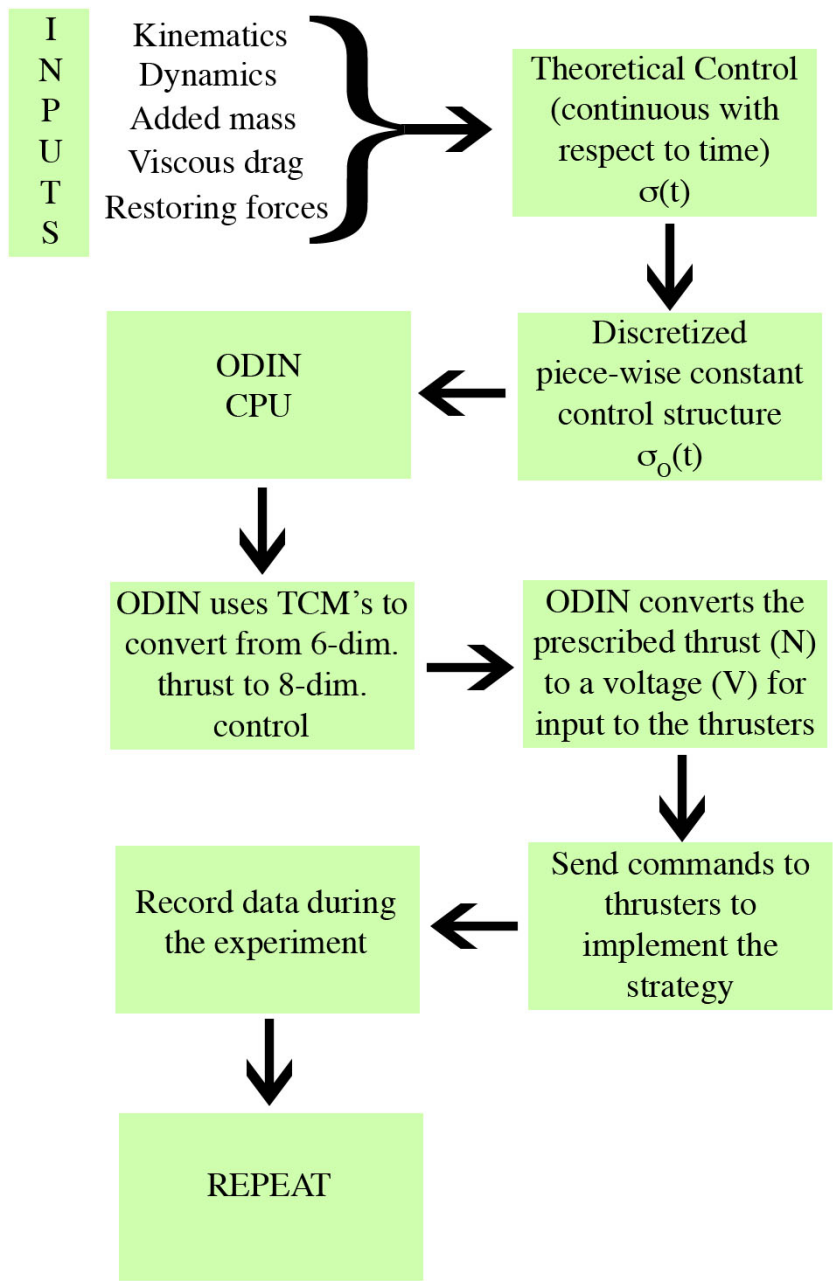


Figure 18: Control design to implementation flow chart.

tion procedure at the beginning of each trajectory. To begin with a stable, submerged vehicle, we implement a closed-loop initialization. This positions the vehicle at $\eta_{init} = (0, 0, 1.5, 0, 0, 0)$ and stabilizes depth, roll, pitch and yaw by use of ODIN's on-board PID controller. The depth is chosen to fully submerge the vehicle, reduce free surface effects and also allow for substantial distance from the bottom of the pool to realize nontrivial dives. We are able to stabilize at different depths and orientations, however, this is rarely necessary.

We are now prepared to discuss the experimental results gathered from the implementation of geometrically designed control strategies onto the test-bed underwater vehicle ODIN.

6.4 Experimental Results

In the following sections, we present the experimental data collected from the implementation of the missions outlined in the previous chapter. In all the graphs, the solid (blue) line represents the actual evolution of ODIN and the dash dot (red) line represents the theoretical evolution of ODIN. The theoretical evolution is determined by numerically integrating the second-order dynamic system of equations, including the actual controls which ODIN applied during the experiment. We use this theoretical evolution because some thrusts which ODIN applied were not implemented exactly as prescribed. When presented, the evolution of the applied control will be displayed by a solid (blue) line; labeling on the graphs will distinguish controls from vehicle position and orientation.

For these experiments, all controls are implemented in completely open-loop. Thus, there is no feedback controller in operation nor any corrective measure accounting for transient thruster response or other deviations from the desired input thrust strategy. Since the development of the geometric theory was heavily model based, we will keep things as pure as possible to demonstrate its effectiveness.

6.4.1 Mission 1

In Section 5.5.1, we calculated the control structure for realizing a pure heave motion of 2.5 meters. Here, we present the implementation of the computed control. As mentioned in Section 6.3, we first need to transform the continuous control strategy into a piece-wise constant control strategy. For the transformation, we would like the work done on the system to be equivalent for both sets of controls. To do this, we make sure that the integral of the two control strategies are equal.

The control given by $\sigma^3(t)$ in Section 5.5.1 is a fourth-degree polynomial with one root in $[0, 8]$ at the point $t = 5.573$ seconds. We note here that the design of the control structure, as done in Sections 5.5.1-5.5.7, is such that there is at most one root in the reparameterized interval for each control. Since we are decoupling the motions of the trajectory as well as starting and ending at zero velocity, each concatenated section intuitively has one acceleration phase and one deceleration phase, which necessarily have opposite sign for the control. Thus, there can be at most one root. Since we include dissipation, there may be motions which only utilize the viscous drag to stop and thus do not require a control

input to decelerate. In general, we may choose $\tau(t)$ as we wish and obtain controls with as many roots in the reparameterized time interval as desired, however this type of control design is impractical for implementation and the functions describing the control can get very complicated.

We continue with the transformation by considering the integral of $\sigma^3(t)$ over the time intervals $[0, 5.573]$ seconds and $[5.573, 8]$ seconds. Since we want a constant control, we simply divide the integral by the length of the associated interval to effectively compute the average work done over each time interval. Computing, we get that the PWC control structure is given by

$$\sigma^3(t) = \begin{cases} 30.04 \text{ N} & t \in [0, 5.573] \\ -24.557 \text{ N} & t \in [5.573, 8]. \end{cases} \quad (6.3)$$

Thus, we implement a constant control force of 30.04 N for 5.573 seconds, then implement a constant control force of -24.557 N for 2.427 seconds to realize the desired motion. However, as mentioned previously, ODIN can not instantaneously switch the thrust from positive to negative. Thus, anytime we change the value of a control, we connect it to the next control via a linear function over a time interval of length 0.9 seconds. Doing this for the PWC control strategy above gives the time-discretized implementable control structure presented in Table 6. This control strategy was implemented onto ODIN and the experimental results are displayed in Fig. 19. Note first that the vehicle started at the point $\eta_{init} = (0, 0, 1.5, 0, 0, 0)$. This is due to the initial closed-loop dive and stabilization. Unless

Time (s)	Applied Thrust (6-dim.) (N)
0	(0,0,0,0,0,0)
0.9	(0,0,30.04,0,0,0)
6.473	(0,0,30.04,0,0,0)
7.373	(0,0,-24.557,0,0,0)
9.8	(0,0,-24.557,0,0,0)
10.7	(0,0,0,0,0,0)

Table 6: Discretized control structure for a 2.5 m pure heave without buoyancy compensation.

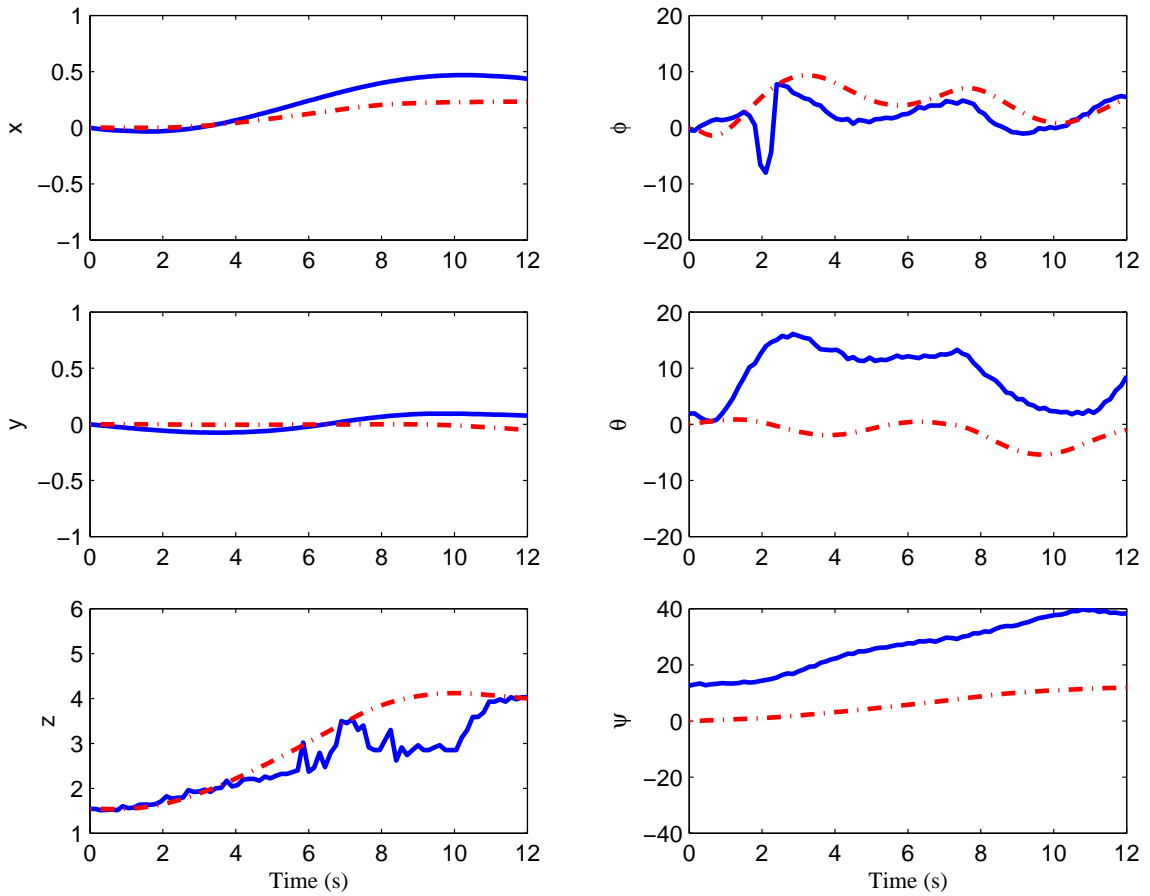


Figure 19: Pure heave trajectory ending at $\eta_f = (0, 0, 4, 0, 0, 0)$ excluding buoyancy.

mentioned otherwise, every trajectory presented will have this same initial configuration.

The heave evolution displays some noise which is related to both the sensor noise and the

AD/DA conversion on-board ODIN when taking the data from the pressure sensor and converting it into a depth measurement to be written to a digital file. Besides the anomaly around $t = 7$ seconds, we see a nice evolution which realizes the prescribed destination. There is a small surge displacement due to the parasite pitch and roll evolutions caused by transient thruster response, and the fact that all the thrusters are not identical. Since we are not running any sort of feedback loop, these discrepancies are minimal and expected.

Examining the evolution of the angles ϕ , θ and ψ , we notice two features. First, the angles do not stay constant over the duration of the motion as prescribed. For the pitch (ϕ) and roll (θ) components, this is a result of an imbalance in the thrust output of the four vertical thrusters. As described in Appendix B.2, each thruster has a unique voltage to thrust relationship which is estimated by use of a piecewise-linear function. The yaw (ψ) component deviation can be attributed to momenta generated by the spinning of the thruster propellers and the imbalance in the thrusters. Secondly, the initial and final values of the angles are not always zero. This artifact will be seen in future experiments in the sections to follow and the explanation is consistent throughout. In the yaw component, this is expected because there are no righting forces or moments acting to correct the displacement. Every effort is made to keep the yaw angle zero at the beginning of experiments in which heading angle is important. For this pure heave motion, the yaw angle has little impact on the realization of η_{final} . However, the situation is different for pitch and roll. Here, restoring forces and moments act to keep the vehicle in a stable equilibrium position where $\phi = \theta = 0$. At the beginning of the trajectory, we stabilize the vehicle by use of a closed-loop control strategy. During this closed-loop initialization, the vehicle is by use of an on-board

PID controller to maintain a 1.5 m depth as well as $\phi = \theta = 0$. Small perturbations in these three components occur based on thruster imbalance and implementing feedback corrections from the PID controller. Each mission is started when ODIN is stable in this closed-loop initialization, but we cannot guarantee that pitch, roll and yaw are collectively zero simultaneously as they are constantly changing. At the end of the prescribed mission, the pitch and roll angles should be zero since the controls are all turned off and the righting moments act to return to the stable equilibrium. In some experiments, we see that these angles are not zero at the end of the trajectory. This is mainly due to the merging of the data collected on board ODIN and the horizontal positioning data collected from the video camera located on the 10 m diving platform. Since there is no way to exactly sync the time between the two data sources, a discrepancy in initial and final times may arise when merging the data together. When merging, the smallest data set determines the size of all other data sets. Thus, some data sets may be truncated based on the length of the video or the data collected from on-board ODIN. This may also contribute to nonzero initial angles as well.

Since we know that ODIN is positively buoyant by 1.3 N, we can include compensation for this force by subtracting this force at each step. The implemented control strategy is presented in Table 7. Here we see that we must apply more force to accelerate against the positive buoyancy, however the deceleration phase uses less force. This control strategy was implemented onto ODIN and the results are presented in Fig. 20.

The Fig. 20 displays a very similar evolution to that seen in Fig. 19. A slightly different pitch and roll evolution cause a large surge displacement. It is significant to note that

Time (s)	Applied Thrust (6-dim.)
0	(0,0,0,0,0,0)
0.9	(0,0,31.34,0,0,0)
6.473	(0,0,31.34,0,0,0)
7.373	(0,0,-23.257,0,0,0)
9.8	(0,0,-23.257,0,0,0)
10.7	(0,0,0,0,0,0)

Table 7: Discretized control structure for a 2.5 m pure heave including buoyancy compensation.

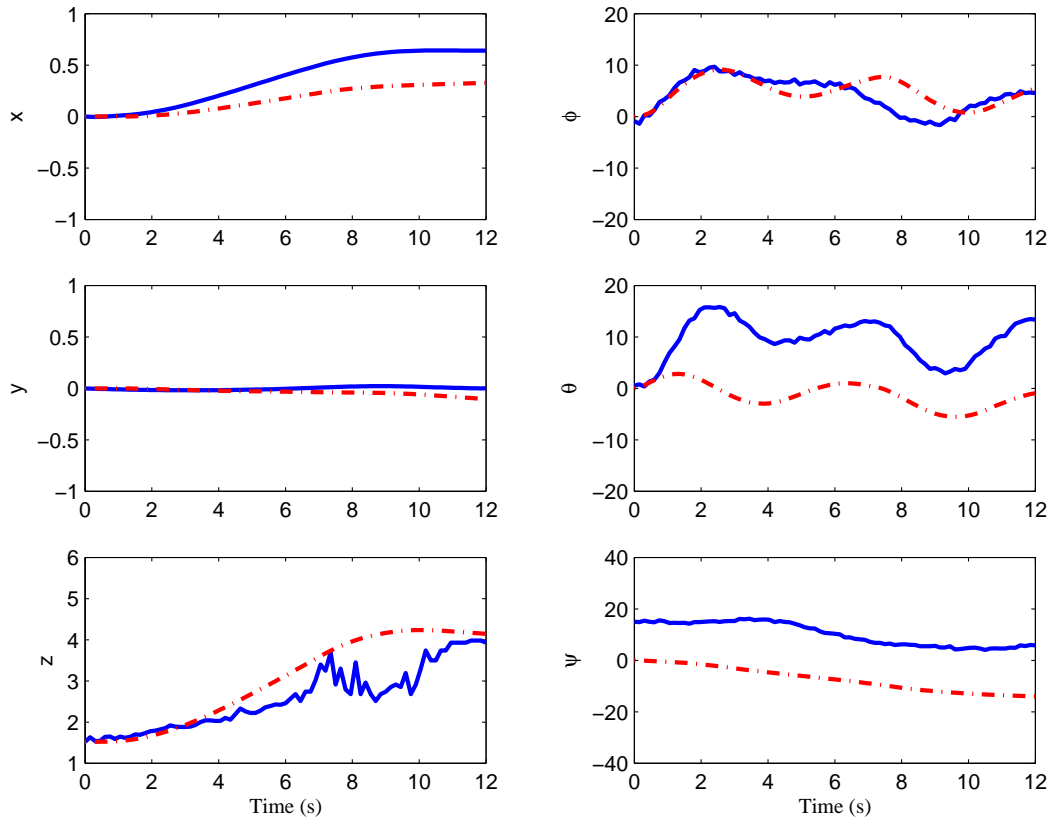


Figure 20: Pure heave trajectory ending at $\eta_f = (0, 0, 4, 0, 0, 0)$ including buoyancy.

both trajectories properly achieved the desired displacement in heave. Due to the chosen reparameterization, the relatively small buoyancy force can be considered negligible with respect to the magnitude of the computed controls.

The experimental results presented in this section match very well with theoretical predictions. The results validate the control design procedure as well as the drag coefficient estimation for heave. We note that the restoring force arising from buoyancy may not be a factor for motions which prescribe a heave displacement with an appropriately chosen reparameterization.

6.4.2 Mission 2

In this section, we present the implementation of two control strategies designed to realize a final configuration of $\eta_{final} = (5, 0, 1.5, 0, 0, 0)$. The first strategy presented applies the control strategy to realize a pure surge in the absence of restoring forces (i.e., 1.3 N positive buoyancy). The second implementation takes into account that ODIN is positively buoyant.

The discretization of the continuous control strategy to a PWC control strategy is outlined in Section 6.3, so it is not repeated here. The PWC control strategy presented in Table 5 was implemented onto ODIN, and the results are displayed in Fig. 21. Examining this result, we see that the vehicle accurately realized the 5 m surge displacement which again validates the control design method as well as the drag estimation for surge. There is a constant positive pitch angle throughout this experiment which may be attributed to the thrusters not applying their force on the same horizontal plane as C_G , which is contrary to our assumptions. Additionally, we clearly see that for this trajectory we cannot neglect the buoyancy force. The evolution of z slowly rises from the initial depth of 1.5 m to a depth

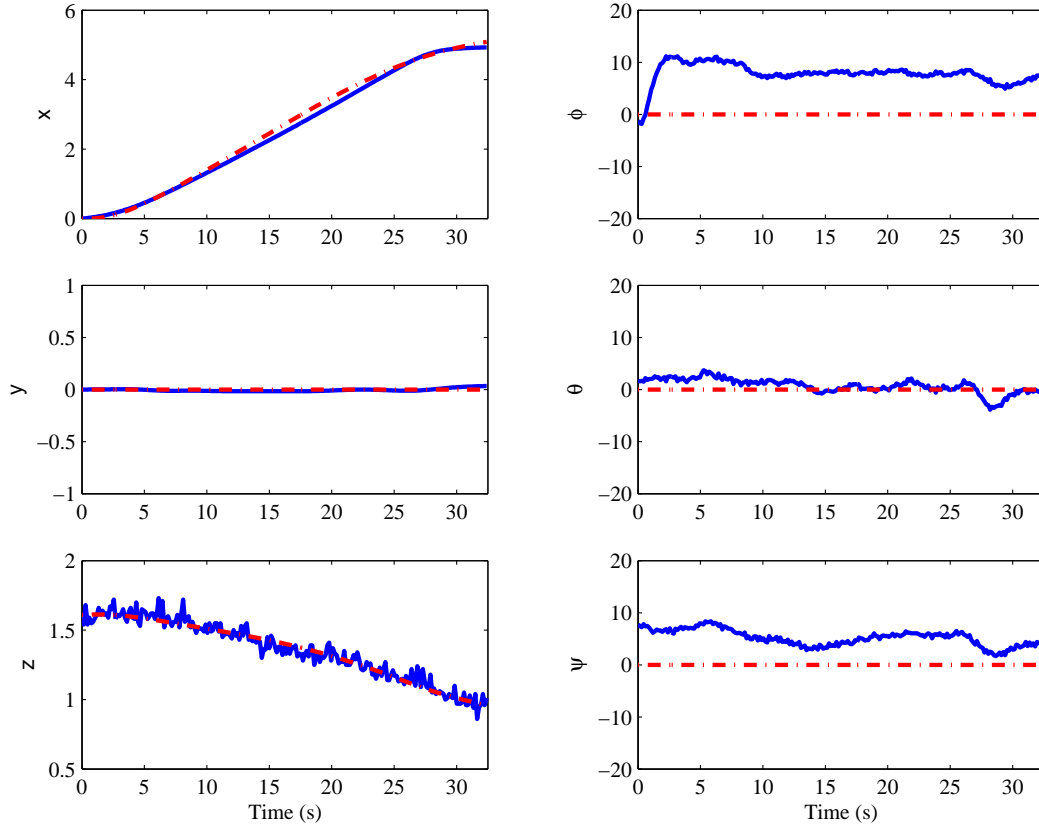


Figure 21: Pure surge trajectory ending at $\eta_f = (5, 0, 1.5, 0, 0, 0)$ excluding buoyancy.

of around 1 m, which is a direct result of the omission of a heave control to compensate for the net positive buoyancy.

For a comparison, we implemented the control strategy given in Table 5 with the addition of a constant 1.3 N force in pure heave. The implementation results are presented in Fig. 22. The results of this implementation are similar to those shown earlier with the exception of the depth evolution. Including the compensation for the net positive buoyancy of ODIN results in realizing the surge displacement while maintaining a constant depth of 1.5 m. There is a slight upward trend in the z evolution, suggesting that ODIN may be slightly more positively buoyant than the assumed 1.3 N.

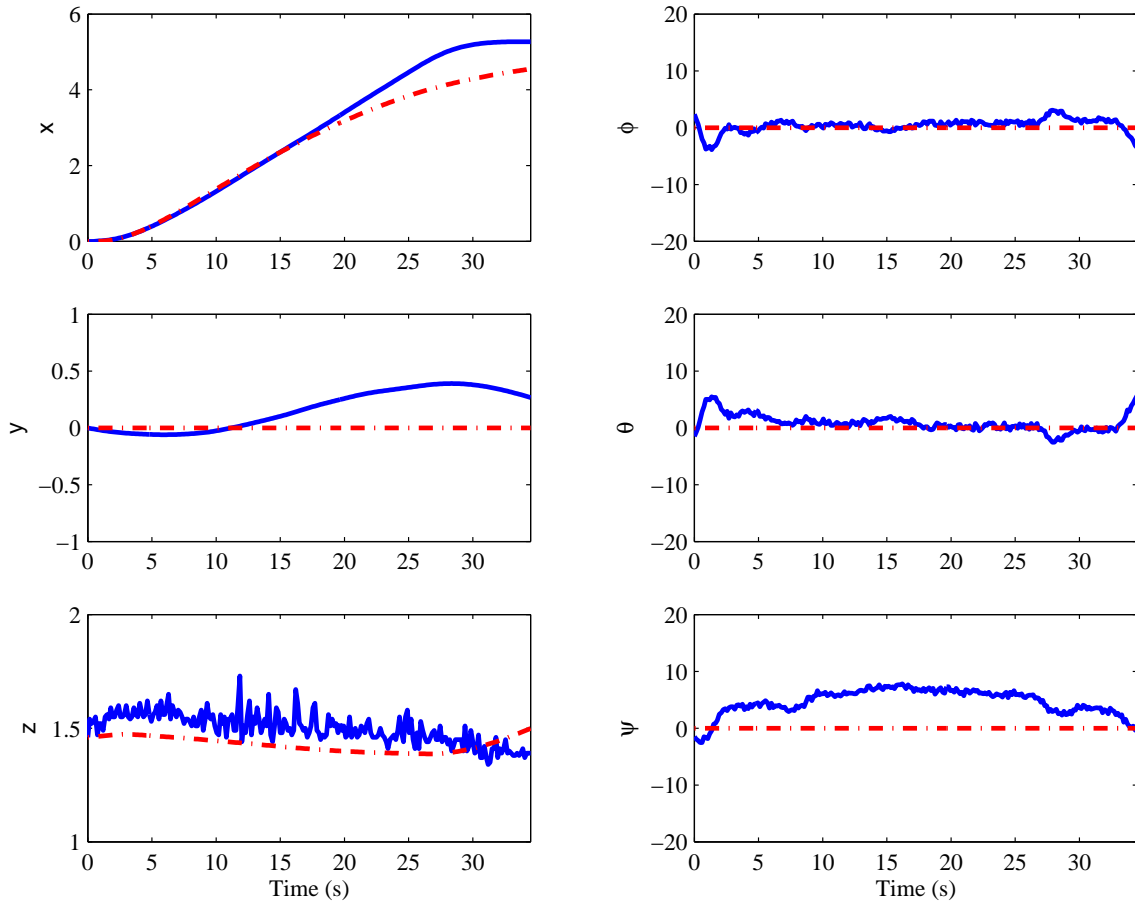


Figure 22: Pure surge trajectory ending at $\eta_f = (5, 0, 1.5, 0, 0, 0)$ including buoyancy.

6.4.3 Mission 3

The previous two missions were straightforward in their design and implementation and only dealt with the restoring force arising from the net buoyancy of the vehicle. Here we prescribe a pitch orientation during the trajectory which induces forces and righting moments upon the vehicle. These forces and moments need to be compensated to realize the desired motion. To demonstrate this need, we implement a control strategy designed under

the assumption that $C_G = C_B$; this practically implies that no righting moments are present for a pitch or roll evolution.

By design, this control strategy is supposed to drive the vehicle from the origin to $\eta_{final} = (1.25, 0, 2.165, 0, 0, 0)$. However, as mentioned before, we begin each trajectory at $z = 1.5$ m. Hence, here we seek to drive the vehicle from $\eta_{init} = (0, 0, 1.5, 0, 0, 0)$ to $\eta_{final} = (1.25, 0, 3.665, 0, 0, 0)$.

Converting the continuous controls given in Eqs. (5.43) and (5.45) gives the PWC implementable control presented in Table 8. Notice that there is no control applied in $\sigma^5(t)$ after $t = 7.7$ seconds. The results of this implementation are presented in Fig. 23, and we clearly see that the pitch angle was not held during the body-pure heave portion of the trajectory.

Time (s)	Applied Thrust (6-dim.) (N)
0	(0,0,0,0,0,0)
0.9	(0,0,0,0,7.19,0)
4.872	(0,0,0,0,7.19,0)
5.772	(0,0,0,0,-0.38,0)
6.8	(0,0,0,0,-0.38,0)
7.7	(0,0,30.04,0,0,0)
13.273	(0,0,30.04,0,0,0)
14.173	(0,0,-24.557,0,0,0)
16.6	(0,0,-24.557,0,0,0)
17.5	(0,0,0,0,0,0)

Table 8: Discretized control structure for trajectory ending at $\eta_f = (1.25, 0, 3.665, 0, 0, 0)$ excluding potential forces.

Along with the evolution of the vehicle, we also present the relevant controls applied by ODIN during the implementation of the strategy presented in Table 8. In Fig. 23, we see a

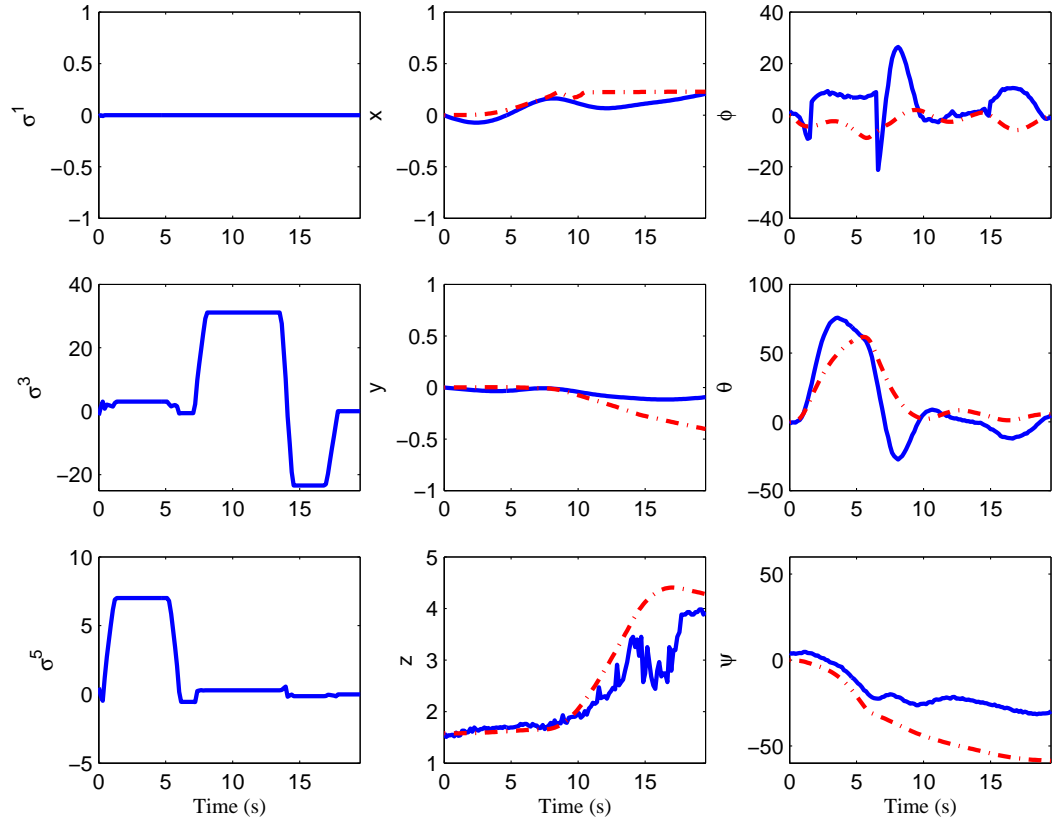


Figure 23: Trajectory ending at $\eta_f = (1.25, 0, 3.665, 0, 0, 0)$ excluding potential forces.

small control applied in $\sigma^5(t)$ from $t \approx 7.5$ s to $t \approx 14$ s. This is a parasite control which ODIN applied but which was not requested. This parasite control arises because of the nonzero dimension of the null space in each of the thrust conversion matrices (TCMs) given in Eqs. (5.1) and (5.2). In particular, there are infinitely many ways to achieve a prescribed six-dimensional control by use of eight thrusters as configured on ODIN. Further details and a more in-depth analysis directly related to the test-bed AUV ODIN can be found in Hanai et al. (2003).

Examining the evolution of the vehicle, we see that there is essentially no displacement in the x -direction and the z displacement exceeds the prescribed amount both theoretically

and actually. Since the pitch angle was not maintained during the body-pure heave motion, no surge displacement could be realized and the vehicle performed an almost pure dive. Since the body-pure heave control was parameterized to travel the length of the hypotenuse of the triangle with sides $x = 1.25$ m and $z = 2.165$ m, it was designed to displace ODIN 2.5 m, which is exactly what it did albeit in the wrong direction. It is difficult to discern whether or not the applied σ^5 control was appropriate or not. There is some overshooting initially which is expected, however the control is terminated before any stabilization occurs. From these data, it is clear that the potential forces arising from induced righting moments cannot be neglected. We continue by presenting the implementation of the control strategies given in Eqs. (5.50) and (5.51).

The inclusion of the restoring forces for the following strategies assumes a reparameterization $\tau_\theta(t)$ for the integral curve following X_5 , which starts and ends with zero velocity as well as ends with zero acceleration. The $\tau_\theta(t)$ chosen for this strategy yields Eqs. (5.50) and (5.51) which have no roots for $t \in [0, 5]$ seconds. This means that, in the design of the PWC control, we will only apply a constant positive control for $\sigma^5(t)$ during this time interval. In the fully actuated scenario, we calculate the appropriate $\sigma^1(t)$ and $\sigma^3(t)$ controls for this constant value of $\sigma^5(t)$ to be $\sigma^1(t) = -0.824$ N and $\sigma^3(t) = 1.006$ N for $t \in [0, 5]$. These forces are different from those given in Eq. (5.46) since the force applied in roll given by the PWC control implies a different resulting angle ϕ from that given by the continuously evolving control. This is an artifact of transforming a continuously evolving control into a piece-wise constant control. The inclusion of these forces will demonstrate the assertion presented in Remark 5.1. For $t > 5$ seconds, we apply a control to counter

the forces given in Eq. (5.46). We give the PWC controls in Table 9 for the case where ODIN only uses vertical thrusters, and in Table 10 for the fully-actuated scenario. The implementation of the respective control strategies are presented in Figs. 24 and 25. The results from the two implementations including restoring forces presented in Figs. 24 and 25 are quite similar and match much better with our theoretical predictions than the results given in Fig. 23. The pitch evolution is almost identical except for the larger overshoot at the beginning of the fully-actuated case. This is probably a result of the initial start-up friction within the thrusters, which is not necessarily the same for each experiment. The main difference is seen in the x evolution. In the under-actuated scenario, ODIN actually exceeds the prescribed surge displacement while the fully-actuated case achieves the desired motion almost exactly. This results from the under-actuated vehicle not being able to apply a force in surge to counter the small coupled force which arises from the induced righting force upon listing. The difference in surge between the two experiments is approximately 10%, however, it is noticeable and certainly not negligible. One concern with the experimental implementation of these strategies is that the pitch angle did not stabilize until midway through the body-pure heave segment of the trajectory. Thus, we wish to consider other control methods to ensure accuracy in realizing the prescribed trajectories.

We conclude this section by presenting two alternate approaches to achieving the prescribed pure rotation in the first segment of this decoupled trajectory. The first approach omits the assumption that $\tau''(5) = 0$ and reverts back to the original definition of the reparameterization function. This choice initially yields a control for $\sigma^5(t)$ which has one root for $t \in [0, 5]$ seconds, although when we include the compensating force in $\sigma^5(t)$ to get

Time (s)	Applied Thrust (6-dim.) (N)
0	(0,0,0,0,0,0)
0.9	(0,0,1.006,0,5.392,0)
4.513	(0,0,1.006,0,5.392,0)
5.413	(0,0,1.006,0,5.392,0)
6.8	(0,0,1.006,0,5.392,0)
7.7	(0,0,31.166,0,4.2553,0)
13.273	(0,0,31.166,0,4.2553,0)
14.173	(0,0,-23.431,0,4.2553,0)
16.6	(0,0,-23.431,0,4.2553,0)
17.5	(0,0,0,0,0,0)

Table 9: Discretized control structure for trajectory ending at $\eta_f = (1.25, 0, 3.665, 0, 0, 0)$ including potential forces using only vertical thrusters.

Time (s)	Applied Thrust (6-dim.) (N)
0	(0,0,0,0,0,0)
0.9	(-0.824,0,1.006,0,5.392,0)
4.513	(-0.824,0,1.006,0,5.392,0)
5.413	(-0.824,0,1.006,0,5.392,0)
6.8	(-0.824,0,1.006,0,5.392,0)
7.7	(-0.65,0,31.166,0,4.2553,0)
13.273	(-0.65,0,31.166,0,4.2553,0)
14.173	(-0.65,0,-23.431,0,4.2553,0)
16.6	(-0.65,0,-23.431,0,4.2553,0)
17.5	(0,0,0,0,0,0)

Table 10: Discretized control structure for trajectory ending at $\eta_f = (1.25, 0, 3.665, 0, 0, 0)$ including potential forces for a fully-actuated system.

$\check{\sigma}(t)$, this root vanishes. Hence, when calculating the PWC control, we calculate the acceleration and deceleration control values for $\check{\sigma}^5(t)$ for $t \in [0, 5]$ based on the location of the initial root of $\sigma^5(t)$. The PWC control strategy is given in Table 11; we omit the surge and heave controls here to compare this strategy to that presented in Fig. 24. Our focus is on the evolution of θ throughout this motion. The experimental data are presented in Fig. 26.

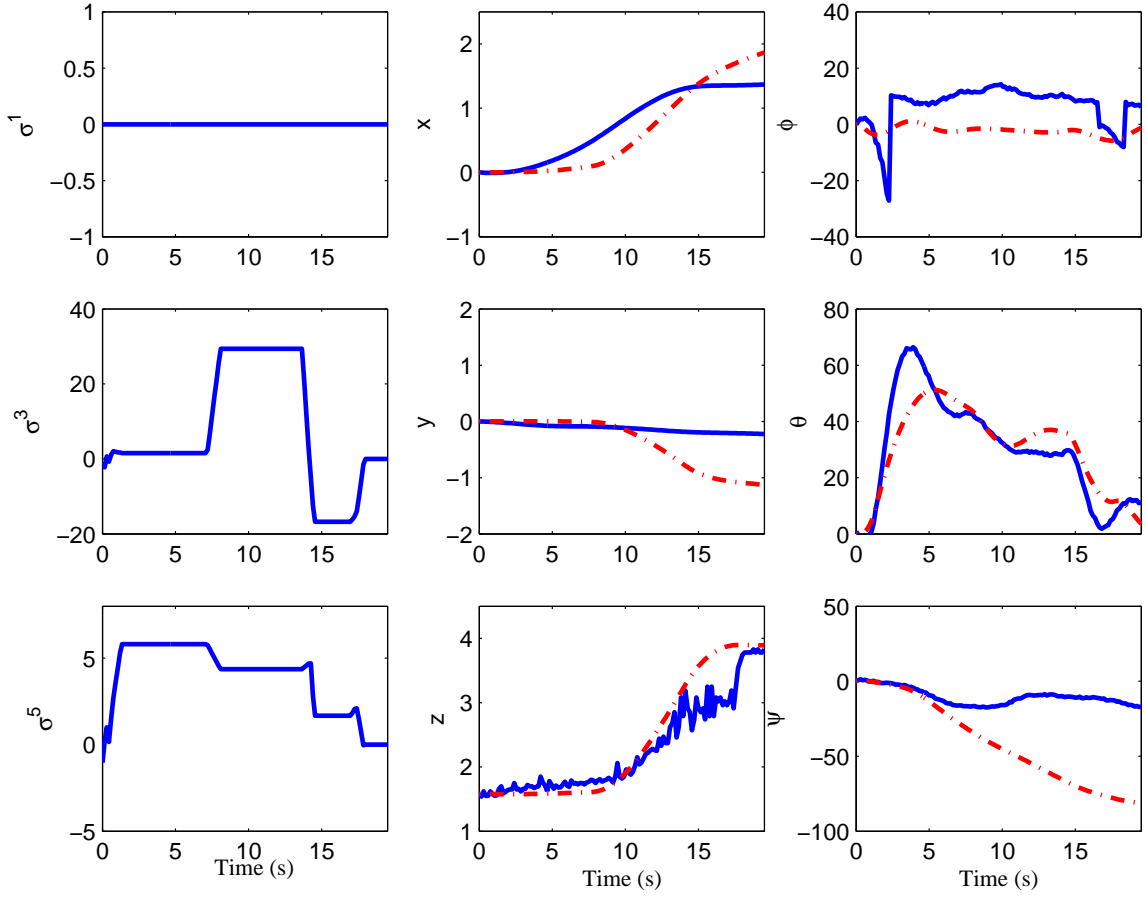


Figure 24: Trajectory ending at $\eta_f = (1.25, 0, 3.665, 0, 0, 0)$ including potential forces using only vertical thrusters.

As previously noted, the only difference between the control strategy in Table 11 and that presented in Table 9 is in $\sigma^5(t)$ for $t \in [0, 6.8]$ and the associated value calculated for $\sigma^3(t)$ with respect to the constant control. Comparing the implementation of these strategies, we see that the heave and surge evolutions are similar. Although the initial overshoot in pitch is larger for the evolution presented in Fig. 26, the pitch evolution stabilizes around 35° for the duration of the body-pure heave motion. Thus, the reduction in applied control during the pitch displacement helped to damp the system and resulted in

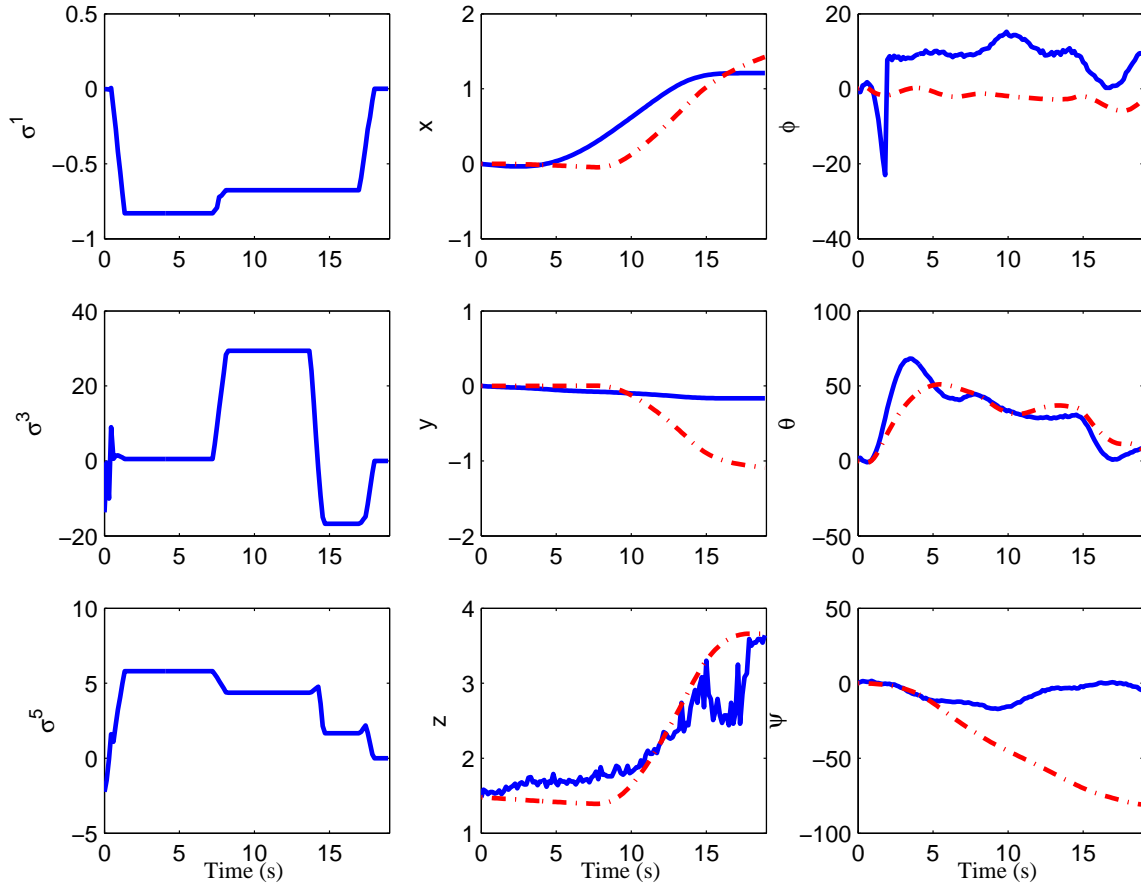


Figure 25: Trajectory ending at $\eta_f = (1.25, 0, 3.665, 0, 0, 0)$ including potential forces for a fully-actuated ODIN.

a more desirable scenario to realize the prescribed mission. Here we see an example where the theory and practical implementation do not coincide. Theoretical development and computation imply that the control strategy presented in Eqs. (5.50) and (5.51) provide the correct control for the prescribed mission. However, converting this theory into a strategy which is implementable onto the test-bed vehicle considered here, renders it undesirable as a practical application. Thus, we must understand the constant interplay between theory and practice including the strengths and downfalls on each side. Testing multiple control

Time (s)	Applied Thrust (6-dim.) (N)
0	(0,0,0,0,0,0)
0.9	(0,0,1.03,0,5.182,0)
4.513	(0,0,1.03,0,5.182,0)
5.413	(0,0,1.154,0,3.923,0)
6.8	(0,0,1.154,0,3.923,0)
7.7	(0,0,31.166,0,4.2553,0)
13.273	(0,0,31.166,0,4.2553,0)
14.173	(0,0,-23.431,0,4.2553,0)
16.6	(0,0,-23.431,0,4.2553,0)
17.5	(0,0,0,0,0,0)

Table 11: Discretized control structure for trajectory ending at $\eta_f = (1.25, 0, 3.665, 0, 0, 0)$ including potential forces using alternate approach #1.

strategies for the same trajectory allows us to consider modifications to the theoretical design and control construction which may not be apparent otherwise.

With this in mind, we abandon the geometric theory altogether and present a second alternative method to realize a pure rotation. In this method, we simply apply the control to compensate for the induced forces and moments for the prescribed angle of inclination. Thus, for $t \in [0, 5]$ seconds, we prescribe $\sigma(t)$ to be the negative of the vector given in Eq. (5.46). We present this method of restoring force compensation for both the under (only vertical thrusters) and fully-actuated scenarios. The under-actuated control is presented in Table 12 and the implementation is displayed in Fig. 27. The fully-actuated control is presented in Table 13 and the implementation is displayed in Fig. 28. We remark that, for the implementation presented in Fig. 28, a feedback control was applied on the yaw control to help maintain a near-zero heading angle. For unknown reasons, this control strategy repeatedly produced poor results when implemented in a fully open-loop situation.

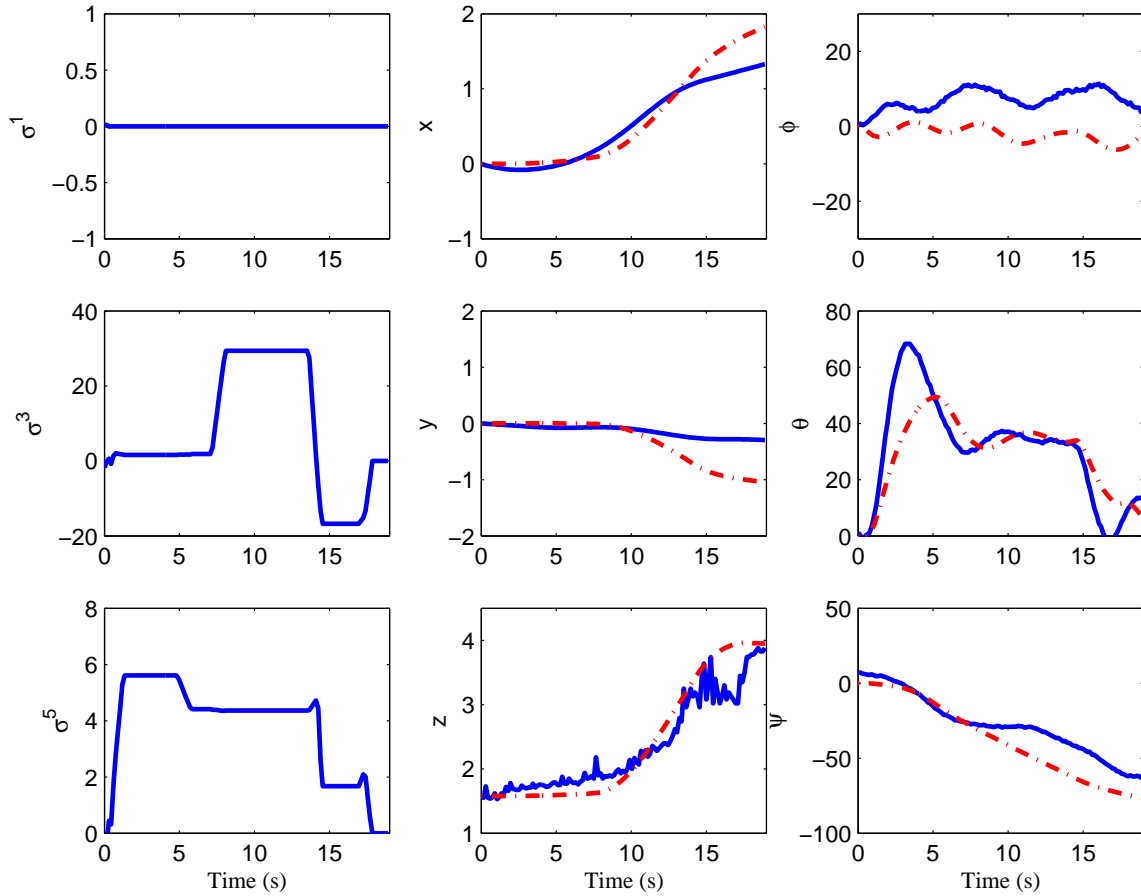


Figure 26: Trajectory ending at $\eta_f = (1.25, 0, 3.665, 0, 0, 0)$ including potential forces using alternate approach #1.

Time (s)	Applied Thrust (6-dim.) (N)
0	(0,0,0,0,0,0)
0.9	(0,0,1.126,0,4.2553,0)
5.9	(0,0,1.126,0,4.2553,0)
6.8	(0,0,31.166,0,4.2553,0)
12.73	(0,0,31.166,0,4.2553,0)
13.273	(0,0,-23.431,0,4.2553,0)
15.7	(0,0,-23.431,0,4.2553,0)
16.6	(0,0,0,0,0,0)

Table 12: Discretized control structure for trajectory ending at $\eta_f = (1.25, 0, 3.665, 0, 0, 0)$ including potential forces using alternate approach #2 using only vertical thrusters.

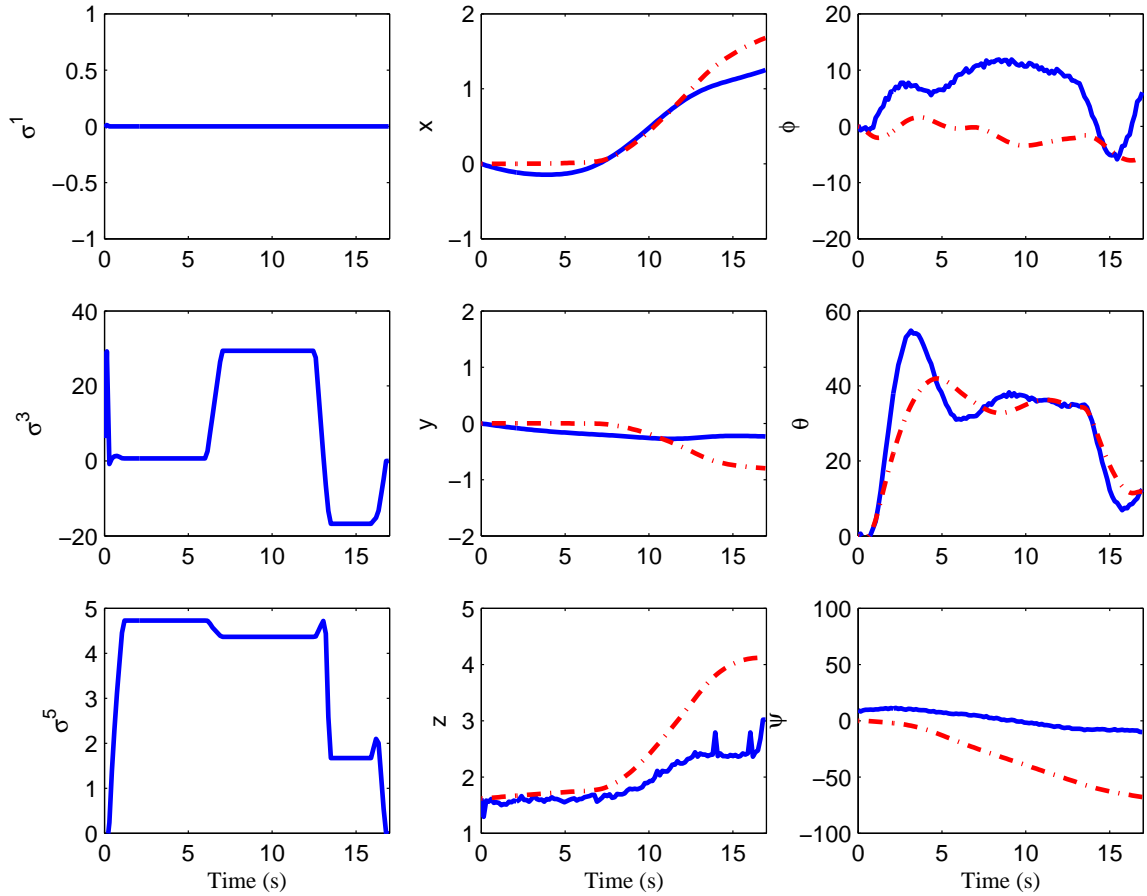


Figure 27: Trajectory ending at $\eta_f = (1.25, 0, 3.665, 0, 0, 0)$ including potential forces using alternate approach #2 using only vertical thrusters.

We comment that all experiments conducted on this day displayed erratic yaw behavior. This behavior was not experienced during other testing days, and the source of the erratic behavior was not fully investigated.

The experimental results shown in Figs. 27 and 28 matched well with theoretical predictions and produced comparable results to those seen earlier in this section. We notice that the heave evolution is slightly less than previously seen, although it is within an acceptable range of the target value. Remarkably, the pitch evolution is greatly improved. The

Time (s)	Applied Thrust (6-dim.) (N)
0	(0,0,0,0,0,0)
0.9	(-0.65,0,1.126,0,4.2553,0)
5.9	(-0.65,0,1.126,0,4.2553,0)
6.8	(-0.65,0,31.166,0,4.2553,0)
12.73	(-0.65,0,31.166,0,4.2553,0)
13.273	(-0.65,0,-23.431,0,4.2553,0)
15.7	(-0.65,0,-23.431,0,4.2553,0)
16.6	(0,0,0,0,0,0)

Table 13: Discretized control structure for trajectory ending at $(1.25, 0, 3.665, 0, 0, 0)$ including potential forces using alternate approach #2.

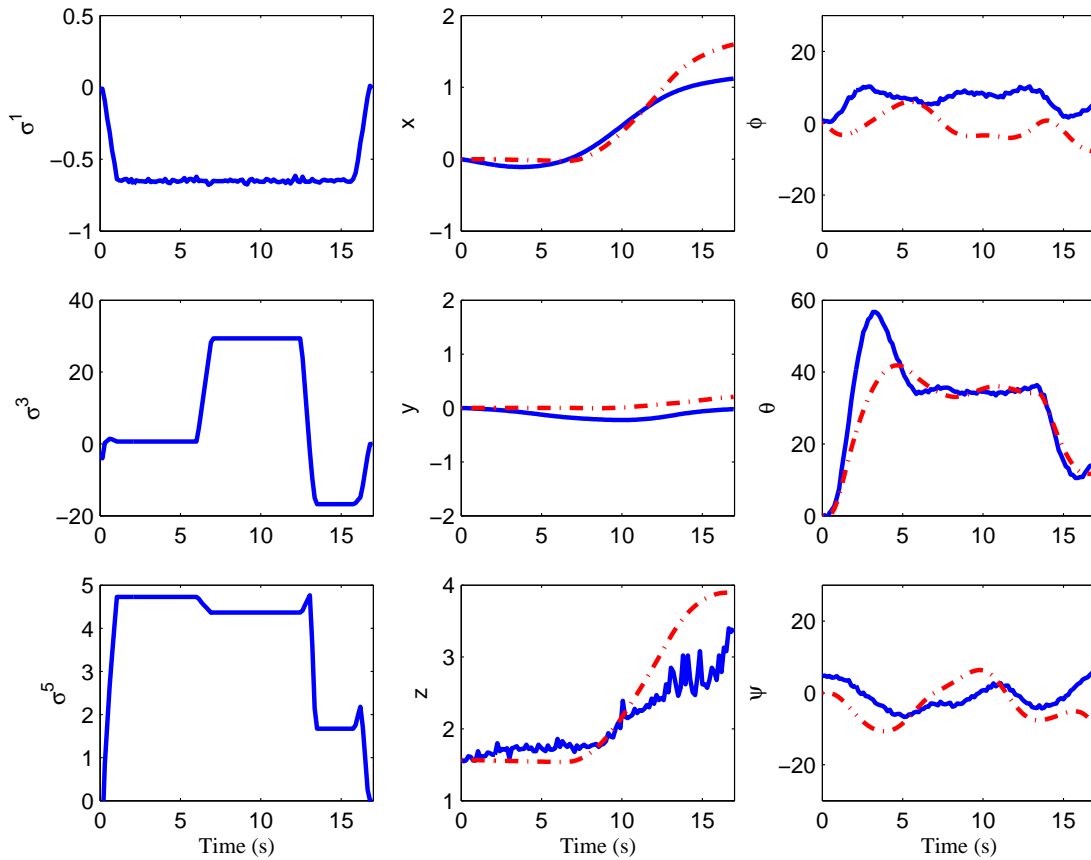


Figure 28: Trajectory ending at $\eta_f = (1.25, 0, 3.665, 0, 0, 0)$ including potential forces using alternate approach #2.

overshoot is smaller than that seen in previously presented data and we observe that a very stable and consistent pitch angle is maintained throughout the entire second leg (body-pure heave) of the trajectory. The Fig. 27 displays a slight dip in pitch just before the body-pure heave motion starts, however even this evolution is better than any other presented previously.

Given the results shown in this section, we will follow the second alternate control design method when prescribing a pure rotation to be stabilized throughout another concatenated motion. In particular, if we need to realize a motion while holding a pitch or roll inclination, we will simply apply the appropriate compensation for the induced forces for approximately five seconds and then apply the geometrically computed control strategy with the restoring force and moment compensation appropriately included within the control.

In the following section, we examine a pure roll trajectory to further validate the findings here, and determine an appropriate stabilization time.

6.4.4 Mission 4

In this section, we display the results of the implementation of the different control strategies designed to realize a pure roll. We present the implemented strategies for the angles $\phi = \pi/8, \pi/6$ and $\pi/4$ radians. The estimated drag terms used in the calculation of the control strategies as presented in Section 5.5.4 are given by $D_4 = 27, 37.2$ and 37.15 kg m^2 , respectively.

We begin by considering the applied compensation control method which is simply applying the control to counteract the forces and moments induced upon listing. Since this control structure is already piece-wise constant, we can readily implement it onto ODIN by inserting the appropriate linear junctions. In particular, for $\phi = \pi/8$

$$\sigma(t) = \begin{cases} (0, 0, 0, 0, 0, 0) & t \in [0, 0.9] \\ (0, 0.497, 1.201, 3.257, 0, 0) & t \in [0.9, 10.9] \\ (0, 0, 0, 0, 0, 0) & t \in [10.9, 11.8], \end{cases} \quad (6.4)$$

for $\phi = \pi/6$,

$$\sigma(t) = \begin{cases} (0, 0, 0, 0, 0, 0) & t \in [0, 0.9] \\ (0, 0.65, 1.126, 4.2553, 0, 0) & t \in [0.9, 10.9] \\ (0, 0, 0, 0, 0, 0) & t \in [10.9, 11.8], \end{cases} \quad (6.5)$$

and for $\phi = \pi/4$,

$$\sigma(t) = \begin{cases} (0, 0, 0, 0, 0, 0) & t \in [0, 0.9] \\ (0, 0.919, 0.919, 6.018, 0, 0) & t \in [0.9, 10.9] \\ (0, 0, 0, 0, 0, 0) & t \in [10.9, 11.8]. \end{cases} \quad (6.6)$$

The implementation results from these strategies are shown in Figs. 29-31, respectively.

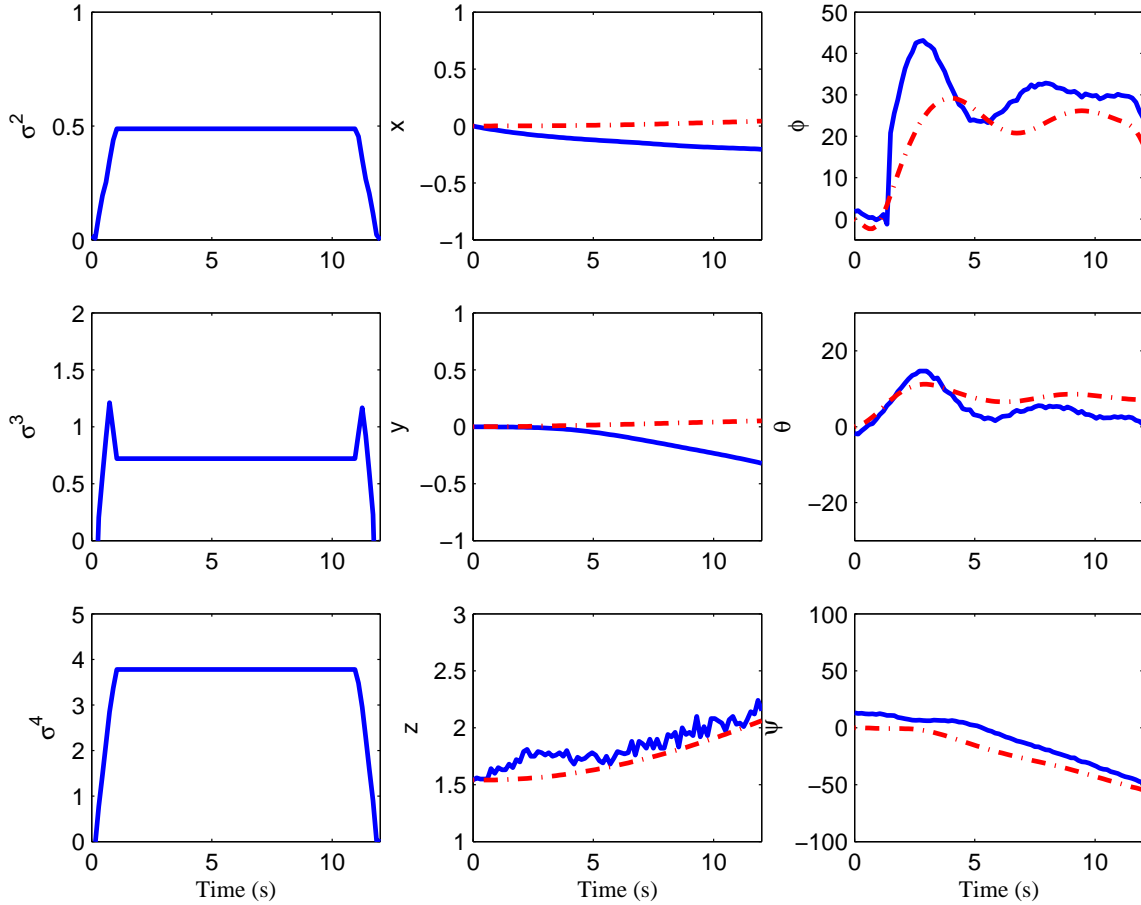


Figure 29: Pure roll for $\phi = \pi/8$ radians using the applied compensation control method.

Our main concern in these experiments is the evolution of the roll component. In all three figures, we see a considerable overshoot followed by a rapid settling to a fairly constant control. We first note that all of the evolutions stabilized at a larger angle than prescribed, whereas the discrepancy lessened as the angle increased in size. This may be linked to the control of the thrusters or to a small difference in the location of C_B with respect to C_G than what is assumed.

For $\phi = \pi/8, \pi/6$ radians we notice that there is more pronounced rebound effect from the initial overshooting and that it takes a longer time to damp the oscillations than observed

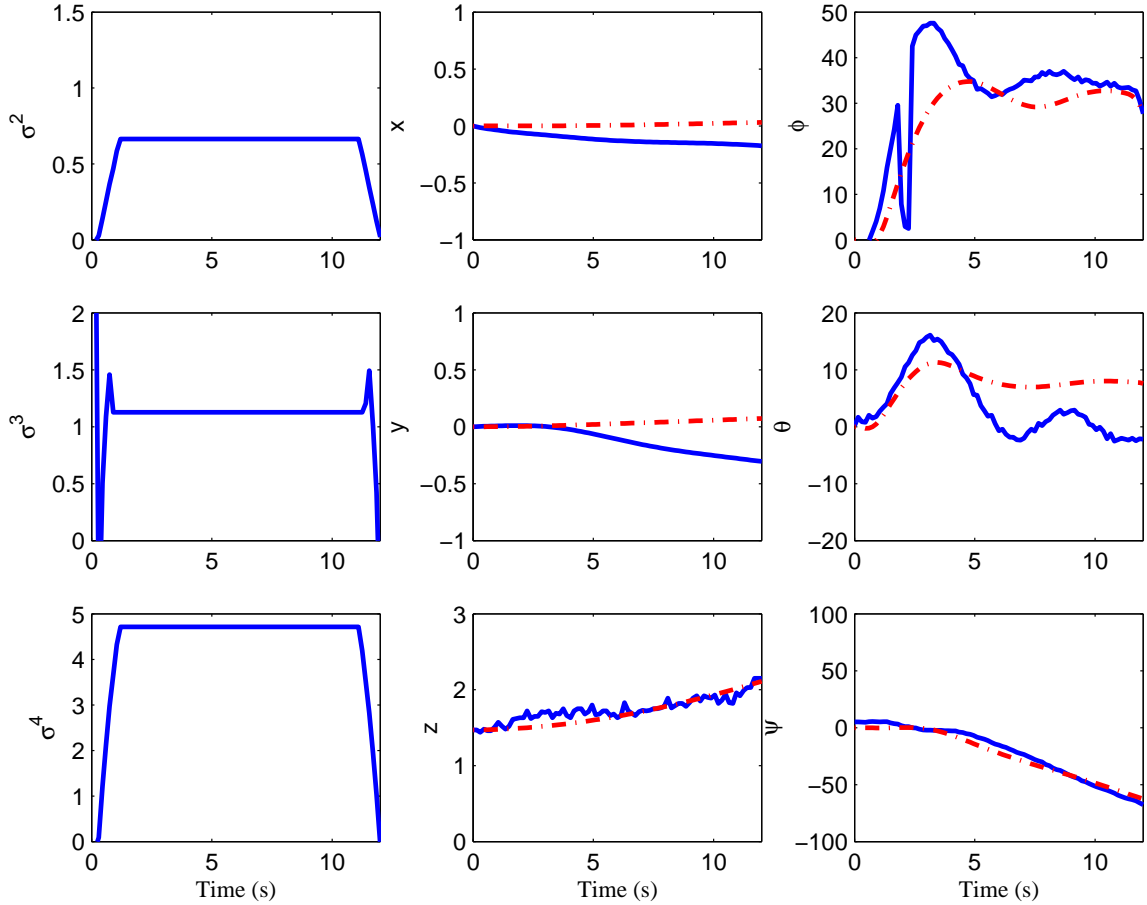


Figure 30: Pure roll for $\phi = \pi/6$ radians using the applied compensation control method.

in the experiment when $\phi = \pi/4$ radians. The direct application of the compensative forces results in a greater overshoot relative to the prescribed angle of inclination for the smaller angles. Since we do not slow the rotational acceleration of the vehicle, we are relying on the viscous drag to damp the system. There are two main reasons for this overshoot. First, there may be an overestimate in the calculation of the drag moment versus velocity relation. Second, the overshooting may be a result of the piece-wise constant requirement for implementation of the control strategies onto ODIN. Without the ability to implement a continuously evolving thrust strategy, we expect such behavior.

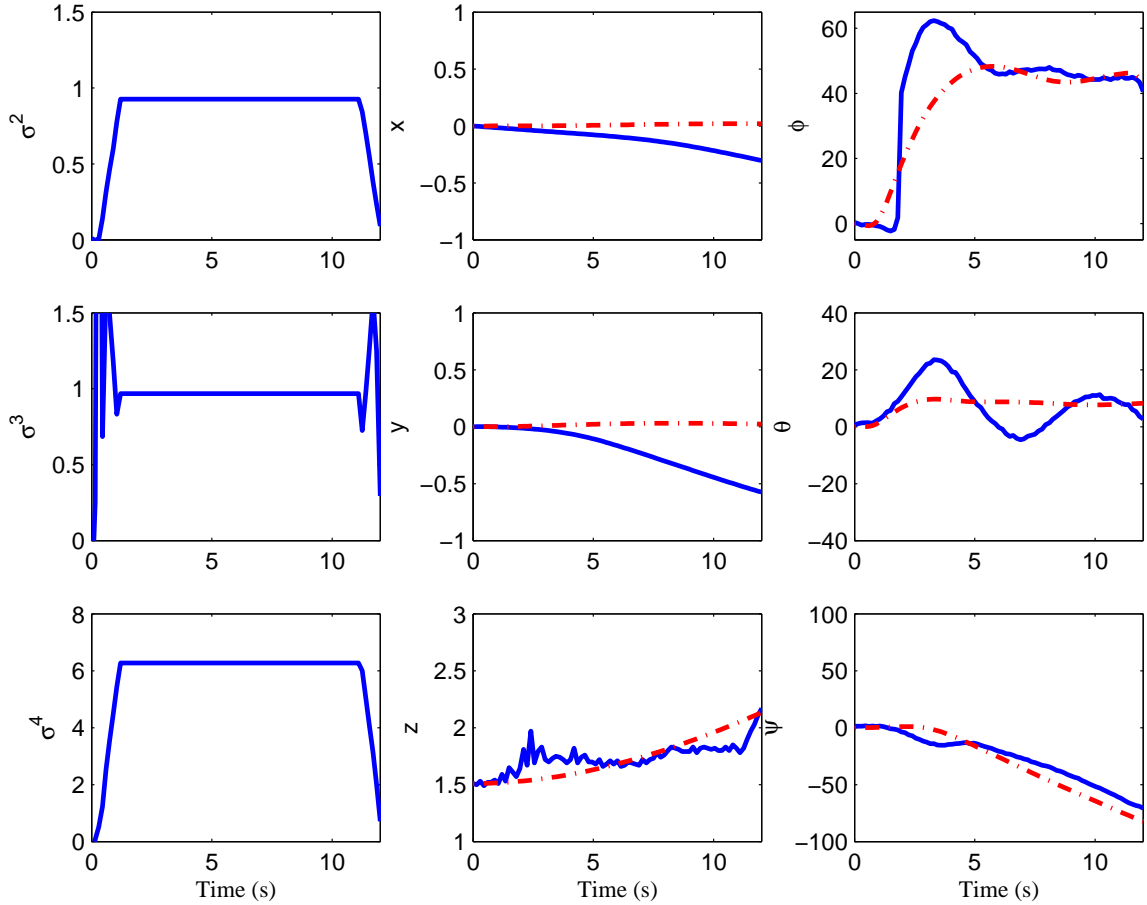


Figure 31: Pure roll for $\phi = \pi/4$ radians using the applied compensation control method.

Next, we consider the implementation of the control strategies designed by use of a choice of $\tau(t)$ which does not guarantee that $\tau''(5) = 0$. We refer to this design as the ramped control method. Again we consider $\phi = \pi/8, \pi/6$ and $\pi/4$ radians. By design and choice of reparameterization, the control $\sigma^4(t)$ has one root for $t \in [0, 5]$ seconds. We use this value of t to determine the limits of integration when computing the PWC controls. Since there is only one root, we only assign two separate controls over the interval of zero to five seconds. Upon computing the PWC control for $\sigma^4(t)$, we then compute the associated sway and heave forces from the value of ϕ obtained by use of Eq. (5.55) and inserting that

into Eq. (5.52). The computed control then has two phases for $t \in [0, 5]$ seconds. The first phase is basically an applied compensation control method for a slightly larger angle than prescribed and the second phase corresponds to a slightly smaller angle than we prescribed. We present the computed PWC controls in Tables 14-16 with the implementation results contained in Figs. 32-34, respectively.

Time (s)	Applied Thrust (6-dim.) (N)
0	(0,0,0,0,0,0)
0.9	(0,0.566,1.17,3.706,0,0)
4.71	(0,0.566,1.17,3.706,0,0)
5.61	(0,0.454,1.22,2.97,0,0)
6.8	(0,0.454,1.22,2.97,0,0)
7.7	(0,0.497,1.201,3.257,0,0)
10.9	(0,0.497,1.201,3.257,0,0)
11.8	(0,0,0,0,0,0)

Table 14: Discretized control structure for a pure roll of $\phi = \pi/8$ radians using the ramped control method.

Time (s)	Applied Thrust (6-dim.) (N)
0	(0,0,0,0,0,0)
0.9	(0,0.761,1.05,4.98,0,0)
4.86	(0,0.761,1.05,4.98,0,0)
5.76	(0,0.590,1.159,3.86,0,0)
6.8	(0,0.590,1.159,3.86,0,0)
7.7	(0,0.65,1.126,4.2553,0,0)
10.9	(0,0.65,1.126,4.2553,0,0)
11.8	(0,0,0,0,0,0)

Table 15: Discretized control structure for a pure roll of $\phi = \pi/6$ radians using the ramped control method.

As seen in the applied control method, the ramped control method also produces overshooting and problems with damping the oscillations in the pitch evolution. However, in the

Time (s)	Applied Thrust (6-dim.) (N)
0	(0,0,0,0,0,0)
0.9	(0,1.14,0.623,7.47,0,0)
5.04	(0,1.14,0.623,7.47,0,0)
5.94	(0,0.827,1.003,5.413,0,0)
6.8	(0,0.827,1.003,5.413,0,0)
7.7	(0,0.919,0.919,6.018,0,0)
10.9	(0,0.919,0.919,6.018,0,0)
11.8	(0,0,0,0,0,0)

Table 16: Discretized control structure for a pure roll of $\phi = \pi/4$ radians using the ramped control method.

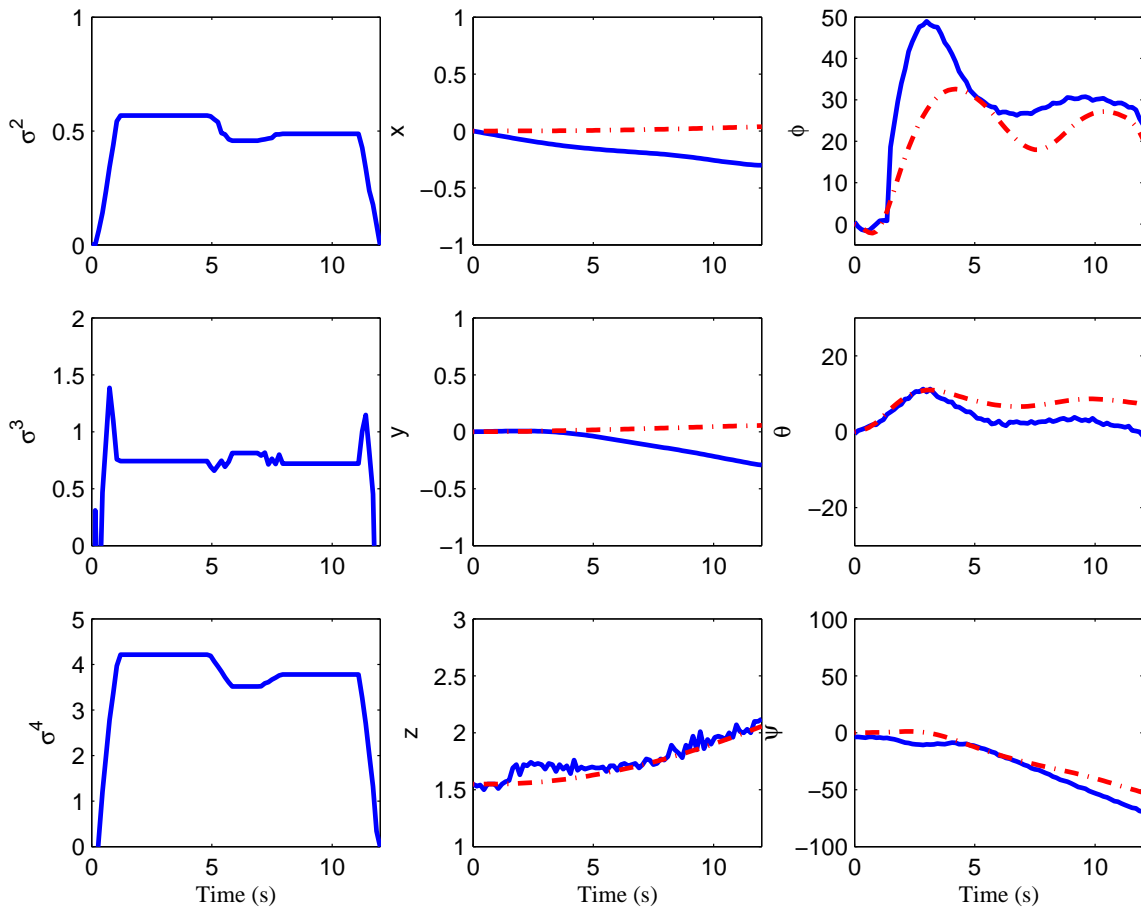


Figure 32: Pure roll for $\phi = \pi/8$ radians designed from theory.

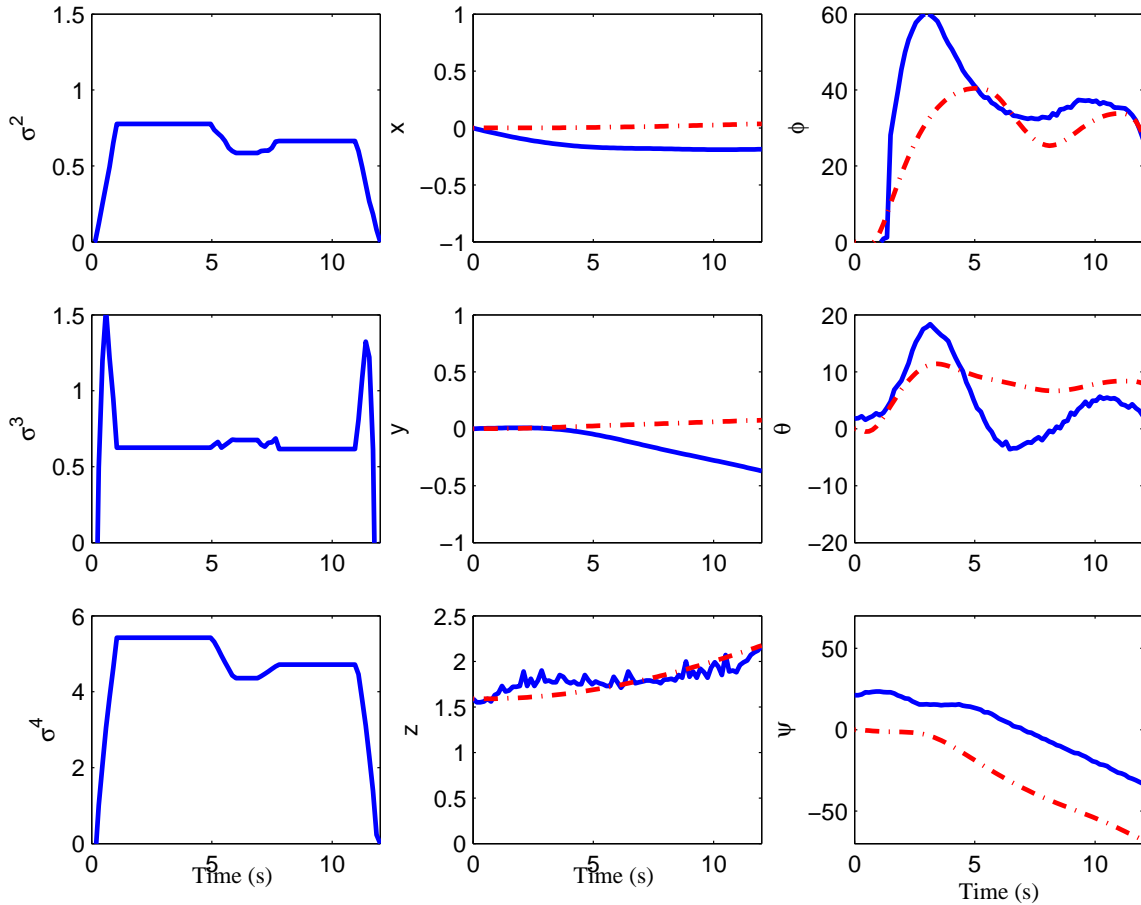


Figure 33: Pure roll for $\phi = \pi/6$ radians designed from theory.

ramped control method, the characteristics on stability and consistency are reversed with respect to the size of the angle. Here the smaller angle ($\phi = \pi/8$) displays a more suitable evolution than that observed for $\phi = \pi/4$ radians. The opposite effect is occurring in the later experiments since we are essentially providing a deceleration phase which is needed by the small angles to recover from the large initial impulse provided by the thrusters. The larger angles are not as effected by this initial impulse response as the righting arm aids in the deceleration process, and as a result, ODIN tends to fall back down below the prescribed angle before the applied forces for the second portion of the trajectory begin.

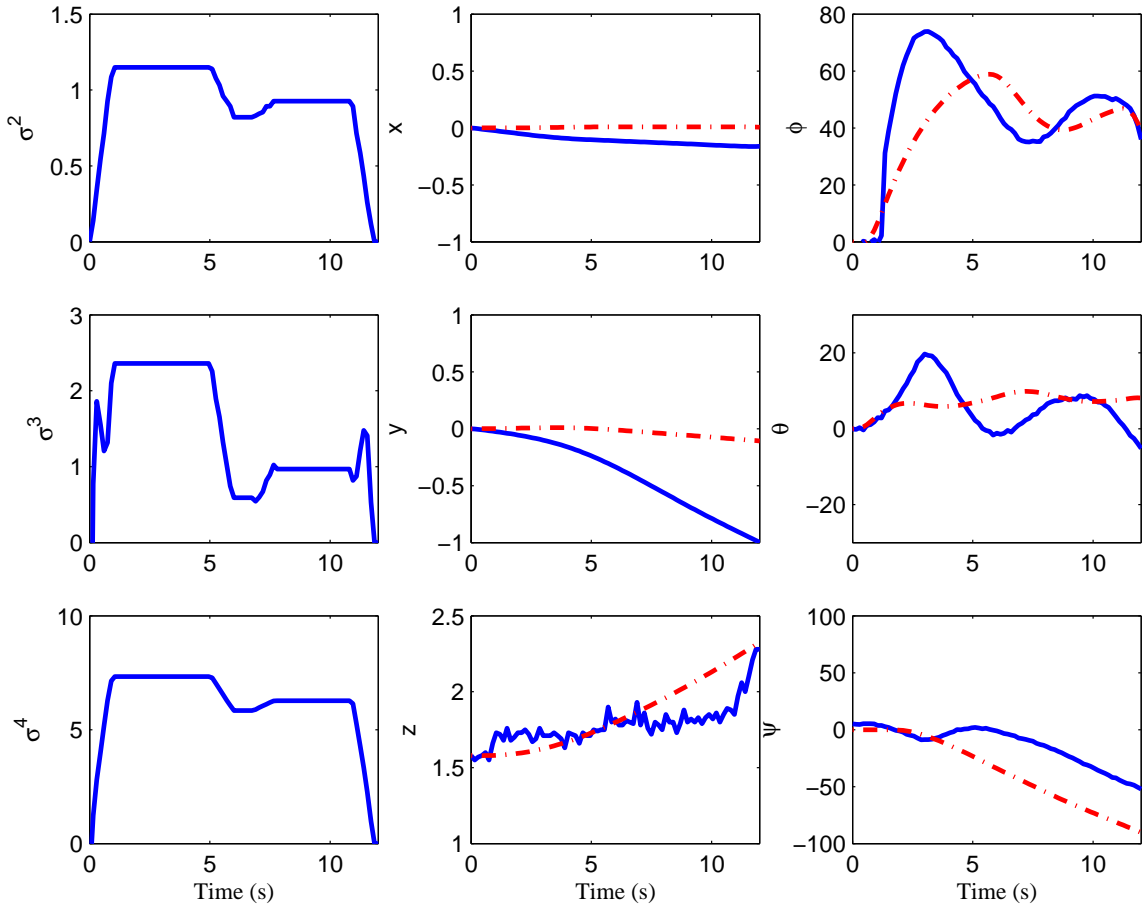


Figure 34: Pure roll for $\phi = \pi/4$ radians designed from theory.

The third method for realizing a pure rotational motion outlined in Section 5.5.4 is the same as the ramped control method except we choose $\tau(t)$ such that $\tau''(5) = 0$. Since we provided an example of such a trajectory design and implementation in Sections 5.5.3 and 6.4.3, respectively, we omit the details here. The results for this method are similar to those presented in the ramped control method. The Fig. 25 presents the experimental results for a pitch angle of $30^\circ = \pi/6$ radians. We observe a similar poor evolution of the pitch angle as in the figures from the ramped control method experiments.

The results shown here suggest that a hybrid method be used to successfully reduce the overshooting and produce a stable and maintainable pure pitch or roll. This corresponds to the final method presented in Section 5.5.4. In this method, we generate a continuous compensation control for the righting moment and the induced forces and moments from the prescribed list angle. The main problem with this method still hinges on the fact that ODIN is unable to accept a continuously evolving control strategy. Thus, we are back to computing a PWC control for this method which, in most ways, defeats the purpose of this method's design. Investigation into the implementation of trajectories designed by use of this method is not active due to the practical constraints of our test-bed vehicle.

From this discussion, we again conclude that the applied compensation control method is the best all around procedure for achieving and stabilizing a pitch or roll angle during a given mission. From the results presented in the previous sections, we realize that we need to allow five seconds for stabilization of the prescribed angle before beginning the next leg of a concatenated trajectory. This is the method we will implement on future control strategies which need to maintain a prescribed angle during a body-pure translational motion.

6.4.5 Mission 5

In this section, we present the implementation results of the two control strategies designed in Section 5.5.5. The intent of these missions is to allow the vehicle to point a forward-looking camera downward while realizing a transect line of a seabed survey. We remark that

in the design stage of the control structure as presented in Section 5.5.5, we do not impose bounds on the control, thus the value of θ can be chosen as any value $-\pi/2 \leq \theta \leq \pi/2$. However, for implementation purposes, we must consider the limitations of our physical actuators which do indeed have force output constraints (see Appendix B.2 for details on ODIN’s thruster bounds). The bounds imposed by ODIN’s thrusters restrict our choice of theta to $\theta > -23^\circ$. This is the reason for the choice of $\theta = -20^\circ$. This may seem a bit small for the practical application considered, however note that we are only demonstrating the applicability and implementability of geometric methods in path planning and construction.

Continuing on, we now present the PWC control for the initial rotation and single transect line. From the experimental results presented in Section 6.4.3, the initial rotation is achieved by applying the appropriate control to compensate for $\theta = -20^\circ$ for a duration of five seconds. This is followed by the discretized controls to realize the surge displacement which also accounts for ODIN’s positive buoyancy. The controls presented in Table 17

Time (s)	Applied Thrust (6-dim.) (N)
0	(0,0,0,0,0,0)
0.9	(0.445,0,-1.126,0,-2.911,0)
5.9	(0.445,0,-1.126,0,-2.911,0)
6.8	(10.425,0,0.302,0,-2.911,0)
26.78	(10.425,0,0.302,0,-2.911,0)
27.68	(10.425,0,2.378,0,-2.911,0)
31.85	(-3.395,0,2.378,0,-2.911,0)
32.75	(-3.395,0,2.378,0,-2.911,0)
37.7	(-3.395,0,2.378,0,-2.911,0)
38.6	(0,0,0,0,0,0)

Table 17: Discretized control structure for a single transect of a seabed survey mission.

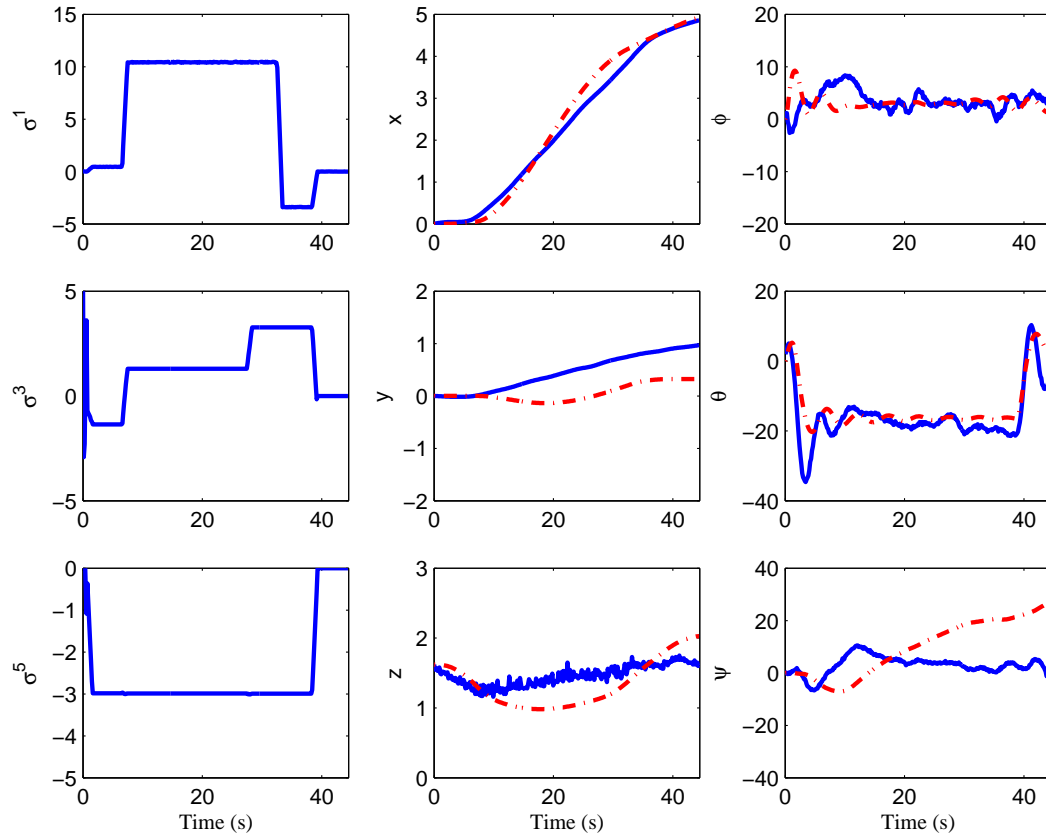


Figure 35: Single transect of the seabed survey mission.

give the strategy to realize the initial rotation and the five-meter transect. The experimental results from the implementation of this control strategy onto ODIN are shown in Fig. 35. We note here that the σ^3 control (body-pure heave) applied during the experiment does not match well with the prescribed values given in Table 17 for $t \in [6.8, 26.78]$ seconds. This often happens in experimentation and here we attribute it to the thruster model used, along with the conversion from a six-dimensional input control strategy to an eight-dimensional output thrust (see e.g., Hanai et al. (2003)). The controls presented in Fig. 35 are the actual controls applied by ODIN during the experiment.

As outlined in the control design phase, we only need to show a concatenated sway on this motion to define an L-shaped trajectory which can then be put together repeatedly to construct an entire survey mission. Since the first 38.6 seconds will be the same, we present only the PWC controls for the concatenated sway motion in Table 18. For this portion of the trajectory, we also account for ODIN's net positive buoyancy. The entire

Time (s)	Applied Thrust (6-dim.) (N)
38.6	(0.445,13.298,0.174,0,-2.911,0)
45.593	(0.445,13.298,0.174,0,-2.911,0)
48.493	(0.445,-9.041,0.174,0,-2.911,0)
51.5	(0.445,-9.041,0.174,0,-2.911,0)
52.4	(0,0,0,0,0,0)

Table 18: Discretized control structure for a concatenated sway motion of a transect of a seabed survey mission.

L-shaped trajectory was implemented onto ODIN with the experimental results presented in Fig. 36.

Since the trajectory shown in Fig. 36 contains the single transect, and the experimental results are similar, we focus on discussing the entire L-shaped trajectory. The surge evolution is precisely what we expected with a five-meter displacement and then relatively constant during the sway motion. There is a slight negative surge displacement for $t > 40$ seconds, which is due to a positive yaw angle present during this time interval. Since the yaw was evolving during the surge motion, we see an evolving sway which should not be present for $t \in [5, 39]$ seconds. The actual sway displacement from the prescribed controls ($t \in [39, 53]$ seconds) was only around 1.5 m with a slight reverse in direction at the very end. Since the drag coefficient estimations were verified in surge for the same velocity, and

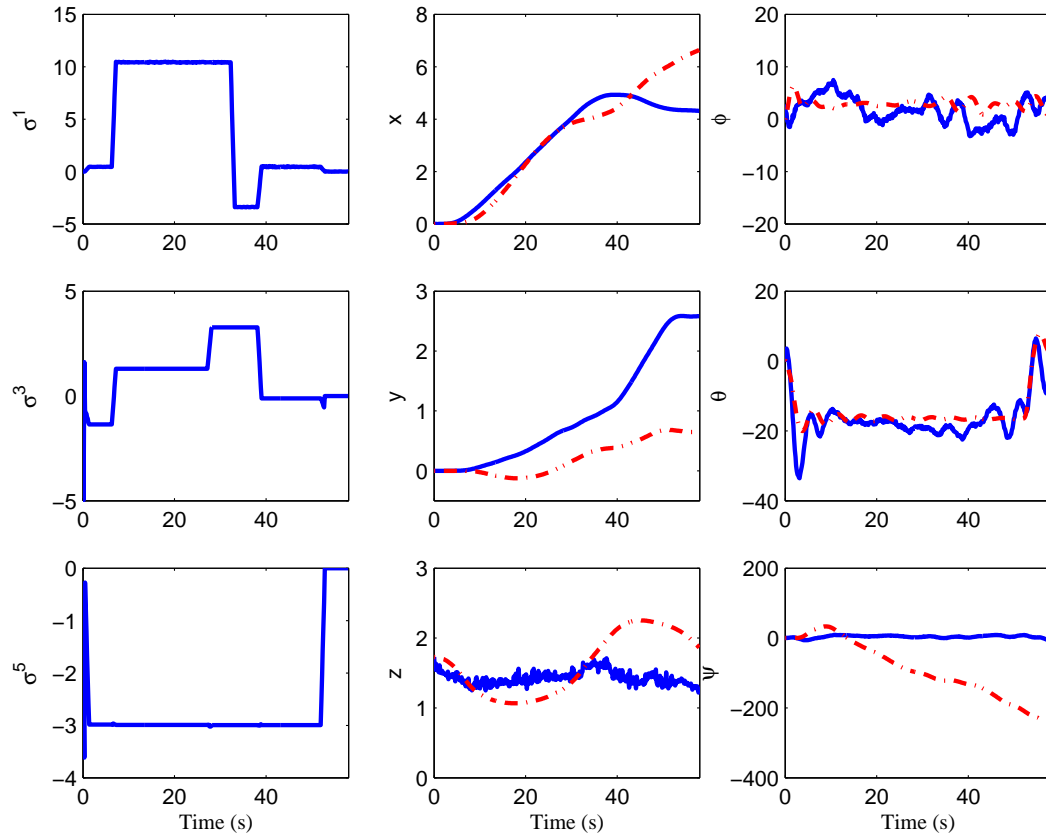


Figure 36: Transect of the seabed survey mission with concatenated sway motion.

surge and sway are equivalent with respect to their drag estimations, this discrepancy may be a result of the thruster response to the input control. During the concatenated trajectory shown in Fig. 36, a feedback control was implemented on the yaw control to eliminate a yaw drift which was occurring during the transition from surge to sway. Since the PID controller was operating and constantly correcting any yaw deviation, we see a large deviation between the actual and theoretical evolutions for ψ . Since the theoretical control is based on the actual applied controls, we see this artifact. This causes the theoretical x and y evolution to also display discrepancies from the actual evolution.

The heave evolution is relatively constant with a slight trend towards the free surface after $t = 40$ seconds. The correlation between the theoretical and actual evolutions here is a result of the σ^3 control not matching the prescribed values well. Of particular interest is the pitch evolution. The response looks good at first, and is consistent throughout the trajectory, but it never really stabilizes and is consistently greater than the -20° prescribed. Due to the lack of symmetry in forward and reverse thrust application of the thrusters, there is one direction of rotation which is preferred over the other. In the case of pitch, the preferred direction is positive, as observed from the experimental results shown in Section 6.4.3. Here, the prescribed negative pitch along with the compensation for ODIN's net buoyancy pushes the physical limits of the thrusters.

6.4.6 Mission 6

As described in Section 5.5.6, we wish to examine a cylinder by use of a linear trajectory with a simultaneous yawing motion. From the calculations presented earlier, we arrive at the PWC control structure for implementation onto ODIN given in Table 19. Upon the implementation of this control strategy, ODIN displayed some very erratic behavior. First, the yaw control prescribed for $t \in [0, 4.8]$ seconds was much greater than needed and rotated the vehicle almost a full 360° . The result from this was that ODIN was misaligned to begin the second leg of the trajectory and the test needed to be aborted to prevent ODIN from hitting the side of the pool. Hence, we have no data to present for the strategy given in Table 19. The behavior described implies that the drag moment calculated for the yaw di-

Time (s)	Applied Thrust (6-dim.) (N)
0	(0,0,0,0,0,0)
0.9	(0,0,0,0,0,3.365)
3.301	(0,0,0,0,0,3.365)
4.201	(0,0,0,0,0,-1.718)
4.8	(0,0,0,0,0,-1.718)
5.7	(11.084,13.698,0,0,0,-0.322)
7.137	(11.084,13.698,0,0,0,-0.322)
8.037	(11.084,13.698,0,0,0,-1.042)
15.186	(11.084,13.698,0,0,0,-1.042)
15.7	(11.084,13.698,0,0,0,-1.042)
16.086	(11.084,-0.66,0,0,0,-1.042)
16.6	(11.084,-0.66,0,0,0,-1.042)
17.5	(0,0,0,0,0,0)

Table 19: Discretized control structure for cylinder examination.

rection is inaccurate and needs to be re-examined. the behavior implies an over-estimation in the total drag momentum.

While at the testing facility, we were able to modify the existing control structure to yield a trajectory similar to what was proposed. The two computed control strategies are presented in Tables 20 and 21 and the experimental results are displayed in Figs. 37 and 38, respectively. We hope to use the *ad hoc* control strategies as a base to determine the validity of future control structures designed for this mission.

In both of the modified control strategies, the desired sway motion was achieved, however the yaw orientation never reached the -45° as prescribed, although the model predicted that it should with the control which were applied. Recall, that the initially designed yaw control was too large and thus caused disastrous results for implementation. However, in Tables 20 and 21, we have had to increase the yaw control throughout the duration of the

Time (s)	Applied Thrust (6-dim.) (N)
0	(0,0,0,0,0,0)
0.9	(0,0,0,0,0,0.7)
3.301	(0,0,0,0,0,0.7)
4.201	(0,0,0,0,0,-0.36)
4.8	(0,0,0,0,0,-0.36)
5.7	(11.084,13.698,0,0,0,-0.34)
7.137	(11.084,13.698,0,0,0,-0.34)
8.037	(11.084,13.698,0,0,0,-1.242)
15.186	(11.084,13.698,0,0,0,-1.242)
15.7	(11.084,13.698,0,0,0,-1.242)
16.086	(11.084,-0.66,0,0,0,-1.242)
16.6	(11.084,-0.66,0,0,0,-1.242)
17.5	(0,0,0,0,0,0)

Table 20: Modified cylinder examination control strategy #1.

Time (s)	Applied Thrust (6-dim.) (N)
0	(0,0,0,0,0,0)
0.9	(0,0,0,0,0,0.7)
3.301	(0,0,0,0,0,0.7)
4.201	(0,0,0,0,0,-0.36)
4.8	(0,0,0,0,0,-0.36)
5.7	(11.084,13.698,0,0,0,-0.34)
7.137	(11.084,13.698,0,0,0,-0.34)
8.037	(11.084,13.698,0,0,0,-1.642)
15.186	(11.084,13.698,0,0,0,-1.642)
15.7	(11.084,13.698,0,0,0,-1.642)
16.086	(11.084,-0.66,0,0,0,-1.642)
16.6	(11.084,-0.66,0,0,0,-1.642)
17.5	(0,0,0,0,0,0)

Table 21: Modified cylinder examination control strategy #2.

sway motion to reach a slightly negative yaw angle at the termination of the trajectory.

This mission requires further examination with respect to the overall design as well as with the drag coefficient in the yaw direction. However, these preliminary results are

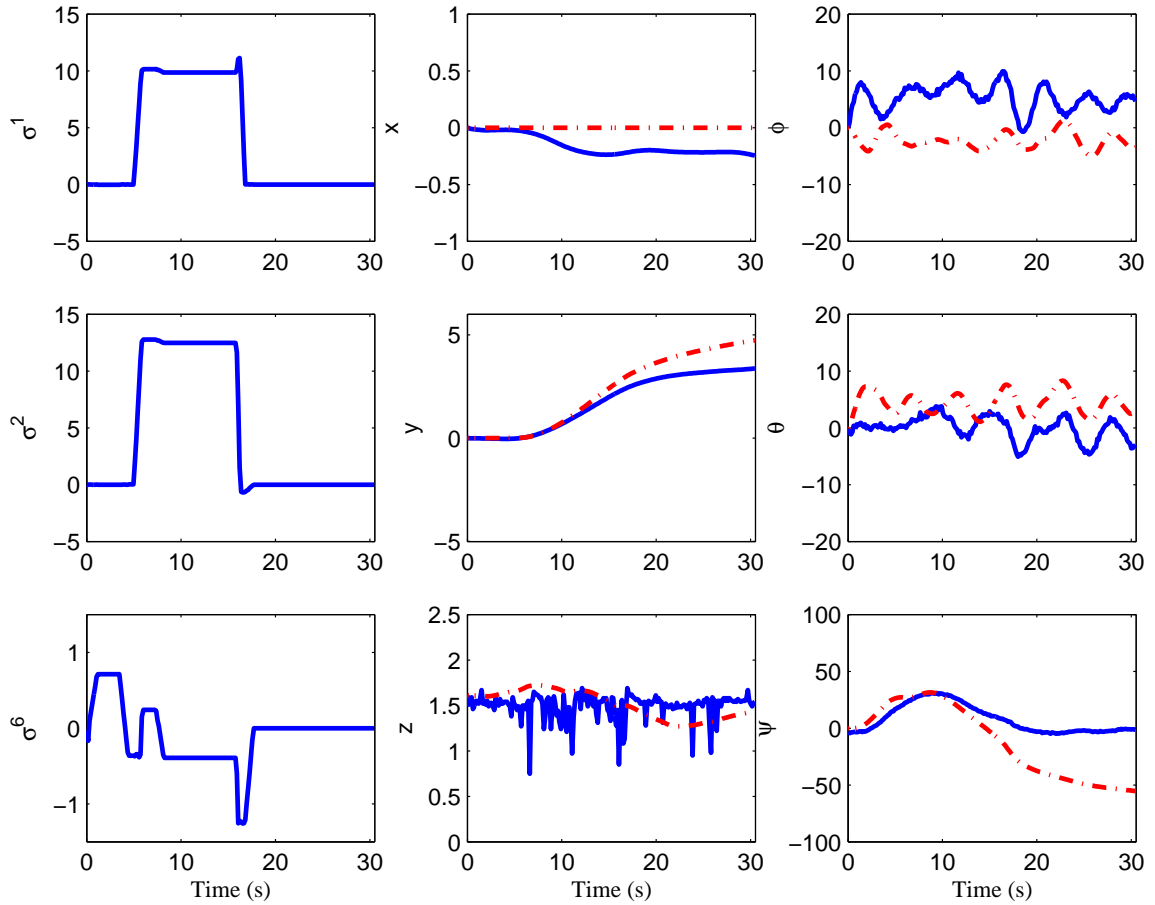


Figure 37: Modified cylinder examination trajectory #1.

promising to be able to produce such a trajectory. We hope to achieve a better estimation of the drag moment in the yaw direction by working backwards from the modified control strategies given in Tables 20 and 21 to find the appropriate theoretical control strategy. This area of research is currently under investigation.

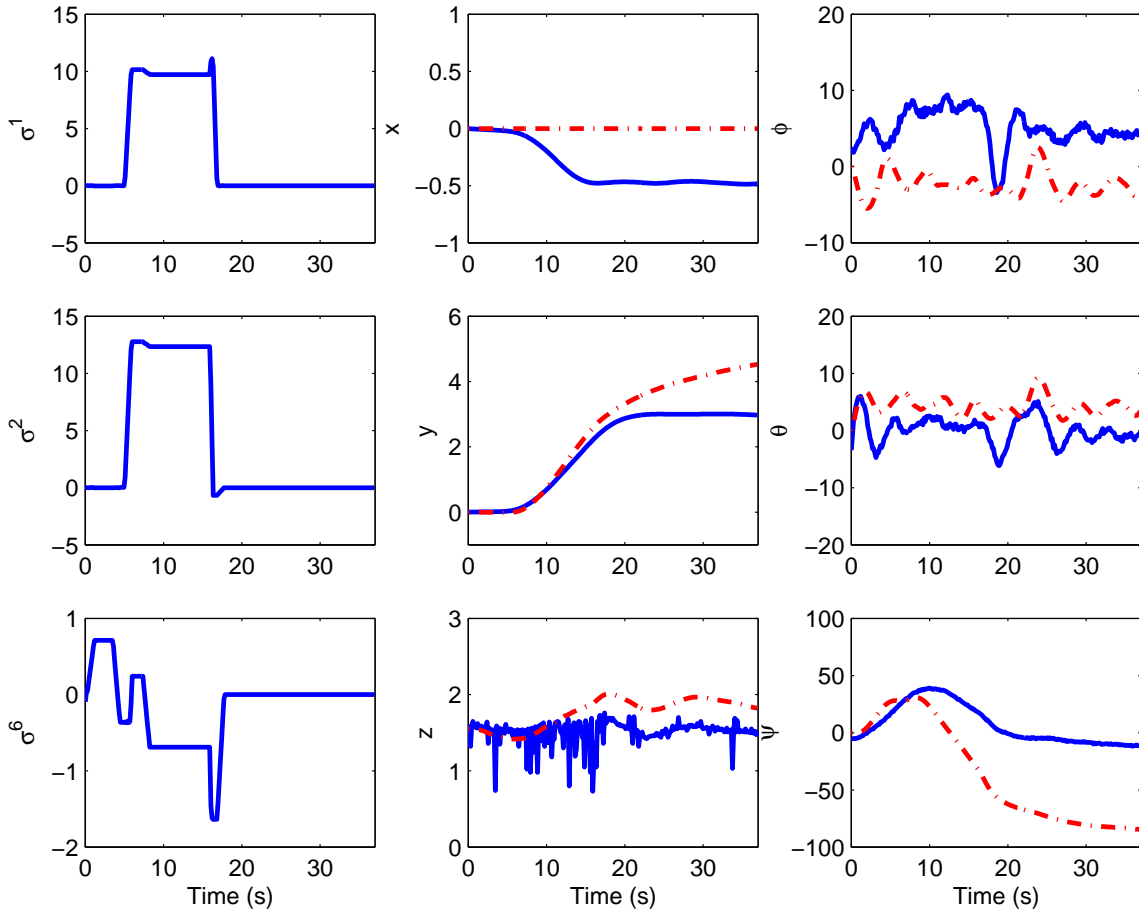


Figure 38: Modified cylinder examination trajectory #2.

6.4.7 Mission 7

For harbor protection, the Department of Homeland Security has shown recent interest in the use of AUVs for searching the hulls of ships before entering port. One portion of the hull which may require a unique motion strategy is the bulbous bow. Here we present the implementation of a control strategy to investigate a bulb at the bow of the ship as de-

signed in Section 5.5.7. As noted previously, the size and shapes of these bulbs can be quite different, thus, we present a general control strategy as defined earlier and make no direct reference to a particular ship or bulb shape.

From the design phase, we see that this is basically two concatenations of trajectories similar to that discussed in Sections 5.5.3 and 6.4.3. From the previous section, we are aware that the initial prescribed rotation of -22.5° is not in the preferred direction and thus we will probably not be able to realize the desired angle nor the desired heave displacement for large angles and large velocities during the heave motion. With this in mind, the reparameterization $\tau(t)$ was chosen such that the heave motion would take 10 seconds in an attempt to keep the control forces small and remain within the physical thruster bounds of ODIN. The continuous control for this mission is discretized into the PWC control to be implemented onto ODIN in Table 22.

Time (s)	Applied Thrust (6-dim.) (N)
0	(0,0,0,0,0,0)
0.9	(0.497,0,-1.201,0,-3.257,0)
5.9	(0.497,0,-1.201,0,-3.257,0)
6.8	(0.497,0,5.086,0,-3.257,0)
12.84	(0.497,0,5.086,0,-3.257,0)
13.74	(0.497,0,-7.184,0,-3.257,0)
17.7	(0.497,0,-7.184,0,-3.257,0)
18.6	(-0.65,0,-1.126,0,4.2553,0)
23.6	(-0.65,0,-1.126,0,4.2553,0)
24.5	(-0.65,0,28.914,0,4.2553,0)
30.073	(-0.65,0,28.914,0,4.2553,0)
30.973	(-0.65,0,-25.683,0,4.2553,0)
33.4	(-0.65,0,-25.683,0,4.2553,0)
34.3	(0,0,0,0,0,0)

Table 22: Discretized control structure for examination of a bulbous bow.

Note again that the initial pitch displacement is achieved by simply applying the compensative forces and moments induced by a list angle of -22.5° . Additionally, the second rotation of 30° in the middle of the trajectory, is achieved in the same way. Both of these pure rotations are applied for five seconds to allow for stabilization in the angular displacement before the heave control is applied. The implementation results for this mission are presented in Fig. 39.

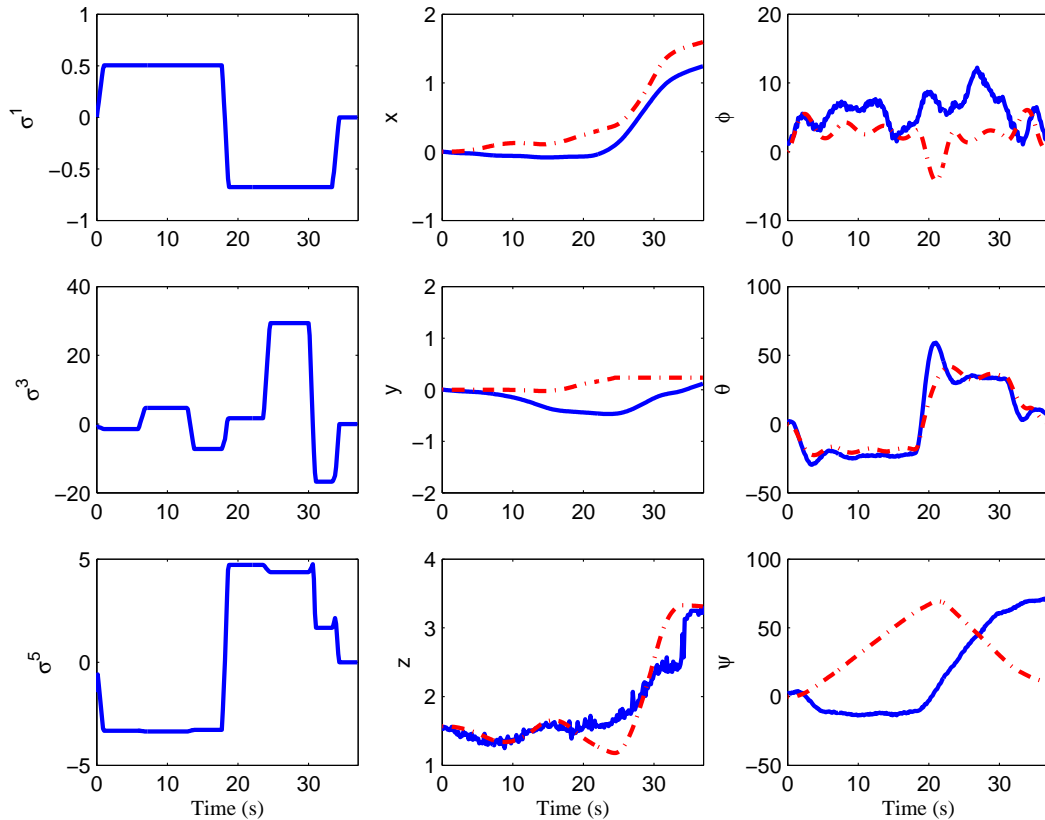


Figure 39: Implementation of trajectory to examine a bulbous bow.

From the geometry of the first rotation and translation of this trajectory, we expect to be at $\eta = (-0.4, 0, 2.42, 0, 0, 0)$ at $t \approx 18$ seconds. From the evolution presented in Fig. 39 we see that this did not happen. The depth and surge components barely evolved at

all. We see a sway displacement of approximately -0.4 m, however this is probably due to transient thruster response, or the current in the pool, more than any other factor. From this, we conclude that the reparameterization was probably taken to be too long of a duration over such a short distance.

On the other hand, the second half of the trajectory matches very well with theoretical predictions. This control strategy is the same one that has been presented and validated earlier. However, the vehicle ended at a shallower depth since the heave displacement was not realized on the previous leg.

It is also significant to note the evolution of the pitch angle over this entire mission. We see relatively small overshooting followed by a very stable and maintained pitch angle during both heave motions. This is a very good result as a switch from a negative angle to positive angle would not intuitively stabilize this rapidly. At the transition, we are prescribing a 52.5° transition in the pitch angle.

6.5 Experimental Summary

In this chapter, we have presented the implementation results of the control strategies designed by use of the geometric control theory derived earlier in this dissertation. Here, we briefly summarize what worked and what did not as well as give a disclaimer on the potential sources of errors in the presented experiments.

For all the implementations, the inclusion of the dissipative forces and moments arising from viscous drag into the geometric framework as presented in this dissertation worked

very well. The estimation for the drag forces corresponding to the translational motions was accurate, but still could be refined through more testing.

As discussed in Sections 6.4.3 and 6.4.4, the drag moments corresponding to pitch and roll motions may be slightly over-estimated. It is difficult to discern the magnitude of an over-estimate in these components because the righting moments also act in a dissipative fashion for rotational motions, which mask the true effect of the viscous drag moment. In Section 6.4.6, we saw that there is clearly an over-estimation in the drag moment for the yaw motion. The majority of the drag moment in yaw is due to the appendages, which include the thrusters and the arms attaching them to ODIN's hull. As presented in Appendix B.1, this moment was calculated by use of a published drag coefficient which may not be accurate for this specific application. Since there are no righting moments in yaw, a slight over-application of force is very noticeable.

The inclusion of the restoring forces and moments into the theoretical structure was unsuccessful. We were able to present an *ad hoc* method to include their effects so that implementation was possible, however the practicality of designing an on-board algorithm which uses the method proposed here is unlikely. The inclusion of the restoring forces and moments will require the characterization of a different kinematic reduction than the one presented in this dissertation. This kinematic reduction may reduce a dynamic system with a drift vector field to a kinematic system also having drift, or optimally to a driftless kinematic system. This is a very interesting area for further research.

Moving from theory to implementation was neither a trivial nor exact process in this research. The control strategies calculated in Chapter 5 were generated as continuous func-

tions with respect to time, whereas the input control implemented onto the test-bed vehicle was required to be a piece-wise constant function with respect to time. Additionally, changes between piece-wise constant control inputs must be made over a 0.9 second time interval. These two constraints provide a significant hurdle in the transformation from theory to implementation. And thus, the transformation of the control strategies is probably the largest source of error. However, there is no real way to quantify this error since the theoretical control strategies cannot be implemented onto the same test-bed vehicle at this time.

The majority of the control strategies implemented onto the test-bed vehicle were done so fully in open-loop. Since the control strategies were designed to be model based, this type of implementation tested the extent of the path planning and control design algorithm. However, without the use of a feedback controller, any small disturbance is seen and exacerbated throughout the entire experiment. Most of this disturbance comes from the thrusters on the vehicle. As noted previously, each thruster is unique and has a nonlinear relationship between input voltage and output thrust. Additionally, the *dead zone* about zero is also different between thrusters. This uniqueness usually leads to a misappropriation of thrust which usually results in a deviation in yaw due to the lack of restoring forces. This yaw deviation then affects all components in the evolution of the trajectory.

The other source of error arising from the thrusters is the conversion from a six-dimensional input control to the eight independent thrusters. Although this does not effect the implementation directly, it does arise in the data analysis. The transformation is exact, however the dimension of the null space is two. Thus, in the conversion from the applied eight-

dimensional control back to the six-dimensional control, forces may arise in one component of the control which were not initially prescribed. As previously mentioned, more details can be found in Hanai et al. (2003).

Other small sources of error related to this research arise from sensor and measurement error when determining the relative position of ODIN within the pool. These errors are based on the accuracy of the inertial measurement unit, pressure sensor and the post processing of the horizontal positioning data from the video recordings.

Overall, the implementation of open-loop control strategies developed by use of a kinematic reduction, as defined previously in this dissertation, was successful. For the majority of the scenarios presented in Sections 6.4.1-6.4.7, ODIN was able to realize the prescribed configuration η_{final} by use of a fully open-loop control strategy implementation.

Chapter 7

Generalization to Other Vehicles

The beauty of the geometric control theory presented in this study is its wide ranging applicability to many different mechanical systems. In particular, the applicability of the theory to multiple types of underwater vehicles.

To make a generalization of the theory presented in this dissertation to another type of a vehicle, only slight modifications to the parameters need to be made. Assuming that the vehicle has three planes of symmetry, which is common for AUVs, the basic foundations and formulations do not change. Of course the physical quantities need to be altered such as the mass, added mass and inertia terms; this corresponds to the generation of a new kinetic energy metric. The viscous drag forces and moments need to be estimated so that $\tilde{\nabla}$ gives the correct covariant derivative in the calculation of the controls. And, the restoring forces of buoyancy and gravity need to be appropriately accounted for.

Other than the primary physical properties, the major difference lies in the input control vector fields. Since these are the basis for determining the decoupling vector fields for the system, the control strategy design depends upon an accurate representation of the forces and moments used to control the vehicle.

With these slight alterations, we can apply the same procedure outlined in Section 5.2, and the sections following it, to design control strategies for other underwater vehicles. Here, we present one generalization of ODIN and another corresponding to a torpedo-shaped AUV.

7.1 ODIN Generalization

From the description of ODIN given in Section 5.1, we remark that the notion of a six dimensional control may not be the most appropriate formulation when considering under-actuation. Since ODIN uses eight actuators to control her motion in six degrees-of-freedom, there is redundancy built into the system. Due to this redundancy, there is not a one to one correspondence between the loss of a degree of freedom and the loss of an actuator.

Although theoretically, a six-dimensional input control scheme makes sense, the under-actuation analysis and practical implementation onto a vehicle utilizing an eight-dimensional control loses some of the geometric beauty we are trying to exploit. To this end, we present an alternate set of input control vector fields $\mathbb{J} = \{\mathbb{J}_1, \dots, \mathbb{J}_8\}$. These vector fields directly correspond to the forces applied by each individual thruster. Thus, when we consider an under-actuated situation, the loss of an actuator is equivalent to the elimination of one input control vector field.

By use of the measurements contained within Fig. 40, the previous definitions of m_i and j_i for $i = 1, 2, 3$ and a little trigonometry we can calculate the eight input vector fields correlating to ODIN's eight thrusters. We note that the thrusters are numbered beginning with the forward horizontal on the starboard side followed by the associated vertical thruster and continuing clockwise around the vehicle. Thus, for the input vector fields, an odd subscript corresponds to a horizontal thruster and an even subscript corresponds to a vertical thruster. We also assume the notation that $\{X_1, \dots, X_6\}$ is the standard basis for $\mathbb{R}^3 \times \text{SO}(3)$.

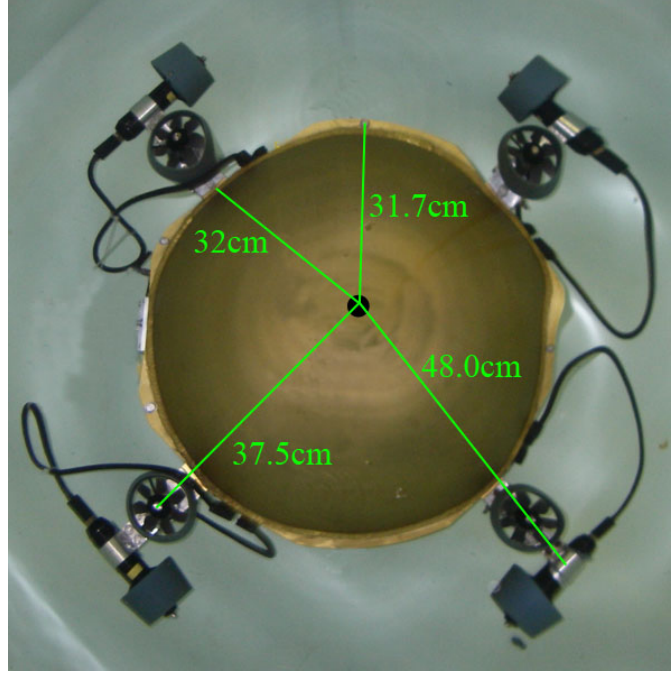


Figure 40: ODIN's external dimensions.

$$\begin{aligned}
 \mathbb{J}_1 &= -\frac{\sin 45^\circ}{m_1} X_1 + \frac{\cos 45^\circ}{m_2} X_2 + \frac{0.480}{j_3} X_6 \\
 \mathbb{J}_3 &= \frac{\sin 45^\circ}{m_1} X_1 + \frac{\cos 45^\circ}{m_2} X_2 - \frac{0.480}{j_3} X_6 \\
 \mathbb{J}_5 &= \frac{\sin 45^\circ}{m_1} X_1 - \frac{\cos 45^\circ}{m_2} X_2 + \frac{0.480}{j_3} X_6 \\
 \mathbb{J}_7 &= -\frac{\sin 45^\circ}{m_1} X_1 - \frac{\cos 45^\circ}{m_2} X_2 - \frac{0.480}{j_3} X_6 \\
 \mathbb{J}_2 &= -\frac{1}{m_3} X_3 - \frac{\sin 45^\circ \times 0.375}{j_1} X_4 - \frac{\cos 45^\circ \times 0.375}{j_2} X_5 \\
 \mathbb{J}_4 &= -\frac{1}{m_3} X_3 - \frac{\sin 45^\circ \times 0.375}{j_1} X_4 + \frac{\cos 45^\circ \times 0.375}{j_2} X_5 \\
 \mathbb{J}_6 &= -\frac{1}{m_3} X_3 + \frac{\sin 45^\circ \times 0.375}{j_1} X_4 + \frac{\cos 45^\circ \times 0.375}{j_2} X_5 \\
 \mathbb{J}_8 &= -\frac{1}{m_3} X_3 + \frac{\sin 45^\circ \times 0.375}{j_1} X_4 - \frac{\cos 45^\circ \times 0.375}{j_2} X_5
 \end{aligned} \tag{7.1}$$

The first thing to remark is that the rank of the input distribution is greater than the dimension of the configuration space. This implies that the vehicle is *over-actuated*. The first under-actuated scenario would occur with the loss of three actuators since the loss of any two of the input control vector fields given in Eq. (7.1) still results in six linearly independent vector fields which form a basis for $\mathbb{R}^3 \times \text{SO}(3)$.

This formulation is currently under investigation to calculate decoupling vector fields and design trajectories for an under-actuated ODIN based on an eight-dimensional input control scheme.

Remark 7.1. Many vehicles are designed similar to ODIN in that there is actuator redundancy built-in. For these vehicles, an under-actuated condition (loss of a thruster) may reduce the controllability of the system simply due to the reduction of available thrust from the remaining actuators. For example, ODIN uses four thrusters to realize pitch angles. It has been seen in one application that losing one of these thrusters restricts the maximum inclination which can be achieved. This remark is to make note that the term *under-actuated* may have different connotations when considering different input control schemes and thrusters with limited bounds as this occurs in practice.

7.2 Torpedo-Shaped Vehicle

In this section, we present a generalization of the theory presented in this study to the control design for a torpedo-shaped vehicle similar to those discussed in the Introduction

and pictured in Figs. 1-3. We consider a few control schemes and calculate their corresponding decoupling vector fields. Some applications are presented which are best suited for this type of motion planning. Details of the calculations made in this section can be found in Smith et al. (2008b).

For the following examples, we assume we have a REMUS AUV, but we simplify the model a bit by assuming that $C_G = C_B$ and that the vehicle is neutrally buoyant. Since it has a torpedo shape, we note that the vehicle has three planes of symmetry. The kinetic energy metric is thus assumed to be diagonal and is given by

$$\begin{aligned}\mathbb{G} &= \text{diag}(m_1, m_2, m_3, j_1, j_2, j_3) \\ &= \text{diag}(31.43, 66, 66, 0.0704, 4.88, 4.88),\end{aligned}\tag{7.2}$$

where the first terms are the translational added mass terms with units of kilograms and the final three are the rotational added mass terms with units kg m^2 . The six principal drag coefficients are given by $\{D_1 = 3.9 \text{ kg/m}, D_2 = 131 \text{ kg/m}, D_3 = 131 \text{ kg/m}, D_4 = 0.13 \text{ kg m}^2, D_5 = 188 \text{ kg m}^2, D_6 = 94 \text{ kg m}^2$. The mass of the vehicle is assumed to be 30.5 kg. Hydrodynamic parameters and coefficients for the considered vehicle were taken from Presterio (2001).

For the first scenario, we assume that we can control surge (propeller in the rear), pitch (foil in front or rear) and yaw (rudder in rear). By use of a rudder and a foil to control pitch and yaw implies that we must also include a surge component to realize these rotations. We take the input vector fields for the mechanical system to be $\mathbb{T}_1 =$

$(1/m_1, 0, 0, 0, 0, 0)^t$, $\mathbb{T}_2 = (1/m_1, 0, 0, 0, \phi/j_2, 0)^t$, and $\mathbb{T}_3 = (1/m_1, 0, 0, 0, 0, \psi/j_3)^t$.

Here, ϕ and ψ represent the angle of rotation that the vehicle experiences after one time step. In this simplified scenario, to realize a rotation, we fix the fins or rudders in a given position and apply a surge which implements the rotation along with the surge motion. Note that here we do not concern ourselves with the precise performance characteristics of the fins and rudders. We assume that there is a higher level control system or some *a priori* knowledge of the mechanics of the fins and rudders which allows us to determine the input control vector fields.

Recall from the definition of an affine connection, that the map $(X, Y) \rightarrow \tilde{\nabla}_X Y$ is \mathbb{R} -bilinear. Thus, $\tilde{\nabla}_{W+X}(Y + Z) = \tilde{\nabla}_W(Y + Z) + \tilde{\nabla}_X(Y + Z) = \tilde{\nabla}_W Y + \tilde{\nabla}_W Z + \tilde{\nabla}_X Y + \tilde{\nabla}_X Z$ for vector fields W, X, Y, Z . This bilinearity suggests that we should express the input vector fields as $\mathbb{T}_2 = \mathbb{I}_1^{-1} + \phi\mathbb{I}_5^{-1}$, $\mathbb{T}_3 = \mathbb{I}_1^{-1} + \psi\mathbb{I}_6^{-1}$ and $\mathbb{T}_4 = \mathbb{I}_1^{-1} + \phi\mathbb{I}_5^{-1} + \psi\mathbb{I}_6^{-1}$, where $\{\mathbb{I}_1^{-1}, \dots, \mathbb{I}_6^{-1}\}$ are the input vector fields defined as the columns of the inverse of the kinetic energy metric.

A direct calculation for this three input system shows that \mathbb{T}_1 is a decoupling vector field, and is the only decoupling vector field for this system. The only kinematic motion for the system is a pure surge. Thus, this scenario does not lend well to motion by use of kinematic motions.

Adding to this scenario, we consider an operational situation in which the vehicle has a rear propeller to provide surge and independently actuated fins to control roll, pitch and yaw. The input control vector fields are $\mathbb{T}_1 = (1/m_1, 0, 0, 0, 0, 0)^t$, $\mathbb{T}_2 = (1/m_1, 0, 0, 0, \phi/j_2, 0)^t$, $\mathbb{T}_3 = (1/m_1, 0, 0, 0, 0, \psi/j_3)^t$ and $\mathbb{T}_4 = (1/m_1, 0, 0, -\theta/j_1, 0, 0)^t$. This case

is analyzed similarly to the previous case. The calculations yield the axial vector field $V = h_1\mathbb{T}_1 + h_4\mathbb{T}_4$ as decoupling. This scenario produces the kinematic motions defined by a pure surge, a pure roll or the axial motion (see Definition 5.3) given by a simultaneous roll and surge motion.

Upon close examination of the previous two examples, we see that we must have direct control (i.e., the control is contained within the span of the input control vector fields) upon sway or heave to produce a decoupling vector field which acts upon an axis different from the body-fixed x-axis (body-pure surge direction). This restriction results from the simplified, six-dimensional input control model chosen for this example. For operational reasons, a torpedo-shaped AUV would probably not be designed to directly control such motions. For illustrative purposes only, we assume that we have a pure heave control available to the vehicle. This motion adds the input vector field $\mathbb{T}_5 = (0, 0, 1/m_3, 0, 0, 0)^t$ to the previous four considered.

Remark 7.2. We would like to remark that for a specific vehicle, torpedo-shaped or other, it is likely that the notion of three pure forces and three pure torques acting at C_G is not a realistic or valid assumption. As shown in Section 7.1 and in Bullo & Lynch (2001), there are alternate formulations for the input control vector fields to a mechanical system. For the example presented in this section, we use this simplified model to demonstrate the general applicability of the control design technique to vehicles other than ODIN.

The decoupling vector fields, calculated for the system with input control vector fields $\{\mathbb{T}_1, \mathbb{T}_2, \mathbb{T}_3, \mathbb{T}_4, \mathbb{T}_5\}$, are $V_\alpha = h_1\mathbb{T}_1 + h_2\mathbb{T}_2 + h_5\mathbb{T}_5$ and $V_\beta = h_1\mathbb{T}_1 + h_2\mathbb{T}_2 + h_4\mathbb{T}_4$.

It should be clear that V_α restricts vehicle movement to the vertical plane, and that the kinematic motions defined by V_α would be useful for motion planning operations which require the vehicle to travel along a straight line transect while maintaining a prescribed distance above a topographically complex seabed, such as photographing coral reefs *in situ*. Other applications include transects which require the vehicle to remain within a certain isopycnal, isothermal or isohaline.

Proposition 7.1. *The torpedo-shaped submerged rigid body with input control vector fields $\{\mathbb{T}_1, \mathbb{T}_2, \mathbb{T}_4\}$ is kinematically controllable.*

Proof: A simple calculation shows that $\{\mathbb{T}_1, \mathbb{T}_2, \mathbb{T}_4, [\mathbb{T}_1, \mathbb{T}_4], [\mathbb{T}_2, \mathbb{T}_4], [\mathbb{T}_4[\mathbb{T}_2, \mathbb{T}_4]]\}$ are six linearly independent vector fields which span $SE(3)$. Applying Proposition 4.1 gives the result.

Since its kinematic motions allow us to reach the entire configuration space, we will use V_β for our trajectory design. Based on its geometry, the torpedo-shaped AUV is primarily used in straight line transect surveys and data collects. The long, narrow body shape provides a large drag resistance in yaw and pitch which helps maintain a consistent heading angle and depth. The missions can be long transects following a particular property in the water column or an exhaustive back and forth or "mowing the lawn" trajectory to completely cover a certain area of the ocean. In either scenario, the AUV must be able to do more than just a pure surge, and possibly a rotation.

Let us consider the mission of searching for a lost vessel. In this scenario, we would have a general area, say $10 \text{ km} \times 10 \text{ km}$, within which to search. One solution is to use the

exhaustive back and forth search to photograph the entire area by use of side-scan sonar or CCD cameras for later review. This mission requires the vehicle to realize a sequence of parallel paths connected at the ends by a turn around loop; just as you would imagine mowing a rectangular lawn. Such motions can be planned by use of the integral curves of the decoupling vector field V_β , even though we do not have direct control on the yaw component to turn the vehicle around. Consider the first two transects of such a trajectory as shown in Fig. 41. Clearly, if we can realize the path in Fig. 41, we can complete the survey by concatenating many of these together. The first transect is realized via $V_1 = h_1\mathbb{T}_1$, a pure surge motion. The turn-arounds at each end are handled by first rolling 90° via $V_2 = h_4\mathbb{T}_4$ and then following the integral curves of $V_3 = h_2\mathbb{T}_2$ to realize the turn. Note here, that for this chosen motion, the system experiences a centripetal acceleration in the body-pure heave direction, which is why we must include \mathbb{T}_5 as an input control vector field to the dynamic system. Inclusion of \mathbb{T}_5 is a result of the chosen input control model along with the choice of trajectory that the vehicle must realize. We remind the reader that the control inputs used to follow the decoupling vector fields belong to the kinematic class \mathcal{U}_{kin} of inputs, in particular, they are velocity control inputs. When calculating the dynamic (i.e., acceleration) control inputs, we must remember that $\mathcal{U}_{kin} \subset \mathcal{U}_{dyn}$, and hence we may need a larger set of dynamic input controls to realize a prescribed motion controlled by kinematic inputs. For example, a body-pure heave acceleration can be realized by implementing a dynamic control in surge and pitch. However, in the control design scheme presented in this dissertation, we control only the velocities, and thus do not have a pure dynamic control on surge and/or pitch.

After the turn around, we can follow V_2 with $-\phi$ in the roll component implying that the fins have been repositioned to realize the negative of the angular displacement achieved in V_2 . This causes the AUV to roll back upright and then it is able to begin another transect by following $V_5 = V_1$. Also note that, along a given transect, the AUV could implement

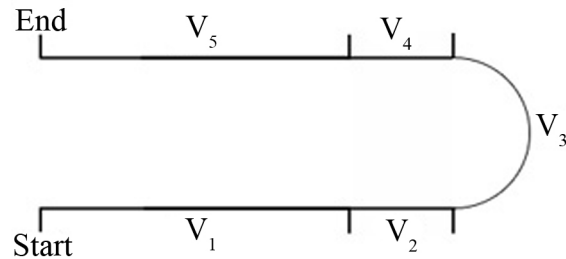


Figure 41: Two transects connected by turn around loop.

constant depth survey or bottom tracking mode since $V_4 = h_2\mathbb{T}_2$ is a decoupling vector field for the system. By Proposition 7.1, we have shown that by use of only V_β , the vehicle is kinematically controllable, and the chosen kinematic motion can be realized with input control vectors $\{\mathbb{T}_1, \mathbb{T}_2, \mathbb{T}_4, \mathbb{T}_5\}$. By use of this trajectory design, we can use the tools presented in Chapter 5 to calculate the controls necessary to complete this trajectory.

In the presentation of this example, we assume that the controls are direct applications of forces and torques at the center of gravity. This assumption is quite limiting when considering practical applications as done in this study. Following the lines of the previous section and selecting controls similar to that done in Bullo & Lynch (2001), we can create an alternate geometric representation of this system and apply the techniques developed in this study to calculate decoupling vector fields for motion planning.

Chapter 8

Further Research

8.1 Control Strategy Implementation onto other Vehicles

The efforts of this research have successfully bridged the gap between theory and implementation by extending the notion of a kinematic reduction and decoupling vector field by use of them to design open-loop controls which include forces encountered by an actual underwater vehicle. However, the implementation of the computed control strategies has only been carried out on the Omni-Directional Intelligent Navigator. To truly display the generality and overall applicability of this extension of geometric control theory, we propose the design and implementation of control strategies onto other autonomous underwater vehicles.

Torpedo-shaped vehicles such as those discussed in the Introduction would be of primary interest. Applications to box-shaped ROV-type vehicles would also warrant investigation. Due to the shape of these vehicles, the available motions may be limited at the outset (i.e., a torpedo-shaped vehicle would not move in a pure sway direction). This simplifies the problem from a control standpoint, yet also brings up new challenges in the way of different geometries to consider and exploit.

Additionally, it would be of interest to implement our control strategies onto a vehicle designed to handle a continuously evolving control structure. This would allow us to di-

rectly implement the computed strategies and would lead to a more accurate representation of the applied theory.

There are many different types of vehicles currently in use and it would be of interest to know those which could benefit most from control strategies designed by use of the methods presented in this study.

8.2 Alternate Inclusion of Restoring Forces

Here we propose an alternate method for the inclusion of the restoring forces arising from gravity and buoyancy via a perturbation method. As seen in Section 5.5, these restoring forces are small compared to the control forces, but they are still within the same order of magnitude. Thus, from a practical point of view, we see the restoring forces as $\mathcal{O}(1)$, and thus perturbation theory is not a viable option. However, from a theoretical point of view, this approach is interesting, and is thus included as a matter of completeness of the geometric control portion of this dissertation.

Additionally, the work presented in Leonard (1995) and Leonard & Krishnaprasad (1995) examine small amplitude ($\mathcal{O}(\epsilon)$), sinusoidal forcing for the control of underwater vehicles and other left-invariant systems on Lie groups. For such a scenario, a perturbation approach may be practically applicable for the incorporation of the restoring forces into the control design. To this end, we consider the following perturbation theory approach.

We first assume that we know how to solve the following affine connection control system on a matrix Lie group G

$$\tilde{\nabla}_{\gamma'} \gamma' = \sum_{i=1}^m \tilde{\mathbb{I}}_i(\gamma(t)) \sigma_i(t), \quad (8.1)$$

through the use of kinematic reductions and decoupling vector fields.

We now consider the forced affine connection control system as defined in Section 2.4.4 given by

$$\tilde{\nabla}_{\gamma'} \gamma' = \mathbb{G}^\# P(\gamma(t)) + \sum_{i=1}^m \tilde{\mathbb{I}}_i(\gamma(t)) \sigma_i(t), \quad (8.2)$$

where $P : G \rightarrow T^*G$ is the potential force as defined in Eq. (2.79).

Assumption 8.1. The potential force is assumed small, i.e., $P = \epsilon P_1$, $0 \leq \epsilon \ll 1$.

This assumption depends on the precise definition of the word *small*. As we develop this theory in more depth we intend to include more precise bounds for the applicability of this assumption. For now, this is simply an idea of another method to include forces arising from a potential. Continuing, we take the controls to be

$$\sigma_i = \sigma_{i,0} + \epsilon \sigma_{i,1}, \quad (8.3)$$

which implies

$$\gamma' = \gamma'_0 + \epsilon \gamma'_1 + \mathcal{O}(\epsilon^2). \quad (8.4)$$

Proposition 8.1. *Under Assumption 8.1 we have that γ_0 satisfies*

$$\tilde{\nabla}_{\gamma'_0} \gamma'_0 = \sum_{i=1}^m \tilde{\mathbb{I}}_i(\gamma_0(t)) \sigma_{i,0}(t). \quad (8.5)$$

Proof. This follows when inserting σ_i and P and collecting terms of same order. \square

As previously, we assume that the kinetic energy is given by a left-invariant Riemannian metric \mathbb{G} as $\mathbb{G}(g)(g \cdot \xi, g \cdot \eta) = \mathbb{I}(\xi, \eta)$. Then, Eq. (8.2) can be rewritten as

$$\dot{g} = g \cdot \xi \quad (8.6)$$

$$\dot{\xi} = -\frac{1}{2} \langle \xi : \xi \rangle - \mathbb{I}^{-1} D \xi - \mathbb{I}^{-1} (dV|_g \cdot g) + \sum_{i=1}^m \tilde{\mathbb{I}}_i^{-1} \sigma_i(t) \quad (8.7)$$

where $-dV|_g \cdot g = T_I^* L_g(-dV|_g) \in T_I G = \mathfrak{g}$ is the restoring forces and moments in the body-fixed frame, $D : \mathfrak{g} \rightarrow \mathfrak{g}^*$ gives the dissipative forces and moments from viscous drag, and the *symmetric product* $\langle \cdot : \cdot \rangle : \mathfrak{g} \times \mathfrak{g} \rightarrow \mathfrak{g}$ is given by

$$\langle \xi : \eta \rangle := -\mathbb{I}^{-1} (\text{ad}_\xi^* \mathbb{I} \eta + \text{ad}_\eta^* \mathbb{I} \xi), \quad (8.8)$$

which is seen to be bilinear and symmetric.

Example 8.1 (The submerged rigid body). Here we re-examine the submerged rigid body and apply our new formulation. The configuration manifold is $Q = SE(3)$. Here we define the inertia tensor as $\mathbb{I} = \text{diag}(J, M)$, where $J = \text{diag}(j_1, j_2, j_2)$ is the inertia matrix for the

body and $M = \text{diag}(m_1, m_2, m_3)$ includes added masses. Since, for $\Omega, v \in \mathbb{R}^3$, we have

$$\text{ad}_{(\Omega, v)} = \begin{bmatrix} \widehat{\Omega} & 0 \\ \widehat{v} & \widehat{\Omega} \end{bmatrix}, \quad (8.9)$$

the symmetric product is given by

$$\langle (\Omega, v) : (\Gamma, w) \rangle = \mathbb{I}^{-1} \begin{bmatrix} \Omega \times (J\Gamma) + \Gamma \times (J\Omega) + v \times (Mw) + w \times (Mv) \\ \Omega \times (Mw) + \Gamma \times (Mv) \end{bmatrix}. \quad (8.10)$$

Under Assumption 8.1 we have that $V = \epsilon V_1$ and $\xi = \xi_0 + \epsilon \xi_1 + \mathcal{O}(\epsilon^2)$, where $\dot{\gamma} = \dot{g} \cdot g \cdot \xi$. Proposition 8.1 describes the dynamics of the zero order system. The following proposition describes the first order dynamics.

Proposition 8.2. *Let $g_0(t)$ denote the solution to $\dot{g}_0 = g_0 \cdot \xi_0$ and define $h := g \cdot g_0^{-1}$. Then we have*

$$\dot{h} = \epsilon h \cdot \text{Ad}_{g_0}(\xi_1) + \mathcal{O}(\epsilon^2), \quad (8.11)$$

$$\dot{\xi}_1 = -\langle \xi_0 : \xi_1 \rangle - \mathbb{I}^{-1} D\xi_1 - \mathbb{I}^{-1} (dV_1|_{g_0} \cdot g_0) + \sum_{i=1}^m \tilde{\mathbb{I}}_i^{-1} \sigma_{i,1}(t). \quad (8.12)$$

Proof. The expression for $\dot{\xi}_1$ follows from insertion and collecting terms of order $\mathcal{O}(\epsilon)$.

The expression for \dot{h} is calculated as follows

$$\dot{h} = \dot{g} \cdot g_0^{-1} - g \cdot g_0^{-1} \cdot \dot{g}_0 \cdot g_0^{-1} \quad (8.13)$$

$$= g \cdot \xi \cdot g_0^{-1} - g \cdot \xi_0 \cdot g_0^{-1} \quad (8.14)$$

$$= h \cdot g_0 \cdot \xi \cdot g_0^{-1} - h \cdot g_0 \cdot \xi_0 \cdot g_0^{-1} \quad (8.15)$$

$$= h \cdot (\text{Ad}_{g_0}(\xi - \xi_0)) \quad (8.16)$$

$$= \epsilon h \cdot \text{Ad}_{g_0}(\xi_1) + \mathcal{O}(\epsilon^2). \quad (8.17)$$

□

By use of the Magnus expansion (see Magnus (1954)) we get that h is given by

$$h(t) = h_0 \exp \left(\epsilon \int_0^t \text{Ad}_{g_0(s)}(\xi_1(s)) ds + \mathcal{O}(\epsilon^2) \right). \quad (8.18)$$

The equations of motion for ξ_1 reduce to the linear control problem

$$\dot{x} = A(t)x + Bu(t), \quad x(T) = \xi_{1,\text{desired}} + z(T), \quad \dot{z} = A(t)z - f(t), \quad (8.19)$$

where

$$A(t) = -\langle \xi_0(t) : \cdot \rangle - \mathbb{I}^{-1}D, \quad B = [\tilde{\mathbb{I}}_1^{-1} \cdots \tilde{\mathbb{I}}_m^{-1}], \quad (8.20)$$

$$u(t) = \begin{bmatrix} \sigma_{1,1}(t) \\ \vdots \\ \sigma_{m,1}(t) \end{bmatrix}, \quad f(t) = -\mathbb{I}^{-1}(dV_1|_{g_0(t)} \cdot g_0(t)). \quad (8.21)$$

By use of this approach we are able to split the problem into two sub-problems. First we do motion planing for the zero order system by use of decoupled motion planning. Then we insert the zero order solution into the first order equations which is a linear control system for the velocity. This kinematic system is controllable if the time dependent equivalent of the Kalman rank condition is satisfied, in particular if

$$\left[B_0 \quad B_1(t_0) \quad \cdots \quad B_k(t_0) \quad \cdots \right], \quad B_0 = B, B_{i+1} = A(t)B_i(t) - \frac{d}{dt}B_i(t) \quad (8.22)$$

has full rank for some $k \in \mathbb{N}$ and some $t_0 \in [0, T]$. This result is Corollary 3.5.18 in Sontag (1998). The control giving the desired end point $x(T) = x_f$ at time T is given by Eq. (3.2.3) in Sontag (1998) as

$$u(t) = B^T \Phi(T, t)^T \left(\int_0^T \Phi(T, s) B B^T \Phi(T, s)^T ds \right)^{-1} (x_f - \Phi(T, 0)x(0)), \quad (8.23)$$

where Φ is the fundamental solution to $\dot{X} = A(t)X$.

Thus, we have an alternate method to compute controls for a submerged rigid body subjected to viscous drag and restorative forces and moments. We remark again that, this approach must heed Assumption 8.1 and is likely not implementable onto underwater vehicles subjected to large restoring forces and moments. Although, small amplitude forcing is a viable control method, as is presented in the two previously cited references at the beginning of this section. Thus, a perturbation approach is worthy of investigation, at least if only purely theoretical.

8.3 Design of Algorithm for On-Board Computations

To extend the application of this theory, it would be an area of further research to design an algorithm which operates on-board the vehicle to compute the decoupling vector fields and designs the control strategies as outlined in this dissertation. As discussed previously, the decoupling vector fields and the controls are currently calculated by hand and uploaded to the vehicle for autonomous implementation.

Ideally, the user would simply send a configuration η_{final} for the vehicle to realize. The vehicle would then assess its condition and determine the possible integral curves along which it can travel. Once a path is found, the parameterization $\tau(t)$ can be chosen based on available battery power and any time constraint prescribed in which to complete the maneuver.

Coupling the trajectory design strategy discussed in this dissertation with one or more of the closed-loop controllers discussed in Sections 3.3.1-3.3.5 would greatly increase the autonomy of an underwater vehicle by combining a path planning algorithm for any under-actuated scenario with a robust feedback controller for tracking the computed trajectory. This algorithm could exploit the strengths of each part of the control design and implementation. Since the geometric design is model based, the motion planning, trajectory design and control design would be vehicle specific and quite accurate. By use of a feedback or adaptive controller, the vehicle would be able to counteract any disturbances encountered along the way, thus ensuring a successful arrival at the desired location.

Chapter 9

Conclusions and Recommendations

9.1 Theoretical Conclusions and Recommendations

We began this study by presenting the equations of motion for a submerged rigid body by use of classical mechanics and well known tools from the community of naval architects and ocean engineers. By use of this base as a parallel, we derived these equations by use of the framework of differential geometry. This derivation showed how the representation of a simple mechanical system, such as a submerged rigid body, arises naturally on a differentiable manifold. By use of the Levi-Civita affine connection, we demonstrated the notion of geometric acceleration along a curve or trajectory for the system. This then led to the development of the dynamic equations of motion for a submerged rigid body.

Having expressed these equations under a different architecture only begs for exploration. Recently, much work has been done in the study of mechanical systems through the application of geometric control theory. From representation of different systems to generating motion planning algorithms, geometric control has become a useful tool to exploit the symmetries and inherent nonlinearities found in many controlled systems.

In this study, we set out to extend what is seemingly to most a purely mathematical exercise in notation, to a practically implementable control strategy for a test-bed AUV. The area of focus for the design of the control strategy was the notion of a kinematic reduction

of rank one, which is a decoupling vector field. The integral curves of such vector fields provide solutions to the motion planning problem. The pleasant thing about the kinematic reduction is that it reduces the second-order system of equations to a driftless first-order control system. Chosen properly, the controlled trajectories of this first-order system are also a solution to the second-order system.

In Section 2.4.3, we present a modification to the Levi-Civita connection which allows the connection to incorporate viscous damping. This modification then extends through to re-characterize a decoupling vector field to be able to handle motion planning and control strategy design for a rigid body submerged in a viscous fluid.

To extend the theory all the way to the practical implementation onto a test-bed vehicle, potential forces must also be accounted for. In Section 4.4, we present a method to incorporate such forces arising from gravity and buoyancy experienced by a real vessel by redefining the reparameterization of motion along the integral curves of the decoupling vector fields.

Combining these two extensions, we were able to construct dynamic controls which solve the motion planning problem for a submerged rigid body. However, the practical implementation of these controls was not straightforward, as we will discuss later. The experimental results obtained led us to consider an alternate input control representation for the vehicle ODIN. Additionally, we propose further research to consider an alternate approach to the inclusion of the potential forces as explained in the next section.

The forces arising from a potential function come from gravity and buoyancy for a submerged rigid body. These forces act based on the configuration of the body and are not

dependent upon the velocity or acceleration. Due to this relationship, the control system representing a system subjected to potential forces inevitably has a drift. This precludes these forces from being included in the kinematic reduction and hence being accounted for by the decoupling vector fields. Thus, at this stage, the use of decoupled motion planning for systems subjected to potential forces is not recommended. Although, workarounds for implementation and *ad hoc* inclusion of these forces is achievable.

9.2 Experimental Conclusions and Recommendations

Taking a purely theoretical concept and implementing it into practice is a very challenging and frustrating experience. This has been learned first hand on multiple occasions throughout the course of this study. First, no matter how good the theory works on paper, or seems to make sense in your head, something always arises that you forgot to include or should not have assumed negligible. Secondly, even when the theory is complete, you can not expect the mechanical system to function similarly every time, or even function at all for that matter!

What we really have to understand is, when bridging the gap from theory to implementation, we must understand the constant interplay between the two. It is not what you forgot to include, it is what the experimental data are telling you that is missing. This interplay is clearly evident in the inclusion of the potential forces into the framework of differential geometry via decoupled motion planning.

During the development of the theory, the inclusion of potential forces was very unclear. Not until repeated experiments were implemented, control strategies were constructed in an *ad hoc* manner and results were meticulously analyzed did we gain any insight into how these forces may arise naturally in the geometric setting.

We presented a few methods for including these forces depending upon the situation and magnitude of the desired angle. The reason for suggesting multiple strategies is that the pure theoretically derived control as suggested in Section 4.4 could not have been implemented. As mentioned earlier, ODIN is unable to apply a continuously evolving thrust strategy. Thus, all controls needed to be converted to piece-wise linear functions. For most cases, this corresponded to an over-estimate for one time regime and an under-estimate in another.

Regardless of this constraint, we were able to design and successfully implement multiple control strategies constructed by use of decoupled motion planning techniques stemming from a kinematic reduction. With the exception of the discrepancy seen in the drag coefficient for yaw in Section 6.4.6, the extension of the kinematic reduction to incorporate dissipative drag forces is excellent. We have shown good agreement between theoretical predictions and experimental data with regard to the incorporation of viscous drag in five degrees-of-freedom. The compensation for potential forces resulting from buoyancy alone are rather straightforward and was incorporated into the control design without any problems, and it produced favorable results.

These favorable results are seen in each of the missions presented in this study. We will remark again that the control strategies were applied without a feedback control or closed-

loop of any sort. Since the derivation of the theory was heavily model based, the calculated controls implemented in open-loop were able to effectively steer the vehicle blindly to the desired location. Utilizing the presented algorithm for mission planning and control design coupled with a feedback controller such as those discussed in Sections 3.3.1-3.3.5, would be a great combination for use on an underwater vehicle. By combining the strengths of both control methods, an effective hybrid controller, that is model specific for trajectory and control design and adaptive for implementation, could be produced.

The results obtained from this study further emphasize the fact that the representation of a mechanical system via differential geometric concepts and ideas is not just a change of notation for the same equations of motion, but a presentation with a much richer inherent structure. It is this geometric presentation which deserves further study and analysis in the area of motion planning for a submerged rigid body and mechanical systems in general.

Appendix A

Differential Geometry

The purpose of this appendix is to provide the basic definitions and concepts of differential geometry used in this study. A thorough treatment of all the tools used to derive the geometric mechanical framework presented warrants much more than just this appendix entry. The basic notation used throughout this research and in this section follows closely to that in Bullo & Lewis (2005a). This reference contains a more detailed investigation of the topics highlighted here, but is still brief in its treatment. Before we introduced the rigid body equations of motion, we gave a few references for a more in-depth survey of the topics required. These references apply for this section and we merely repeat them for completeness and add a few other texts which one may find useful.

Four excellent references for an introduction to differential geometry are Boothby (1986), Abraham & Marsden (1978), Abraham et al. (1986) and the comprehensive five volumes of Spivak (1979). For the basics on manifolds and tensors, we recommend Warner (1971). The texts do Carmo (1992) and do Carmo (1976) provide a comprehensive introduction to Riemannian geometry. And, the classical text for the study of affine differential geometry is Kobayashi & Nomizu (1963). We do not intend to be complete in our coverage here, and urge the interested, or confused, reader to seek any of these or other reference on the topics for a deeper understanding of such a beautiful area of mathematics.

A.1 Manifolds and Submanifolds

The study of differential geometry is the extension of differential calculus to spaces which are more general than \mathbb{R}^n . Since Euclidean space can be rather restrictive, we prefer to work in more complex spaces to define our mechanical systems so that inherent structure and nonlinearities can be exploited.

The basic object of differential geometry is a manifold, this is basically the initial extension of Euclidean space to a more abstract mathematical object. We begin here with some basic topological definitions and then proceed onto the definition of a manifold and submanifold.

We define n -dimensional Euclidean space as $\mathbb{R}^n = \{a | a = (a_1, a_2, \dots, a_n), a_i \in \mathbb{R}\}$ for $n \in \mathbb{Z}^+$. Here we assume that if $n = 0$, \mathbb{R}^0 is a point, and if $n = 1$, $\mathbb{R}^1 = \mathbb{R}$ is the real line. The i^{th} canonical coordinate function on \mathbb{R}^n is the function $r_i : \mathbb{R}^n \rightarrow \mathbb{R}$ defined by

$$r_i(a) = a_i, \tag{A-1}$$

where $a = (a_1, \dots, a_n) \in \mathbb{R}^n$. If $f : X \rightarrow \mathbb{R}^n$, then

$$f_i = r_i \circ f, \tag{A-2}$$

where f_i is the i^{th} component function of f .

For a point $p \in \mathbb{R}^n$, we denote the open ball of radius r centered at p by $B_p(r)$. The open cube of side length $2r$ centered about the origin is denoted as $C(r)$ and is given by

$$C(r) = \{(a_1, \dots, a_n) \in \mathbb{R}^n : |a_i| < r, \forall i\}. \quad (\text{A-3})$$

In this section and the rest of this appendix, we will use the term neighborhood to mean an open neighborhood. And we will denote the closure of a subset S of a topological space by \bar{S} . For a function φ on a topological space, we take the support of φ to be

$$\text{supp } \varphi = \overline{\varphi^{-1}(\mathbb{R} - \{0\})}. \quad (\text{A-4})$$

If $\alpha = (\alpha_1, \dots, \alpha_n)$ is an n-tuple of non-negative integers, then we set $[\alpha] = \sum \alpha_i$, $\alpha! = \alpha_1! \alpha_2! \cdots \alpha_n!$ and $\frac{\partial^\alpha}{\partial r^\alpha} = \frac{\partial^{[\alpha]}}{\partial r_1^{\alpha_1} \cdots \partial r_n^{\alpha_n}}$.

Suppose that $f : \mathbb{R}^n \rightarrow \mathbb{R}$, $1 \leq i \leq n$ and $t \in (t_1, \dots, t_n) \in \mathbb{R}^n$, then we denote the partial derivative of f with respect to r_i at t by

$$\left. \frac{\partial}{\partial r_i} \right|_t (f) = \left. \frac{\partial f}{\partial r_i} \right|_t = \lim_{h \rightarrow 0} \frac{f(t_1, \dots, t_{i-1}, t_i + h, t_{i+1}, \dots, t_n) - f(t)}{h}. \quad (\text{A-5})$$

Now, we proceed with the following definitions which will build up our language appropriately to define the object known as a manifold. Since we will only define the terms directly included in the definition of a manifold, we assume that the reader has a basic knowledge of general set theoretic topology.

Definition A.1 (Topological space). A *topological space* M is a set, together with a topology $T \subset \mathcal{P}(M)$ which satisfies the following properties:

- i) $M \in T$
- ii) $\emptyset \in T$
- iii) For any collection $\{U_\alpha\}_{\alpha \in A} \subset T$, $\cup_{\alpha \in A} U_\alpha \in T$
- iv) For any finite collection $\{U_1, \dots, U_n\} \subset T$, $U_1 \cap \dots \cap U_n \in T$.

Definition A.2 (Continuous). Given two topological spaces M and N , a function $\psi : M \rightarrow N$ is *continuous* if and only if $\psi^{-1}(U)$ is open in M for any open $U \subset N$; the inverse image of open sets is open.

Definition A.3 (Homeomorphism). Given two topological spaces M and N , a continuous function $\psi : M \rightarrow N$ is a *homeomorphism* if ψ has a continuous inverse $\psi^{-1} : N \rightarrow M$.

Definition A.4 (Hausdorff). We say that a topological set M is *Hausdorff* if for any two distinct points $p, q \in M$ there exists two open sets U_p, U_q such that $p \in U_p$, $q \in U_q$ and $U_p \cap U_q = \emptyset$.

Definition A.5 (Locally Euclidean). A *locally Euclidean space* M of dimension n is a Hausdorff topological space M for which each point has a neighborhood which is homeomorphic to an open subset of \mathbb{R}^n (Euclidean space).

Definition A.6 (Second countable). A topological space M is *second countable* if it satisfies the second axiom of countability, i.e., the space has a countable topological basis.

Definition A.7 (Coordinates). Suppose M is a topological space. If φ is a homeomorphism of a connected, open set $U \subset M$ onto an open subset of \mathbb{R}^n then we call φ a coordinate

map. The functions $x_i = r_i \circ \varphi$ are called the coordinate functions, and the pair (U, φ) is referred to as a coordinate system. Sometimes (U, φ) is denoted $(U, (x_1, \dots, x_n))$. In other texts, a coordinate system is sometimes called a (coordinate) chart. The coordinate system, or chart, basically puts coordinates onto open sets similarly to how we put latitude and longitude coordinates onto the sphere.

These definitions give us the structure of the space involved in a manifold, we now need only to define the differential component or the portion which allows us to consider differential calculus in multiple dimensions on abstract spaces.

Definition A.8 (Atlas). For $1 \leq r \leq \infty$, a C^r -atlas for a set M is a collection $\mathcal{A} = \{(U_\alpha, \varphi_\alpha)\}_{\alpha \in A}$ of coordinate systems such that, $M = \cup_{\alpha \in A} U_\alpha$ and whenever $U_\alpha \cap U_\beta \neq \emptyset$ we have that $\varphi_\alpha(U_\alpha \cap U_\beta)$ and $\varphi_\beta(U_\alpha \cap U_\beta)$ are open subsets of \mathbb{R}^n and the overlap map given by $\varphi_{\alpha\beta} \triangleq \varphi_\beta \circ \varphi_\alpha^{-1}|_{\varphi_\alpha(U_\alpha \cap U_\beta)}$, is a C^r -diffeomorphism from $\varphi_\alpha(U_\alpha \cap U_\beta)$ to $\varphi_\beta(U_\alpha \cap U_\beta)$.

We will define two C^r -atlases to be equivalent if their union is also a C^r -atlas. Under this equivalence relation, we define a C^r -differentiable structure on M to be an equivalence class of atlases.

We are now ready to present the formal definition of a C^r -differentiable manifold. We follow this definition with a few examples.

Definition A.9 (Differentiable manifold). For $1 \leq r \leq \infty$, a C^r -differentiable manifold of dimension n is a pair (M, F) consisting of a n -dimensional, locally Euclidean, Hausdorff, second countable topological space M together with a C^r -atlas F .

With the exception of the following examples, we will assume that for the rest of this appendix we will only deal with smooth, or class C^∞ -differentiable manifolds. The term manifold will be understood to mean a smooth differential manifold.

As a first example of a manifold, we let S be an arbitrary set and define a coordinate system on S in the following way: $\{U_x, \varphi_x\}_{x \in S}$ where $U_x = \{x\}$ and $\varphi_x(x) = 0$. This is a very degenerate example and produces a zero-dimensional manifold with topology defined by the differential structure as the discrete topology. Note that this manifold will not be second countable unless S itself is.

A common example of a manifold in three space is the 2-sphere. This is a regular surface in Euclidean three space and is easily seen as a union of open sets of \mathbb{R}^2 . In this example it is easily seen that when two of these open sets overlap, the change from one to the other can be performed in a differential manner. Here we consider the d -sphere given by the set $S^d = \{a \in \mathbb{R}^{d+1} \mid \sum_{i=1}^{d+1} a_i^2 = 1\}$. Let $n = (0, \dots, 0, 1)$ and $s = (0, \dots, 0, -1)$, which would represent the north and south pole respectively for the two-sphere. Then, we take as the differential structure the maximal collection containing $(S^d - n, \pi_n)$ and $(S^d - s, \pi_s)$ where π_n and π_s are stereographic projections from n and s respectively.

Let $V = L(n)$ be the set of all $n \times n$ real matrices which is a vector space of dimension n^2 . The determinant function $\det : L(n) \rightarrow \mathbb{R}$ is continuous and $\det^{-1}(\mathbb{R} - \{0\})$ is an open subset of $L(n)$. Thus, $\det^{-1}(\mathbb{R} - \{0\})$ defines a manifold of dimension n^2 , and this is commonly referred to as $GL(n)$ or the set of all invertible matrices.

Finally, any open subset U of a differentiable manifold (M, F_M) is itself a differentiable manifold with the inherited differentiable structure $F_U = \{(U_\alpha \cap U, \varphi_\alpha|_{U_\alpha \cap U}) : (U_\alpha, \varphi_\alpha) \in$

$F_M\}$. The idea of a subset also being a manifold brings to question the notion of the existence of a submanifold. This is indeed an object of differential geometry and worthy of its own definition.

Definition A.10 (Submanifold). For $1 \leq r \leq \infty$, a subset S of a C^r -manifold M is a C^r -submanifold if, for each point $x \in S$, there is a coordinate chart (U, φ) for M with $x \in U$ and such that φ takes its values in a product $\mathbb{R}^k \times \mathbb{R}^{n-k}$ and $\varphi(U \cap S) = \varphi(U) \cap \varphi(\mathbb{R}^k \times \{0\})$.

By this definition, a coordinate chart for S is then given by $(U \cap S, \varphi|_{(U \cap S)})$. If the submanifold S has a well-defined dimension as a manifold, we denote the dimension of S as $\dim(S)$. If the original manifold also has a well-defined dimension, then we can speak of the codimension of S which is given by $\dim(M) - \dim(S)$.

This now gives us the base space or configuration space within which we can construct the equations which define the mechanical systems considered in this dissertation. We now continue by defining the space of positions and velocities.

A.2 Tangent and Cotangent Bundles

In this section we introduce the notion of a tangent bundle along with its dual object the cotangent bundle. In geometric mechanics, the manifold gives the positions of the system whereas the tangent bundle to this configuration space is the set of positions and velocities. Here we emphasize the fact that velocities do not exist on their own, and we can only discuss velocity at a position.

To begin, let us assume that we have a smooth manifold M of dimension n . Now, consider the collection $G_U : U \rightarrow \mathbb{R}$ of all smooth (C^∞) mappings on an open subset $U \subseteq M$. It is easily verified (see e.g., Boothby (1986)) that G_U is a commutative algebra over \mathbb{R} . Given $p \in M$, define G_p as the algebra of smooth functions defined on some open neighborhood of p . Here we identify two functions defined on open sets containing p to be equivalent, or have the same germ at p , if they agree on some neighborhood of p . The equivalence classes are called germs, and we will abuse notation and denote the set of germs at p by G_p .

Definition A.11 (Tangent vector). A *tangent vector to M at p* is a mapping $X_p : G_p \rightarrow \mathbb{R}$ such that for all $a, b \in \mathbb{R}$ and $f, g \in G_p$ satisfy

- i) $X_p(af + bg) = a(X_p f) + b(X_p g)$
- ii) $X_p(fg) = (X_p f)g(p) + f(p)(X_p g)$,

with the vector space operations defined by $(X_p + Y_p)f = X_p f + Y_p f$ and $(aX_p)f = a(X_p f)$.

Definition A.12 (Dual vector space). The *dual vector space* to a real vector space V is the vector space of linear functions $f : V \rightarrow \mathbb{R}$. We denote the dual space of a vector space V by V^* . The dimension of the dual space is the same as the dimension of the original vector space.

The tangent space $T_p M$ to M at p is the set of all mappings X_p which satisfy the conditions in Definition A.11. For a manifold M , denote by TM the disjoint union $TM = \dot{\cup}_{p \in M} T_p M$. This collection is itself a differentiable manifold called the tangent bundle. We

can also define the cotangent space at p , T_p^*M , which is the dual vector space to T_pM . The cotangent bundle is then given by $T^*M = \dot{\cup}_{p \in M} T_p^*M$.

We will now demonstrate how to assign a differential structure to these vector bundles to show that they are, in fact differentiable manifolds. Let M be a smooth manifold with differentiable structure F . Let $TM = \dot{\cup}_{p \in M} T_pM$ and $T^*M = \dot{\cup}_{p \in M} T_p^*M$. Then define the natural projections π_1 and π_2 as follows

$$\pi_1 : TM \rightarrow M, \quad \pi_1(\nu) = p, \text{ if } \nu \in T_pM \quad (\text{A-6})$$

$$\pi_2 : T^*M \rightarrow M, \quad \pi_2(\tau) = p, \text{ if } \tau \in T_p^*M. \quad (\text{A-7})$$

Let $(U, \varphi) \in F$ with coordinate functions x_1, \dots, x_n . For all $\nu \in \pi_1^{-1}(U)$ and $\tau \in (\pi_2)^{-1}(U)$, define $\tilde{\varphi}_1 : \pi_1^{-1}(U) \rightarrow \mathbb{R}^{2n}$ and $\tilde{\varphi}_2 : (\pi_2)^{-1}(U) \rightarrow \mathbb{R}^{2n}$ by

$$\tilde{\varphi}_1(\nu) = (x_1(\pi_1(\nu)), \dots, x_n(\pi_1(\nu)), dx_1(\nu), \dots, dx_n(\nu)) \quad (\text{A-8})$$

$$\tilde{\varphi}_2(\tau) = (x_1(\pi_2(\tau)), \dots, x_n(\pi_2(\tau)), \tau \left(\frac{\partial}{\partial x_1} \right), \dots, \tau \left(\frac{\partial}{\partial x_n} \right)), \quad (\text{A-9})$$

where dx_i and $\partial/\partial x_i$ are the differentials of the coordinate functions $\{x_1, \dots, x_n\}$ on TM and its dual space T^*M , respectively. Now, if (U, φ) and $(V, \psi) \in F$, then we can see that $\tilde{\psi}_1 \circ \tilde{\varphi}_1^{-1}$ is a smooth function. We can form a basis for a topology on TM using the collection $\{\tilde{\varphi}_1^{-1}(W), (U, \varphi)\}$, where W is open in \mathbb{R}^{2n} . This makes TM a locally Euclidean, second countable space of dimension $2n$. The differentiable structure \tilde{F} for TM can be taken to be the maximal collection containing $\{(\pi_1^{-1}(U), \tilde{\varphi}_1)\}$.

This construction now defines a differentiable manifold of dimension $2n$ which we refer to as the tangent bundle. A similar construction can be done for T^*M which results in the cotangent bundle.

A.3 Vector and Covector Fields

In the previous section we saw two examples (the tangent and cotangent bundles) of the geometric object called a bundle. Here we will only cover the preliminaries and necessary tools needed to understand the concepts of a vector bundle, a section of a bundle and a tensor bundle. With these notions, we then give the definitions of vector and covector fields.

Generally speaking, a bundle is an object containing a total space (TM in the case of the tangent bundle), a base space (M in the case of the tangent bundle) and a projection (π_{TM} in the case of the tangent bundle). We define the fiber of a point in the base space as the preimage of the point under the projection map. As done with the construction of a manifold, we begin locally. We also assume that everything is of class C^∞ .

Definition A.13 (Local vector bundle). Let $U \subset \mathbb{R}^n$ and $V \subset \mathbb{R}^m$ be open sets, then a *local vector bundle* is a product $U \times \mathbb{R}^k$.

Definition A.14 (Local vector bundle map). Let $U \times \mathbb{R}^k$ and $V \times \mathbb{R}^l$ be local vector bundles and $r \in \mathbb{N} \cup \{\infty\}$. A C^r -*local vector bundle map* is a map $g : U \times \mathbb{R}^k \rightarrow V \times \mathbb{R}^l$ such that $g(x, v) = (g_1(x), g_2(x) \cdot v)$, where $g_1 : U \rightarrow V$ and $g_2 : U \rightarrow L(\mathbb{R}^k; \mathbb{R}^l)$ are of class C^r . If g_1 is a C^r -diffeomorphism and $g_2(x)$ is an isomorphism for each $x \in U$, then the map g is a C^r -*local vector bundle isomorphism*.

Definition A.15 (Vector bundle). A *vector bundle* is a set S with an atlas $A = \{U_a, \varphi_a\}_{a \in \mathcal{A}}$ where $\text{im}(\varphi_a)$ is a local vector bundle and for which the overlap maps are local vector bundle isomorphisms.

The base space B of a vector bundle V is the set of all $v \in V$ with the property that there exists an admissible vector bundle coordinate system (\mathcal{V}, ψ) such that $\psi(v) = (x, 0) \in U \times \mathbb{R}^k$. Thus, we can define $b = \psi^{-1}(x, 0)$. This resulting map is referred to as the vector bundle projection and is written as the vector bundle $\pi : V \rightarrow B$. For $b \in B$, the set $\pi^{-1}(b)$ is the fiber over b and is written as V_b .

Definition A.16 (Section of a vector bundle). The *section of a vector bundle* $\pi : V \rightarrow B$ is a smooth map $\xi : B \rightarrow V$ for which $\pi \circ \xi = \text{id}_B$. We will denote the sections of V by $\Gamma(V)$ under the assumption that they are of class C^∞ .

Now, given a vector bundle $\pi : V \rightarrow B$ we can associate different vector bundles over B which are constructed from the vector bundle V . One construction leading to three separate objects is of particular interest here.

For $r, s \in \mathbb{N}$, let $T_s^r V$ be the vector bundle over B whose fiber over $b \in B$ is the set of (r, s) -tensors on V_b . In the specific case where $B = M$ and $V = TM$ is the tangent bundle, the sections of $T_s^r TM$ are called (r, s) -tensor fields on M . The three important tensor fields here are given in the following definition.

Definition A.17 (Vector field). A smooth *vector field* on M is a smooth $(1, 0)$ -tensor field on M . A smooth *covector field* on M is a smooth $(0, 1)$ -tensor field on M . And, a smooth

Riemannian metric \mathbb{G} on M is a smooth $(0, 2)$ -tensor field on M with the property that $\mathbb{G}(p)$ is an inner product on T_pM .

Thus, a vector field on M is an element of $\Gamma(TM)$ and it assigns, in a smooth way, a tangent vector to each point of the manifold. This, in a sense, defines a flow through or along the manifold.

Following this flow of a vector field on a manifold has applications in the realm of mechanical systems and trajectory design. The trajectory planning used in the body of this dissertation uses the concatenation of integral curves of vector fields. Here we give the precise definition of an integral curve for a smooth vector field.

Definition A.18 (Differentiable curve). A *differentiable curve* $\gamma : I \rightarrow M$ is an integral curve for a vector field X if $\gamma'(t) = X(\gamma(t))$ for every $t \in I$.

A.3.1 Lie Bracket

The use of vector fields in differential geometry is quite widespread. Their applications are diverse within the theory, yet we will consider them in the context of differential equations and differential operators. In this way, we can use vector fields to differentiate functions as well as other vector fields. Let us first consider the differential of a function.

Definition A.19 (Tangent map). Given a function $f : M \rightarrow N$ between two smooth manifolds, let $p \in M$ and let $[\gamma]_p \in T_pM$ represent the tangent vector corresponding to γ at p .

Then $f \circ \gamma$ is a curve at $f(p)$ and we can write $Tf([\gamma]_p) = [f \circ \gamma]_{f(p)}$. This then defines the *tangent map* $Tf : TM \rightarrow TN$ of f .

Definition A.20 (Differential). Given $f \in C^r(M)$, we have $Tf : TM \rightarrow T\mathbb{R}$. Since $T\mathbb{R} \simeq \mathbb{R} \times \mathbb{R}$ we can write $Tf(v_p) = (f(p), \alpha_f(p) \cdot v_p)$ for $\alpha_f(p) \in L(T_p M; \mathbb{R}) = T_p^* M$, and we refer to $\alpha_f(p)$ as the *differential of f at p* . We denote this covector by $df(x)$ and the C^{r-1} section $p \mapsto df(p)$ of $T^* M$ is denoted by df .

Contracting this differential with a vector field $X \in \Gamma(TM)$ we get the following important object which provides a convenient method of representing vector fields in coordinates.

Definition A.21 (Lie derivative). If $p \in M$, $X \in \Gamma^r(TM)$ and $f \in C^r(M)$, then the function $\mathcal{L}_X f \in C^{r-1}(M)$ defined by $p \mapsto df(p) \cdot X(p)$ is the *Lie derivative of f with respect to X* .

The properties of the Lie derivative follow similarly to that of the standard derivative. The map $f \rightarrow \mathcal{L}_X f$ is \mathbb{R} -linear with respect to vector addition and scalar multiplication, and the standard product rule applies: $\mathcal{L}_X(fg) = (\mathcal{L}_X f)g + f(\mathcal{L}_X g)$. By use of this later relation, we suppose that we have $X, Y \in \Gamma^\infty(TM)$ and consider the map $f \rightarrow \mathcal{L}_X \mathcal{L}_Y f - \mathcal{L}_Y \mathcal{L}_X f$. The expression depends only upon first derivatives of the function f as the second derivatives cancel. This new vector field associated with both X and Y deserves its own definition.

Definition A.22 (Lie bracket). For $X, Y \in \Gamma^\infty(TM)$, the vector field $[X, Y]$ defined by $\mathcal{L}_{[X, Y]}f = \mathcal{L}_X\mathcal{L}_Yf - \mathcal{L}_Y\mathcal{L}_Xf$ for $f \in C^\infty(M)$ is called the *Lie bracket of X and Y* and is the Lie derivative of Y with respect to X ; $[X, Y] = \mathcal{L}_XY$.

In the coordinate system (x^1, \dots, x^n) , the Lie bracket $[X, Y]$ is given by

$$[X, Y]^i = \frac{\partial Y^i}{\partial x^j}X^j - \frac{\partial X^i}{\partial x^j}Y^j, \quad i \in \{1, \dots, n\}. \quad (\text{A-10})$$

At this point, it is not intuitively clear what the Lie bracket represents. However, we add some insight through the following properties and demonstrate a useful characteristic of the Lie bracket with regard to the flow of vector fields.

Proposition A.1. *For all $f, g \in C^\infty(M)$ and for all $X, Y, Z \in \Gamma^\infty(TM)$, the Lie bracket has the following properties:*

- i) $[X, Y] = -[Y, X]$
- ii) $[X + Y, Z] = [X, Z] + [Y, Z]$
- iii) $[fX, gY] = fg[X, Y] + f(\mathcal{L}_Xg)Y - g(\mathcal{L}_Yf)X$, and
- iv) $[X, [Y, Z]] + [Y, [Z, X]] + [Z, [X, Y]] = 0$

The proofs of each of these facts is easily verified by use of the definition and the coordinate representation of the Lie bracket. To determine kinematic controllability of a mechanical system, we must examine the involutive closure of the distribution of the input control vector fields with respect to the Lie bracket. We denote this involutive closure by $Lie^{(\infty)}(Y)$, where Y is a distribution of vector fields. We denote $Lie^{(0)}(Y) = Y$, and

inductively define the distributions $Lie^{(l)}(\mathbf{Y})$ on M by

$$Lie^{(l)}(\mathbf{Y})_x = Lie^{(l-1)}(\mathbf{Y})_x + \text{Span}_{\mathbb{R}}\{[X, Z](x) | X \in \Gamma^\infty(Lie^{(l_1)}(\mathbf{Y})), \\ Z \in \Gamma^\infty(Lie^{(l_2)}(\mathbf{Y})), l_1 + l_2 = l - 1\}, \quad (\text{A-11})$$

for $l \in \mathbb{N}$. For a fixed $x \in M$, there exists a smallest integer $K(x)$ such that $Lie^{(l)}(\mathbf{Y})_x = Lie^{(K(x))}(\mathbf{Y})_x$ for all $l \geq K(x)$. The distribution we call the involutive closure is defined by doing this for each $x \in M$.

Next, we define the domain of a vector field to be the subset $\text{dom}(X) \subset \mathbb{R} \times M$ given by $\text{dom}(X) = \{(t, x) | t \in I(X, x)\}$ where $I(X, x)$ is the largest interval on which an integral curve for X can be defined. If $\text{dom}(X) = \mathbb{R} \times M$, we call the vector field X complete. The flow of X is a map from $\text{dom}(X)$ to M which assigns to $(t, x) \in \text{dom}(X)$ the point $\gamma(t) \in M$ where γ is the maximal integral curve of X at x . The image of (t, x) under the flow is written as $\mathcal{F}_t^X(x)$. By use of this terminology, we now present a Proposition from Bullo & Lewis (2005a) which gives a more intuitive notion of the Lie bracket. Basically, this proposition says that if you follow the flow of a vector field X , then follow the flow of a vector field Y , then $-X$, then $-Y$ for the same amount of time along each, then if we return to the same point, we have $[X, Y] = 0$. In particular, the Lie bracket is a measure of how well the vector fields commute with each other.

Proposition A.2. *Let $X, Y \in \Gamma^\infty(TM)$ and let $x \in M$. Define a curve γ at x by*

$$\gamma(t) = \mathcal{F}_{\sqrt{t}}^{-Y} \circ \mathcal{F}_{\sqrt{t}}^{-X} \circ \mathcal{F}_{\sqrt{t}}^Y \circ \mathcal{F}_{\sqrt{t}}^X(x). \quad (\text{A-12})$$

Then γ is differentiable and $\gamma'(0) = [X, Y](x)$. Moreover, if X and Y are complete, then $[X, Y] = 0$ for all $x \in M$ if and only if $\mathcal{F}_t^X \circ \mathcal{F}_s^Y = \mathcal{F}_s^Y \circ \mathcal{F}_t^X$ for all $s, t \in \mathbb{R}$.

A.4 Affine Differential Geometry

Thus far, we have developed the abstract notion of a manifold (configuration space) in which we can describe a mechanical system as well as define its associated velocities via the tangent bundle. To properly deal with dynamic systems, we need to develop the proper notion for acceleration. This step requires a bit more effort along with the definition of an affine connection.

For example, let us suppose that we have a manifold M of dimension two embedded in \mathbb{R}^3 , and let $\gamma : I \rightarrow M$ be a parameterized curve in M with $V : I \rightarrow \mathbb{R}^3$ a vector field along γ tangent to M . If we simply consider the vector $\frac{dV}{dt}(t)$ for $t \in I$, we are not guaranteed that this vector is an element of the tangent plane of M , $T_\gamma M$. This shows that the idea of differentiating a vector field is not an intrinsic geometric concept. We solve this dilemma by considering the orthogonal projection of $\frac{dV}{dt}(t)$ onto $T_\gamma M$ which yields the derivative of V as seen from M . This covariant derivative generalizes the notion of directional derivative, usually denoted by $\frac{DV}{dt}(t)$ and, when $V = d\gamma/dt$, produces what we think of in Euclidean space as the acceleration to the curve γ .

The concept of a covariant derivative presents the opportunity to be able to define a geodesic (curve with zero acceleration) and the notion of curvature on more general spaces

than Riemannian manifolds. This abstract notion of the differentiation of vector fields is now referred to as an affine connection and gives rise to the more general geometric area of affine differential geometry.

A.4.1 Affine Connections

The heart of affine differential geometry lies with the affine connection.

Definition A.23 (Affine connection). A C^r -affine connection on M assigns to the pair $(X, Y) \in \Gamma^r(TM) \times \Gamma^{r+1}(TM)$ a vector field $\nabla_X Y \in \Gamma^r(TM)$ which satisfies the following properties:

- i) the map $(X, Y) \rightarrow \nabla_X Y$ is \mathbb{R} -bilinear,
- ii) $\nabla_{fX} Y = f\nabla_X Y$ for each $X \in \Gamma^r(TM), Y \in \Gamma^{r+1}(TM)$ and $f \in C^r(M)$ and
- iii) $\nabla_X fY = f\nabla_X Y + (\mathcal{L}_X f)Y$ for each $X \in \Gamma^r(TM), Y \in \Gamma^{r+1}(TM)$ and $f \in C^{r+1}(M)$.

We refer to the vector field $\nabla_X Y$ as the covariant derivative of Y with respect to X . It is common to consider the covariant derivative along a curve γ ; in this case, we will use the notation $\nabla_{\gamma'(t)} Y$. With this notation, we can present the definition of a geodesic of an affine connection to be a curve $\gamma : I \rightarrow M$ such that $\nabla_{\gamma'(t)} \gamma'(t) = 0$.

In general, there are many different affine connections with properties suited for their specific application. For our application, we will be interested in an affine connection which is derived from a Riemannian metric (e.g., the kinetic energy metric \mathbb{G} given in Eq. (2.48))

on the manifold M . This specific affine connection is called the Levi-Civita connection and is characterized in the following theorem.

Theorem A.1. *If M is a C^{r+1} -Riemannian manifold, then there exists a unique C^r -affine connection ∇ on M such that*

- i) $\nabla \mathbb{G} = 0$ (i.e., ∇ is a metric connection) and
- ii) $\nabla_X Y - \nabla_Y X = [X, Y]$ for all $X, Y \in \Gamma^{r+1}(TM)$.

A proof of this result can be found in Bullo & Lewis (2005a).

For completeness, we also demonstrate how the affine connection can be displayed in local coordinates. Let ∇ be an affine connection on M , and let (x^1, \dots, x^n) be coordinates for the chart (U, φ) . For any $i, j \in \{1, \dots, n\}$, $\nabla_{\frac{\partial}{\partial x^i}} \frac{\partial}{\partial x^j}$ is a vector field on U and is hence a linear combination of the vector fields $\{\frac{\partial}{\partial x^1}, \dots, \frac{\partial}{\partial x^n}\}$. For n^3 uniquely defined functions $\Gamma_{ij}^k : U \rightarrow \mathbb{R}$ with $i, j, k \in \{1, \dots, n\}$ we can write

$$\nabla_{\frac{\partial}{\partial x^i}} \frac{\partial}{\partial x^j} = \Gamma_{ij}^k \frac{\partial}{\partial x^k}. \quad (\text{A-13})$$

These n^3 functions are called the Christoffel symbols for ∇ in the chart (U, φ) . For our application, the Christoffel symbols are the functions which account for the coriolis and centripetal forces arising from the assumption that the earth fixed frame is not rotating.

A.4.2 Symmetric Product

Another key component of affine differential geometry is the notion of the symmetric product. As applied to the formulation of rigid body kinematics, the symmetric product is fundamental in determining the controllability of a given system.

Definition A.24 (Symmetric product). If ∇ is an affine connection on a manifold M , the *symmetric product corresponding to ∇* is the operation which assigns to vector fields X and Y the vector field $\langle X : Y \rangle = \nabla_X Y + \nabla_Y X$.

A.5 Lie Groups

In the study of rigid body kinematics, an important type of manifold arises naturally from the inherent structure and symmetries of the mechanical system. The Lie group and its associated Lie algebra are used to exploit such inherent properties for the analysis and control of the system. These matrix objects form a vast area of mathematics and much literature has been published on the study of them alone. Here we only aim to give the basic definitions and derive the necessary tools used in the body of this dissertation.

We begin by recalling from basic abstract algebra that a group is a set G together with an associative binary operation which is closed under inverses and has an identity element. We define a topological group as a group G which is also a topological space and, for

$(a, b) \in G \times G$ and $a \in G$, the maps $(a, b) \mapsto ab$ and $a \mapsto a^{-1}$ are continuous. This leads us to our main definition.

Definition A.25 (Lie group). A *Lie group* is a topological group which is also a manifold with a C^∞ structure such that the group operation and the inverse operation are C^∞ functions.

The simplest example of a Lie group is \mathbb{R}^n with the operation $+$. For a slightly more complicated example, consider the two link manipulator. This mechanical system has as its configuration space the torus or $S^1 \times S^1$. If we consider S^1 as the quotient group \mathbb{R}/\mathbb{Z} we have a group structure on the circle. The functions $x \mapsto \cos 2\pi x$ and $x \mapsto \sin 2\pi x$ are smooth functions on \mathbb{R}/\mathbb{Z} and demonstrate that the circle is also a Lie group. It is easy to show the extension that the direct product of Lie groups is again a Lie group, hence the torus is a Lie group. For more details on this example or to see other mechanical systems whose configuration spaces are also Lie groups, see Bullo et al. (2002) and Bullo & Lewis (2005a).

With reference to the modeling of mechanical systems, the Lie groups which we will be interested in are matrix Lie groups. Notice that the set of all $n \times n$ invertible matrices composed of real entries with the binary operation of matrix multiplication is a Lie group. This set is referred to as the general linear group and is denoted $GL(n, \mathbb{R})$. The identity element is given by I_n and the inverse of an element $A \in GL(n, \mathbb{R})$ is A^{-1} .

Definition A.26 (Lie subgroup). Let G be a Lie group. A *Lie subgroup* of G is a subgroup $H \subset G$ for which the inclusion map $i_H : H \rightarrow G$ is an injective immersion.

Definition A.27 (Matrix Lie group). A *matrix Lie group* is a subgroup of $GL(n, \mathbb{R})$.

A direct consequence of the definition of a matrix Lie group is that the group of rotations $SO(3)$ and the group of rigid displacements $SE(3)$ are both matrix Lie groups.

In a matrix Lie group, we can define the matrix commutator $[\cdot, \cdot] : \mathbb{R}^{n \times n} \times \mathbb{R}^{n \times n} \rightarrow \mathbb{R}^{n \times n}$ as $[A, B] = AB - BA$. Additionally, we call $A \in \mathbb{R}^{n \times n}$ a one-parameter subgroup generator of G if $\mathbb{R} \ni t \mapsto \exp(tA) \in \mathbb{R}^{n \times n}$ takes values in G . The set of these generators, forms an algebra on the Lie group $G \subset GL(n, \mathbb{R})$. If this set of generators is also closed under the matrix commutator, we refer to this subspace as the matrix Lie algebra. This is just one example of a broader object introduced in the following section.

A.5.1 Lie Algebras

Each matrix Lie group gives rise to a corresponding matrix Lie algebra. In fact, there is a one-to-one correspondence between connected k -dimensional subgroups $G \subset GL(n, \mathbb{R})$ and k -dimensional matrix Lie algebras (see e.g., Warner (1971)). Here we introduce the Lie algebra and demonstrate that every Lie group has an associated Lie algebra.

Definition A.28 (Lie algebra). A *Lie algebra* V is a \mathbb{R} -vector space along with a bilinear operation $[\cdot, \cdot] : V \times V \rightarrow V$ called the bracket which is anti-commutative and satisfies the Jacobi identity.

A relevant example is that the vector space $\Gamma^\infty(TM)$ of all smooth vector fields on a smooth manifold M is a Lie algebra with respect to the operation of Lie bracket.

For any Lie group G , given $a \in G$ we can define the linear maps of left and right translations $L_a : G \rightarrow G$ and $R_a : G \rightarrow G$ by $L_a(b) = ab$ and $R_a(b) = ba$ respectively. Both of these maps are diffeomorphisms, and have inverses. Let the dual of a linear map A be represented by A^* . Then, the dual maps of left and right translation are isomorphisms.

Definition A.29 (Left-invariant). A vector field X on G is *left-invariant* if $L_g^*X = X$ for all $g \in G$. Equivalently, X is left-invariant if $X(g \star h) = T_h L_g(X(h))$ for all $g, h \in G$.

Note that replacing left with right and L_g with R_g defines a right-invariant vector field. Here we choose to consider the left-invariant case only. We identify a left-invariant vector field by their value at the identity via $X(g) = T_e L_g(X(e))$ and we will denote the left-invariant vector field on G defined by $\xi_L = \xi \in T_e G$ as ξ_L . These left-invariant vector fields have the following properties.

Proposition A.3. *For a Lie group G ,*

- i) left-invariant vector fields are smooth;*
- ii) the set of left-invariant vector fields of G ($\mathcal{L}(G)$) is a Lie subalgebra of $\Gamma^\infty(TG)$ and*
- iii) the vector spaces $T_e G$ and $\mathcal{L}(G)$ are isomorphic by the vector space isomorphism $T_e G \ni X_e \rightarrow (X_e)_L \in \mathcal{L}(G)$. Additionally, $\dim(G) = \dim(T_e G) = \dim(\mathcal{L}(G))$.*

We refer the reader to Warner (1971) and Bullo & Lewis (2005a) for a proof of these properties. This then leads us into the definition of a Lie algebra.

Definition A.30 (Characterization of the Lie algebra). The Lie algebra \mathfrak{g} of a Lie group G is the tangent space at the identity $T_e G$ with the bracket $[\xi, \eta] = [\xi_L, \eta_L](e)$.

An equivalent definition of a Lie algebra to that presented here is given by Warner (1971) to be the set of left-invariant vector fields.

Appendix B

Ancillary Data Collected

B.1 Drag Force Estimations

In this appendix, we present the procedure for estimating the total viscous drag forces and moments acting on ODIN. As remarked in Section 2.4.3, the contribution of the drag forces and moments are assumed quadratic with respect to the velocity of the vehicle. We also assume that the matrix representing the drag forces and moments is diagonal, see Section 2.3.2.

As presented in Allmendinger (1990), the drag force imparted by a viscous fluid on ODIN, denoted D_{ODIN} , can be broken down into two main components, the drag from the bare hull (D_{Sphere}), and the drag from the appendages ($D_{Appendages}$). In particular,

$$D_{ODIN} = D_{Sphere} + D_{Appendages}. \quad (\text{B-1})$$

We assume that the bare hull of ODIN is a sphere with a diameter of 0.64m. The appendages we consider are:

- (i) Tether connector (cylinder)
- (ii) Keel mounted rubber pipe fitting (cylinder)
- (iii) Arms holding the thrusters (rectangular solids)

(iv) Thrusters normal to the direction of motion; broken down into the trapezoidal thruster tops and the cylindrical thruster bodies

For the hull and each appendage, we know that the drag force is a function of velocity given by $D = 1/2 C_D \rho A |\nu| \nu$, where C_D is the non-dimensional drag coefficient, ρ is the fluid density, A is the representative area and ν is the representative velocity of ODIN.

The viscous drag forces for ODIN's spherical hull can be broken down into three main components

$$D_{Sphere}(\nu) = \frac{1}{2} C_f \rho A |\nu| \nu + \frac{1}{2} C_r \rho A |\nu| \nu + \frac{1}{2} C_w \rho A |\nu| \nu, \quad (B-2)$$

where

$$C_f = \text{Frictional resistance coefficient}, \quad (B-3)$$

$$C_r = \text{Residual resistance coefficient or pressure/form drag coefficient}, \quad (B-4)$$

$$C_w = \text{Wave-making resistance coefficient}, \quad (B-5)$$

and A is the projected frontal area (C_r) or the total surface area (C_f).

Since we consider a deeply submerged body, and thus an unbounded fluid, we may assume that $C_w = 0$. For the range of velocities considered in the experiments, the Reynolds number is approximately 10^5 . Published values for the frictional drag coefficient give $0.003 \leq C_f \leq 0.007$ depending if one uses Blasius boundary layer theory, Schoenherr's

flat-plate theory, or calculates the value by use of an ITTC-type equation⁹ similar to Eq. (61) on p. 252 of Allmendinger (1990). For moderate Reynolds numbers, such as those experienced here, the majority of the drag force experienced by a sphere is due to pressure gradients induced from separation. This drag force is referred to as pressure drag or form drag and is dependent upon the shape of the body. For a sphere, there is a stagnation point, or region of relatively high pressure, directly at the front. There is a reduced pressure region aft of the body within the separated wake resulting from the continuity of the free-stream pressure away from the body and outside the area of separation. Thus, there is a considerable pressure gradient between the front and rear of the sphere which results in a residual or pressure resistance coefficient C_r which is two orders of magnitude larger than C_f . Values of C_r for a general body are usually found via model testing. For our case of a sphere, multiple references exist providing such drag coefficients. In this dissertation, we choose to follow the data presented in Table 2.2 of Newman (1977). For the range of velocities considered in this dissertation, we estimate $0.4 \leq C_D < 0.6$ depending upon the Reynolds number. We remark here that C_D as given in Table 2.2 of Newman (1977) is a total drag coefficient and its estimation includes the effects of frictional resistance as well as pressure drag.

For rotational motions, the viscous drag moments resulting only from the sphere are due to frictional resistance. We calculate $C_f = 0.00469$ by use of Eq. (61) in Allmendinger (1990). The viscous drag moments are then calculated by $D_{Sphere}(\Omega) = 1/2 C_f \rho A_s |v| v r$, where A_s is the surface area of the sphere, $v = \Omega r$ is the linear velocity of a point on

⁹ITTC - International Towing Tank Conference

the surface of the sphere, Ω is the corresponding angular velocity of the point and r is the sphere radius.

For the appendages, Allmendinger (1990) gives typical drag coefficients for different types of protrusions from the body. The author mentions that the presented values are total drag coefficients as the drag tests do not break out individual coefficients. Of the aforementioned appendages we consider for ODIN, the drag coefficients are all equal to 1.2, and the representative area is the projected frontal area. This again assumes that pressure drag is dominant. We assume that these coefficients are constant with respect to the range of Reynolds numbers considered. When calculating the viscous drag momentum for each appendage, we compute the drag force with respect to the linear velocity of the appendage and multiply this by the moment arm. We assume that the length of the moment arm is the distance from O_B to the center of gravity of the appendage.

For the hull and each appendage, we calculate the drag forces (moments) separately for every 0.01 m/s (rad/sec) over the velocity range of zero to one m/s (rad/sec). We do this for each of the six independent velocity motions, taking into account that some appendages do not contribute a drag force or moment for some motions. In particular, the keel mounted rubber pipe fitting contributes a negligible drag moment during yawing motions. Summing the drag forces together for each velocity interval gives us the total drag force/moment for ODIN discretized over the operational velocity regime.

The data allow us to plot the total drag force or moment on ODIN with respect to velocity for each of the six degree-of-freedom motions. These forces and moments are shown in Figs. 42-47.

We are interested in finding $F_i(\gamma'(t)) = D_i$ for $i = \{1, \dots, 6\}$, such that the total viscous drag force can be expressed as $D_{ODIN}(\nu) = D_i \nu_i^2$ for $i = 1, 2, 3$ and the drag momenta as $D_{ODIN}(\Omega) = D_i \Omega_i^2$ for $i = 4, 5, 6$, as defined in Section 2.4.3. This will allow us to incorporate the drag forces into the affine connection $\tilde{\nabla}$. To do this, we calculate a best fit quadratic polynomial, with no linear or constant terms, to the drag force (moment) versus velocity relation for ODIN's velocity which is prescribed by the parameterization $\tau(t)$.

During the experimental trials, the calculated drag coefficients D_i were tested for several velocities within ODIN's operational range. The experimental data matched well with theoretical predictions. We omit the details of these experiments, as the results are contained within the results presented in Chapter 6.

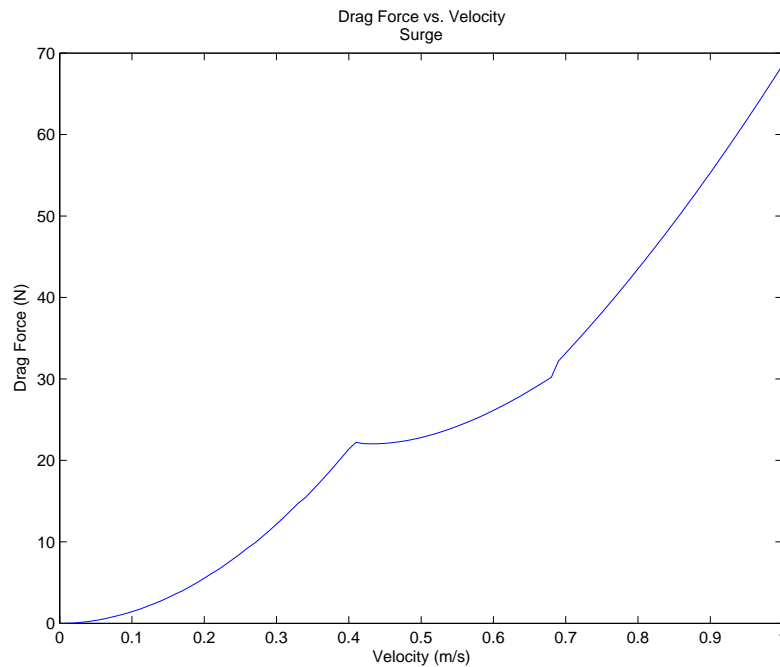


Figure 42: Drag force versus velocity in the surge direction.

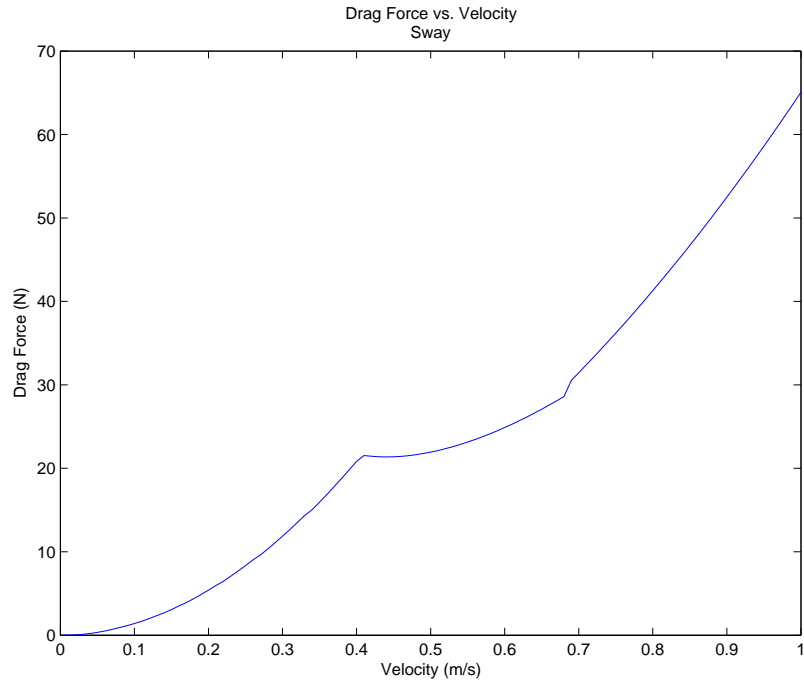


Figure 43: Drag force versus velocity in the sway direction.

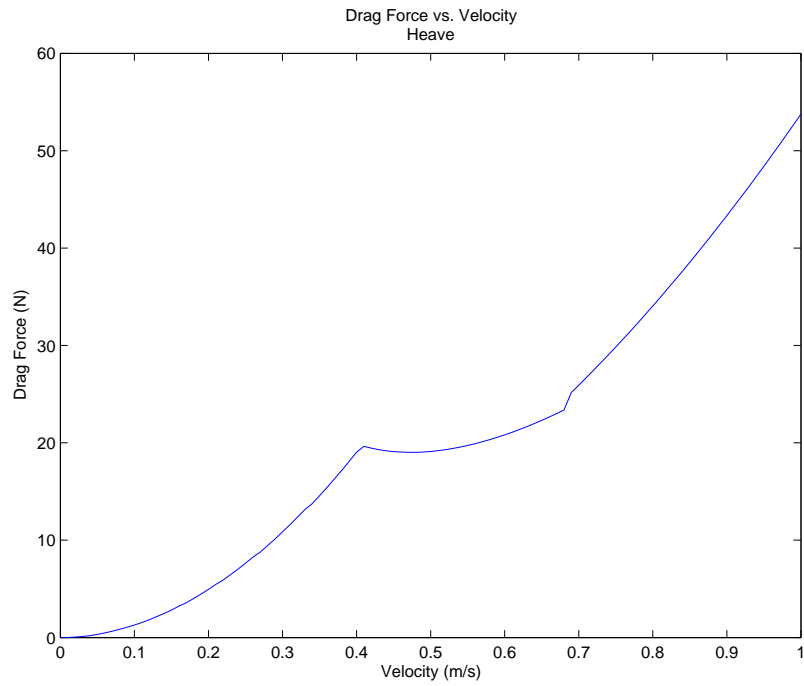


Figure 44: Drag force versus velocity in the heave direction.

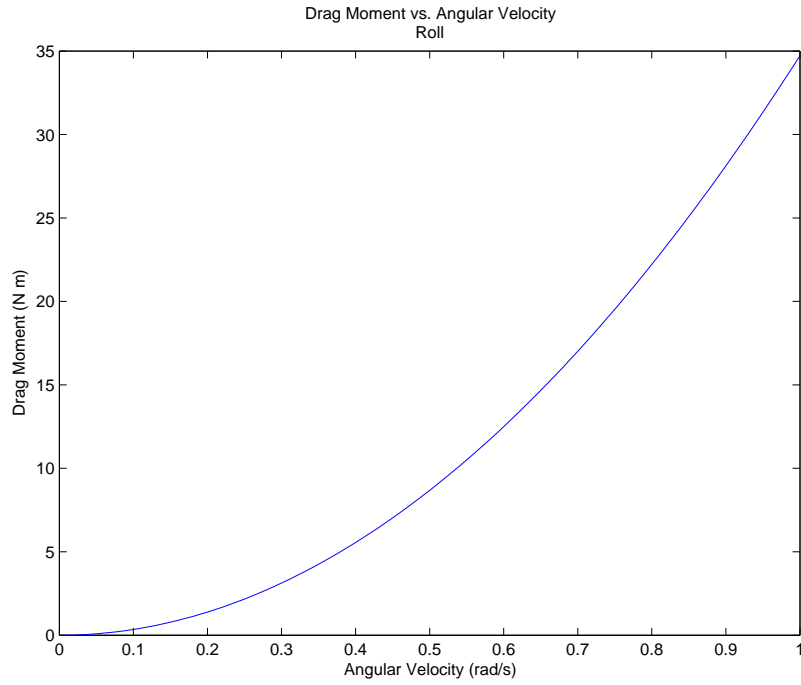


Figure 45: Drag moment versus velocity in the roll direction.

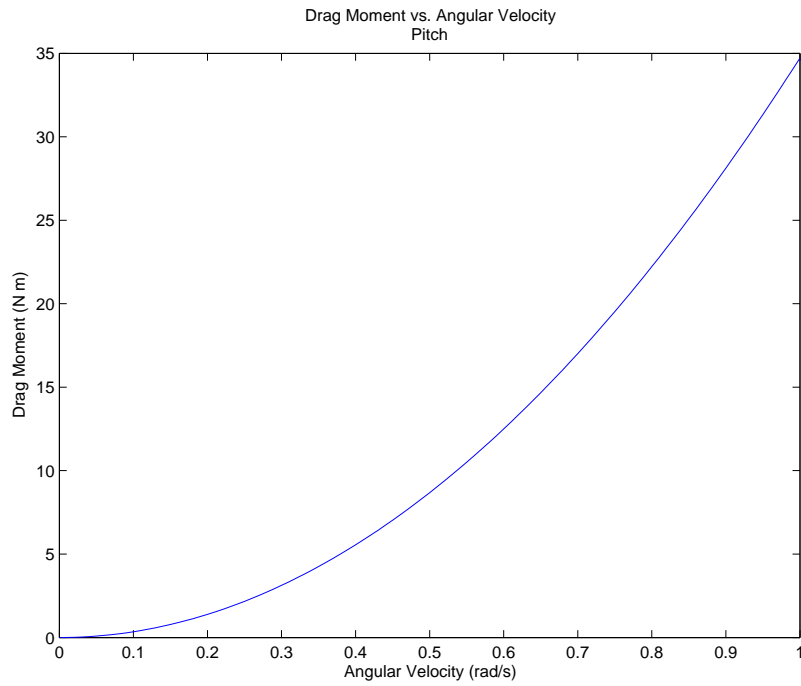


Figure 46: Drag moment versus velocity in the pitch direction.

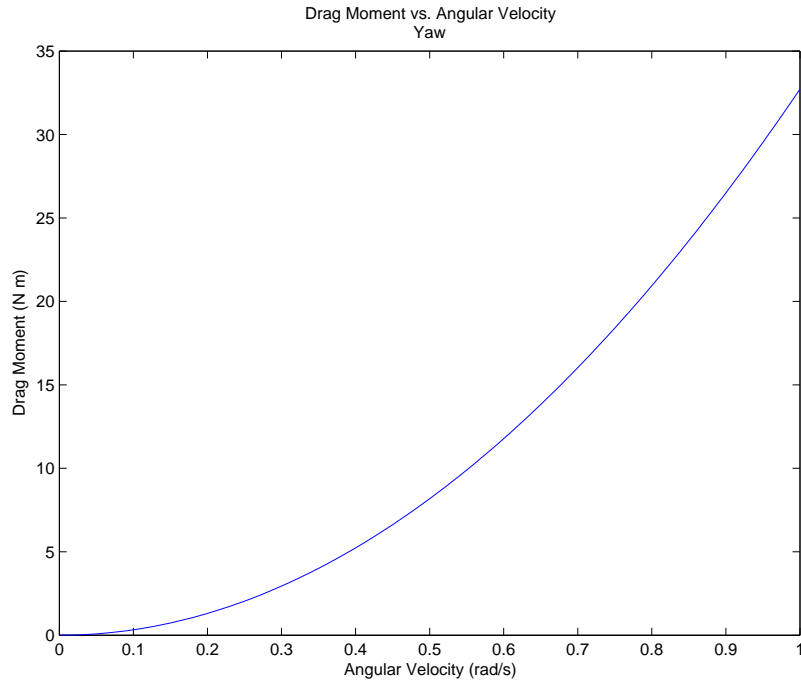


Figure 47: Drag moment versus velocity in the yaw direction.

B.2 Thruster Calibrations

For propulsion, ODIN uses eight Model 300 DC brushless thrusters manufactured by Tec-
 nadyne. A typical thruster of this type operates by use of ± 12 vdc instrumentation power.
 However, ODIN's on-board power supply is ± 24 vdc. Thus, the thrusters used on ODIN
 were modified by Tecnydyne to operate by use of a higher instrumentation power supply.
 This modification caused the thrusters to have a different output response from the general
 model produced by Tecnydyne. This discrepancy, the fact that no two thrusters are identical
 in their response and the nonlinearity of the response prompted us to develop our own rela-
 tionship between the input control voltage supplied and the output force provided by each

thruster. Implementing this relationship gives ODIN a more accurate means to appropriately balance the thruster forces over the duration of experiment.

To this end, we attached each thruster to a lever arm which was attached to a calibrated *SBO – 300* strain gauge from Transducer Technologies. The set-up can be seen in Fig. 48. The experiment consisted of inputting an evolving voltage to the thruster and measuring

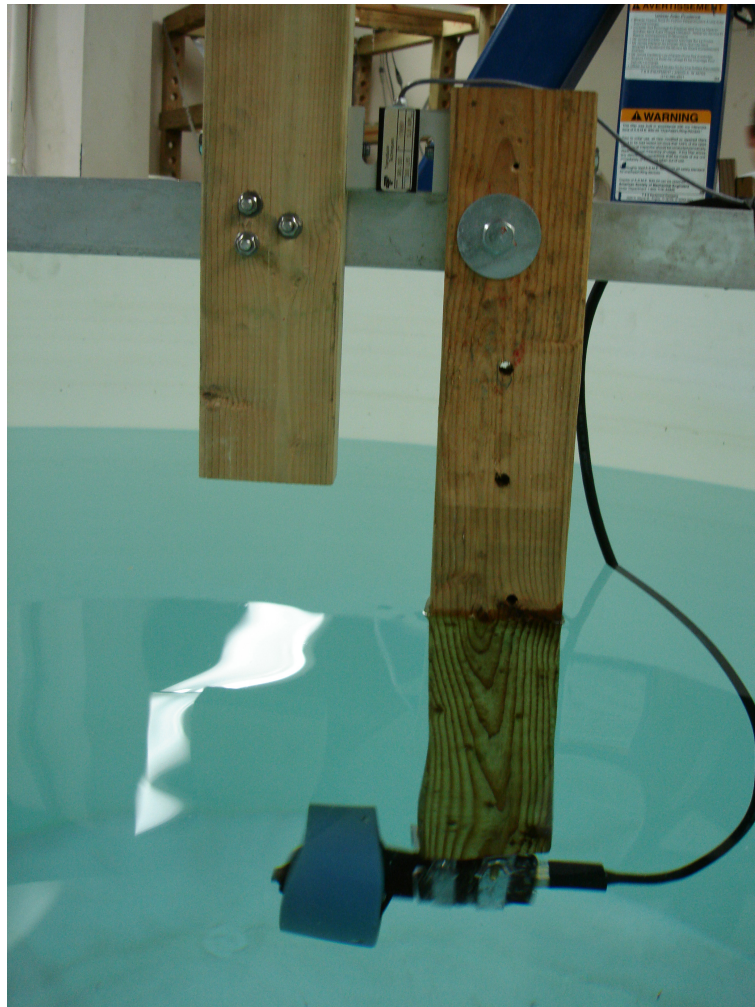


Figure 48: Lever and strain gauge set-up for thruster testing.

the obtained output thrust via the strain gauge. The input control voltage for the thrusters is $\pm 5\text{vdc}$. The thruster experiment was designed to ramp up the voltage from zero to five

volts over a period of 12 seconds, remain at five volts for four seconds, slowly decrease the voltage back to zero over a period of 36 seconds, remain at zero volts for four seconds, ramp the voltage down to negative five volts over a period of 12 seconds, remain at negative five volts for four seconds and then slowly return back to zero volts over a period of 36 seconds. There is also a 12 second period of zero voltage linking the ramping. This control function was generated and periodically repeated by use of an oscilloscope. An example of one of the 120 second experiments is displayed in Fig. 49. The experiment was implemented twice on each thruster in a manner such that the same thruster was not tested two times in a row. The input voltage is piecewise linear and has two different slopes (in absolute value),

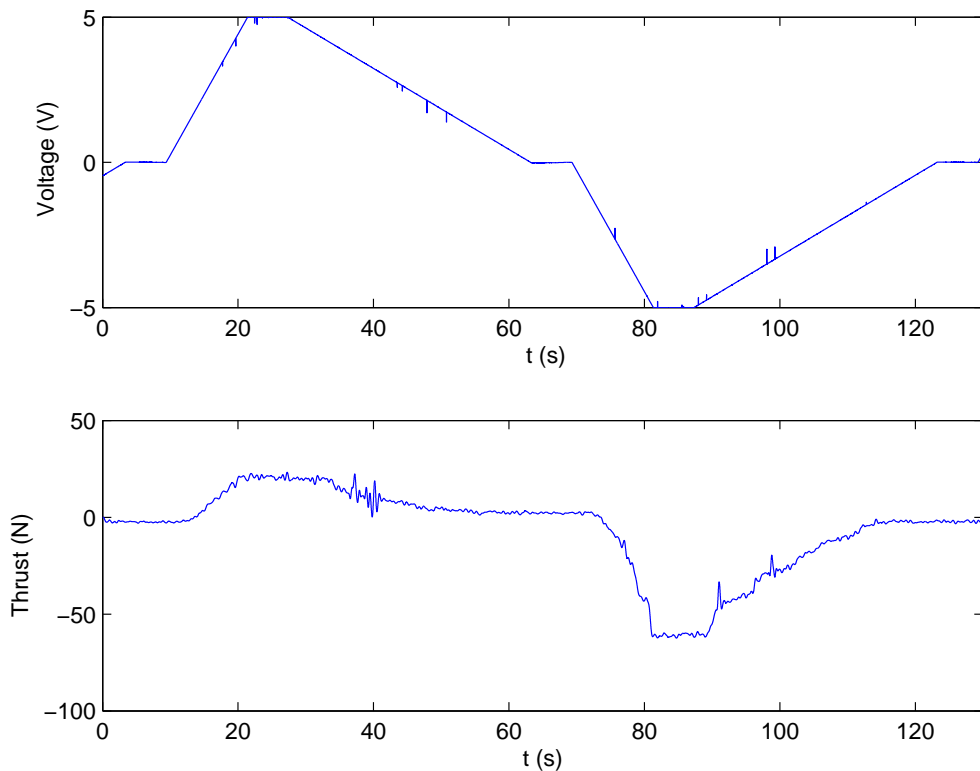


Figure 49: Example thruster testing experiment.

the steepest slope is $\pm \frac{5}{12} \approx 0.4167 \text{ V.s}^{-1}$ and the other slope is $\pm \frac{5}{36} \approx 0.1389 \text{ V.s}^{-1}$. Note that Fig. 49 only gives the general shape. The evolution of the input voltage is not identical for all experiments as it depends on when the experiment was started.

From the data collected during the thruster testing, we produced three relations between the input voltage and output thrust for each thruster depending upon the operational range of the control voltage supplied to the thrusters. For instance, we found that the output force was constant for input voltages greater than 4.7 volts, which is consistent with the specifications supplied by the manufacturer. Since we limit the input control voltage to $\pm 4\text{vdc}$ on ODIN, this artifact occurring at 4.7 volts is of no concern.

If we consider a voltage saturation for ODIN of ± 3 volts, we can produce a quadratic relation between the input voltage and output thrust as seen in Table 23. For the experi-

Thruster	Negative voltage	Positive voltage
γ_0 (1-1)a	$-3.46215V^2 - 2.63523V - 0.12753$	$1.09476V^2 - 0.15750V - 0.05080$
γ_0 (1-1)b	$-3.11660V^2 - 2.10045V - 0.06296$	$1.12414V^2 - 0.27956V - 0.03655$
γ_2 (2-1)a	$-2.88466V^2 - 2.70058V - 0.20480$	$0.95790V^2 + 0.00690V - 0.08197$
γ_2 (2-1)b	$-3.14098V^2 - 2.71371V - 0.11672$	$0.78653V^2 + 0.32292V - 0.11863$
γ_5 (3-2)a	$-3.26816V^2 - 1.24481V + 0.13550$	$1.50571V^2 - 1.25503V + 0.10270$
γ_5 (3-2)b	$-3.32461V^2 - 0.96436V + 0.19446$	$1.28571V^2 - 0.55066V - 0.02555$
γ_7 (4-2)a	$-3.64455V^2 - 3.73341V - 0.26599$	$1.11431V^2 - 0.55043V + 0.05459$
γ_7 (4-2)b	$-3.80241V^2 - 3.14260V - 0.18896$	$1.15922V^2 - 0.50911V + 0.00900$
γ_1 (1-2)a	$1.04202V^2 - 0.20031V - 0.10681$	$-3.00451V^2 + 2.84851V - 0.33671$
γ_1 (1-2)b	$1.06910V^2 + 0.16107V - 0.05069$	$-2.83625V^2 + 2.42950V - 0.20207$
γ_3 (2-2)a	$1.27374V^2 + 0.09759V - 0.06513$	$-4.09301V^2 + 4.67127V - 0.48047$
γ_3 (2-2)b	$1.49976V^2 + 0.99821V + 0.02330$	$-3.32802V^2 + 3.06366V - 0.35159$
γ_4 (3-1)a	$1.12854V^2 + 0.12025V - 0.11241$	$-3.15976V^2 + 1.73817V - 0.03584$
γ_4 (3-1)b	$1.12031V^2 + 0.47704V + 0.00688$	$-3.13741V^2 + 1.52644V + 0.08825$
γ_6 (4-1)a	$0.79355V^2 - 0.59009V - 0.12001$	$-2.63043V^2 + 2.36388V - 0.18109$
γ_6 (4-1)b	$1.16489V^2 + 0.50174V + 0.01482$	$-2.85908V^2 + 2.62864V - 0.17827$

Table 23: Quadratic Thrust/Voltage relationship for a control voltage range of $[-3, 3]$.

ments conducted in this study, we used a piece-wise linear relationship between the input voltage and output thrust. This relation has junctions at $\pm 0.5, \pm 1, \pm 2$ and ± 3 volts. The associated force values are given in Table 24. Here, the force is zero for a voltage between -0.5 and 0.5 volts, so we do not include these values in the table. Also, note that in Table 24 there are ten thrusters listed. ODIN operates with eight thrusters and has two spare in case of mechanical failure. Additionally, the position and rotation direction of each thruster is accounted for when computing the transformation from the six degree of freedom inputs to the eight dimensional applied control structure.

Thruster	-3V	-2V	-1V	1V	2V	3V
T_1	7.339249	2.416353	0.034123	-0.127279	-3.566529	-13.823253
T_2	-14.109838	-4.849457	-0.122768	0.232395	1.754468	5.795801
T_3	-18.557354	-5.718503	-0.063300	0.192645	1.659656	7.108828
T_4	6.007828	2.265985	0.807578	-0.815440	-3.725631	-13.341294
T_5	-13.149951	-5.249596	-0.240330	0.104070	1.685122	5.144876
T_6	5.481753	2.141444	0.269373	-0.195448	-4.007460	-11.327850
T_7	-10.783574	-4.041258	-0.291837	0.446474	1.439093	4.526483
T_8	7.339249	2.416353	0.034123	-0.127279	-3.566529	-13.823253
T_9	5.481753	2.141444	0.269373	-0.195448	-4.007460	-11.327850
T_{10}	-14.109838	-4.849457	-0.122768	0.232395	1.754468	5.795801

Table 24: Piece-wise linear Thrust/Voltage relationship for a control voltage range of $[-3, 3]$.

B.3 Water Sampling Data

The trajectory design method presented in this research is model-based, and thus depends on the characteristics of the fluid surrounding ODIN. In particular, fluctuations in water temperature and chlorine content affect the density of the water, which in turn affect the hydrodynamic coefficients used for ODIN. For example, ODIN’s buoyancy is given by

$B = \rho g \mathcal{V}$ where ρ is the fluid density, $g = 9.81 \text{ m/s}^2$ is the gravitational constant and \mathcal{V} is the submerged volume of ODIN. Since \mathcal{V} and g are constants, B is directly proportional to ρ . The purpose of this Appendix is to show that the water contained within the diving well at the Duke Kahanamoku Aquatic Complex can be assumed to remain at a constant temperature and density.

For each experiment conducted, we measured the water temperature and density. The chlorination of the pool is controlled, the chemical composition of the water remains constant¹⁰, and thus has no effect upon the density.

The temperature of the water was measured by use of a standard mercury thermometer which is accurate to $\pm 0.5^\circ\text{C}$. The density of the water was calculated by weighing a 10 mL water sample, measured by use of a volumetric flask, on a balance accurate to $\pm 0.001 \text{ g}$.

For the dates of the experiments included in Chapter 6, the water temperature was a constant 28° Centigrade and the water density was an average 997.018 kg m^3 . Due to the consistency in the temperature and density of the water sampled, we assume that $\rho = 997 \text{ kg m}^3$ in all of our experiments.

B.4 Thruster Protection Circuit

As an additional safeguard to avoid damage to the thrusters, we wired a capacitor and Metal Oxide Varistor (MOV) in parallel into the voltage output to the thruster. The capacitor is a $2200\mu\text{F}$ at 35V, the MOV has a $V_{max}(\text{DC})=31\text{V}$. These are needed since ODIN operates on

¹⁰This was analyzed and verified. Results are omitted as they are out of the scope of this research.

a 24V system, even though we are only allowing a ± 3 volt current to pass through to the thrusters. A circuit diagram is shown in Fig. 50.

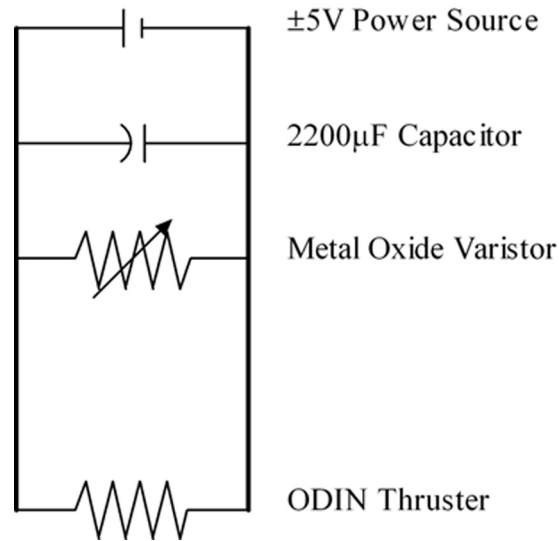


Figure 50: Circuit diagram for thruster protection.

The meaning for this circuit implementation is to prohibit high voltage from passing through to the thruster. This will act as a failsafe to protect the thruster. As current passes from the power output, it sees a capacitor, an MOV, and the thruster (which can be viewed as a simple resistor). Current always takes the path of least resistance. MOVs are widely used for voltage protection. The MOV is put in place to clamp transient voltages thus diverting a potentially high surge current from entering the main circuit which would burn the thruster. At low voltages, the MOV has a very high resistance, passing very little current. At high clamping voltages, the MOV has very low resistance, causing the voltage surge to travel into the MOV suppressing the applied voltage.

Appendix C

Proof of Theorem 5.2

Here we present the additional computations necessary to prove Theorem 5.2. We assume that we have an under-actuated control system for the submerged rigid body with input control vectors \mathcal{I}_m^{-1} for $m < 6$. We have already presented the computations for single and two-input systems in Sections 5.2.2 and 5.2.3, so we start the computations here with three-input systems.

C.1 Three Input Systems

Consider a three input system ($m = 3$) where the geometric acceleration is given by

$$\nabla_{\gamma'}\gamma' = \sum_{a=1}^3 \tilde{\mathbb{I}}_a^{-1}(\gamma(t))\sigma^a(t).$$

To simplify computations, we divide the three input systems into all translational inputs, all rotational inputs, and the two mixed input scenarios.

C.1.1 Three Translational Inputs

Consider a three input system in which all inputs are translational ($\mathcal{I}_3^{-1} = \{\mathbb{I}_1^{-1}, \mathbb{I}_2^{-1}, \mathbb{I}_3^{-1}\}$).

$$\nabla_{\gamma'}\gamma = \mathbb{I}_1^{-1}\sigma^1 + \mathbb{I}_2^{-1}\sigma^2 + \mathbb{I}_3^{-1}\sigma^3$$

We are interested in finding a vector field V such that $V \in \mathcal{I}_3^{-1}$ and $\nabla_V V \in \mathcal{I}_3^{-1}$. Thus, we are interested in calculating $\nabla_A B$ for $A, B \in \mathcal{I}_3^{-1}$. From Section 5.2.2, we know that

$$\mathbb{G}(\nabla_{\mathbb{I}_1^{-1}}\mathbb{I}_1^{-1}, X_i) = 0,$$

$$\mathbb{G}(\nabla_{\mathbb{I}_2^{-1}}\mathbb{I}_2^{-1}, X_i) = 0,$$

and

$$\mathbb{G}(\nabla_{\mathbb{I}_3^{-1}}\mathbb{I}_3^{-1}, X_i) = 0,$$

for $i = 1, \dots, 6$, which implies $\nabla_{\mathbb{I}_1^{-1}}\mathbb{I}_1^{-1} = \nabla_{\mathbb{I}_2^{-1}}\mathbb{I}_2^{-1} = \nabla_{\mathbb{I}_3^{-1}}\mathbb{I}_3^{-1} = 0$. From Section 5.2.3 we

know that

$$\nabla_{\mathbb{I}_1^{-1}}\mathbb{I}_2^{-1} = \nabla_{\mathbb{I}_2^{-1}}\mathbb{I}_1^{-1} = -\frac{1}{2j_3}(m_1 - m_2)X_6$$

From Section 5.3 we have that

$$\nabla_{\mathbb{I}_1^{-1}}\mathbb{I}_3^{-1} = \nabla_{\mathbb{I}_3^{-1}}\mathbb{I}_1^{-1} = -\frac{1}{2j_3}(m_1 - m_2)X_6,$$

and

$$\nabla_{\mathbb{I}_2^{-1}}\mathbb{I}_3^{-1} = \nabla_{\mathbb{I}_3^{-1}}\mathbb{I}_2^{-1} = -\frac{1}{2j_3}(m_1 - m_2)X_6.$$

Thus, by use of Eq. (5.5), we get

$$\begin{aligned} \nabla_V V \equiv & \frac{1}{2}(h_1 h_2 (\nabla_{\mathbb{I}_1^{-1}}\mathbb{I}_2^{-1} + \nabla_{\mathbb{I}_2^{-1}}\mathbb{I}_1^{-1}) + h_1 h_3 (\nabla_{\mathbb{I}_1^{-1}}\mathbb{I}_3^{-1} + \nabla_{\mathbb{I}_3^{-1}}\mathbb{I}_1^{-1}) \\ & + h_2 h_3 (\nabla_{\mathbb{I}_2^{-1}}\mathbb{I}_3^{-1} + \nabla_{\mathbb{I}_3^{-1}}\mathbb{I}_2^{-1})) \pmod{\mathcal{I}_3^{-1}} \end{aligned}$$

Substituting the results from above, for a given vector field $V \in \mathcal{I}_3^{-1}$,

$$\begin{aligned} \nabla_V V \equiv & \frac{1}{2}(h_1 h_2 (-\frac{1}{j_3}(m_1 - m_2)\mathbb{I}_6^{-1}) \\ & + h_1 h_3 (\frac{1}{j_2}(m_1 - m_3)\mathbb{I}_5^{-1}) + h_2 h_3 (-\frac{1}{j_1}(m_2 - m_3)\mathbb{I}_4^{-1})) \pmod{\mathcal{I}_3^{-1}} \end{aligned}$$

Note that in order for $\nabla_V V \in \mathcal{I}_3^{-1}$, two or three of h_1, h_2, h_3 must be zero. Thus, the only decoupling vector fields for system consisting of translational inputs are $V = h_a \mathbb{I}_a^{-1}$ for

$a \in \mathcal{U}$. This observation gives the following theorem.

Theorem C.1. *For a kinetically unique system with $\mathcal{I}_3^{-1} = \{\mathbb{I}_1^{-1}, \mathbb{I}_2^{-1}, \mathbb{I}_3^{-1}\}$, a vector field $V \in \mathcal{I}^{-1}$ is decoupling if and only if V has all but one of its components equal to zero. In particular, it has the form $V = h_a \mathbb{I}_a^{-1}$ for $a \in \mathcal{U}$, which are the pure translational motions.*

Proof. From Section C.1.1, we see that at least two of h_1, h_2, h_3 must be zero to satisfy the conditions in Eq. (5.5). This gives the result. \square

Remark C.1. Assuming exactly two of the m_i 's are equal, we get additional decoupling vector fields which are the axial motions $V = h_a \mathbb{I}_a^{-1} + h_b \mathbb{I}_b^{-1}$, where $m_a = m_b$ and $m_a \neq m_c$.

Remark C.2. If $m_a = m_b = m_c$, then every vector field $V \in \mathcal{I}_3^{-1}$ is decoupling since $\nabla_V V = 0$.

C.1.2 Three Rotational Inputs

Consider a three input system in which all inputs are rotational.

$$\nabla_{\gamma'} \gamma = \mathbb{I}_4^{-1} \sigma^4 + \mathbb{I}_5^{-1} \sigma^5 + \mathbb{I}_6^{-1} \sigma^6$$

Using the information from Table 4, we know that for a given vector field $V \in \mathcal{I}_3^{-1} = \{\mathbb{I}_4^{-1}, \mathbb{I}_5^{-1}, \mathbb{I}_6^{-1}\}$, and by use of Eq. (5.5), we get

$$\begin{aligned} \nabla_V V \equiv & \frac{1}{2} (h_4 h_5 (\nabla_{\mathbb{I}_4^{-1}} \mathbb{I}_5^{-1} + \nabla_{\mathbb{I}_5^{-1}} \mathbb{I}_4^{-1}) + h_4 h_6 (\nabla_{\mathbb{I}_4^{-1}} \mathbb{I}_6^{-1} + \nabla_{\mathbb{I}_6^{-1}} \mathbb{I}_4^{-1}) \\ & + h_5 h_6 (\nabla_{\mathbb{I}_5^{-1}} \mathbb{I}_6^{-1} + \nabla_{\mathbb{I}_6^{-1}} \mathbb{I}_5^{-1})) \pmod{\mathcal{I}_3^{-1}}, \end{aligned}$$

which then reduces to

$$\begin{aligned}\nabla_V V &\equiv \frac{1}{2}(h_4 h_5 (-\frac{1}{j_3}(j_1 - j_2)\mathbb{I}_6^{-1}) \\ &+ h_4 h_6 (\frac{1}{j_2}(j_1 - j_3)\mathbb{I}_5^{-1}) + h_5 h_6 (-\frac{1}{j_1}(j_2 - j_3)\mathbb{I}_4^{-1})) \pmod{\mathcal{I}_3^{-1}}.\end{aligned}$$

We see that $\nabla_V V \in \mathcal{I}^{-1}$ for all $V \in \mathcal{I}^{-1}$, thus each vector field $V \in \mathcal{I}^{-1}$ is decoupling.

C.1.3 Mixed Translational and Rotational Inputs

2 Translational, 1 Rotational

1,2,4

Here we consider a three input system where the inputs are

$$\nabla_{\gamma'} \gamma = \mathbb{I}_1^{-1} \sigma^1 + \mathbb{I}_2^{-1} \sigma^2 + \mathbb{I}_4^{-1} \sigma^4$$

From this we come up with the following for a given vector field \mathbf{V} ,

$$\nabla_V V = \frac{1}{2} \left(h_1 h_2 \left(\frac{1}{j_3} (m_2 - m_1) X_6 \right) + h_2 h_4 \left(\frac{m_2}{m_3} X_3 \right) \right)$$

Thus, either h_1 and h_4 are zero, or h_2 is zero. Thus, the decoupling vector fields are of the form $V = h_1 \mathbb{I}_1^{-1} + h_4 \mathbb{I}_4^{-1}$ or $V = h_2 \mathbb{I}_2^{-1}$.

1,2,5

Here we consider a three input system where the inputs are

$$\nabla_{\gamma'} \gamma = \mathbb{I}_1^{-1} \sigma^1 + \mathbb{I}_2^{-1} \sigma^2 + \mathbb{I}_5^{-1} \sigma^5$$

From this we come up with the following for a given vector field \mathbf{V} ,

$$\nabla_V V = \frac{1}{2} \left(h_1 h_2 \left(\frac{1}{j_3} (m_2 - m_1) X_6 \right) + h_1 h_5 \left(-\frac{m_1}{m_3} X_3 \right) \right)$$

Thus, either h_1 is zero, and the decoupling vector fields are of the form $V = h_2\mathbb{I}_2^{-1} + h_5\mathbb{I}_5^{-1}$ or $h_2 = h_5 = 0$ and the decoupling vector fields are $V = h_1\mathbb{I}_1^{-1}$.

1,2,6

Here we consider a three input system where the inputs are

$$\nabla_{\gamma'}\gamma = \mathbb{I}_1^{-1}\sigma^1 + \mathbb{I}_2^{-1}\sigma^2 + \mathbb{I}_6^{-1}\sigma^6$$

From this we come up with the following for a given vector field V ,

$$\nabla_V V = \frac{1}{2} \left(h_1 h_2 \left(\frac{1}{j_3} (m_1 - m_2) X_6 \right) + h_1 h_6 \left(\frac{m_1}{m_2} \right) X_2 + h_2 h_6 \left(-\frac{m_2}{m_1} \right) X_1 \right)$$

Thus, since $\nabla_V V \in \mathcal{I}^{-1}$ for all V , every vector field $V \in \mathcal{I}^{-1}$ is decoupling.

2,3,4

Here we consider a three input system where the inputs are

$$\nabla_{\gamma'}\gamma = \mathbb{I}_2^{-1}\sigma^2 + \mathbb{I}_3^{-1}\sigma^3 + \mathbb{I}_4^{-1}\sigma^4$$

From this we come up with the following for a given vector field V ,

$$\nabla_V V = \frac{1}{2} \left(h_2 h_3 \left(\frac{1}{j_1} (m_3 - m_2) X_4 \right) + h_2 h_4 \left(\frac{m_2}{m_3} \right) X_3 + h_3 h_4 \left(-\frac{m_3}{m_2} \right) X_2 \right)$$

Thus, since $\nabla_V V \in \mathcal{I}^{-1}$ for all V , every vector field $V \in \mathcal{I}^{-1}$ is decoupling.

2,3,5

Here we consider a three input system where the inputs are

$$\nabla_{\gamma'}\gamma = \mathbb{I}_2^{-1}\sigma^2 + \mathbb{I}_3^{-1}\sigma^3 + \mathbb{I}_5^{-1}\sigma^5$$

From this we come up with the following for a given vector field V ,

$$\nabla_V V = \frac{1}{2} \left(h_2 h_3 \left(\frac{1}{j_1} (m_3 - m_2) X_4 \right) + h_3 h_5 \left(\frac{m_3}{m_1} \right) X_1 \right)$$

Thus, either h_3 is zero, and the decoupling vector fields are of the form $V = h_2 \mathbb{I}_2^{-1} + h_5 \mathbb{I}_5^{-1}$ or $h_2 = h_5 = 0$ and the decoupling vector fields are $V = h_3 \mathbb{I}_3^{-1}$.

2,3,6

Here we consider a three input system where the inputs are

$$\nabla_{\gamma'} \gamma = \mathbb{I}_2^{-1} \sigma^2 + \mathbb{I}_3^{-1} \sigma^3 + \mathbb{I}_6^{-1} \sigma^6$$

From this we come up with the following for a given vector field V ,

$$\nabla_V V = \frac{1}{2} \left(h_2 h_3 \left(\frac{1}{j_1} (m_3 - m_2) X_4 \right) + h_2 h_6 \left(-\frac{m_2}{m_1} \right) X_1 \right)$$

Thus, either h_2 is zero, and the decoupling vector fields are of the form $V = h_3 \mathbb{I}_3^{-1} + h_6 \mathbb{I}_6^{-1}$ or $h_3 = h_6 = 0$ and the decoupling vector fields are $V = h_2 \mathbb{I}_2^{-1}$.

1,3,4

Here we consider a three input system where the inputs are

$$\nabla_{\gamma'} \gamma = \mathbb{I}_1^{-1} \sigma^1 + \mathbb{I}_3^{-1} \sigma^3 + \mathbb{I}_4^{-1} \sigma^4$$

From this we come up with the following for a given vector field V ,

$$\nabla_V V = \frac{1}{2} \left(h_1 h_3 \left(-\frac{1}{j_2} (m_3 - m_2) X_5 \right) + h_3 h_4 \left(-\frac{m_3}{m_2} \right) X_2 \right)$$

Thus, either h_3 is zero, and the decoupling vector fields are of the form $V = h_1 \mathbb{I}_1^{-1} + h_4 \mathbb{I}_4^{-1}$ or $h_1 = h_4 = 0$ and the decoupling vector fields are $V = h_3 \mathbb{I}_3^{-1}$.

1,3,5

Here we consider a three input system where the inputs are

$$\nabla_{\gamma'}\gamma = \mathbb{I}_1^{-1}\sigma^1 + \mathbb{I}_3^{-1}\sigma^3 + \mathbb{I}_5^{-1}\sigma^5$$

From this we come up with the following for a given vector field \mathbf{V} ,

$$\nabla_V V \frac{1}{2} \left(h_1 h_3 \left(-\frac{1}{j_2} (m_3 - m_2) X_5 \right) + h_3 h_5 \left(\frac{m_3}{m_1} \right) X_1 + h_1 h_5 \left(-\frac{m_1}{m_3} \right) X_3 \right)$$

Thus, since $\nabla_V V \in \mathcal{I}^{-1}$ for all \mathbf{V} , every vector field $V \in \mathcal{I}^{-1}$ is decoupling.

1,3,6

Here we consider a three input system where the inputs are

$$\nabla_{\gamma'}\gamma = \mathbb{I}_1^{-1}\sigma^1 + \mathbb{I}_3^{-1}\sigma^3 + \mathbb{I}_6^{-1}\sigma^6$$

From this we come up with the following for a given vector field \mathbf{V} ,

$$\nabla_V V = \frac{1}{2} \left(h_1 h_3 \left(-\frac{1}{j_2} (m_3 - m_2) X_5 \right) + h_1 h_6 \left(\frac{m_1}{m_2} \right) X_2 \right)$$

Thus, either h_1 is zero, and the decoupling vector fields are of the form $V = h_3 \mathbb{I}_3^{-1} + h_6 \mathbb{I}_6^{-1}$
or $h_3 = h_6 = 0$ and the decoupling vector fields are $V = h_1 \mathbb{I}_1^{-1}$.

2 Rotational, 1 Translational

1,4,5

Here we consider a three input system where the inputs are

$$\nabla_{\gamma'}\gamma = \mathbb{I}_1^{-1}\sigma^1 + \mathbb{I}_4^{-1}\sigma^4 + \mathbb{I}_5^{-1}\sigma^5$$

From this we come up with the following for a given vector field \mathbf{V} ,

$$\nabla_V V = \frac{1}{2} \left(h_1 h_5 \left(-\frac{m_1}{m_3} \right) X_3 + h_4 h_5 \left(\frac{1}{j_3} (j_2 - j_1) \right) X_6 \right)$$

Thus, either h_5 is zero, and the decoupling vector fields are of the form $V = h_1 \mathbb{I}_1^{-1} + h_4 \mathbb{I}_4^{-1}$ or $h_1 = h_4 = 0$ and the decoupling vector fields are $V = h_5 \mathbb{I}_5^{-1}$.

1,4,6

Here we consider a three input system where the inputs are

$$\nabla_{\gamma'} \gamma = \mathbb{I}_1^{-1} \sigma^1 + \mathbb{I}_4^{-1} \sigma^4 + \mathbb{I}_6^{-1} \sigma^6$$

From this we come up with the following for a given vector field V ,

$$\nabla_V V = \frac{1}{2} \left(h_1 h_6 \left(\frac{m_1}{m_2} \right) X_2 + h_4 h_6 \left(\frac{1}{j_2} (j_1 - j_3) \right) X_5 \right)$$

Thus, either h_6 is zero, and the decoupling vector fields are of the form $V = h_1 \mathbb{I}_1^{-1} + h_4 \mathbb{I}_4^{-1}$ or $h_1 = h_4 = 0$ and the decoupling vector fields are $V = h_6 \mathbb{I}_6^{-1}$.

1,5,6

Here we consider a three input system where the inputs are

$$\nabla_{\gamma'} \gamma = \mathbb{I}_1^{-1} \sigma^1 + \mathbb{I}_5^{-1} \sigma^5 + \mathbb{I}_6^{-1} \sigma^6$$

From this we come up with the following for a given vector field V ,

$$\nabla_V V = \frac{1}{2} \left(h_1 h_5 \left(-\frac{m_1}{m_3} \right) X_3 + h_1 h_6 \left(\frac{m_1}{m_2} \right) X_2 + h_5 h_6 \left(\frac{1}{j_1} (j_3 - j_2) \right) X_4 \right)$$

In this scenario, two of $\{h_1, h_5, h_6\}$ must be zero. Thus, the decoupling vector fields are just the pure vector fields $V = h_a \mathbb{I}_a^{-1}$ for $a \in \{1, 5, 6\}$.

2,4,5

Here we consider a three input system where the inputs are

$$\nabla_{\gamma'}\gamma = \mathbb{I}_2^{-1}\sigma^2 + \mathbb{I}_4^{-1}\sigma^4 + \mathbb{I}_5^{-1}\sigma^5$$

From this we come up with the following for a given vector field V ,

$$\nabla_V V = \frac{1}{2} \left(h_2 h_4 \left(\frac{m_2}{m_3} \right) X_3 + h_4 h_5 \left(\frac{1}{j_3} (j_2 - j_1) \right) X_6 \right)$$

Thus, either h_4 is zero, and the decoupling vector fields are of the form $V = h_2 \mathbb{I}_2^{-1} + h_5 \mathbb{I}_5^{-1}$

or $h_2 = h_5 = 0$ and the decoupling vector fields are $V = h_4 \mathbb{I}_4^{-1}$.

2,4,6

Here we consider a three input system where the inputs are

$$\nabla_{\gamma'}\gamma = \mathbb{I}_2^{-1}\sigma^2 + \mathbb{I}_4^{-1}\sigma^4 + \mathbb{I}_6^{-1}\sigma^6$$

From this we come up with the following for a given vector field V ,

$$\nabla_V V = \frac{1}{2} \left(h_2 h_4 \left(\frac{m_2}{m_3} \right) X_3 + h_2 h_6 \left(-\frac{m_2}{m_1} \right) X_1 + h_4 h_6 \left(\frac{1}{j_2} (j_1 - j_3) \right) X_5 \right)$$

In this scenario, two of $\{h_2, h_4, h_6\}$ must be zero. Thus, the decoupling vector fields are just the pure vector fields $V = h_a \mathbb{I}_a^{-1}$ for $a \in \{2, 4, 6\}$.

2,5,6

Here we consider a three input system where the inputs are

$$\nabla_{\gamma'}\gamma = \mathbb{I}_1^{-1}\sigma^1 + \mathbb{I}_4^{-1}\sigma^4 + \mathbb{I}_6^{-1}\sigma^6$$

From this we come up with the following for a given vector field V ,

$$\nabla_V V = \frac{1}{2} \left(h_2 h_6 \left(-\frac{m_2}{m_1} \right) X_1 + h_5 h_6 \left(\frac{1}{j_1} (j_3 - j_2) \right) X_4 \right)$$

Thus, either h_6 is zero, and the decoupling vector fields are of the form $V = h_2 \mathbb{I}_2^{-1} + h_5 \mathbb{I}_5^{-1}$ or $h_2 = h_5 = 0$ and the decoupling vector fields are $V = h_6 \mathbb{I}_6^{-1}$.

3,4,5

Here we consider a three input system where the inputs are

$$\nabla_{\gamma'} \gamma = \mathbb{I}_3^{-1} \sigma^3 + \mathbb{I}_4^{-1} \sigma^4 + \mathbb{I}_5^{-1} \sigma^5$$

From this we come up with the following for a given vector field V ,

$$\nabla_V V = \frac{1}{2} \left(h_3 h_4 \left(-\frac{m_3}{m_2} \right) X_2 + h_3 h_5 \left(\frac{m_3}{m_1} \right) X_1 + h_4 h_5 \left(\frac{1}{j_3} (j_2 - j_1) \right) X_6 \right)$$

In this scenario, two of $\{h_3, h_4, h_5\}$ must be zero. Thus, the decoupling vector fields are just the pure vector fields $V = h_a \mathbb{I}_a^{-1}$ for $a \in \{3, 4, 5\}$.

3,4,6

Here we consider a three input system where the inputs are

$$\nabla_{\gamma'} \gamma = \mathbb{I}_3^{-1} \sigma^3 + \mathbb{I}_4^{-1} \sigma^4 + \mathbb{I}_6^{-1} \sigma^6$$

From this we come up with the following for a given vector field V ,

$$\nabla_V V = \frac{1}{2} \left(h_3 h_4 \left(-\frac{m_3}{m_2} \right) X_2 + h_4 h_6 \left(\frac{1}{j_2} (j_1 - j_3) \right) X_5 \right)$$

Thus, either h_4 is zero, and the decoupling vector fields are of the form $V = h_3 \mathbb{I}_3^{-1} + h_6 \mathbb{I}_6^{-1}$ or $h_3 = h_6 = 0$ and the decoupling vector fields are $V = h_4 \mathbb{I}_4^{-1}$.

3,5,6

Here we consider a three input system where the inputs are

$$\nabla_{\gamma'}\gamma = \mathbb{I}_1^{-1}\sigma^1 + \mathbb{I}_4^{-1}\sigma^4 + \mathbb{I}_6^{-1}\sigma^6$$

From this we come up with the following for a given vector field V ,

$$\nabla_V V = \frac{1}{2} \left(h_3 h_5 \left(\frac{m_3}{m_1} \right) X_1 + h_5 h_6 \left(\frac{1}{j_1} (j_3 - j_2) \right) X_4 \right)$$

Thus, either h_5 is zero, and the decoupling vector fields are of the form $V = h_3 \mathbb{I}_3^{-1} + h_6 \mathbb{I}_6^{-1}$ or $h_3 = h_6 = 0$ and the decoupling vector fields are $V = h_5 \mathbb{I}_5^{-1}$.

The above calculations lead us to the following theorems on three-input systems.

Theorem C.2. *Suppose we have a kinetically unique three input system which is a coordinate field such that there are two translational inputs and one rotational input. Then, every a vector field $V \in \mathcal{I}^{-1}$ is decoupling.*

Proof. See above calculations. □

Theorem C.3. *Suppose we have a kinetically unique three input system which is a coordinate field such that there are two rotational inputs and one translational input. Then, the decoupling vector fields are the pure motions.*

Theorem C.4. *Suppose we have a kinetically unique three input system which is an axial field plus another input vector field but the system is not a coordinate field; ($\mathcal{I}_3^{-1} = \{\mathbb{I}_a^{-1}, \mathbb{I}_{a+3}^{-1}, \mathbb{I}_b^{-1}\}$ where $a \in \mathcal{U}$ and $b \neq a$ or $a + 3$). The decoupling vector fields are the axial motions, $V = h_c \mathbb{I}_c^{-1} + h_{c+3} \mathbb{I}_{c+3}^{-1}$ for $c \in \mathcal{U}$ and c acting on the principal axis not acted upon by a or b .*

Theorems C.2 and C.3 characterize decoupling vector fields for the mixed three input system. More decoupling vector fields exist if the kinetically unique assumption is relaxed.

C.2 Four Input Systems

Consider a four input system ($m = 4$) where the geometric acceleration is given by

$$\nabla_{\gamma'}\gamma' = \sum_{a=1}^4 \tilde{\mathbb{I}}_a^{-1}(\gamma(t))\sigma^a(t).$$

In this section we omit calculations since they are similar to those seen earlier.

C.2.1 Three Translation, One Rotation

1,2,3,4

Here we consider a four input system where the inputs are

$$\nabla_{\gamma'}\gamma' = \mathbb{I}_1^{-1}\sigma^1 + \mathbb{I}_2^{-1}\sigma^2 + \mathbb{I}_3^{-1}\sigma^3 + \mathbb{I}_4^{-1}\sigma^4$$

From this we come up with the following for a given vector field V ,

$$\begin{aligned} \nabla_V V &\equiv \frac{1}{2}(h_1 h_2 \left(\frac{1}{j_3}(m_2 - m_1)X_6 + h_1 h_3 \left(-\frac{1}{j_2}(m_3 - m_2)X_5\right.\right. \\ &\quad \left.\left.+ h_2 h_3 \left(\frac{1}{j_1}(m_3 - m_2)X_4 + h_3 h_4 \left(-\frac{m_3}{m_2}X_2\right)\right)\right) \pmod{\mathcal{I}_4^{-1}} \\ &\equiv \frac{1}{2}(h_1 h_2 \left(\frac{1}{j_3}(m_2 - m_1)X_6 + h_1 h_3 \left(-\frac{1}{j_2}(m_3 - m_2)X_5\right)\right) \pmod{\mathcal{I}_4^{-1}} \end{aligned}$$

Thus, either h_1 is zero, and the decoupling vector fields are of the form $V = h_2\mathbb{I}_2^{-1} + h_3\mathbb{I}_3^{-1} + h_4\mathbb{I}_4^{-1}$ or $h_2 = h_3 = 0$ and the decoupling vector fields are $V = h_1\mathbb{I}_1^{-1} + h_4\mathbb{I}_4^{-1}$.

1,2,3,5

Here we consider a four input system where the inputs are

$$\nabla_{\gamma'}\gamma = \mathbb{I}_1^{-1}\sigma^1 + \mathbb{I}_2^{-1}\sigma^2 + \mathbb{I}_3^{-1}\sigma^3 + \mathbb{I}_5^{-1}\sigma^5$$

From this we come up with the following for a given vector field V ,

$$\begin{aligned}\nabla_V V &\equiv \frac{1}{2}(h_1 h_2 \left(\frac{1}{j_3}(m_2 - m_1)X_6 + h_1 h_3 \left(-\frac{1}{j_2}(m_3 - m_2)X_5\right.\right. \\ &\quad \left.\left.+ h_2 h_3 \left(\frac{1}{j_1}(m_3 - m_2)X_4 + h_1 h_5 \left(-\frac{m_1}{m_3}X_3 + h_3 h_5 \left(\frac{m_3}{m_1}X_1\right)\right)\right)\right) \pmod{\mathcal{I}_4^{-1}} \\ &\equiv \frac{1}{2}(h_1 h_2 \left(\frac{1}{j_3}(m_2 - m_1)X_6 + h_2 h_3 \left(\frac{1}{j_1}(m_3 - m_2)X_4\right)\right) \pmod{\mathcal{I}_4^{-1}}\end{aligned}$$

Thus, either h_2 is zero, and the decoupling vector fields are of the form $V = h_1 \mathbb{I}_1^{-1} + h_3 \mathbb{I}_3^{-1} + h_5 \mathbb{I}_5^{-1}$ or $h_1 = h_3 = 0$ and the decoupling vector fields are $V = h_2 \mathbb{I}_2^{-1} + h_5 \mathbb{I}_5^{-1}$.

1,2,3,6

Here we consider a four input system where the inputs are

$$\nabla_{\gamma'}\gamma = \mathbb{I}_1^{-1}\sigma^1 + \mathbb{I}_2^{-1}\sigma^2 + \mathbb{I}_3^{-1}\sigma^3 + \mathbb{I}_6^{-1}\sigma^6$$

From this we come up with the following for a given vector field V ,

$$\begin{aligned}\nabla_V V &\equiv \frac{1}{2}(h_1 h_2 \left(\frac{1}{j_3}(m_2 - m_1)X_6 + h_1 h_3 \left(-\frac{1}{j_2}(m_3 - m_2)X_5\right.\right. \\ &\quad \left.\left.+ h_2 h_3 \left(\frac{1}{j_1}(m_3 - m_2)X_4 + h_1 h_6 \left(\frac{m_1}{m_2}X_2\right)\right)\right) \pmod{\mathcal{I}_4^{-1}} \\ &\equiv \frac{1}{2}(h_1 h_3 \left(-\frac{1}{j_2}(m_3 - m_2)X_5 + h_2 h_3 \left(\frac{1}{j_1}(m_3 - m_2)X_4\right)\right) \pmod{\mathcal{I}_4^{-1}}\end{aligned}$$

Thus, either h_3 is zero, and the decoupling vector fields are of the form $V = h_1 \mathbb{I}_1^{-1} + h_2 \mathbb{I}_2^{-1} + h_6 \mathbb{I}_6^{-1}$ or $h_1 = h_2 = 0$ and the decoupling vector fields are $V = h_3 \mathbb{I}_3^{-1} + h_6 \mathbb{I}_6^{-1}$.

The above calculations lead to the following theorem.

Theorem C.5. *Suppose that we have a kinetically unique four input system with input vectors $\mathcal{I}_4^{-1} = \{\mathbb{I}_1^{-1}, \mathbb{I}_2^{-1}, \mathbb{I}_3^{-1}, Y_d\}$ where $d \in \mathcal{V}$. Then the decoupling vector fields for the corresponding affine connection control system are the axial fields $V = h_{d-3}Y_{d-3} + h_d Y_d$ or coordinate fields $V = h_a \mathbb{I}_a^{-1} + h_b \mathbb{I}_b^{-1} + h_d Y_d$.*

C.2.2 Three Rotation, One Translation

We continue on by considering the systems with three rotational inputs and one translational input.

1,4,5,6

Here we consider a four input system where the inputs are

$$\nabla_{\gamma'} \gamma = \mathbb{I}_1^{-1} \sigma^1 + \mathbb{I}_4^{-1} \sigma^4 + \mathbb{I}_5^{-1} \sigma^5 + \mathbb{I}_6^{-1} \sigma^6$$

From this we come up with the following for a given vector field V ,

$$\begin{aligned} \nabla_V V &\equiv \frac{1}{2} \left(h_1 h_5 \left(-\frac{m_1}{m_3} \right) X_3 + h_1 h_6 \left(\frac{m_1}{m_2} \right) X_2 + h_4 h_5 \left(\frac{1}{j_3} (j_2 - j_1) \right) X_6 \right. \\ &\quad \left. + h_4 h_6 \left(\frac{1}{j_2} (j_1 - j_3) \right) X_5 + h_5 h_6 \left(\frac{1}{j_1} (j_3 - j_2) \right) X_4 \right) \pmod{\mathcal{I}_4^{-1}} \\ &\equiv \frac{1}{2} \left(h_1 h_5 \left(-\frac{m_1}{m_3} \right) X_3 + h_1 h_6 \left(\frac{m_1}{m_2} \right) X_2 \right) \pmod{\mathcal{I}_4^{-1}} \end{aligned}$$

Thus, either h_1 is zero, and the decoupling vector fields are of the form $V = h_4 \mathbb{I}_4^{-1} + h_5 \mathbb{I}_5^{-1} + h_6 \mathbb{I}_6^{-1}$ or $h_5 = h_6 = 0$ and the decoupling vector fields are $V = h_1 \mathbb{I}_1^{-1} + h_4 \mathbb{I}_4^{-1}$.

2,4,5,6

Here we consider a four input system where the inputs are

$$\nabla_{\gamma'}\gamma = \mathbb{I}_2^{-1}\sigma^2 + \mathbb{I}_4^{-1}\sigma^4 + \mathbb{I}_5^{-1}\sigma^5 + \mathbb{I}_6^{-1}\sigma^6$$

From this we come up with the following for a given vector field V ,

$$\begin{aligned}\nabla_V V &\equiv \frac{1}{2}(h_2 h_4 \left(\frac{m_2}{m_3}\right) X_3 + h_2 h_6 \left(-\frac{m_2}{m_1}\right) X_1 + h_4 h_5 \left(\frac{1}{j_3}(j_2 - j_1)\right) X_6 \\ &\quad + h_4 h_6 \left(\frac{1}{j_2}(j_1 - j_3)\right) X_5 + h_5 h_6 \left(\frac{1}{j_1}(j_3 - j_2)\right) X_4) \pmod{\mathcal{I}_4^{-1}} \\ &\equiv \frac{1}{2}(h_2 h_4 \left(\frac{m_2}{m_3}\right) X_3 + h_2 h_6 \left(-\frac{m_2}{m_1}\right) X_1) \pmod{\mathcal{I}_4^{-1}}\end{aligned}$$

Thus, either h_2 is zero, and the decoupling vector fields are of the form $V = h_4 \mathbb{I}_4^{-1} + h_5 \mathbb{I}_5^{-1} + h_6 \mathbb{I}_6^{-1}$ or $h_4 = h_6 = 0$ and the decoupling vector fields are $V = h_2 \mathbb{I}_2^{-1} + h_5 \mathbb{I}_5^{-1}$.

3,4,5,6

Here we consider a four input system where the inputs are

$$\nabla_{\gamma'}\gamma = \mathbb{I}_3^{-1}\sigma^3 + \mathbb{I}_4^{-1}\sigma^4 + \mathbb{I}_5^{-1}\sigma^5 + \mathbb{I}_6^{-1}\sigma^6$$

From this we come up with the following for a given vector field V ,

$$\begin{aligned}\nabla_V V &\equiv \frac{1}{2}(h_3 h_4 \left(-\frac{m_3}{m_2}\right) X_2 + h_3 h_5 \left(\frac{m_3}{m_1}\right) X_1 + h_4 h_5 \left(\frac{1}{j_3}(j_2 - j_1)\right) X_6 \\ &\quad + h_4 h_6 \left(\frac{1}{j_2}(j_1 - j_3)\right) X_5 + h_5 h_6 \left(\frac{1}{j_1}(j_3 - j_2)\right) X_4) \pmod{\mathcal{I}_4^{-1}} \\ &\equiv \frac{1}{2}(h_3 h_4 \left(-\frac{m_3}{m_2}\right) X_2 + h_3 h_5 \left(\frac{m_3}{m_1}\right) X_1) \pmod{\mathcal{I}_4^{-1}}\end{aligned}$$

Thus, either h_3 is zero, and the decoupling vector fields are of the form $V = h_4 \mathbb{I}_4^{-1} + h_5 \mathbb{I}_5^{-1} + h_6 \mathbb{I}_6^{-1}$ or $h_4 = h_5 = 0$ and the decoupling vector fields are $V = h_3 \mathbb{I}_3^{-1} + h_6 \mathbb{I}_6^{-1}$.

Theorem C.6. *Suppose that we have a kinetically unique four input system with input vectors $\mathcal{I}_4^{-1} = \{\mathbb{I}_4^{-1}, \mathbb{I}_5^{-1}, \mathbb{I}_6^{-1}, \mathbb{I}_a^{-1}\}$ where $a \in \mathcal{U}$. Then the decoupling vector fields for the corresponding affine connection control system are the axial fields $V = h_a \mathbb{I}_a^{-1} + h_{a+3} \mathbb{I}_{a+3}^{-1}$ or coordinate fields $V = h_4 \mathbb{I}_4^{-1} + h_5 \mathbb{I}_5^{-1} + h_6 \mathbb{I}_6^{-1}$.*

C.2.3 Two Translation, Two Rotation

Now we consider the system of two translational and two rotational inputs. We divide this section into two parts.

Two principal axes repeated

1,2,4,5

Here we consider a four input system where the inputs are

$$\nabla_{\gamma'} \gamma = \mathbb{I}_1^{-1} \sigma^1 + \mathbb{I}_2^{-1} \sigma^2 + \mathbb{I}_4^{-1} \sigma^4 + \mathbb{I}_5^{-1} \sigma^5$$

From this we come up with the following for a given vector field V ,

$$\begin{aligned} \nabla_V V \equiv & \frac{1}{2} (h_1 h_2 \left(\frac{1}{j_3} (m_2 - m_1) X_6 + h_1 h_5 \left(-\frac{m_1}{m_3} \right) X_3 \right. \\ & \left. + h_4 h_5 \left(\frac{1}{j_3} (j_2 - j_1) X_6 + h_2 h_4 \left(\frac{m_2}{m_3} \right) X_3 \right) \right) \pmod{\mathcal{I}_4^{-1}} \end{aligned}$$

1,3,4,6

Here we consider a four input system where the inputs are

$$\nabla_{\gamma'} \gamma = \mathbb{I}_1^{-1} \sigma^1 + \mathbb{I}_3^{-1} \sigma^3 + \mathbb{I}_4^{-1} \sigma^4 + \mathbb{I}_6^{-1} \sigma^6$$

From this we come up with the following for a given vector field V ,

$$\begin{aligned}\nabla_V V &\equiv \frac{1}{2}(h_1 h_3(-\frac{1}{j_2}(m_3 - m_2)X_5 + h_1 h_6(\frac{m_1}{m_2})X_2 \\ &\quad + h_4 h_6(\frac{1}{j_2}(j_1 - j_3)X_5 + h_3 h_4(-\frac{m_3}{m_2})X_2) \pmod{\mathcal{I}_4^{-1}}\end{aligned}$$

2,3,5,6

Here we consider a four input system where the inputs are

$$\nabla_{\gamma'} \gamma = \mathbb{I}_2^{-1} \sigma^2 + \mathbb{I}_3^{-1} \sigma^3 + \mathbb{I}_5^{-1} \sigma^5 + \mathbb{I}_6^{-1} \sigma^6$$

From this we come up with the following for a given vector field V ,

$$\begin{aligned}\nabla_V V &\equiv \frac{1}{2}(h_2 h_3(\frac{1}{j_1}(m_3 - m_2)X_4 + h_2 h_6(-\frac{m_2}{m_1})X_1 \\ &\quad + h_3 h_5(\frac{m_3}{m_1})X_1 + h_5 h_6(\frac{1}{j_1}(j_3 - j_2)X_4) \pmod{\mathcal{I}_4^{-1}}\end{aligned}$$

From the above calculations, and given $a, b, c \in \mathcal{U}$ and that the input vector fields are $\mathcal{I}_4^{-1} = \{\mathbb{I}_a^{-1}, \mathbb{I}_b^{-1}, \mathbb{I}_{a+3}^{-1}, \mathbb{I}_{b+3}^{-1}\}$. Then, for a given vector field $V \in \mathcal{I}^{-1}$,

$$\begin{aligned}\nabla_V V &\equiv \frac{1}{2}(h_a h_b(\frac{1}{j_c}(m_b - m_a)\mathbb{I}_{c+3}^{-1}) + \epsilon_{abc} h_a h_{b+3}(\frac{m_a}{m_c}\mathbb{I}_c^{-1}) \\ &\quad + \epsilon_{abc} h_b h_{a+3}(\frac{m_b}{m_c}\mathbb{I}_c^{-1}) + h_{a+3} h_{b+3}(\frac{1}{j_c}(j_b - j_a)\mathbb{I}_{c+3}^{-1})) \pmod{\mathcal{I}_4^{-1}},\end{aligned}$$

where ϵ_{abc} is the standard permutation symbol.

Theorem C.7. *Suppose that we have a kinetically unique four input system with input vectors $\mathcal{I}_4^{-1} = \{\mathbb{I}_a^{-1}, \mathbb{I}_b^{-1}, \mathbb{I}_{a+3}^{-1}, \mathbb{I}_{b+3}^{-1}\}$ where $a, b \in \mathcal{U}$, then the decoupling vector fields are either the pure vector fields $V = h_i \mathbb{I}_i^{-1}$ for $i \in \{a, b, a + 3, b + 3\}$ or the axial fields $V = h_i \mathbb{I}_i^{-1} + h_{i+3} Y_{i+3}$ where $i = a$ or $i = b$.*

Remark C.3. From Section C.2.3, we see that if $m_a = m_b$, then additional decoupling

vector fields for the system are the axial motions plus a multiple of the other translational input vector field, $V = h_a \mathbb{I}_a^{-1} + h_b \mathbb{I}_b^{-1} + h_i \mathbb{I}_i^{-1}$ where $i = a + 3$ or $i = b + 3$. And, if $j_a = j_b$, then additional decoupling vector fields for the system are of the form $V = h_{a+3} \mathbb{I}_{a+3}^{-1} + h_{b+3} \mathbb{I}_{b+3}^{-1}$.

One principal axis repeated

1,2,4,6

Here we consider a four input system where the inputs are

$$\nabla_{\gamma'} \gamma = \mathbb{I}_1^{-1} \sigma^1 + \mathbb{I}_2^{-1} \sigma^2 + \mathbb{I}_4^{-1} \sigma^4 + \mathbb{I}_6^{-1} \sigma^6$$

From this we come up with the following for a given vector field V ,

$$\begin{aligned} \nabla_V V &\equiv \frac{1}{2} (h_1 h_2 \left(\frac{1}{j_3} (m_2 - m_1) X_6 + h_1 h_6 \left(\frac{m_1}{m_2} \right) X_2 + h_2 h_4 \left(\frac{m_2}{m_3} \right) X_3 \right. \\ &\quad \left. + h_2 h_6 \left(-\frac{m_2}{m_1} \right) X_1 + h_4 h_6 \left(\frac{1}{j_2} (j_1 - j_3) X_5 \right) \right) \pmod{\mathcal{I}_4^{-1}} \\ &\equiv \frac{1}{2} (h_2 h_4 \left(\frac{m_2}{m_3} \right) X_3 + h_4 h_6 \left(\frac{1}{j_2} (j_1 - j_3) X_5 \right) \pmod{\mathcal{I}_4^{-1}} \end{aligned}$$

Thus, either h_4 is zero, and the decoupling vector fields are of the form $V = h_1 \mathbb{I}_1^{-1} + h_2 \mathbb{I}_2^{-1} + h_6 \mathbb{I}_6^{-1}$ or $h_2 = h_6 = 0$ and the decoupling vector fields are $V = h_1 \mathbb{I}_1^{-1} + h_4 \mathbb{I}_4^{-1}$.

1,2,5,6

Here we consider a four input system where the inputs are

$$\nabla_{\gamma'} \gamma = \mathbb{I}_1^{-1} \sigma^1 + \mathbb{I}_2^{-1} \sigma^2 + \mathbb{I}_5^{-1} \sigma^5 + \mathbb{I}_6^{-1} \sigma^6$$

From this we come up with the following for a given vector field V ,

$$\begin{aligned}
\nabla_V V &\equiv \frac{1}{2}(h_1 h_2 \left(\frac{1}{j_3}(m_2 - m_1)X_6 + h_1 h_6 \left(\frac{m_1}{m_2}\right)X_2 + h_1 h_5 \left(-\frac{m_1}{m_3}\right)X_3\right. \\
&\quad \left.+ h_2 h_6 \left(-\frac{m_2}{m_1}\right)X_1 + h_5 h_6 \left(\frac{1}{j_1}(j_3 - j_2)X_4\right) \pmod{\mathcal{I}_4^{-1}}\right) \\
&\equiv \frac{1}{2}(h_1 h_5 \left(-\frac{m_1}{m_3}\right)X_3 + h_5 h_6 \left(\frac{1}{j_1}(j_3 - j_2)X_4\right) \pmod{\mathcal{I}_4^{-1}}
\end{aligned}$$

Thus, either h_5 is zero, and the decoupling vector fields are of the form $V = h_1 \mathbb{I}_1^{-1} + h_2 \mathbb{I}_2^{-1} + h_6 \mathbb{I}_6^{-1}$ or $h_1 = h_6 = 0$ and the decoupling vector fields are $V = h_2 \mathbb{I}_2^{-1} + h_5 \mathbb{I}_5^{-1}$.

1,3,4,5

Here we consider a four input system where the inputs are

$$\nabla_{\gamma'} \gamma = \mathbb{I}_1^{-1} \sigma^1 + \mathbb{I}_3^{-1} \sigma^3 + \mathbb{I}_4^{-1} \sigma^4 + \mathbb{I}_5^{-1} \sigma^5$$

From this we come up with the following for a given vector field V ,

$$\begin{aligned}
\nabla_V V &\equiv \frac{1}{2}(h_1 h_3 \left(-\frac{1}{j_2}(m_3 - m_2)X_5 + h_1 h_5 \left(-\frac{m_1}{m_3}\right)X_3 + h_3 h_4 \left(-\frac{m_3}{m_2}\right)X_2\right. \\
&\quad \left.+ h_3 h_5 \left(\frac{m_3}{m_1}\right)X_1 + h_4 h_5 \left(\frac{1}{j_3}(j_2 - j_1)X_6\right) \pmod{\mathcal{I}_4^{-1}}\right) \\
&\equiv \frac{1}{2}(h_3 h_4 \left(-\frac{m_3}{m_2}\right)X_2 + h_4 h_5 \left(\frac{1}{j_3}(j_2 - j_1)X_6\right) \pmod{\mathcal{I}_4^{-1}}
\end{aligned}$$

Thus, either h_4 is zero, and the decoupling vector fields are of the form $V = h_1 \mathbb{I}_1^{-1} + h_3 \mathbb{I}_3^{-1} + h_5 \mathbb{I}_5^{-1}$ or $h_3 = h_5 = 0$ and the decoupling vector fields are $V = h_1 \mathbb{I}_1^{-1} + h_4 \mathbb{I}_4^{-1}$.

1,3,5,6

Here we consider a four input system where the inputs are

$$\nabla_{\gamma'} \gamma = \mathbb{I}_1^{-1} \sigma^1 + \mathbb{I}_3^{-1} \sigma^3 + \mathbb{I}_5^{-1} \sigma^5 + \mathbb{I}_6^{-1} \sigma^6$$

From this we come up with the following for a given vector field V ,

$$\begin{aligned}\nabla_V V &\equiv \frac{1}{2}(h_1 h_3 (-\frac{1}{j_2}(m_3 - m_2)X_5 + h_1 h_5 (-\frac{m_1}{m_3})X_3 + h_1 h_6 (\frac{m_1}{m_2})X_2 \\ &\quad + h_3 h_5 (\frac{m_3}{m_1})X_1 + h_5 h_6 (\frac{1}{j_1}(j_3 - j_2)X_4) \pmod{\mathcal{I}_4^{-1}} \\ &\equiv \frac{1}{2}(h_1 h_6 (\frac{m_1}{m_2})X_2 + h_5 h_6 (\frac{1}{j_1}(j_3 - j_2)X_4) \pmod{\mathcal{I}_4^{-1}}\end{aligned}$$

Thus, either h_6 is zero, and the decoupling vector fields are of the form $V = h_1 \mathbb{I}_1^{-1} + h_3 \mathbb{I}_3^{-1} + h_5 \mathbb{I}_5^{-1}$ or $h_1 = h_5 = 0$ and the decoupling vector fields are $V = h_3 \mathbb{I}_3^{-1} + h_6 \mathbb{I}_6^{-1}$.

2,3,4,5

Here we consider a four input system where the inputs are

$$\nabla_{\gamma'} \gamma = \mathbb{I}_2^{-1} \sigma^2 + \mathbb{I}_3^{-1} \sigma^3 + \mathbb{I}_4^{-1} \sigma^4 + \mathbb{I}_5^{-1} \sigma^5$$

From this we come up with the following for a given vector field V ,

$$\begin{aligned}\nabla_V V &\equiv \frac{1}{2}(h_2 h_3 (\frac{1}{j_1}(m_3 - m_2)X_4 + h_2 h_4 (\frac{m_2}{m_3})X_3 + h_3 h_4 (-\frac{m_3}{m_2})X_2 \\ &\quad + h_3 h_5 (\frac{m_3}{m_1})X_1 + h_4 h_5 (\frac{1}{j_3}(j_2 - j_1)X_6) \pmod{\mathcal{I}_4^{-1}} \\ &\equiv \frac{1}{2}(h_3 h_5 (\frac{m_3}{m_1})X_1 + h_4 h_5 (\frac{1}{j_3}(j_2 - j_1)X_6) \pmod{\mathcal{I}_4^{-1}}\end{aligned}$$

Thus, either h_5 is zero, and the decoupling vector fields are of the form $V = h_2 \mathbb{I}_2^{-1} + h_3 \mathbb{I}_3^{-1} + h_4 \mathbb{I}_4^{-1}$ or $h_3 = h_4 = 0$ and the decoupling vector fields are $V = h_2 \mathbb{I}_2^{-1} + h_5 \mathbb{I}_5^{-1}$.

2,3,4,6

Here we consider a four input system where the inputs are

$$\nabla_{\gamma'} \gamma = \mathbb{I}_2^{-1} \sigma^2 + \mathbb{I}_3^{-1} \sigma^3 + \mathbb{I}_4^{-1} \sigma^4 + \mathbb{I}_6^{-1} \sigma^6$$

From this we come up with the following for a given vector field V ,

$$\begin{aligned}\nabla_V V &\equiv \frac{1}{2}(h_2 h_3 \left(\frac{1}{j_1}(m_3 - m_2)X_4 + h_2 h_4 \left(\frac{m_2}{m_3}\right)X_3 + h_2 h_6 \left(-\frac{m_2}{m_1}\right)X_1\right. \\ &\quad \left.+ h_3 h_4 \left(-\frac{m_3}{m_2}\right)X_2 + h_4 h_6 \left(\frac{1}{j_2}(j_1 - j_3)X_5\right)\right) \pmod{\mathcal{I}_4^{-1}} \\ &\equiv \frac{1}{2}(h_2 h_6 \left(-\frac{m_2}{m_1}\right)X_1 + h_4 h_6 \left(\frac{1}{j_2}(j_1 - j_3)X_5\right)) \pmod{\mathcal{I}_4^{-1}}\end{aligned}$$

Thus, either h_6 is zero, and the decoupling vector fields are of the form $V = h_2 \mathbb{I}_2^{-1} + h_3 \mathbb{I}_3^{-1} + h_4 \mathbb{I}_4^{-1}$ or $h_2 = h_4 = 0$ and the decoupling vector fields are $V = h_3 \mathbb{I}_3^{-1} + h_6 \mathbb{I}_6^{-1}$.

Suppose that $a, b, c \in \mathcal{U}$ and the input vector fields are $\mathcal{I}_4^{-1} = \{\mathbb{I}_a^{-1}, \mathbb{I}_b^{-1}, \mathbb{I}_{a+3}^{-1}, \mathbb{I}_{c+3}^{-1}\}$.

Then, for a given vector field $V \in \mathcal{I}^{-1}$,

$$\nabla_V V \equiv \frac{1}{2}(\epsilon_{abc} h_b h_{a+3} \left(\frac{m_b}{m_c} Y_c\right) + h_{a+3} h_{c+3} \left(\frac{1}{j_b}(j_a - j_c) \mathbb{I}_{b+3}^{-1}\right)) \pmod{\mathcal{I}^{-1}}.$$

Theorem C.8. *Suppose that we have a kinetically unique four input system with input vectors $\mathcal{I}^{-1} = \{\mathbb{I}_a^{-1}, \mathbb{I}_b^{-1}, \mathbb{I}_{a+3}^{-1}, \mathbb{I}_{c+3}^{-1}\}$ where $a, b, c \in \mathcal{U}$, then the decoupling vector fields are the axial motions $V = h_a \mathbb{I}_a^{-1} + h_{a+3} \mathbb{I}_{a+3}^{-1}$ or the coordinate motions $V = h_a \mathbb{I}_a^{-1} + h_b \mathbb{I}_b^{-1} + h_{c+3} \mathbb{I}_{c+3}^{-1}$.*

Remark C.4. From Section C.2.3, we see that if $j_a = j_c$ then h_b or h_{a+3} must be zero, and additional decoupling vector fields are the axial motions plus a multiple of the other rotational input vector field, $V = h_a \mathbb{I}_a^{-1} + h_{a+3} \mathbb{I}_{a+3}^{-1} + h_{c+3} \mathbb{I}_{c+3}^{-1}$.

We conclude this section on four input systems with this general remark.

Remark C.5. It is interesting to note that in Sections C.2.2, C.2.3 and C.2.3, letting $m_1 = m_2 = m_3$ and $j_1 = j_2 = j_3$ yields no additional decoupling vector fields for the affine

connection control system with four input vector fields.

C.3 Five Input Systems

Consider a five input system ($m = 5$) where the geometric acceleration is given by

$$\nabla_{\gamma'}\gamma' = \sum_{a=1}^5 \tilde{\mathbb{I}}_a^{-1}(\gamma(t))\sigma^a(t).$$

C.3.1 Three Translation, Two Rotation

1,2,3,4,5

Here we consider a five input system where the inputs are

$$\nabla_{\gamma'}\gamma = \mathbb{I}_1^{-1}\sigma^1 + \mathbb{I}_2^{-1}\sigma^2 + \mathbb{I}_3^{-1}\sigma^3 + \mathbb{I}_4^{-1}\sigma^4 + \mathbb{I}_5^{-1}\sigma^5$$

From this we come up with the following for a given vector field V ,

$$\begin{aligned} \nabla_V V &\equiv \frac{1}{2}(h_1 h_2 \left(\frac{1}{j_3}(m_2 - m_1)X_6 + h_1 h_3 \left(-\frac{1}{j_2}(m_3 - m_2)X_5 + h_1 h_5 \left(-\frac{m_1}{m_3}\right)X_3\right.\right. \\ &\quad \left. + h_2 h_3 \left(\frac{1}{j_1}(m_3 - m_2)X_4 + h_2 h_4 \left(\frac{m_2}{m_3}\right)X_3 + h_3 h_4 \left(-\frac{m_3}{m_2}\right)X_2\right.\right. \\ &\quad \left. + h_3 h_5 \left(\frac{m_3}{m_1}\right)X_1 + h_4 h_5 \left(\frac{1}{j_3}(j_2 - j_1)X_6\right) \pmod{\mathcal{I}_5^{-1}}\right) \\ &\equiv \frac{1}{2}(h_1 h_2 \left(\frac{1}{j_3}(m_2 - m_1)X_6 + h_4 h_5 \left(\frac{1}{j_3}(j_2 - j_1)X_6\right) \pmod{\mathcal{I}_5^{-1}}\right) \end{aligned}$$

Thus, one of $\{h_1, h_2\}$ and one of $\{h_4, h_5\}$ must be zero. Thus, the decoupling vector fields

are the coordinate fields $V = h_2\mathbb{I}_2^{-1} + h_3\mathbb{I}_3^{-1} + h_4\mathbb{I}_4^{-1}$ or $V = h_1\mathbb{I}_1^{-1} + h_3\mathbb{I}_3^{-1} + h_5\mathbb{I}_5^{-1}$,

or the axial fields plus and additional input vector $V = h_2\mathbb{I}_2^{-1} + h_3\mathbb{I}_3^{-1} + h_5\mathbb{I}_5^{-1}$ or $V =$

$h_1\mathbb{I}_1^{-1} + h_3\mathbb{I}_3^{-1} + h_4\mathbb{I}_4^{-1}$.

1,2,3,4,6

Here we consider a five input system where the inputs are

$$\nabla_{\gamma'}\gamma = \mathbb{I}_1^{-1}\sigma^1 + \mathbb{I}_2^{-1}\sigma^2 + \mathbb{I}_3^{-1}\sigma^3 + \mathbb{I}_4^{-1}\sigma^4 + \mathbb{I}_6^{-1}\sigma^6$$

From this we come up with the following for a given vector field V ,

$$\begin{aligned}\nabla_V V &\equiv \frac{1}{2}(h_1 h_2 \left(\frac{1}{j_3}(m_2 - m_1)X_6 + h_1 h_3 \left(-\frac{1}{j_2}(m_3 - m_2)X_5 + h_1 h_6 \left(\frac{m_1}{m_2}\right)X_2\right.\right. \\ &\quad \left. + h_2 h_3 \left(\frac{1}{j_1}(m_3 - m_2)X_4 + h_2 h_4 \left(\frac{m_2}{m_3}\right)X_3 + h_3 h_4 \left(-\frac{m_3}{m_2}\right)X_2\right.\right. \\ &\quad \left. + h_2 h_6 \left(-\frac{m_2}{m_1}\right)X_1 + h_4 h_6 \left(\frac{1}{j_2}(j_1 - j_3)X_5\right) \pmod{\mathcal{I}_5^{-1}} \\ &\equiv \frac{1}{2}(h_1 h_3 \left(-\frac{1}{j_2}(m_3 - m_2)X_5 + h_4 h_6 \left(\frac{1}{j_2}(j_1 - j_3)X_5\right) \pmod{\mathcal{I}_5^{-1}}\end{aligned}$$

Thus, one of $\{h_1, h_3\}$ and one of $\{h_4, h_6\}$ must be zero. Thus, the decoupling vector fields are the coordinate fields $V = h_2\mathbb{I}_2^{-1} + h_3\mathbb{I}_3^{-1} + h_4\mathbb{I}_4^{-1}$ or $V = h_1\mathbb{I}_1^{-1} + h_2\mathbb{I}_2^{-1} + h_6\mathbb{I}_6^{-1}$, or the axial fields plus and additional input vector $V = h_2\mathbb{I}_2^{-1} + h_3\mathbb{I}_3^{-1} + h_6\mathbb{I}_6^{-1}$ or $V = h_1\mathbb{I}_1^{-1} + h_2\mathbb{I}_2^{-1} + h_4\mathbb{I}_4^{-1}$.

1,2,3,5,6

Here we consider a five input system where the inputs are

$$\nabla_{\gamma'}\gamma = \mathbb{I}_1^{-1}\sigma^1 + \mathbb{I}_2^{-1}\sigma^2 + \mathbb{I}_3^{-1}\sigma^3 + \mathbb{I}_5^{-1}\sigma^5 + \mathbb{I}_6^{-1}\sigma^6$$

From this we come up with the following for a given vector field V ,

$$\begin{aligned}
\nabla_V V &\equiv \frac{1}{2} \left(h_1 h_2 \left(\frac{1}{j_3} (m_2 - m_1) X_6 + h_1 h_3 \left(-\frac{1}{j_2} (m_3 - m_2) X_5 + h_1 h_5 \left(-\frac{m_1}{m_3} \right) X_3 \right. \right. \right. \\
&\quad \left. \left. + h_2 h_3 \left(\frac{1}{j_1} (m_3 - m_2) X_4 + h_1 h_6 \left(\frac{m_1}{m_2} \right) X_2 + h_2 h_6 \left(-\frac{m_2}{m_1} \right) X_1 \right. \right. \right. \\
&\quad \left. \left. + h_3 h_5 \left(\frac{m_3}{m_1} \right) X_1 + h_5 h_6 \left(\frac{1}{j_1} (j_3 - j_2) X_4 \right) \right) \pmod{\mathcal{I}_5^{-1}} \\
&\equiv \frac{1}{2} \left(h_2 h_3 \left(\frac{1}{j_1} (m_3 - m_2) X_4 + h_5 h_6 \left(\frac{1}{j_1} (j_3 - j_2) X_4 \right) \right) \pmod{\mathcal{I}_5^{-1}}
\end{aligned}$$

Thus, one of $\{h_2, h_3\}$ and one of $\{h_5, h_6\}$ must be zero. Thus, the decoupling vector fields are the coordinate fields $V = h_1 \mathbb{I}_1^{-1} + h_3 \mathbb{I}_3^{-1} + h_5 \mathbb{I}_5^{-1}$ or $V = h_1 \mathbb{I}_1^{-1} + h_2 \mathbb{I}_2^{-1} + h_6 \mathbb{I}_6^{-1}$, or the axial fields plus and additional input vector $V = h_1 \mathbb{I}_1^{-1} + h_2 \mathbb{I}_2^{-1} + h_5 \mathbb{I}_5^{-1}$ or $V = h_1 \mathbb{I}_1^{-1} + h_3 \mathbb{I}_3^{-1} + h_6 \mathbb{I}_6^{-1}$.

Suppose we have a five input system $\mathcal{I}_5^{-1} = \{\mathbb{I}_1^{-1}, \mathbb{I}_2^{-1}, \mathbb{I}_3^{-1}, \mathbb{I}_a^{-1}, \mathbb{I}_b^{-1}\}$ with $a, b \in \mathcal{V}$, then

$$\begin{aligned}
\nabla_V V &\equiv [h_{a-3} h_{b-3} \left(-\frac{1}{j_{c-3}} (m_{a-3} - m_{b-3}) \right) \\
&\quad + h_a h_b \left(-\frac{1}{j_{c-3}} (j_{a-3} - j_{b-3}) \right)] Y_c \pmod{\mathcal{I}_5^{-1}}
\end{aligned}$$

where $c \in \mathcal{V}$ and $a, b \neq c$.

Theorem C.9. *Suppose that we have a kinetically unique five input system with input vectors $\mathcal{I}_5^{-1} = \{\mathbb{I}_1^{-1}, \mathbb{I}_2^{-1}, \mathbb{I}_3^{-1}, \mathbb{I}_a^{-1}, \mathbb{I}_b^{-1}\}$ where $a, b \in \mathcal{V}$, then the decoupling vector fields are the axial motions plus a multiple of a translational input $V = h_{i-3} Y_{i-3} + h_j \mathbb{I}_j^{-1} + h_i Y_i$ where $i = a$ or $i = b$ and $j \in \mathcal{U} - \{a - 3, b - 3\}$ or the coordinate motions $V = h_i \mathbb{I}_i^{-1} + h_j \mathbb{I}_j^{-1} + h_k \mathbb{I}_k^{-1}$ where $i = a$ or $i = b$ and $j, k \in \mathcal{U} - \{i - 3\}$.*

Remark C.6. Assuming that $m_{a-3} = m_{b-3}$, additional decoupling vector fields are given

by $V = h_i \mathbb{I}_i^{-1} + h_c \mathbb{I}_c^{-1} + h_a \mathbb{I}_a^{-1} + h_b \mathbb{I}_b^{-1}$ where $i = a - 3$ or $i = b - 3$ and $c \in \mathcal{U} - \{a - 3, b - 3\}$. Assuming that $j_{a-3} = j_{b-3}$, additional decoupling vector fields are given by $V = h_1 \mathbb{I}_1^{-1} + h_2 \mathbb{I}_2^{-1} + h_3 \mathbb{I}_3^{-1} + h_i \mathbb{I}_i^{-1}$ where $i = a$ or $i = b$.

C.3.2 Two Translation, Three Rotation

1,2,4,5,6

Here we consider a five input system where the inputs are

$$\nabla_{\gamma'} \gamma = \mathbb{I}_1^{-1} \sigma^1 + \mathbb{I}_2^{-1} \sigma^2 + \mathbb{I}_4^{-1} \sigma^4 + \mathbb{I}_5^{-1} \sigma^5 + \mathbb{I}_6^{-1} \sigma^6$$

From this we come up with the following for a given vector field V ,

$$\begin{aligned} \nabla_V V &\equiv \frac{1}{2} (h_1 h_2 \left(\frac{1}{j_3} (m_2 - m_1)\right) X_6 + h_1 h_5 \left(-\frac{m_1}{m_3}\right) X_3 + h_1 h_6 \left(\frac{m_1}{m_2}\right) X_2 \\ &+ h_2 h_4 \left(\frac{m_2}{m_3}\right) X_3 + h_2 h_6 \left(-\frac{m_2}{m_1}\right) X_1 + h_4 h_5 \left(\frac{1}{j_3} (j_2 - j_1)\right) X_6 \\ &+ h_4 h_6 \left(\frac{1}{j_2} (j_1 - j_3)\right) X_5 + h_5 h_6 \left(\frac{1}{j_1} (j_3 - j_2)\right) X_4) \pmod{\mathcal{I}_5^{-1}} \\ &\equiv \frac{1}{2} (h_1 h_5 \left(-\frac{m_1}{m_3}\right) X_3 + h_2 h_4 \left(\frac{m_2}{m_3}\right) X_3) \pmod{\mathcal{I}_5^{-1}} \end{aligned}$$

Thus, one of $\{h_1, h_5\}$ and one of $\{h_2, h_4\}$ must be zero. Thus, the decoupling vector fields are the coordinate fields $V = h_4 \mathbb{I}_4^{-1} + h_5 \mathbb{I}_5^{-1} + h_6 \mathbb{I}_6^{-1}$ or $V = h_1 \mathbb{I}_1^{-1} + h_2 \mathbb{I}_2^{-1} + h_6 \mathbb{I}_6^{-1}$, or the axial fields plus and additional input vector $V = h_2 \mathbb{I}_2^{-1} + h_5 \mathbb{I}_5^{-1} + h_6 \mathbb{I}_6^{-1}$ or $V = h_1 \mathbb{I}_1^{-1} + h_4 \mathbb{I}_4^{-1} + h_6 \mathbb{I}_6^{-1}$.

1,3,4,5,6

Here we consider a five input system where the inputs are

$$\nabla_{\gamma'} \gamma = \mathbb{I}_1^{-1} \sigma^1 + \mathbb{I}_3^{-1} \sigma^3 + \mathbb{I}_4^{-1} \sigma^4 + \mathbb{I}_5^{-1} \sigma^5 + \mathbb{I}_6^{-1} \sigma^6$$

From this we come up with the following for a given vector field V ,

$$\begin{aligned}
\nabla_V V &\equiv \frac{1}{2}(h_1 h_3 (-\frac{1}{j_2}(m_3 - m_2)X_5 + h_1 h_5 (-\frac{m_1}{m_3})X_3 + h_1 h_6 (\frac{m_1}{m_2})X_2 \\
&\quad + h_3 h_4 (-\frac{m_3}{m_2})X_2 + h_3 h_5 (\frac{m_3}{m_1})X_1 + h_4 h_5 (\frac{1}{j_3}(j_2 - j_1)X_6 \\
&\quad + h_4 h_6 (\frac{1}{j_2}(j_1 - j_3)X_5 + h_5 h_6 (\frac{1}{j_1}(j_3 - j_2)X_4) \pmod{\mathcal{I}_5^{-1}} \\
&\equiv \frac{1}{2}(h_1 h_6 (\frac{m_1}{m_2})X_2 + h_3 h_4 (-\frac{m_3}{m_2})X_2) \pmod{\mathcal{I}_5^{-1}}
\end{aligned}$$

Thus, one of $\{h_1, h_6\}$ and one of $\{h_3, h_4\}$ must be zero. Thus, the decoupling vector fields are the coordinate fields $V = h_4 \mathbb{I}_4^{-1} + h_5 \mathbb{I}_5^{-1} + h_6 \mathbb{I}_6^{-1}$ or $V = h_1 \mathbb{I}_1^{-1} + h_3 \mathbb{I}_3^{-1} + h_5 \mathbb{I}_5^{-1}$, or the axial fields plus and additional input vector $V = h_3 \mathbb{I}_3^{-1} + h_5 \mathbb{I}_5^{-1} + h_6 \mathbb{I}_6^{-1}$ or $V = h_1 \mathbb{I}_1^{-1} + h_4 \mathbb{I}_4^{-1} + h_5 \mathbb{I}_5^{-1}$.

2,3,4,5,6

Here we consider a five input system where the inputs are

$$\nabla_{\gamma'} \gamma = \mathbb{I}_2^{-1} \sigma^2 + \mathbb{I}_3^{-1} \sigma^3 + \mathbb{I}_4^{-1} \sigma^4 + \mathbb{I}_5^{-1} \sigma^5 + \mathbb{I}_6^{-1} \sigma^6$$

From this we come up with the following for a given vector field V ,

$$\begin{aligned}
\nabla_V V &\equiv \frac{1}{2}(h_2 h_3 (\frac{1}{j_1}(m_3 - m_2)X_4 + h_2 h_4 (\frac{m_2}{m_3})X_3 + h_2 h_6 (-\frac{m_2}{m_1})X_1 \\
&\quad + h_3 h_4 (-\frac{m_3}{m_2})X_2 + h_3 h_5 (\frac{m_3}{m_1})X_1 + h_4 h_5 (\frac{1}{j_3}(j_2 - j_1)X_6 \\
&\quad + h_4 h_6 (\frac{1}{j_2}(j_1 - j_3)X_5 + h_5 h_6 (\frac{1}{j_1}(j_3 - j_2)X_4) \pmod{\mathcal{I}_5^{-1}} \\
&\equiv \frac{1}{2}(h_2 h_6 (-\frac{m_2}{m_1})X_1 + h_3 h_5 (\frac{m_3}{m_1})X_1) \pmod{\mathcal{I}_5^{-1}}
\end{aligned}$$

Thus, one of $\{h_2, h_6\}$ and one of $\{h_3, h_5\}$ must be zero. Thus, the decoupling vector fields are the coordinate fields $V = h_4 \mathbb{I}_4^{-1} + h_5 \mathbb{I}_5^{-1} + h_6 \mathbb{I}_6^{-1}$ or $V = h_2 \mathbb{I}_2^{-1} + h_3 \mathbb{I}_3^{-1} + h_4 \mathbb{I}_4^{-1}$,

or the axial fields plus and additional input vector $V = h_2\mathbb{I}_2^{-1} + h_4\mathbb{I}_4^{-1} + h_5\mathbb{I}_5^{-1}$ or $V = h_3\mathbb{I}_3^{-1} + h_4\mathbb{I}_4^{-1} + h_6\mathbb{I}_6^{-1}$.

Suppose we have a five input system $\mathcal{I}_5^{-1} = \{\mathbb{I}_a^{-1}, \mathbb{I}_b^{-1}, \mathbb{I}_4^{-1}, \mathbb{I}_5^{-1}, \mathbb{I}_6^{-1}\}$ with $a, b \in \mathcal{U}$, then

$$\nabla_V V \equiv [h_a h_{b+3} \left(\frac{m_a}{m_c}\right) + h_b h_{a+3} \left(\frac{m_b}{m_c}\right)] \mathbb{I}_c^{-1} \pmod{\mathcal{I}_5^{-1}}$$

where $c \in \mathcal{U}$ and $a, b \neq c$.

Theorem C.10. *Suppose that we have a kinetically unique five input system with input vectors $\mathcal{I}_5^{-1} = \{\mathbb{I}_a^{-1}, \mathbb{I}_b^{-1}, \mathbb{I}_4^{-1}, \mathbb{I}_5^{-1}, \mathbb{I}_6^{-1}\}$ where $a, b \in \mathcal{U}$, then the decoupling vector fields are the axial motions plus a multiple of a rotational input $V = h_{i+3}Y_{i+3} + h_j\mathbb{I}_j^{-1} + h_iY_i$ where $i = a$ or $i = b$ and $j \in \mathcal{V} - \{a+3, b+3\}$, the coordinate motion $V = h_4\mathbb{I}_4^{-1} + h_5\mathbb{I}_5^{-1} + h_6\mathbb{I}_6^{-1}$ or the coordinate motion $V = h_a\mathbb{I}_a^{-1} + h_b\mathbb{I}_b^{-1} + h_i\mathbb{I}_i^{-1}$ where $i \in \mathcal{V} - \{a+3, b+3\}$.*

Remark C.7. Assuming that the system is not kinematically unique in any way does not yield any additional decoupling vector fields.

C.4 Six Input Systems

A six input system ($m = 6$) is a fully actuated affine connection control system, and it is known that every vector field $V \in \mathcal{I}^{-1}$ ($\mathcal{I}_6^{-1} = \{\mathbb{I}_1^{-1}, \mathbb{I}_2^{-1}, \mathbb{I}_3^{-1}, \mathbb{I}_4^{-1}, \mathbb{I}_5^{-1}, \mathbb{I}_6^{-1}\}$) is a decoupling vector field.

References

- Abraham, R. & Marsden, J. (1978), *Foundations of Mechanics*, Second edn, Addison Wesley, Reading, MA.
- Abraham, R., Marsden, J. & Ratiu, T. (1986), *Manifolds, Tensor Analysis, and Applications*, Second edn, Academic Press, New York.
- Abraham, R. & Ratiu, T. (1999), *Introduction to Mechanics and Symmetry*, Second edn, Springer-Verlag, New York–Heidelberg–Berlin. Number 17 in Texts in Applied Mathematics.
- Allmendinger, E. E. (1990), *Submersible Vehicle Design*, SNAME.
- Ardema, M. D. (2005), *Newton-Euler Dynamics*, Springer, New York.
- Arnol'd, V. (1978), *Mathematical Methods of Classical Mechanics*, First edn, Springer-Verlag, New York–Heidelberg–Berlin. Number 60 in Graduate Texts in Mathematics.
- Bhattacharyya, R. (1978), *Dynamics of Marine Vehicles*, John Wiley & Sons.
- Bloch, A. (2003), *Nonholonomic Mechanics and Control*, Springer-Verlag, New York-Heidelberg-Berlin. Volume 24 of Interdisciplinary Applied Mathematics.
- Bluefin Robotics Corporation (2008), 'Bluefin-12', <http://www.bluefinrobotics.com/>. viewed May 2008.
- Bonnard, B. (1984), 'Controllabilité de systemès mécaniques sur les groupes de lie', *SIAM Journal on Control and Optimization* **22(5)**, 711–722.
- Boothby, W. (1986), *An Introduction to Differentiable Manifolds and Riemannian Geometry*, Number 125 in Pure and Applied Mathematics, Second edn, Academic Press, Inc., Orlando, FL.
- Brockett, R. (1993), Hybrid models for motion control systems, in 'Essays in Control: Perspectives in the Theory and its Applications', Birkhäuser, Boston, MA, pp. 29–53.
- Bullo, F., A.D., L. & K.M., L. (2002), Controllable kinematic reductions for mechanical systems: concepts, computational tools, and examples., in 'Proceedings of MTNS02', University of Notre Dame.
- Bullo, F., Leonard, N. & Lewis, A. (2000), 'Controllability and motion algorithms for underactuated lagrangian systems on lie groups', *Institute of Electrical and Electronics Engineers. Transactions on Automatic Control* **45(8)**, 1437–1454.
- Bullo, F. & Lewis, A. D. (2005a), *Geometric Control of Mechanical Systems*, Springer.

- Bullo, F. & Lewis, A. D. (2005*b*), ‘Low-order controllability and kinematic reductions for affine connection control systems’, *SIAM Journal on Control and Optimization* **44**(3), 885–908.
- Bullo, F. & Lynch, K. (2001), ‘Kinematic controllability for decoupled trajectory planning in underactuated mechanical systems’, *IEEE Transactions. Robotics and Automation* **17**(4), 402–412.
- Canny, J. F. (1988), *The Complexity of Robot Motion Planning*, MIT Press, Cambridge, MA.
- Choi, S. & Yuh, J. (1996), ‘Design of advanced underwater robotic vehicle and graphic workstation’, *International Journal of Autonomous Robots* **3**(2/3), 187–194.
- Chyba, M., Haberkorn, T., Smith, R. N. & Choi, S. (2008*a*), ‘Design and implementation of time efficient trajectories for an underwater vehicle’, *Ocean Engineering* **35**(1), 63–76.
- Chyba, M., Haberkorn, T., Smith, R. N., Singh, S. & Choi, S. (2008*b*), ‘Increasing underwater vehicle autonomy by reducing energy consumption’, *Ocean Engineering: Special Edition on AUVs*. Accepted, to appear.
- Chyba, M., Haberkorn, T., Smith, R. & Wilkens, G. (2008*c*), ‘A geometrical analysis of trajectory design for underwater vehicles’, *Discrete and Continuous Dynamical Systems-B*. Accepted, to appear.
- Chyba, M. & Smith, R. N. (2008), A first extension of geometric control theory to underwater vehicles, in ‘Proceedings of the 2008 IFAC Workshop on Navigation, Guidance and Control of Underwater Vehicles’, Killaloe, Ireland.
- Cousteau, J.-M. (2004), ‘To go where no man has gone before...’, http://www.oceanfutures.org/features/2004/dispatch_02_04_a.php. viewed May 2008.
- Dalsmo, M. & van der Schaft, A. (1998), ‘On representations and integrability of mathematical structures in energy-conserving physical systems’, *SIAM Journal on Control and Optimization* **37**(1), 54–91.
- do Carmo, M. (1976), *Differential Geometry of Curves and Surfaces*, Prentice-Hall, Inc., Upper Saddle River, New Jersey.
- do Carmo, M. (1992), *Riemannian Geometry*, Birkhauser, Boston.
- Fossen, T. I. (1994), *Guidance and Control of Ocean Vehicles*, John Wiley & Sons.
- Frazzoli, E., Daleh, M. & Feron, E. (2002), ‘Real-time motion planning for agile autonomous vehicles’, *AIAA Journal of Guidance, Control and Dynamics* **25**(1), 116–129.

- GlobalSecurity.org (2008), 'Uss george h.w. bush', <http://www.globalsecurity.org/military/systems/ship/bulbous-bow.htm>. viewed May 2008.
- Hanai, A., Choi, H., Choi, S. & Yuh, J. (2003), Minimum energy based fine motion control of underwater robots in the presence of thruster nonlinearity, *in* 'Proceedings of IEEE/RSJ International Conference on Intelligent Robots and Systems', Las Vegas, Nevada, USA, pp. 559–564.
- Healey, A. & Lienard, D. (1993), 'Multivariable sliding mode control for autonomous diving and steering of unmanned underwater vehicles', *IEEE Journal of Oceanic Engineering* **18(3)**, 327–339.
- Hydroid, LLC (2008), 'Remus 600', <http://www.hydroidinc.com/remus600.html>. viewed May 2008.
- Imlay, F. (1961), The complete expressions for added mass of a rigid body moving in an ideal fluid, Technical Report DTMB 1528, David Taylor Model Basin, Washington D.C.
- Kato, N. (1995), Applications of fuzzy algorithm to guidance and control of underwater vehicles, *in* J. Yuh, ed., 'Underwater Robotic Vehicles: Design and Control', TSI, Albuquerque, NM.
- Kobayashi, S. & Nomizu, K. (1963), *Foundations of Differential Geometry, Volumes I and II*, Interscience Publishers, New York. Number 15 in Interscience Tracts in Pure and Applied Mathematics.
- Lamb, H. (1945), *Hydrodynamics*, 6th edn, Dover Publications.
- Lamb, H. (1961), *Dynamics*, University Press, Cambridge.
- Leonard, N. (1996), Stabilization of steady motions of an underwater vehicle, *in* 'Proceedings of the 35th IEEE Conference on Decision and Control'.
- Leonard, N. (1997), 'Stability of a bottom-heavy underwater vehicle.', *Automatica* **33(3)**, 331–346.
- Leonard, N. E. (1994), Control synthesis and adaptation for an underactuated autonomous underwater vehicle, Research report t.r. 94-58, Department of Electrical Engineering, Institute for Systems Research, University of Maryland, College Park, MD.
- Leonard, N. E. (1995), Periodic forcing, dynamics and control of underactuated spacecraft and underwater vehicles, *in* 'Proceedings of the 34th IEEE Conference on Decision and Control', New Orleans, Louisiana, pp. 3980–3985.
- Leonard, N. & Krishnaprasad, P. (1995), 'Motion control of drift-free, left-invariant systems on lie groups', *IEEE Transactions on Automatic Control* **40(9)**, 1539–1554.

- Lewis, A. D. (2007), ‘Is it worth learning differential geometric methods for modelling and control of mechanical systems?’, *Robotica* **25(6)**, 765–777.
- Lewis, H. W. (1997), *The Foundations of Fuzzy Control*, Plenum Press, New York, NY.
- Lynch, K., Shiroma, N., Arai, H. & Tanie, K. (1998), Motion planning for a 3-DOF robot with a passive joint, in ‘Proceedings of IEEE International Conference on Robotics and Automation’, Leuven, Belgium, pp. 927–932.
- Lynch, K., Shiroma, N., Arai, H. & Tanie, K. (2000), ‘Collision-free trajectory planning for a 3-DOF robot with a passive joint’, *Journal of the Society of Instrument & Control Engineers* **19(12)**, 1171–1184.
- Magnus, W. (1954), ‘On the exponential solution of differential equations for a linear operator’, *Comm. Pure Applied Mathematics* **VII**, 649–673.
- Marsden, J. (1992), *Lectures on Mechanics*, Cambridge University Press, New York–Port Chester–Melbourne–Sydney. Number 174 in London Mathematical Society Lecture Note Series.
- McIsaac, K. & Ostrowski, J. (2001), Steering algorithms for dynamic robotic locomotion systems, in B. Donald, K. Lynch & D. Rus, eds, ‘Algorithmic and Computational Robotics: New Directions’, A.K. Peters, Natick, MA, pp. 221–231.
- Meriam, J. & Kraige, L. (1997), *Engineering Mechanics, DYNAMICS*, 4th edn, John Wiley & Sons, Inc., New York.
- Newman, J. (1977), *Marine Hydrodynamics*, MIT Press, Cambridge, MA.
- Pappas, G., Lafferriere, G. & Sastry, S. (2000), ‘Hierarchically consistent control systems’, *IEEE Transactions on Automatic Control* **45(6)**, 1144–60.
- Prestero, T. (2001), Verification of a six-degree of freedom simulation model for the remus autonomous underwater vehicle, Master’s thesis, Massachusetts Institute of Technology and Woods Hole Oceanographic Institution, Joint Program in Applied Ocean Science and Engineering.
- Reif, J. H. (1987), Complexity of the generalized mover’s problem, in J. T. Schwartz, M. Sharir & J. Hopcroft, eds, ‘Planning, Geometry and Complexity of Robot Motion’, Ablex Publishing Corporation, pp. 267–281.
- Sagatun, S. (1992), Modeling and Control of Underwater Vehicles: A Lagrangian Approach, Dr.ing. thesis, Dept. of Engineering Cybernetics, The Norwegian Institute of Technology, Trondheim, Norway.
- SilverStar (2008), ‘A block diagram of a pid controller’, <http://en.wikipedia.org/wiki/Image:Pid-feedback-nct-int-correct.png>. viewed May 2008.

- Smith, R. N., Chyba, M. & Singh, S. B. (2008a), Submerged rigid body subject to dissipative and potential forces, *in* 'Proceedings of the IEEE Region 10 Colloquium and Third International Conference on Industrial and Information Systems', Kharagpur, India. Submitted.
- Smith, R. N., Chyba, M., Wilkens, G. & Catone, C. (2008b), A geometrical approach to the motion planning problem for a submerged rigid body. Submitted to the International Journal of Control.
- SNAME (1950), Nomenclature for treating the motion of a submerged body through a fluid, Technical and Research Bulletin No. 1-5, The Society of Naval Architects and Marine Engineers.
- Sontag, E. (1998), *Mathematical Control Theory: Deterministic Finite Dimensional Systems*, Second edn, Springer-Verlag, New York. Volume 6 of TAM.
- Spivak, M. (1979), *A Comprehensive Introduction to Differential Geometry*, Second edn, Publish or Perish, Inc., Berkeley, CA. Volumes 1–5.
- StoneAerospace, Inc. (2008a), 'Depthx', <http://www.stoneaerospace.com/products-pages/products-DEPTHX.php>. viewed May 2008.
- StoneAerospace, Inc. (2008b), 'Endurance', <http://www.stoneaerospace.com/products-pages/products-ENDURANCE.php>. viewed May 2008.
- Sussmann, H. & Jurdjevic, V. (1972), 'Controllability of nonlinear systems', *Journal of Differential Equations* **12**, 95–116.
- Tsukamoto, C., Yuh, J., Choi, S., Lee, W. & Lorentz, J. (1999), 'Experimental study of advanced controllers for an underwater robotic vehicle thruster system', *International Journal of Intelligent Automation and Soft Computing* **5(3)**, 225–238.
- van der Schaft, A. (2000), 'Port-controlled hamiltonian systems: Towards a theory for control and design of nonlinear physical systems', *Journal of the Society of Instrument & Control Engineers* **39(2)**, 91–98.
- Warner, F. (1971), *Foundations of Differentiable Manifolds and Lie Groups*, Revised edn, Scott, Foresman and Co., Glenview, IL-London.
- Webb Research Corporation (2008), <http://www.webbresearch.com/slocum.htm>. viewed May 2008.
- Yoerger, D. & Slotine, J. (1985), 'Robust trajectory control of underwater vehicles', *IEEE Journal of Oceanic Engineering* **10(4)**, 462–470.
- Yuh, J. (1990), 'A neural net controller for underwater robotic vehicles', *IEEE Journal of Oceanic Engineering* **15(3)**, 161–166.

Yuh, J. (1996), 'An adaptive and learning control system for underwater robots', *Proceedings of 13th World Congress International Federation of Automatic Control* **A**, 145–150.